Tampere University

MARIA KOIVISTO

Functional Human Cell-Based Cardiac Tissue Model with Contraction Force Measurements

Tampere University Dissertations 843

Tampere University Dissertations 843

MARIA KOIVISTO

Functional Human Cell-Based Cardiac Tissue Model with Contraction Force Measurements

ACADEMIC DISSERTATION
To be presented, with the permission of
the Faculty of Medicine and Health Technology
of Tampere University,
for public discussion in the auditorium F114
of the Arvo Building, Arvo Ylpön katu 34, Tampere,
on 13 October 2023, at 12 o'clock.

ACADEMIC DISSERTATION
Tampere University, Faculty of Medicine and Health Technology
Finland

Responsible supervisor and Custos	Professor h.c. Tuula Heinonen Tampere University Finland	
Supervisor	PhD Tarja Toimela Tampere University Finland	
Pre-examiners	Docent Virpi Talman University of Helsinki Finland	PhD Enrico Accastelli TissUse GmbH Germany
Opponent	Professor Robert Passier University of Twente Netherlands	

The originality of this thesis has been checked using the Turnitin OriginalityCheck service.

Cover design: Roihu Inc.

ISBN 978-952-03-3008-8 (print)
ISBN 978-952-03-3009-5 (pdf)
ISSN 2489-9860 (print)
ISSN 2490-0028 (pdf)
http://urn.fi/URN:ISBN:978-952-03-3009-5

Carbon dioxide emissions from printing Tampere University dissertations have been compensated.

PunaMusta Oy – Yliopistopaino
Joensuu 2023

PREFACE

This thesis was done during 2017–2023 in the Faculty of Medicine and Health Technology, Tampere University. The work was performed in the Finnish Centre for Alternative Methods (FICAM) during 2017–2020 and, after FICAM's research group fusion with Greco Lab in 2021, the work was formally continued in the Finnish Hub for Development and Validation of Integrated Approaches (FHAIVE). Professor Jari Hyttinen, head of BioMediTech unit at the Faculty of Medicine and Health Technology / Computational Biophysics and Imaging Group (CBIG) provided resources during the finalising of the PhD thesis.

This work was financially supported by the project funding from Academy of Finland (310347), and by personal grants from Emil Aaltonen Foundation, Juliana von Wendt Foundation, and Pirkanmaa Cultural Foundation (50211545), as well as by the Faculty of Medicine and Health Technology doctoral research funding. Open access publishing was supported by Tampere University Library Open Access support funding.

I wish to express my gratitude to my both supervisors Professor (hc) Tuula Heinonen, Dos., PhD, ERT and Tarja Toimela, PhD. Thank you Tuula for giving me the opportunity to do this PhD work in FICAM. The advises and support I received from both of you were invaluable in my PhD journey. I learned so much from you both.

I'm grateful to the pre-examiners Docent Virpi Talman, PhD and Enrico Accastelli, PhD for their insightful comments on my thesis. Moreover, I'm grateful to Professor Robert Passier, PhD for agreeing to act as the opponent in my public defence.

I want to thank my thesis follow-up committee members Associate Professor Sampo Tuukkanen, PhD and Professor Timo Ylikomi, MD, PhD for their valuable advises in the yearly meetings.

I would also like to thank all my co-authors. This work required a lot of multidisciplinary teamwork, and it would not have been possible without you. Especially, the tight collaboration in the InVitroCardio project with Sampo Tuukkanen, Juhani Virtanen, PhD and Milad Mosallaei, PhD was crucial for my PhD work.

I also want to thank the members of the research group, including former FICAM members. Thank you for your help in the lab, with GLP, and especially for the invigorating coffee breaks. The team spirit in FICAM was excellent and I'm glad I got to be part of the group. I will remember my time in FICAM warmly.

Lastly, I want to thank my husband Mike for the enormous amount of support and encouragement that you have given me during this PhD journey. You are my rock. And my wind.

Tampere, August 2023

Maria

ABSTRACT

Adverse cardiac effects are a major reason for drug attrition during drug development and for post-approval market withdrawals. Therefore, drug development would greatly benefit from tests that better predict human cardiac function. Due to intrinsic species-to-species differences in the functionality of the heart, nonclinical animal testing does not fully represent the effects of the drugs on human. Thus, there is a need for reliable, human cell -based standardised *in vitro* models for cardiotoxicity and drug efficacy testing.

The aim of this thesis was to develop a functional human cell -based cardiac tissue model that mimics the adult human heart and to develop a contraction force measurement system for measuring the cardiac contractility of the cardiac tissue model. The cardiac tissue model that was optimised in this thesis consisted of human induced pluripotent stem cell (hiPSC)-derived cardiomyocytes that are cocultured with preformed human adipose stromal cells (hASC) and human umbilical vein endothelial cells (HUVEC) vascular-like networks. The model was characterized structurally, in gene expression levels, and functionally. For measuring the cardiac contraction force, piezoelectric cantilever sensors with single axis and dual axis sensor designs were developed. The cell culture method was adjusted according to the sensor designs. The functionality of the cardiac tissue model and contraction force measurement technology were confirmed by known inotropic drug exposures.

The results show that the coculture with the vascular-like networks improved the cardiomyocyte maturity and the tissue like structure of the model. The cardiomyocytes in the model showed improved organization and morphology, well-developed sarcomeres, and cell-cell connections. The gene expression of the cardiac tissue model also showed characteristics of the adult human heart. The functional characterization with known reference compounds showed that the model had good predictivity with high correlation to human data. The developed piezoelectric contraction force sensors were suitable for measuring the contraction force of cardiac tissue constructs. Both positive and negative inotropic effects including different mechanisms were measurable in the model with the system.

In conclusion, the developed cardiac tissue model mimics the myocardium structure and functionality. The model is suitable for testing cardiotoxicity and efficacy of acute drug-induced effects on human heart. Moreover, the functionality of the cardiac tissue model with the developed contraction force measurement system was shown on a proof-of-concept level.

TIIVISTELMÄ

Sydämeen kohdistuvat lääkkeiden haittavaikutukset ovat yksi suurimpia syitä lääkeainekandidaattien hylkäämiselle sekä jo markkinoille vietyjen lääkkeiden poisvedoille. Nykyiset menetelmät lääkkeiden turvallisuuden ja tehokkuuden testaamiseen eivät ennusta lääkkeiden vaikutuksia ihmiselle riittävän tarkasti. Koska sydänten toiminnassa on lajikohtaisia eroja, eläinkokeissa ei välttämättä tunnisteta kaikkia ihmisen sydämelle haitallisia aineita. Tätä varten tarvitaan toiminnaltaan mahdollisimman hyvin ihmisen sydänkudosta vastaavia ihmissolupohjaisia sydänkudosmalleja.

Tämän väitöskirjan tavoitteena oli kehittää toiminnallinen sydänkudosmalli, joka mallintaa aikuisen ihmisen sydäntä, sekä yhdistää tähän malliin sykintävoiman mittaus. Tässä työssä kehitetty sydänkudosmalli koostuu ihmisen rasvan kantasoluista (hASC) ja ihmisen napanuoran laskimon endoteelisoluista (HUVEC) muodostuvasta verisuoniverkostosta, jonka päälle kasvatetaan ihmisen indusoiduista kantasoluista (hiPSC) erilaistetut sydänlihassolut. Tämä sydänkudosmalli karakterisoitiin rakenteellisesti, geenien ilmentymisen tasolla ja toiminnallisesti. Sydänkudosmallien sykintävoimanmittaukseen kehitettiin yksi- ja kaksisuuntaisia pietsosähköisiä sensoreita.

Tulosten perusteella yhteisviljelmä verisuonipohjan kanssa parantaa sydänlihassolujen kypsymistä edistämällä niiden järjestäytymistä ja morfologiaa, sarkomeerirakennetta ja solu-solu-liitoksia. Myös sydänlihassolujen geenien ilmentymisessä oli vastaavuuksia aikuisen sydämeen. Toiminnallinen karakterisointi tunnetuilla sydämeen vaikuttavilla lääkeaineilla osoitti mallin tunnistavan tarkasti aineiden vaikutuksia. Kehitetyt pietsosähköiset voima-anturit soveltuivat sydänmallien sykintävoiman mittaamiseen. Antureiden todettiin pystyvän mittaamaan sekä voimaa eri mekanismein lisäävien että sitä vähentävien aineiden vaikutuksia.

Yhteenvetona voidaan todeta, että työssä kehitetty sydänkudosmalli jäljittelee sydänlihaskudoksen rakennetta ja toimintaa. Malli sopii testaamaan ihmisen

sydämeen kohdistuvia akuutteja lääkeaineiden haittavaikutuksia ja sydänlääkkeiden tehoa. Kehitettyyn sydänkudosmalliin liitetyllä pietsosähköisellä voima-anturilla on potentiaalia voimaankohdistuvien lääkeainevaikutusten testaamiseen.

CONTENTS

Preface iii

Abstract v

Tiivistelmä vii

Abbreviations xi

List of original publications xiii

Author's contribution xiv

1 Introduction 15

2 Theoretical background 18

2.1 Cardiac tissue 18

2.1.1 Structure and function of heart 18

2.1.2 Cardiomyocytes 21

2.1.3 Non-myocytes in heart 24

2.1.4 Cardiac extracellular matrix 25

2.2 Cardiac *in vitro* models 26

2.2.1 Requirements for a model 27

2.2.2 Cardiomyocyte sources 29

2.2.3 Coculture models 32

2.2.4 Cell culture techniques 37

2.3 Functional measurements 39

2.3.1 Electrophysiology and ion fluctuations 39

2.3.2 Contraction movement 41

2.3.3 Contraction force 42

2.4 Inotropic drugs and their mechanisms 48

3 Aims of the study 50

4 Materials and Methods 51

4.1 Ethical considerations 51

4.2 Cardiac tissue model 51

4.2.1 Cells 51
4.2.2 Fibrin 52
4.2.3 Vascular networks 52
4.2.4 Adding the cardiomyocytes 54
4.2.5 Cell culture platforms 55
4.3 Characterization of cardiac tissue model 56
4.3.1 Immunofluorescence 56
4.3.2 Transmission electron microscopy 57
4.3.3 Gene expression 58
4.3.4 Electrophysiology 59
4.4 Contraction force measurement setup 60
4.4.1 Force measurement sensors and data acquisition 60
4.4.2 Environmental control during force measurements 62
4.4.3 Inotropic drug exposures 63
4.5 Force measurement data analysis 63
4.6 Statistical analyses 64

5 Summary of the Results 66
5.1 Cardiac tissue model 66
5.1.1 Structural characterization 68
5.1.2 Gene expression 70
5.1.3 Functional characterization with known drugs with different mechanisms 71
5.2 Contraction force measurements 74
5.2.1 Functional characterisation with known inotropes 76

6 Discussion 78
6.1 Development of the cardiac tissue model 79
6.2 Comparison of cardiac tissue models 85
6.3 Contraction force measurements 88
6.4 Future directions 93

7 Conclusions 96

References 98

Original publications 121

ABBREVIATIONS

AFM	Atomic force microscope
Amp	Amplitude
AP	Action potential
AV	Atrioventricular
bFGF	Basic fibroblast growth factor
BH p-value	Benjamini-Hochberg adjusted p-value
BPM	beats per minute
cAMP	3',5'-cyclic adenosine monophosphate
cDNA	Complementary DNA, synthetic DNA from RNA
CiPA	Comprehensive *in vitro* proarrhythmia assay
cTnT	Cardiac troponin T
DEG	Differentially expressed gene
DMSO	Dimethyl sulfoxide
DNA	Deoxyribonucleic acid
EC_{50}	Half maximal effective concentration
ECG	Electrocardiogram
ECM	Extracellular matrix
EHT	Engineered heart tissue
ESC	Embryonic stem cell
FGF-β	Basic fibroblast growth factor
fps	frames per second
FPD	Field potential duration
GTEx	Genotype-Tissue Expression
hAMSC	Human amniotic mesenchymal stem cells
hASC	Human adipose stromal cell
hESC	Human embryonic stem cell
HERG	Human ether-à-go-go, voltage-gated K^+ channel Kv11.1
hiPSC	Human induced pluripotent stem cell
hiPSC-CM	hiPSC-derived cardiomyocyte
hPSC	Human pluripotent stem cell

HUVEC	Human umbilical vein endothelial cell
IC_{50}	Half maximal inhibitory concentration
ICH	International Council for Harmonisation
MEA	Microelectrode array
mRNA	Messenger ribonucleic acid
MMP	Matrix metalloproteinase
MYH7	β-myosin heavy chain coding gene
MYL2	Myosin light chain-2
MYL7	Myosin light chain-7
NCX	Sodium-calcium exchanger
OoC	Organ-on-a-chip
PBS	Phosphate-buffered saline
PCA	Principal component analysis
PDE	Phosphodiesterase
PDGF-β	Platelet-derived growth factor-β
PDMS	Polydimethylsiloxane
PSC	Pluripotent stem cell
RNA	Ribonucleic acid
SA	Sinoatrial
SERCA	Sarcoplasmic reticulum Ca^{2+}-ATPase
SFSM	Serum free stimulation medium
SNR	Signal-to-noise ratio
SR	Sarcoplasmic reticulum
TdP	Torsades de Pointes
TEM	Transmission electron microscopy
TnC	Troponin C
TnI	Troponin I
TNNT2	Troponin T coding gene
TnT	Troponin T
T-tubule	Transverse tubule
VEGF	Vascular endothelial growth factor
vWf	von Willebrand factor

LIST OF ORIGINAL PUBLICATIONS

The present thesis is based on the following publications which are referred to in the text by their Roman numerals (**study I-IV**)

I **Koivisto M**, Tolvanen TA, Toimela T, Miinalainen I, Kiviaho A, Kesseli J, Nykter M, Eklund L and Heinonen T. Functional human cell-based vascularised cardiac tissue model for biomedical research and testing. Scientific Reports 12(1):13459 (2022)

II Virtanen J, **Toivanen M**, Toimela T, Heinonen T and Tuukkanen S. Direct measurement of contraction force in human cardiac tissue model using piezoelectric cantilever sensor technique. Current Applied Physics 20(1):155-160 (2020)

III Virtanen J*, **Koivisto M***, Toimela T, Vehkaoja A, Heinonen T and Tuukkanen S. Direct measurement of contraction force in cardiac tissue construct in 2D- plane using dual axis cantilever sensor. IEEE Sensors Journal 21(3):2702–2711 (2021)

IV **Koivisto M**, Mosallaei M, Toimela T, Tuukkanen S, Heinonen T. Direct Contraction Force Measurements of Engineered Cardiac Tissue Constructs with Inotropic Drug Exposure. Frontiers in Pharmacology 13:871569 (2022)

* Authors contributed equally

The original publications are reproduced with the permission of the copyright holders. The publication **II** and publication **III** (as an unpublished manuscript) have been used as a part of PhD Thesis of Juhani Virtanen. This dissertation contains unpublished data that is indicated separately in the text.

AUTHOR'S CONTRIBUTION

Study I: The author participated in planning the experiments together with Tuomas Tolvanen, Tarja Toimela and Tuula Heinonen. The author was responsible for performing the experiments (excluding the TEM imaging) and analysing the immunofluorescence images and writing the manuscript together with Tuomas Tolvanen.

Study II: The author was responsible for culturing the cardiac tissue samples. The author was responsible for performing the contraction force measurements with Juhani Virtanen and Tarja Toimela. The author was responsible for writing parts of the manuscript concerning the culturing and measuring the cardiac tissue constructs.

Study III: The author was responsible for culturing the cardiac tissue samples. The author was responsible for performing the contraction force measurements with Juhani Virtanen and Tarja Toimela. The author was responsible for writing parts of the manuscript concerning the culturing, analysing, and measuring the cardiac tissue constructs.

Study IV: The author was responsible for planning the experiments and culturing the cardiac tissue constructs. The author was responsible for performing most parts of the contraction force measurements including drug exposures. The author was responsible for analysing the force measurements data and writing most parts of the manuscript.

1 INTRODUCTION

Cardiovascular diseases are the leading cause of death worldwide (WHO 2021). Therefore, there is a need for new and better cardiac drugs to treat heart function related diseases. In addition to drugs to cure or prevent heart related diseases, better models and tests are needed to predict heart related adverse effects of all drugs and chemicals. The drug development process begins with discovery and development phase which is followed by nonclinical and clinical research phases. After getting approved to enter the market, the post-market safety monitoring phase of the drug is continued (FDA 2020).

Pharmaceutical industry suffers from high attrition rates in drug development (Bowes et al. 2012). Reasons for attrition of drug candidates in clinical trials mainly include lack of efficacy and unacceptable safety (Arrowsmith and Miller 2013; Laverty et al. 2011). Together with hepatotoxicity, cardiotoxicity is the main reason for drug attrition because of unacceptable safety. Adverse cardiac effects are also a leading cause for drug withdrawal at post-approval stage when the drug has passed the clinical trials and entered the market (MacDonald and Robertson 2009; Lasser et al. 2002). As a matter of fact, one third of withdrawals were due to cardiac or cardiovascular safety liabilities during 1998–2008 (MacDonald and Robertson 2009). Detected cardiac adverse drug reactions include arrythmias due to alterations in ion channel function or structure, and cardiac myopathy due to direct cytotoxicity to cardiomyocytes (MacDonald and Robertson 2009). For example, disturbances in ventricular repolarization and QT interval prolongation which predisposes to ventricular Torsades de Pointes (TdP) arrhythmia, may have fatal consequences (Magdy et al. 2018).

The degree of drug attrition and withdrawal due to drug-induced cardiotoxicity shows the inadequacy of nonclinical safety testing. The nonclinical drug safety studies include *in vivo* and *in vitro* testing which are described by the International Council for Harmonisation of Technical Requirements for Pharmaceuticals for Human Use (ICH) guideline *"ICH S7B Non-clinical evaluation of the potential for delayed*

ventricular repolarization (QT interval prolongation) by human pharmaceuticals - Scientific guideline" (EMEA 2006). The animal models do not always accurately predict the effects in human due to intrinsic inter-species differences in cardiac electrophysiology (Mathur et al. 2016). Animal testing is also time-consuming, costly, has low throughput, and requires large compound quantities (Li et al. 2016). The nonclinical *in vitro* testing includes the human ether-à-go-go (hERG) assay to test the effect of a drug on the voltage-gated potassium channel Kv11.1 (Magdy et al. 2018). The blockage of the channel delays the cardiac action potential repolarization which may have fatal consequences (Li et al. 2016). However, the drug-induced effects may target other ion channels and structures in the myocardium with adverse effects (Magdy et al. 2018) which cannot be detected using the current *in vitro* models.

There is a need for human cell -based *in vitro* models that can reliably predict the drug-induced effects in human for safety testing of drugs and other chemicals and for efficacy testing of cardiac drugs (Heinonen 2015). *In vitro* models could reduce the time and cost of drug testing by reducing or replacing animal testing while providing more reliable results with their human cell -based functionality and being ethically preferable. Moreover, *in vitro* cardiac models are needed for biomedical research and testing. Human induced pluripotent stem cells (hiPSC) provide a valuable cell source for these models with their ability to self-renewal and to differentiate to any cell type of the human body including cardiomyocytes. In addition to cardiac tissue models mimicking the normal human myocardium, disease models can be created for testing different treatments (Vunjak-Novakovic et al. 2014). The use of hiPSC also enables the use of patient-specific cardiomyocytes in these disease models (Smith et al. 2017).

The contractility of cardiomyocytes is the key function for the heart as it produces the force for maintain the blood circulation. Patients with impaired cardiac contractility benefit from safe and efficient drugs that increase the cardiomyocyte contractility to support the heart function. However, unwanted increase of cardiomyocyte contractility may cause myocardial hypertrophy, impaired myocardial energetics, and arrythmias. The decrease of contractility is equally harmful with drop of systemic arterial blood pressure, increased heart rate, syncope, and inadequate blood flow to vital organs (Guth et al. 2019). Thus, the drug safety and efficacy testing would benefit from methods to evaluate the drug-induced effects directly on cardiac contractility.

This PhD thesis consists of two main parts: 1) finalising the development of an *in vitro* human cell -based cardiac tissue model and 2) the development of a contraction force measurement system to be used with the above-mentioned model. The cardiac tissue model that has been further developed in this PhD work was based on the work of Vuorenpää et al. in FICAM (Vuorenpää et al. 2014; 2017). In this work, the previously developed model was further optimised, characterised and its functionality was confirmed. Moreover, the cardiac tissue model was slightly modified for the purpose of the contraction force measurements. The modifications were made gradually adapting the model to the requirements set by the force measurement system at its different developmental stages including different sensor designs.

2 THEORETICAL BACKGROUND

2.1 Cardiac tissue

2.1.1 Structure and function of heart

The heart maintains the blood circulation throughout the body by pumping. The organ consists of four chambers, left and right atria and ventricles. The chambers are separated from each other by valves (tricuspid, bicuspid, pulmonary, and aortic) and septa. The valves ensure unidirectional blood flow from atria to ventricles, from the right ventricle to the lungs and from the left ventricle to the body (Weinhaus and Roberts 2009).

The heart wall around the chambers consists of endocardium, myocardium, and epicardium (Figure 1). Endocardium consists of a single endothelial cell layer that forms the lining of the heart chambers and of subendothelial connective tissue (Arackal and Alsayouri 2022). The middle myocardium is the thickest layer of the heart wall. It is the contractile layer containing cardiac muscle cells i.e., cardiomyocytes. The cardiomyocytes are organized in laminar sheets in which they orient in certain direction in each layer (Sands et al. 2008; Tsukamoto et al. 2020). The myocardium is dense with capillaries for blood supply (Vunjak-Novakovic et al. 2010), and innervated to regulate the cardiomyocyte function (Fitzgerald et al. 2009). Epicardium is the outer layer of the heart wall, and it is part of the pericardium that forms a double layer fluid-filled covering that surrounds the heart body (Weinhaus and Roberts 2009).

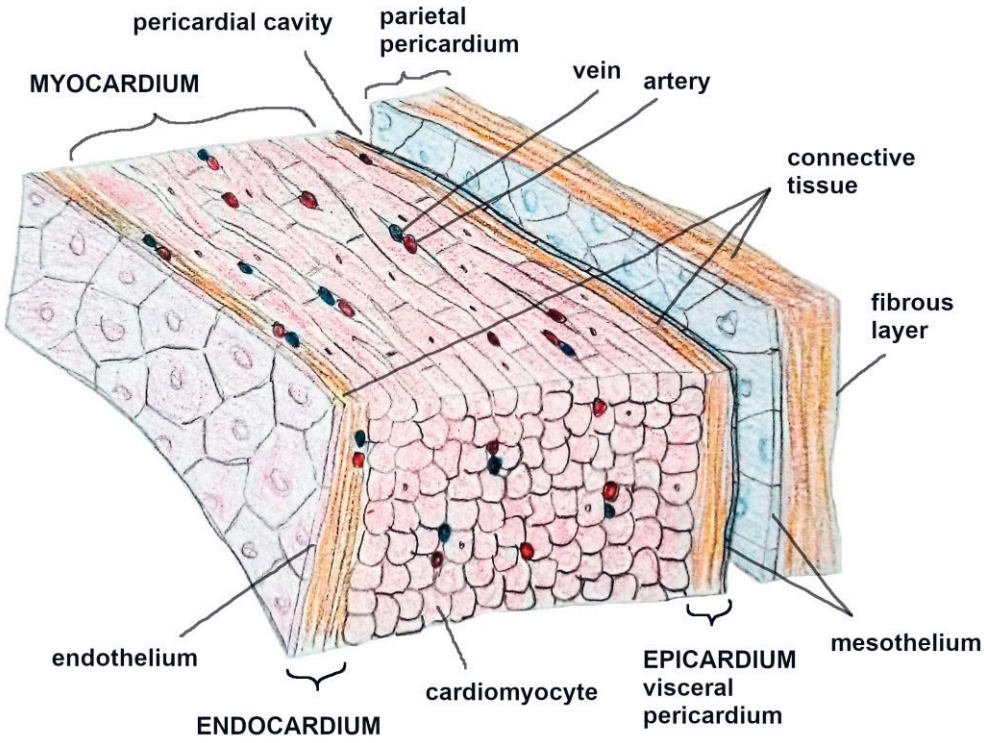

Figure 1. Structure of myocardium as part of the heart wall between endo- and epicardium.

A cardiac contraction that enables the pumping function of the organ is initiated in a sinoatrial (SA) node in right atrium where pacemaker cells spontaneously generate series of electrical impulses. The beat rate is normally under physiological conditions 60–100 beats per minute (BPM) (Laske et al. 2009). Autonomous nervous system together with hormonal inputs regulate the heart rate. Norepinephrine from sympathetic nervous system increases heart rate and contractility while acetylcholine from the parasympathetic nervous system decreases heart rate (Gordan et al. 2015).

The electrical impulses from the SA node cause the depolarization of the atrial myocardium and the atrioventricular (AV) node from which the impulses are further spread through the bundle of His and rapid conduction cells called Purkinje fibres to the ventricular tissues. The conduction system of the heart ensures the correct timing of the atrial and ventricular contractions by rapid and highly coordinated spreading of the electrical impulses (Laske et al. 2009).

The spreading of the electrical impulses in the heart can be detected using an electrocardiogram (ECG) recording (Figure 2). The ECG measures the cumulative electrical field potentials from depolarization and repolarization of the cells in atria and ventricles. The P-wave of the ECG results from depolarization of atria, QRS complex results from the depolarization of the ventricles, and T-wave results from repolarization of the ventricles. Repolarization of atria is normally not detected in ECG because it coincides with the depolarization of the ventricles and is masked under the QRS complex (Dupre et al. 2009).

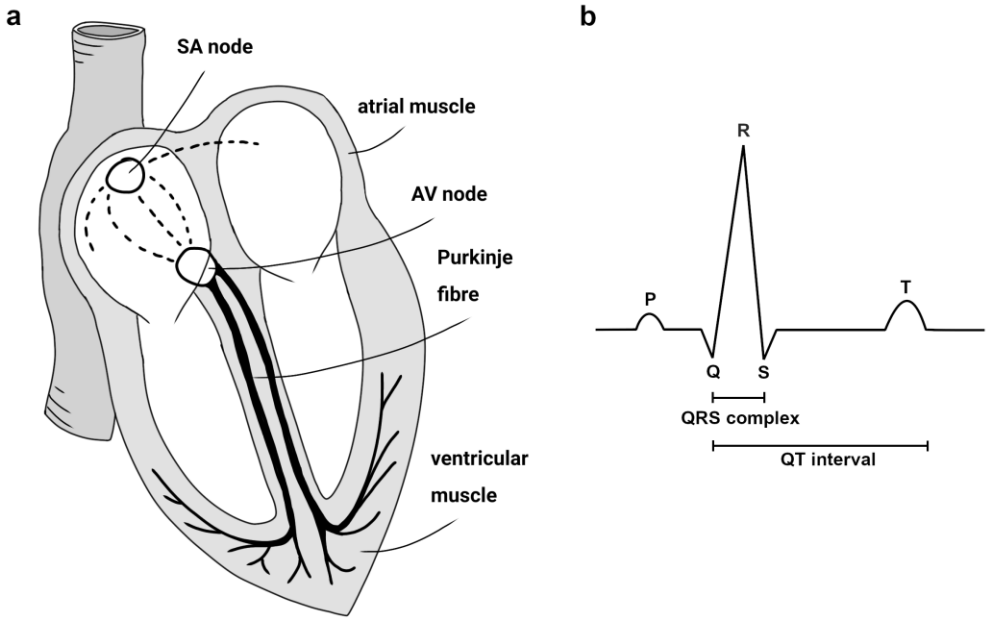

Figure 2. The electrical function of the heart. a) The conduction of electrical impulse in the heart. The action potential is initiated in the SA node, it spreads through the atria, to the AV node and Purkinje fibres, to the ventricular muscle. b) ECG wave represents the atrial depolarization (P-wave), ventricular depolarization (QRS complex), and ventricular repolarization (T-wave).

The ECG recording is an important method to monitor the heart functionality in a clinical setting. Clinically important ECG parameters include the PR interval, the QRS interval, the ST segment, and the QT interval, which reveal the timing of electrical impulse spreading in different parts of the heart. Longer than normal PR and QRS intervals may indicate conduction blocks in the heart while the prolongation of QT interval indicates an increased risk of ventricular tachyarrhythmia (Dupre et al. 2009).

2.1.2 Cardiomyocytes

Cardiomyocytes are the main functional cell type in heart capable of contraction function and thus, pumping of blood. Different types of cardiomyocytes include pacemaker cells, and force-producing atrial and ventricular cardiomyocytes (Talman and Kivelä 2018).

2.1.2.1 Cardiomyocyte structure

Cardiomyocytes are 10–20 μm in diameter and 50–100 μm long cylindrical cells with short branches (Barnett 2009). They are interconnected with each other mechanically via intercalated disks and desmosomes and electrically via gap junctions. The intercalated discs enable force transmission in the tissue. Open gap junctions allow direct passing of electrical signals between neighbouring cardiomyocytes facilitating simultaneous contraction of the cardiac tissue (Barnett 2009). Both mechanical and electrical coupling of cardiomyocytes are critical for the proper function of the tissue.

Majority of the internal volume of cardiomyocytes is devoted to highly organized contractile proteins giving the cells their striated appearance. The contractile subunits, called myofibrils, are oriented along the long axis of the cell. In the myofibrils, the contractile proteins are arranged into small contractile units which are called sarcomeres (Figure 3). At the ends of a sarcomere, there are transverse boundaries formed by α-actinin and actin known as Z-disks. Thin filaments are anchored to each Z-disc. These actin filaments are 1 μm long. Thick filaments are located at the centre of a sarcomere. These myosin filaments are 1.6 μm long, and the region is known as the A-band. The region between the A-bands is called the I-band. The myosin filaments are connected to each other by protein matrix called the M-line (Barnett 2009). The contraction occurs along the longitudinal axis along the sarcomeres. Well-organized sarcomeres are essential for proper contractile function of a cardiomyocyte.

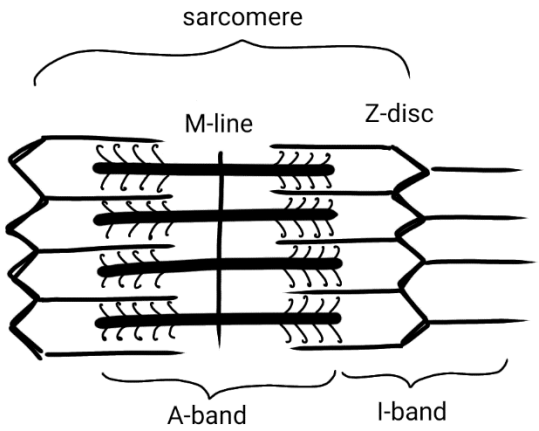

Figure 3. A sarcomere consists of thin filaments, actin, and thick filaments, myosin, arranged between z-discs.

2.1.2.2 Cardiac action potential

Cardiac action potential (AP) has five phases. However, the AP waveform varies among cardiomyocytes in different locations of the heart (Figure 4). The AP waveform varies also with heart rate, developmental stage, and in response to neurohormones and drugs (Santana et al. 2010). The exact composition and function of cardiac ion channels determines the AP waveform (Kussauer et al. 2019).

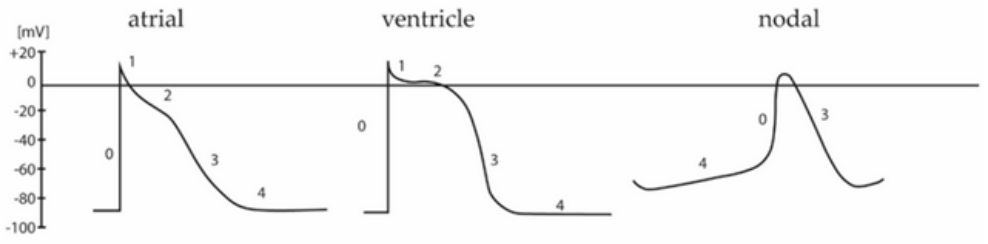

Figure 4. Atrial, ventricular, and nodal action potentials. Atrial and ventricular APs consist of five phases while the nodal AP has three phases, a resting phase (4), a depolarization phase (0) and a repolarization phase (3). The plateau phase (2) is more prominent on ventricular cells than in atrial cells (Kussauer et al. 2019).

At phase 4, cardiomyocytes have a resting membrane potential of -90 mV (Grant 2009). It is the result of difference in concentrations of charged ions across the membrane, mainly K^+ ions at the resting stage (Laske et al. 2009). Phase 0 begins

when the membrane potential becomes depolarised reaching a threshold at -60 to -70 mV. At the threshold potential, voltage-gated Na^+ channels open and an inward Na^+ current (INa) leads to rapid depolarization (Grant 2009; Laske et al. 2009). The rapid depolarization is followed by rapid repolarization at phase 1 caused by transient outward K^+ current (Ito) though voltage-gated K^+ channels. The membrane potential plateaus at phase 2 as the influx of Ca^{2+} ions (current ICa) through the L-type calcium channels is electrically balanced by K^+ efflux through rapid and slow delayed rectifier K^+ channels (currents IKr and IKs, respectively) (Laske et al. 2009). At phase 3, the Ca^{2+} channels begin to close and K^+ efflux increases causing rapid repolarization that restores the membrane potential to the resting stage (Grant 2009; Laske et al. 2009).

2.1.2.3 Excitation-contraction coupling

The cardiac AP initiates an excitation-contraction coupling mechanism. The influx of Ca^{2+} through the L-type Ca^{2+} channels during the plateau causes the release of Ca^{2+} from sarcoplasmic reticulum (SR) by calcium-induced calcium release. The depolarization of the membrane also causes ryanodine receptors in transverse tubules (T-tubules), cell membrane-lined channels filled with extracellular fluid, to trigger the release of calcium from SR (Barnett 2009).

The increased intracellular calcium binds to troponin C (TnC), inducing the sliding of actin and myosin filaments and shortening of the cell. The interaction between the actin and myosin filaments is regulated by troponin and tropomyosin which are attached to actin filaments. Troponin has three subunits: a calcium-binding subunit TnC, inhibitory subunit troponin I (TnI), and subunit connecting the troponin complex to tropomyosin and actin troponin T (TnT) (Barnett 2009). The generated contraction force depends on the amount of Ca^{2+} bound to troponin (Eisner et al. 2017). Relaxation occurs when intracellular Ca^{2+} is transported back to SR by the sarcoplasmic reticulum Ca^{2+}-ATPase (SERCA) and eliminated outside the cell by the sodium–calcium exchanger (NCX) and sarcolemmal Ca^{2+}-ATPase (Bers 2008) or retrieved by mitochondrial Ca^{2+} uniport (Bers 2002).

2.1.3 Non-myocytes in heart

The most abundant cell types in heart are cardiomyocytes, endothelial cells, fibroblasts, perivascular cells (Zhou and Pu 2016), neural cells and immune cells (Zamani et al. 2018). However, the exact proportions of the different cell types have been difficult to determine because of technical limitations and lack of cell type specific markers (Talman and Kivelä 2018). The reported cell compositions differ based on the cell type characterization and quantification methods (Munawar and Turnbull 2021). Recent single cell- and single nucleus RNA sequencing techniques provide new tools to identify cell types based on their transcriptional signatures (Koenig et al. 2022).

Even though the contractile cardiomyocytes are responsible for the main function of the heart, majority of the cells in the heart are non-myocytes (Gray et al. 2018). Cardiomyocytes constitute the majority of the volume in mammalian heart (Tucker et al. 2020; Zhou and Pu 2016). However, they account for only 17.5% to 50% of the cells in the human heart (Koenig et al. 2022; Litviňuková et al. 2020; Tucker et al. 2020).

The different cell types in the heart participate in multicellular crosstalk through cell-cell interactions, paracrine signalling, and extracellular matrix mediated signalling. Together they regulate cellular organization, differentiation, viability, and function (Zamani et al. 2018).

2.1.3.1 Endothelial cells

Endothelial cells constitute 8–17% of the cells in human heart (Koenig et al. 2022; Litviňuková et al. 2020). They form blood vessels, lymphatic vessels (Gray et al. 2018), and endocardium (Tucker et al. 2020). In the myocardium, each cardiomyocyte is located near a capillary to ensure adequate supply of oxygen and nutrients (Hsieh et al. 2006; Zamani et al. 2018). Endothelial cells have important role in mediating cardiomyocyte spatial organization, contraction, survival, and function (Zamani et al. 2018). The cell types communicate through paracrine signalling. Moreover, physical endothelial cell-cardiomyocyte contacts and extracellular vesicles may play a role in their communication. The endothelial cell-cardiomyocyte communication is not yet fully understood (Talman and Kivelä 2018).

2.1.3.2 Fibroblasts

Fibroblasts form 16–32% of the cells in human heart (Koenig et al. 2022; Litviňuková et al. 2020; Tucker et al. 2020). Fibroblasts maintain the myocardial structure by producing extracellular matrix components such as fibronectin, laminin, collagen I and collagen III (Tirziu et al. 2010). They also mediate the cardiomyocyte function by cell-cell interactions and paracrine factors e.g., platelet-derived growth factor-β (PDGF-β) and basic fibroblast growth factor (bFGF). Moreover, fibroblasts participate in transmitting the electrical signalling between cardiomyocytes through gap junctions. Each cardiomyocyte is located next to at least one fibroblast (Zamani et al. 2018). Fibroblasts can also differentiate into myofibroblasts that have increased proliferative and matrix production properties (Tirziu et al. 2010). The fibroblast phenotype is determined by signalling from other neighbouring cells (Gray et al. 2018).

2.1.3.3 Perivascular cells/mural cells

Perivascular cells or mural cells include pericytes and smooth muscle cells. They form 17–21% of the cell in the human heart (Litviňuková et al. 2020). According to Koenig et al. (2022), pericytes form 11% and smooth muscle cells 2% of the cells in the human heart. They are located around vasculature, smooth muscle cells around larger vessels and pericytes around capillaries (Sweeney and Foldes 2018). They regulate the blood flow in the vessels (Talman and Kivelä 2018). Pericytes are also involved in regulation of angiogenesis. Endothelial cell-pericyte contacts maintain the mature vasculature stable, while detachment of pericytes enables angiogenesis (Gray et al. 2018).

2.1.4 Cardiac extracellular matrix

The extracellular matrix (ECM) in myocardium is highly ordered anisotropic structure (Vunjak-Novakovic et al. 2014). The main load-bearing ECM component is collagen, but the myocardial ECM also contains fibronectin, laminin, vitronectin, elastin, hyaluronan, fibrillin, proteoglycans, glycoproteins, periostin (Vunjak-Novakovic et al. 2014; Howard and Baudino 2014). Collagen provides elasticity and integrity of the tissue. Hyaluronan provides a hydrated environment for cellular motility and proliferation. Fibronectin and periostin are key ECM proteins that

interact with other ECM components. Glycoproteins and proteoglycans have roles in signalling, ECM turnover, and binding growth factors and cytokines waiting for release. The exact role of each individual ECM component is complex and has been difficult to precisely characterize (Howard and Baudino 2014).

In addition to the above-mentioned cell-cell communication between the different cell types in heart, the cell-ECM interactions are also important for homeostasis and remodelling of the myocardium. Degradation of ECM can release latent growth factors and cytokines via cleavage by matrix metalloproteinases (MMPs). The myocardial ECM provides attachment points for the cells and supports the densely packed cardiomyocytes and non-myocytes by transducing contraction forces and providing stiffness to the tissue (Vunjak-Novakovic et al. 2014). ECM mediates mechanical signals such as stretch and pressure to the cells. The cell-ECM interactions are essential for maintaining the structural integrity of the heart (Howard and Baudino 2014).

2.2 Cardiac *in vitro* models

Cardiac tissue engineering aims to create cardiac constructs with the structure and functionality of the native myocardium (Vunjak-Novakovic et al. 2010; Mathur et al. 2016). Cardiac *in vitro* models are created for studying heart function in physiological studies, drug screening, and safety pharmacology purposes (Vunjak-Novakovic et al. 2014). In addition to cardiac models mimicking the healthy human heart, disease models including patient-specific models can be created for testing the efficacy of different treatments (Vunjak-Novakovic et al. 2014).

These cardiac tissue models do not aim to mimic the whole organ but rather focus on the functional cardiac muscle tissue, the myocardium. They do not recapitulate the structure of the heart with the atria and ventricles, septa, and valves (Weinhaus and Roberts 2009). Their electrophysiology differs from the electrophysiology of the heart as they do not have SA and AV nodes, or Purkinje fibres for the generation and conduction of the action potential (Laske et al. 2009). Instead, the action potential in the *in vitro* models is typically generated by the spontaneously beating cardiomyocytes instead of the SA node. The action potentials are spread in the tissue model by electrical coupling among the neighbouring cells as it is also in the myocardium. The *in vitro* models are typically not innervated and lack the sympathetic

and parasympathetic stimulation from the autonomous nervous system as well as hormonal stimulation (Gordan et al. 2015). The lack of the nervous system input in these models may affect the obtained responses to drugs whose mechanism targets these functions.

Table 1 presents the summary of different types of models for drug efficacy and safety testing. The details of these models will be elaborated in the following sections.

Table 1. Strengths and weaknesses of different types of models for drug efficacy and safety testing.

Model	Strengths	Weakness
In vivo models (Animal models)	whole heart drug metabolism ICH S7B required	animal vs. human electrophysiology low throughput, expensive ethical issues
Cell lines (Expressing the potassium ion channel Kv11.1)	ICH S7B required	lacks other relevant ion channels lacks other relevant cardiomyocyte structures relatively high false positive rate
Cardiomyocyte monoculture (hiPSC-CM)	relevant ion channels human electrophysiology possibility for patient-specific model	not adult level CM maturity no cell-cell communication with other cell types
Coculture models (hiPSC-CM + one or more cell types)	relevant ion channels human electrophysiology cell-cell communication with relevant cell types improved CM maturity tissue resemblance possibility for patient-specific model	not quite adult level CM maturity more complex than monocultures

CM = cardiomyocyte; hiPSC-CM = human induced pluripotent cell -derived cardiomyocyte

2.2.1 Requirements for a model

A model is a simplified representation of the real biological system. The cardiac *in vitro* models cannot recapitulate the whole complexity of the human heart, but they should replicate the most relevant tissue-specific structures and critical physiological functions of the heart (Vunjak-Novakovic et al. 2014). The key aspects of the model depend on the intended use of the model.

For testing drug-induced cardiac effects in human, the *in vitro* model should reliably mimic the normal functionality of the human heart and contain critical structural

elements that can be vulnerable to drug-induced adverse effects. To achieve proper functionality in the model, certain underlaying structures are needed to produce the required functionality. These structures enable normal cardiac tissue function, in cellular and tissue level.

A critical part of a functional cardiac tissue model are proper electrophysiological properties of the cardiomyocytes. Because the cardiac action potential is composed of the cardiac ion currents (Kussauer et al. 2019), correct composition of the cardiac ion channels is needed to establish matching electrophysiological properties between the model and the target organ. All ion channels that can be vulnerable to drug-induced effects should be present in the model.

Apart from single cell measurement methods, the cardiomyocytes should have proper electrical coupling among them, similar to the native myocardium. Methods that measure more than one cardiomyocyte at a time may require synchronization of the cells to be able to effectively measure their activity. Synchronism of cardiomyocytes is achieved by electrical coupling i.e., gap junctions between the cardiomyocytes (Barnett 2009).

For force measurement applications, it is critical that the cardiac tissue model can produce contraction force. To be able to do that the model needs, in addition to functional ion channels and electrophysiology, functional excitation contraction coupling and contraction machinery. The excitation-contracting coupling depends on the calcium dynamics (Barnett 2009). The cardiomyocytes need functional calcium-induced calcium release mechanism. T-tubules and SR for calcium release are needed for efficient excitation contraction coupling (Ronaldson-Bouchard et al. 2018). Moreover, the contraction machinery needs to consist of well-developed and well-organized sarcomeres. Preferably, the sarcomeres should be aligned both within a cell but also among neighbouring cells similar to the myocardium structure. The alignment of the cardiomyocytes enables the contraction of the tissue in a certain direction, which may be needed to produce measurable force depending on the measurement method (Barnett 2009). Efficient energy conversion with oxidative metabolism instead of glycolysis and high density of mitochondria are also needed (Ronaldson-Bouchard et al. 2018). Moreover, mechanical coupling of the individual cells enables transmission of the force in the engineered cardiac tissue. Mechanical junctions are formed by intercalated discs and desmosomes between cardiomyocytes (Barnett 2009).

Moreover, the optimal model would benefit from a native myocardium type of structure to act as a supporting platform for the cardiomyocytes, and to provide 3D structure and growth factors for the cells. Inclusion of other relevant cell types in the model enables the *in vivo* like cell-cell crosstalk that may be essential for developing the proper functionality. The cell-cell communication among the cardiomyocytes and other cell types in the heart such as fibroblasts and endothelial cells is essential for maintaining the tissue homeostasis in the myocardium (Zamani et al. 2018).

The International Council for Harmonisation (ICH) has given guidelines concerning the nonclinical and clinical cardiotoxicity screening of drugs. The guideline ICH S7B describes the nonclinical evaluation of the potential of a drug to delay ventricular repolarization. The evaluation consists of an *in vitro* assay to test the drug-induced effects on the delayed rectifier potassium current (IKr), and an *in vivo* assay to test drug-induced effects on QT interval in animal models.

The *in vitro* assay utilises cell lines that express voltage-gated potassium channel Kv11.1 (also known as hERG) e.g., recombinant HEK293 line which is an immortalized human embryonic kidney 293 cell line that has been modified to overexpress the HERG potassium channel (Zhou et al. 1998). This assay has sensitivity of 64% and specificity of 88% for QT prolongation (Gintant 2011), which leads to discarding many non-cardiotoxic drug candidates.

Even though the Kv11.1 is a critical channel that needs to be tested for drug-induced QT prolongation and potentially lethal cardiac arrythmia TdP, it is not the only ion channel that can affect the ventricular repolarization. Moreover, the QT interval prolongation alone is not an ideal marker for clinical arrhythmia risk (Magdy et al. 2018). The cardiac action potential is the sum of cardiac ion currents (Kussauer et al. 2019). Therefore, it is not enough to use cell lines expressing only one cardiac ion channel to enable more comprehensive testing if drug-induced effects. Instead, the *in vitro* models should include cardiomyocytes that express all relevant Na^+, K^+ and Ca^{2+} ion channels.

2.2.2 Cardiomyocyte sources

Cardiomyocyte sources for *in vitro* models include primary cardiomyocytes and pluripotent stem cell -derived cardiomyocytes.

2.2.2.1 Primary rodent cardiomyocytes

Primary cardiomyocytes from rodents i.e., rats and mice, have been extensively used in research. They can be obtained from adult or neonatal hearts. Primary adult cardiomyocytes are fully differentiated while the isolation and culture of primary neonatal cardiomyocytes is more straightforward. It is also possible to select primary cardiomyocytes from different parts of the heart such as atria and left ventricle. (Louch et al. 2011).

The freshly isolated primary cardiomyocytes are structurally and functionally more physiologically relevant than immortalized cell lines. However, they easily lose their phenotype and viability during *in vitro* culture (Louch et al. 2011). Thus, they are not well suited for long-term studies. In addition, even though several isolation protocols exist, the isolation of high quality, viable cardiomyocytes in high yield can be challenging (Li et al. 2014; Louch et al. 2011). These cells are not capable of self-renewal *in vitro* and the scale up for high throughput is challenging.

Primary rodent cardiomyocytes are a valuable model for research. However, the electrophysiological properties of human cardiomyocytes are significantly different from cardiomyocytes of other species (Vunjak-Novakovic et al. 2014; Takeda et al. 2018). Inter-species differences exist in ion channels, biological pathways, and pharmacokinetic properties. Therefore, the cardiac models should be preferably human cell -based to recapitulate human heart physiology (Mathur et al. 2016).

2.2.2.2 Primary human cardiomyocytes

Primary human cardiomyocytes fully represent the physiological cellular properties but they are not easily available (Ribeiro et al. 2019). Primary human cardiomyocytes have also the challenges related to isolation and long-term culture similar to the primary rodent cardiomyocytes. The cardiomyocyte quality depends on the isolation process which can be challenging and suffer from low efficiency (Zhou et al. 2022). The cells easily lose their phenotype and viability in culture, and they are not suitable for long-term cultures. The primary cardiomyocytes lack self-renewal capacity and the scale-up for high throughput is difficult.

2.2.2.3 Stem cell -derived cardiomyocytes

Cell sources for human cell -based cardiac *in vitro* models include human embryonic stem cells (hESC) from donated human blastocysts, human induced pluripotent stem cells (hiPSC) that are reprogrammed to pluripotent state from somatic cells, and cardiac progenitor cells from foetal or adult heart. Human pluripotent stem cells (hPSC) i.e., hESC and hiPSC, can differentiate to any cell type of human body including cardiomyocytes, while cardiac progenitor cells are multipotent stem cells with specified lineage to cardiomyocytes, cardiac fibroblasts, and endothelial cells (Vunjak-Novakovic et al. 2014).

Especially, the discovery of reprogramming somatic cells into pluripotent stem cells (Takahashi and Yamanaka 2006; Takahashi et al. 2007) and methods to differentiate them into functional cardiomyocytes have been invaluable for cardiac tissue engineering applications. The hiPSCs provide a cell source with self-renewal capacity and without the ethical controversies related to hESCs. Moreover, the hiPSC-derived cardiomyocytes (hiPSC-CM) enable the generation of patient-specific disease models recapitulating the disease phenotype for personalised medicine (Vunjak-Novakovic et al. 2014; Kussauer et al. 2019).

Various differentiation protocols have been developed for producing hiPSC-CMs. Earlier feeder layer differentiation on END2 mouse endoderm-like cells and embryoid bodies differentiation by creating 3D cell aggregates have been mainly replaced by a more controllable monolayer differentiation method. The initially low yield has also been improved up to 85–90%. Using metabolic enrichment method with sodium lactate the efficiency of producing hiPSC-CMs can be 95% (Mathur et al. 2016).

The utility of hiPSC-CMs for nonclinical drug screening purposes has been demonstrated by several studies (Millard et al. 2018; Blinova et al. 2017). The cells express several relevant ion channels and can be used for detecting concentration-dependent drug-induced effects (Blinova et al. 2017). The comprehensive *in vitro* proarrhythmia assay (CiPA) initiative proposes the use of hiPSC-CMs as a part of the regulatory assessment of drug-induced arrhythmia. The new paradigm includes the evaluation of drug-induced effects on multiple ion channels and not only on the hERG-channel blockade caused QT-prolongation (CiPA 2019; Colatsky et al. 2016).

A challenge related to the use of hiPSC-CMs has been reaching the maturity stage of an adult cardiomyocyte *in vitro*. The hiPSC-CMs resemble more embryonic or foetal than adult cardiomyocytes. There are differences in cell morphology and structure, electrophysiology, calcium handling, and metabolism (Li et al. 2020). They also show immature gene expression (Robertson et al. 2013; Jiang et al. 2018). Typically, hiPSC-CMs are circular, have unorganized myofibrils, show spontaneous electrical activity (Vunjak-Novakovic et al. 2014), immature action potential characteristics, and force of contraction (Munawar and Turnbull 2021). Moreover, their energy metabolism uses glycolysis instead of oxidative phosphorylation of fatty acids (Robertson et al. 2013; Jiang et al. 2018).

The cardiomyocyte maturity can be improved by extending the culture time, applying electrical stimulation, stretch or mechanical loading (Munawar and Turnbull 2021; Magdy et al. 2018). Moreover, the switching from glycolytic to oxidative metabolism has also been shown to improve the cardiomyocyte maturation (Mills et al. 2017; Feyen et al. 2020). The cardiomyocyte maturity can be improved also by creating more *in vivo* like culture conditions such as 3D culture environment and co-culture with other relevant cardiac cells such as fibroblasts and endothelial cells (Robertson et al. 2013; Karbassi et al. 2020).

2.2.3 Coculture models

The inclusion of cardiac nonmyocytes in a coculture model improves the model's resemblance to native myocardium. Compared to models containing only cardiomyocytes, the cell composition of the coculture models matches better to the native cardiac tissue cell composition (Munawar and Turnbull 2021; Zamani et al. 2018). This chapter presents the most common cell type combinations for cardiac coculture models, focusing on the effects of the cocultures on the cardiomyocytes.

2.2.3.1 Cardiomyocytes + fibroblasts

Engineered cardiac tissues including cardiomyocytes and fibroblasts have shown improved electrophysiological properties such as higher beating rate of hiPSC-CMs (Beauchamp et al. 2020), higher synchronicity of mouse ESC -derived cardiomyocytes (Iwamiya et al. 2016; Matsuura et al. 2011) and higher amplitude of contractions of neonatal rat cardiomyocytes (Radisic et al. 2008) compared to

cardiomyocyte only cultures. The improved contractility may be due to enhanced expression of connexin 43 which enables ion flow between adjacent cells (Saini et al. 2015).

The addition of fibroblasts has also been shown to enhance the structural maturation of cardiomyocytes by improving cardiomyocyte elongation and alignment (Beauchamp et al. 2020; Saini et al. 2015). These morphological changes may be induced by MMP-dependent mechanisms (Nichol et al. 2008). Moreover, adding fibroblasts to the cardiac culture has been reported to enhance the expression of cardiac maturation marker *TNNI3* even though the markers *ACTA2*, *MYOM1* and *MYOM2* were downregulated compared to cardiomyocyte only culture (Beauchamp et al. 2020).

Cardiomyocyte and fibroblast coculture models using hiPSC-CMs have been developed by Ronaldson-Bouchard et al. (2018; 2019) and Beauchamp et al. (2020). The cardiac model of Ronaldson-Bouchard et al. (2018; 2019) consisted of hiPSC-CMs and human dermal fibroblasts in 3:1 ratio encapsulated in a fibrin hydrogel that was attached between flexible pillars to introduce passive mechanical stretching. Electrical stimulation was also applied during the 4-week culture time to these 3D tissue structures. They measured the contraction forces in the model by imaging the change of tissue area (Ronaldson-Bouchard et al. 2018).

The cardiac spheroids of Beauchamp et al. (2020) consisted of commercial hiPSC-CMs (iCell^2 cardiomyocytes or Cor.4U cardiomyocytes) and primary human embryonic cardiac fibroblasts in 4:1 ratio. The culture time after spheroid formation was 30 days. They studied the spheroid beating activity using video imaging, and the electrophysiology by patch clamp (Beauchamp et al. 2020). Their model did not include measurement of the beating force.

The exact effects of adding fibroblasts vary depending on the cell source and age of the fibroblasts as well as the ratio of the two cell types (Munawar and Turnbull 2021). Instead of promoting the normal cardiac tissue phenotype, fibroblasts have also been included in cardiac cultures to create disease models for cardiac fibrosis (Sadeghi et al. 2017; Mastikhina et al. 2020).

2.2.3.2 Cardiomyocytes + endothelial cells

One goal of cardiomyocyte-endothelial cell coculture is to create vascularized cardiac tissue constructs (Munawar and Turnbull 2021; Zamani et al. 2018). Endothelial cells form capillary-like structures in culture. Cardiomyocyte coculture with the capillary-like networks has been shown beneficial for the structural organization, long-term survival of the cells, and cardiomyocyte contractility e.g., area of synchronous contraction and sustained contractile function (Garzoni et al. 2009; Narmoneva et al. 2004). In contrast, other studies report no significant changes in cardiomyocyte properties when cultured with endothelial cells. For example, endothelial cells did not significantly affect electrophysiological properties (action potential amplitude or duration, resting membrane potential) (Giacomelli et al. 2017) and contractility (magnitude of contraction, contractile area) (Burridge et al. 2014) of hPSC-derived cardiomyocytes.

In the studies of Burridge et al. (2014) and Giacomelli et al. (2017) the cardiomyocytes and endothelial cells were seeded simultaneously unlike in the studies of Garzoni et al. (2009) and Narmoneva et al. (2004) where the endothelial cells had formed capillary-like networks before cardiomyocyte seeding. The beneficial effects of the endothelial cells were found to be more significant when the endothelial cells had formed capillary-like structure prior to cardiomyocyte seeding compared to simultaneous seeding of cardiomyocytes and endothelial cells in the study of Narmoneva et al. (2004).

Endothelial cells have been shown to slightly reduce the gene expression of cardiac-specific genes coding *NKX2.5* and Troponin T *(TNNT2)* but to have no effect on ion channel genes *CACNA1C*, *SCN5A*, *KCNQ1*, *KCNH2*, *KCNJ12* and *HCN4* or calcium handling proteins *SERCA2A* and *NCX1* (Giacomelli et al. 2017). Burridge et al. (2014) found no significant differences in the gene expression of structural genes *TNNT2* and β-myosin heavy chain (*MYH7*), or cardiomyocyte maturity markers myosin light chain-2 (*MYL2*) and myosin light chain-7 (*MYL7*).

The beneficial effects of the coculture were also found to be greater when using cardiac progenitor cells and early-stage cardiomyocytes (Dunn et al. 2019). The cell-cell communication between cardiomyocytes and endothelial cells appears to be advantageous during cardiomyocyte development (Helle et al. 2021).

Enhanced maturation of hPSC-derived cardiomyocytes has been reported in coculture with hPSC-derived endothelial cells by several studies (Burridge et al. 2014; Giacomelli et al. 2017; Dunn et al. 2019; Helle et al. 2021). The coculture models have been established as small spherical 3D microtissues (Giacomelli et al. 2017; Garzoni et al. 2009) or coculture on a well plate (Helle et al. 2021) or a 3D hydrogel (Burridge et al. 2014). Giacomelli et al. (2017) and Burridge et al. (2014) studied the contractility of their tissue constructs by video imaging.

Inclusion of endothelial cells in implantable cardiac tissue grafts has also been shown to improve the vascularization and functionality of the graft (Sekine et al. 2008). 3D cardiac tissue grafts were created by cell sheet -based technique. Endothelial cells formed networks within cardiomyocyte sheets in the coculture. Four weeks after graft transplantation in infarcted rat hearts, the grafts containing endothelial cells had more capillaries and better contractility compared to cardiomyocyte only grafts. The grafts containing the preformed endothelial cell networks also reduced fibrosis of the tissue (Sekine et al. 2008).

2.2.3.3 Multicellular cocultures

Models consisting of more than two cell types increase the complexity of the model but enable more cell-cell crosstalk between different cell types and better resemblance of the cell composition of native myocardium. One popular cell type combination for engineered cardiac tissue models is the coculture of the three major cell types of the heart: cardiomyocytes, endothelial cells, and fibroblasts. Wagner et al. (2020) developed 3D spheroids of primary rat cardiomyocytes, cardiac rat fibroblasts, and HUVEC. They first created cocultures of cardiomyocytes and fibroblasts using a hanging drop method, and then added the endothelial cells on the spheroids. Their results showed that physiological pro-hypertrophic stimulation with adrenoceptor agonist phenylephrine augmented the spheroid growth, metabolic maturation, and vascularization. The phenylephrine stimulation also improved the amplitude of the contraction movement which was studied video imaging (Wagner et al. 2020).

Giacomelli et al. (2020) developed scaffold-free 3D microtissues including hiPSC-CMs, cardiac endothelial cells, and fibroblasts. They reported that the triculture model improved the cardiomyocytes structural, electrical, mechanical, and metabolic maturity better compared to cardiomyocyte-endothelial cell cocultures. The

enhanced sarcomeric structure, contractility, mitochondrial respiration, and electrophysiological properties in the triculture model were likely due to gap junctions connecting cardiomyocytes and fibroblasts and increased intracellular 3',5'-cyclic adenosine monophosphate (cAMP) level. They studied the contractility using video imaging (Giacomelli et al. 2020).

Other cell type combinations have also been studied. Abulaiti et al. (2020) developed 3D cardiac microtissues consisting of hiPSC-CMs, vascular endothelial, and vascular mural cells. They used a microfluidic chip where the cardiac contraction induces movement of fluorescent particles in a microchannel. The particle displacement was video imaged and used for evaluating fluidic output, pressure, and force (Abulaiti et al. 2020).

Burridge et al. (2014) developed a 3D model composing of hPSC-derived cardiomyocytes, hPSC-derived endothelial cells, and human amniotic mesenchymal stem cells (hAMSC) that were seeded on a hydrogel. They reported improved cardiomyocyte maturation in the triculture model. Studied by video imaging, the contractility properties (magnitude of contraction, contractile area) of the construct were improved in the triculture model compared to cardiomyocyte monocultures, cardiomyocyte-endothelial cell cocultures, and cardiomyocyte-hAMSC cocultures during a 6-week culture period (Burridge et al. 2014). Their results indicate the importance of multicellular interactions for sustaining the cardiomyocyte contractility in longer culture times.

Varzideh et al. (2019) developed 3D microtissues of hESC-derived mesenchymal stem cells and endothelial cells from human umbilical cord with hESC-derived cardiac progenitor cells in ratio 1:1:2. The gene expression and electrophysiological properties were improved in the coculture compared to cardiomyocyte only spheroids. Cardiac progenitor markers *TBX5* and *GATA4* were downregulated and structural maturity markers *MLC2v* and *β-MHC* were upregulated in the coculture. The spontaneous beating rate was decreased and interspike intervals and field potential durations were prolonged in the coculture possibly due to differentiation into ventricular cardiomyocytes or shift to less pacemaking nodal cells (Varzideh et al. 2019).

The benefits of cardiomyocyte coculture models with different nonmyocytes depend also on the cell seeding order and timing. Generally, better results have been obtained if the nonmyocytes have been seeded before cardiomyocytes compared to

seeding nonmyocytes simultaneously with the cardiomyocytes. This could be due to a more favourable culture environment for the cardiomyocytes through ECM deposition by the precultured nonmyocytes (Munawar and Turnbull 2021).

2.2.4 Cell culture techniques

This chapter presents cell culture techniques that can be used for improving the cardiomyocyte properties such as maturity and resemblance to the native myocardium compared to traditional 2D monolayer cultures. These techniques include 2D and 3D cell culture techniques with biomaterials, microfluidic systems and organ-on-a-chip (OoC) technology.

Cell alignment in 2D cultures is beneficial for cardiomyocyte maturity. The alignment can be controlled by micropatterning methods including manipulation of surface topography and microcontact printing of ECM proteins for cell adhesive areas (Mathur et al. 2016).

In addition to 2D cultures, cell culture techniques for creating cardiac *in vitro* models include various methods for creating 3D culture environments for improved physiological relevance. Biomaterials in 3D models can support cell attachment, promote cell alignment, provide favourable mechanical properties for the model such as physiologically relevant stiffness and load transmission. The biomaterials can be degraded during the culture and replaced by cell-secreted ECM proteins (Mathur et al. 2016).

Fibrous scaffolds provide ECM-like architecture to guide spatial organization of cells (Zamani et al. 2018). Synthetic biomaterials enable controlling the scaffolds' mechanical properties, topography, and structure. Frequently used synthetic biomaterials in cardiac tissue engineering are polyurethane, poly e-caprolactone, polylactic acid, polyglycolic acid, and their copolymers (Mathur et al. 2016). Biomaterials such as chitosan nanofibers, fibrous polyurethane, and composite scaffold of nanofibrous yarns containing carbon nanotubes in gelatin methacrylate hydrogel have been reported to improve cardiomyocyte morphology and alignment (Zamani et al. 2018).

Hydrogel materials such as fibrin (Hirt et al. 2014), collagen I (Feng et al. 2014), gelatin methacrylate (Saini et al. 2015), and Matrigel (Li et al. 2017) can be used to

create 3D cardiac constructs. In the method, the cells are mixed into the solution of the hydrogel material before gelation in a mould. Unlike casting in a mould, bioprinting enables precisely organized 3D cultures. ECM proteins such as collagen, gelatin, hyaluronic acid, alginate, and decellularized ECMs can be used as bioinks, or the cells can be bioprinted without a biomaterial. Cellular spreading, deforming the hydrogel, and diffusion of nutrients are critical for proper functionality of the 3D construct (Zamani et al. 2018).

Cell sheet engineering is a method of producing transferable 2D cell sheets that are combined to create 3D structures. The cell sheets can be cocultures (Sekine et al. 2008) or mono-cultured layers of different cell types (Haraguchi et al. 2010), and synchronous beating can be achieved between layers. It is possible to create high cell density constructs but ensuring sufficient diffusion of oxygen and nutrients limits the size of the 3D structures (Zamani et al. 2018).

Microfluidic culture platforms or microphysiological systems enable creating controlled, physiologically relevant 3D microenvironments with increased throughput (Dehne et al. 2017; Mathur et al. 2016; Yang et al. 2021). Moreover, they enable longer culture times due to effective circulation of media. The media flow introduces also shear stress to the cells and enables the monitoring of secreted factors (Zamani et al. 2018). Appropriate level of shear stress improves the differentiated cell phenotype and function of cell types that physiologically experience shear stress such as cardiovascular cells (Leung et al. 2022).

The OoC technology allows electrical and mechanical stimulation of the cells and real-time monitoring through different microsensors embedded in the devices. For example, the platforms can have integrated microelectrodes for measuring the cell behaviour and pH, oxygen, and temperature sensors for monitoring the microenvironment parameters (Paloschi et al. 2021). Moreover, the OoCs enable coculture of different cell types or organ models in separated culture areas which are connected in the microphysiological system by media flow enabling physiological interaction among the different cell types or organ models in the separate compartments (Dehne et al. 2017). The body-on-a-chip platforms enable studying drug efficacy in the target tissue and toxicity in multiple other tissues (Sung et al. 2019).

Heart-on-a-chip models have great potential for various biomedical applications including drug screening (Yang et al. 2021). For example, Zhang et al. (2021)

developed a microfluidic heart-on-a-chip platform with electrical stimulation and recording of hiPSC-CM for testing drug-induced cardiac effects. Marsano et al. (2016) developed a microfluidic heart-on-a-chip platform which applied cyclic mechanical strain to 3D cardiac constructs improving the cardiomyocyte maturation.

2.3 Functional measurements

Several techniques and parameters can be used for studying the functionality of cardiac cell cultures including electrophysiology and ion fluctuations, calcium handling, and contractility (Laurila et al. 2016). Contractility can be studied by measuring mechanical movement or contraction force of the cells.

2.3.1 Electrophysiology and ion fluctuations

A patch clamp measurement is a classical, gold standard method to study cardiac action potential parameters (Meyer et al. 2004). The method can be used for single/dissociated cells (Ronaldson-Bouchard et al. 2018) as well as cell clusters (Beauchamp et al. 2020) or tissue slices (Segev et al. 2016). The basic principle is to contact the cell membrane of the measured cell with a glass pipette creating a strong seal. The method provides detailed information on ion currents of the individual cell (Kussauer et al. 2019). Disadvantages of patch clamp method are that it is a time-consuming, terminal measurement method which requires a skilled user (Laurila et al. 2016; Meyer et al. 2004). The conventional patch clamp is not well suited for high throughput. Automated patch clamp technology has enabled multiple simultaneous measurements and high throughput drug screening applications (Obergrussberger et al. 2021; Kussauer et al. 2019).

Microelectrode array (MEA) is another method to measure the electrical functionality of cardiomyocytes. The MEA measures fluctuations in the extracellular field potential without disturbing the cell cultures or tissue slices that are located on top of the electrodes. As a non-invasive and non-terminal method (Laurila et al. 2016), MEA measurements enable repeated measurements of the same cells during long term cultures. Unlike patch clamp recordings, MEA measurements cannot be used for studying individual ion channels. Instead, the MEA signal is the sum of electrical activity from the excitable cells at the proximity of the recording electrode (Kussauer et al. 2019; Obien et al. 2015). This also means that the MEA detects the

comprehensive drug-induced effects potentially on multiple ion channels (Meyer et al. 2004). Because the recorded signal is the sum of all excitable cells in the proximity of the recording electrode, the measured sample should preferably consist of synchronized cells i.e., cardiomyocytes should have formed electrical coupling among themselves. Recording from unsynchronized cell clusters may impede the analysis of the signal from those electrodes.

The field potential from MEA measurements corresponds to the cardiac AP and ECG recordings (Figure 5). The MEA waveform begins with a strong transient spike resulting from Na^+ influx and depolarization of the cell. It is followed by a gentle incline which results from increasing intracellular calcium level. The field potential ends with a repolarization associated with K^+ efflux. In the MEA signal, field potential duration (FPD) corresponds to the QT interval of the ECG (Kussauer et al. 2019).

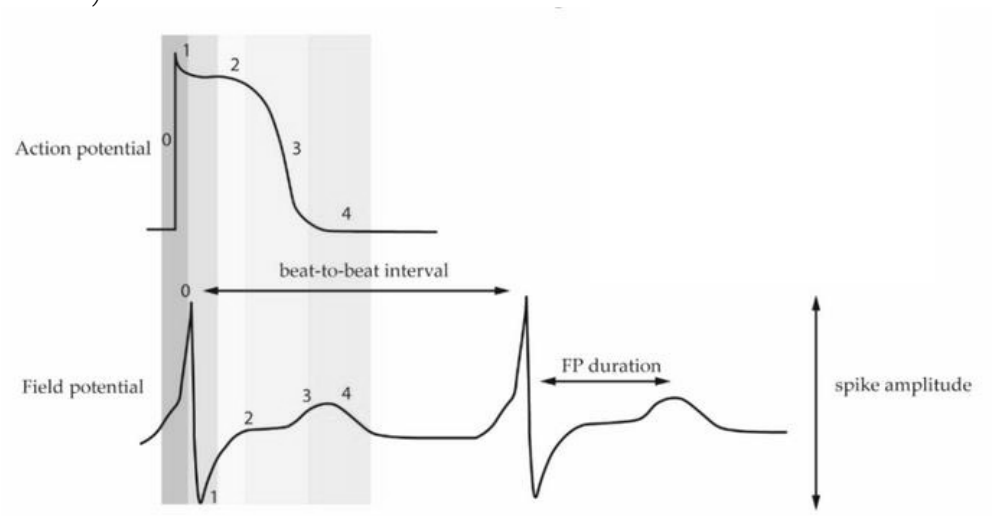

Figure 5. The field potential waveform represents the cardiac action potential phases (Kussauer et al. 2019).

Fluorescent imaging can be used to study the ion fluctuations and voltage changes of cardiomyocytes using voltage-sensitive dyes or calcium indicators. Calcium plays a key role in the excitation-contraction coupling of cardiomyocytes. Thus, calcium imaging has been widely used to study the cardiomyocyte functionality (Sutanto et al. 2020). Fluorescent imaging is a non-invasive method and enables high temporal resolution but the chemicals may interfere with the cells. Available calcium indicators e.g., Fura-2 and Fluo-4 and voltage-sensitive dyes e.g., di-4-ANEPPS are toxic to the

cells. Alternatively, cardiomyocytes can be genetically modified to express fluorescent proteins. Changes of the membrane potential cause conformational changes in these proteins which affects the emission spectra of the fluorescent protein. This method is less harmful for the cells compared to the voltage-sensitive dyes and can be used in longer-term measurements. However, also the voltage-sensitive proteins may affect the functionality of the cardiomyocytes. Regardless of the indicator method, fluorescence imaging provides only relative values of the membrane potential and cannot be used for obtaining absolute voltage values (Laurila et al. 2016; Kussauer et al. 2019).

2.3.2 Contraction movement

Mechanical movement of contracting cardiomyocytes can be studied using impedance assays. In this non-invasive method, the cells are attached as a cell sheet on top of the electrodes. A weak electric current, that is applied between the electrodes, is impeded by the cells. Movement of the cells changes the impedance signal (Laurila et al. 2016). The impedance is also affected by cell density, cell number and the extent of cell adhesion. Impedance measurements reveal information about beating behaviour, proliferation, cell death and viability (Kussauer et al. 2019). Impedance measurements are label-free and allow long-term measurements (Dou et al. 2022).

Cardiomyocyte contractility movement can also be studied using video imaging. It is non-invasive and enables high throughput. The temporal resolution of the recording depends on the frame rate which needs to be high enough to capture the details of beating patterns. For example, a 30–50 ms prolongation of the contraction relaxion phase (typically 500–600 ms if beating rate is 40–60 bpm) could be significant. In addition, the spatial resolution needs to be high enough to detect contraction movements. The displacement of cells between frames is used for determining the contraction movement. Video imaging can be used for studying the contractility of single cells, cell clusters and sheets (Laurila et al. 2016). Dou et al. (2022) studied beating cardiac spheroids of diameter 200–400 μm using video imaging. The movement of the edges was used for calculating the contraction magnitude. However, the measured spheroid shape changes do not directly correlate to the contraction force. For example, cell density and spheroid composition can affect the magnitude of contraction movement (Dou et al. 2022).

2.3.3 Contraction force

Cardiac output is defined as the stroke volume times beat rate. The stroke volume depends on several factors including contractility. Therefore, contractility of cardiac tissue directly affects its main function to maintain the blood circulation through the body. Both increase and decrease in the cardiac contractility can have fatal consequences. The decrease of contractility can cause drop of systemic arterial blood pressure, increased heart rate, syncope, and inadequate blood flow to vital organs, while the increase of contractility can lead to myocardial hypertrophy, impaired myocardial energetics, and arrythmias. Thus, it is important to avoid unwanted drug-induced adverse inotropic effects. However, modulation of cardiac contractility can also be the purpose of a treatment e.g., when augmentation to impaired contractile function is needed (Guth et al. 2019). The safety and efficacy testing of drugs would benefit from methods to measure drug-induced effects on the cardiomyocyte contraction force.

The existing *in vitro* force measurement techniques can be divided to direct and indirect techniques. Direct techniques measure the contraction force with a mechanical force sensor while indirect methods exploit video-based approaches in combination with known material properties to estimate the contraction force. The temporal resolution of the imaging-based contraction force measurement methods depends on the speed of the camera used to acquire them. To accurately capture all cardiomyocyte transient kinetics, they require a high sampling speed of more than 300 frames per second (fps) (van Meer et al. 2019).

Typically, the force is proportional to the number of cells. As some of the measurement techniques are developed for single cell measurements while others for measuring cell clusters, 2D cell layers or tissue-like samples, the measured force values vary greatly. Moreover, the tissue-like samples typically include a biomaterial e.g., fibrin or collagen, to support the cardiomyocytes. The single cell measurement methods allow studying cellular and subcellular structures and electrophysiology but lack cell-cell communication. Measurement methods using 2D cell layers enable also studying these cell-cell junctions that affect action potential propagation and synchronous beating of the cells. The 2D cardiomyocyte monolayers lack the 3D extracellular microenvironment and cell-cell communication with other cell types but they enable high throughput methods. Tissue-like samples include more *in vivo* -like 3D microenvironment, cell organization and junctions (Dou et al. 2022).

2.3.3.1 Direct force measurement techniques

Examples of different types of direct contraction force measurement techniques are presented in Table 2. They include atomic force microscope (AFM), AFM-like microcantilever, direct force transducer, and CellDrum technology.

Table 2. Direct contraction force measurement techniques.

Method	Description	Force	Sample	Bio-material	Reference
AFM	AFM probe brought in contact with cell, deflection measured with laser sensor	vertical: pN to nN range	single cells, cell clusters	-	(Liu et al. 2012; Chang et al. 2013; Saenz Cogollo et al. 2011)
AFM-type micro-cantilever	microcantilever with embedded deflection-sensor brought in contact with cell layer	vertical: 38.6 ± 2.2 N/m^2	2D layer	-	(Gaitas et al. 2015)
Force transducer	tissue attached to force transducer and static attachment point	µN to mN range	circular, fibre, strip-format tissue	fibrin, collagen, decellularized/ infarcted myocardium	(Akiyama et al. 2010; Zimmermann et al. 2002; Eschenhagen et al. 1997; Schwan et al. 2016; Pillekamp et al. 2007; Xi et al. 2010; Sasaki et al. 2018; Turnbull et al. 2014; Mathews et al. 2012; Sondergaard et al. 2012)
CellDrum	cell grown on flexible membrane, deflection-measuring laser sensor and air pressure sensor		2D layer, tissue	-/collagen	(Linder et al. 2010)

AFM = atomic force microscope

AFM consists of a cantilever, a probe, and a laser sensor. The cantilever holds the probe that indents the specimen. The deflection of the cantilever is detected by the laser and photodiodes (Peña et al. 2022). When the AFM probe is brought in contact with the cells, their contraction movement deflects the AFM cantilever. The contraction force can be calculated from the deflection using the spring constant of the cantilever. The AFM is suitable for measuring the small contraction forces of single cardiomyocytes or small cardiomyocyte clusters (Liu et al. 2012). The contraction forces are in pN to nN range, and it is measured in vertical direction. In addition to the contraction force, also cell elasticity, adhesion behaviour, viscoelasticity, and beating frequency can be measured with AFM (Peña et al. 2022). The direct contact of the AFM tip can mechanically stimulate the measured cell and

affect the beating (Dou et al. 2022). This method is not well suited for measuring the contraction forces of engineered cardiac tissues which typically generate contraction forces mainly in the horizontal direction i.e., in the direction of sarcomere orientation. In these cardiac tissues the contraction forces are formed as the sum of several contracting cardiomyocytes in the construct.

Gaitas et al. (2015) developed an AFM-type microcantilever which had an embedded sensing element removing the need of the laser sensor system required in AFM. The cantilevers were 40 μm wide, 150 μm long, and 2 μm thick. They contained a 2 nm/10 nm thick Cr/Au deflection sensing element between polyimide layers. Using a micromanipulator, a small 10 μm × 40 μm area of this cantilever was brought into contact with cardiomyocytes that were cultured as a monolayer (Gaitas et al. 2015). Similar to AFM, also this method measured the vertical force of the cardiomyocyte contraction.

Force transducers can be used for measuring cardiac contraction forces. The sample types for this method include engineered cardiac tissues that consist cardiomyocytes in a biomaterial scaffold or in myocardial ECM. The sample shapes are typically circular, fibre or strip-format so that they can be attached to the force transducer in one end and to a fixed attachment point in the other. Both custom-made (Sondergaard et al. 2012) and commercial (Eschenhagen et al. 1997; Pillekamp et al. 2007; Xi et al. 2010; Akiyama et al. 2010) force transducers have been used. Isometric force transducers (e.g. Eschenhagen et al. 1997; Pillekamp et al. 2007; Zimmermann et al. 2002; Xi et al. 2010) measure the contraction force while the length of the tissue remains constant, which does not correspond to the *in vivo* situation where the length of the cardiac tissue changes during the contraction. The measured forces with force transducer method are generally in μN range but forces up to mN range have been measured (Sasaki et al. 2018). Sample preparation with the biomaterials and attachment to the force transducers add to the complexity of using the method. However, the culture method with the biomaterials enables the samples to have 3D structure.

CellDrum technology measures the contraction force of cardiomyocytes that are grown as monolayers or in collagen-based 3D films on flexible membrane sheets (Linder et al. 2010). The sheet is bulged outwards by air pressure to produce biaxial strain to the cell layer. The cardiomyocyte contraction causes deflection of the sheet which is monitored by a laser sensor. The measured air pressure is used for

calculating mechanical tension (Linder et al. 2010). The CellDrum technology has been commercialised by innoVitro and Nanion as FLEXcyte 96 equipment. It allows simultaneous measurements of 96 parallel cultures (Nanion Technologies 2023).

2.3.3.2 Indirect force measurement techniques

Examples of different indirect i.e., imaging-based contraction force measurement techniques are presented in Table 3. They include microcantilevers, static and elastic pillars, micropillars, microposts, elastic culture substrate, and magnetic beads.

Table 3. Indirect i.e., imaging-based contraction force measurement techniques.

Method	Description	Force	Sample	Bio-material	Reference
Micro-cantilever	cells grown on microcantilever, cantilever deflection imaged	2–10 nN/µm^2	2D layer	-	(Park et al. 2005; Kim et al. 2008)
Static pillars	circular tissue anchored to static pins, movement of the ring imaged	tens of µN	circular tissue	collagen	(Feng et al. 2014)
Elastic pillars	tissue adhered between elastic pillars, deflection of pillars imaged	up to hundreds of µN	strip-format tissue	fibrin, Matrigel, collagen	(Boudou et al. 2012; Hansen et al. 2010; Hirt et al. 2014; Stoehr et al. 2014; Mannhardt et al. 2016; Turnbull et al. 2014; Schaaf et al. 2011)
Micro-pillars	cells between elastic micropillars, deflection of pillars imaged	hundreds of nN	single cells	-	(Kajzar et al. 2008)
Micropost array	cells on elastic micropost array, deflection of posts imaged	nN range	single cells	-	(Rodriguez et al. 2014)
Elastic substrate (TFM)	cells grown on patterned elastic culture substrate	0.4-7 mN/mm^2; ~3 nN/CM	single cells/ cell clusters	-/fibrin	(Kijlstra et al. 2015; Ribeiro et al. 2015; Schaefer and Tranquillo 2016; Hazeltine et al. 2012)
Magnetic beads	magnetic beads attached to CM, change in magnetic field	~10 µN	single cells	-	(Yin et al. 2005)

CM = cardiomyocyte; TFM = traction force microscopy

Cardiomyocyte contraction forces were measured using polydimethylsiloxane (PDMS) microcantilevers by Park et al. (2005) and Kim et al. (2008). The cardiomyocytes were grown on microcantilevers that deflected with cardiomyocyte contraction. The degree of cantilever deflection was detected using video imaging at 30 fps. The contraction force of the cardiomyocyte layer was calculated using the deflection of the cantilever and its mechanical properties (Park et al. 2005; Kim et al. 2008). Kim et al. (2008) tested also longitudinally grooved cantilevers which aligned the cardiomyocytes and increased their contractility compared to flat cantilevers. The method requires the culturing of the cardiomyocytes on the cantilevers which increases the complexity of the method. Moreover, reaching a high level of interconnectedness among the cardiomyocytes on the cantilevers may be difficult. The cardiac cultures do not show physiological tissue structure even if the cardiomyocytes are aligned using the grooved cantilevers.

Feng et al. (2014) created circular cardiac tissues consisting of cardiomyocytes and collagen type I that were attached to two static pillars. The pillars were 17 mm apart and the thickness of the tissue ring was 0.5 mm. The deflection of the ring was imaged at 60 fps and the contraction force was calculated from the ring deflection (Feng et al. 2014). The biomaterial allows 3D structure to the cardiac tissue. However, the method of creating the cardiac ring first in a mould and then transferring it to the pins adds to the complexity of using this method. In addition, the high number of cardiomyocytes required to create the contracting ring in this method decreases its usability.

Elastic pillars have been used for measuring cardiac contraction forces (Boudou et al. 2012; Hansen et al. 2010; Hirt et al. 2014; Stoehr et al. 2014; Mannhardt et al. 2016; Turnbull et al. 2014; Schaaf et al. 2011). A strip-format engineered cardiac tissue was adhered between two elastic pillars whose deflection was imaged at frame rates from 20 fps (Boudou et al. 2012) to 100 fps (Turnbull et al. 2014; Stoehr et al. 2014). The contraction force was calculated from the pillar deflection, silicone post length and radius, and elastic modulus (Schaaf et al. 2011). The engineered cardiac tissue samples consisted of cardiomyocytes in fibrin or collagen type I based scaffold. (Boudou et al. 2012; Hansen et al. 2010; Hirt et al. 2014; Stoehr et al. 2014; Mannhardt et al. 2016; Turnbull et al. 2014; Schaaf et al. 2011). Similar to the previous method also this method allows 3D structure to the cardiac tissue with the biomaterial. Furthermore, the formation of the sample in the mould adds to the complexity of using the method.

Kajzar et al. (2008) used elastic PDMS micropillars for measuring the contraction forces of single cardiomyocytes. Single cells attached between two 10 μm wide micropillars whose distance was 20–30 μm. The deflection of the micropillars was imaged with high scanning speed and the contraction force was calculated from the deflection (Kajzar et al. 2008). As this method is suitable for measuring the contraction forces of single cardiomyocytes, it does not allow physiological 3D structure or cell-cell contracts in the sample. Moreover, the cardiomyocyte attachment in the correct locations between the micropillars may be difficult to control.

Rodriguez et al. (2014) used a micropost array to measure contraction force of cardiomyocytes. The cardiomyocytes were cultured on top of an array of small PDMS microposts (d = 2.3 μm, h = 7.2 μm, 6 μm center-to-center spacing) whose movements were detected using high-speed video imaging at >100 fps. The contraction force was calculated using the deflection of the microposts (Rodriguez et al. 2014). This method is also suitable for measuring single cardiomyocytes and thus does not allow physiological 3D structure or cell-cell contracts in the sample. Moreover, the cardiomyocytes on the micropost arrays showed reduced cell area and elongation compared to cardiomyocytes on flat surfaces (Rodriguez et al. 2014).

Yin et al. (2005) measured contraction forces of single cardiomyocytes using magnetic beads. The magnetic beads were attached to the cells whose movement was monitored with video imaging. The load was controlled by applying magnetic field. The contraction force was calculated from the displacement of the cell and magnitude of the magnetic field (Yin et al. 2005). As also this method is suitable for measuring only single cardiomyocytes, it does not allow physiological 3D structure or cell-cell contracts. In addition, the attachment of the magnetic beads to the cells adds to the complexity of using the method.

Cardiomyocyte contraction forces can be also indirectly measured using elastic culture substrates (Kijlstra et al. 2015; Ribeiro et al. 2015; Schaefer and Tranquillo 2016; Hazeltine et al. 2012) with stiffness typically in range of 1–30 kPa (Dou et al. 2022). In traction force microscopy (TFM), the cardiomyocytes are grown on an elastic culture substrate that is patterned for tracking the movement of the substrate surface e.g., polyacrylamide gel (Ribeiro et al. 2015; Hazeltine et al. 2012) or PDMS substrate patterned with fluorescent beads (Kijlstra et al. 2015). Kijlsta et al. (2015) also used nonpatterned PDMS substrates. In the method of Schaefer and Tranquillo

(2016), the cardiomyocytes were cultured in a fibrin gel on the PDMS substrates. The movement of the beads were imaged at 4–8 fps (Ribeiro et al. 2015; Schaefer and Tranquillo 2016; Hazeltine et al. 2012). The displacement of the beads and mechanical propertied of the elastic substrate are used for calculating the contraction forces generated by single cells or cell clusters (Hazeltine et al. 2012). The method is not well suited for samples with 3D structure as only the forces that cause movement of the substrate get measured.

2.4 Inotropic drugs and their mechanisms

Chronotropy refers to the rate of contraction while inotropy means the level or the strength of contraction (Guth et al. 2019). Inotropes are substances that affect the contraction force of cardiomyocytes. Positive inotropes increase the contraction force whereas negative inotropes decrease it. Most inotropes affect the cardiomyocyte contractility by increasing or decreasing the free cytosolic calcium concentration (Hasenfuss and Teerlink 2011). Inotropes can affect the cytosolic calcium concentration either directly or indirectly via affecting the cAMP concentration. Besides the cytosolic calcium concentration, inotropes can modify the cardiac contractility by targeting the myofilaments. Unspecific negative inotropy can also result from general toxicity, for example after administration of anthracyclines e.g., doxorubicin (van Meer et al. 2019).

Positive inotropes that directly affect the cytosolic calcium concentrations include calcium- and sodium channel agonists and cardiac glycosides (van Meer et al. 2019). Cardiac glycosides e.g., digoxin and ouabain, inhibit the sodium-potassium-ATPase resulting in elevated sodium level which in turn increases intracellular calcium level via the NCX (Hasenfuss and Teerlink 2011). Negative inotropes with direct effect on the intracellular Ca^{2+} concentration include calcium channel blockers e.g., verapamil and nifedipine which inhibit the influx of calcium ions into the cells (van Meer et al. 2019).

Catecholamines, phosphodiesterase (PDE) inhibitors and beta blockers affect the cytosolic calcium levels by affecting the cAMP concentration (van Meer et al. 2019). Catecholamines/beta-adrenoceptor agonists cause their positive inotropic responses by targeting beta-adrenoceptors. These G-protein coupled receptors activate adenylate cyclase enzyme that enhances production of cAMP. The elevated level of

cAMP increases the activation Ca^{2+}-channels and influx of calcium into the cytosol (Overgaard and Džavík 2008). Examples of catecholamines include epinephrine and isoprenaline (van Meer et al. 2019). PDE inhibitors, such as milrinone and rolipram (Mannhardt et al. 2017), produce positive inotropic effects by decreasing cAMP degradation by phosphodiesterase enzyme. Beta blockers/beta-adrenoceptor antagonists e.g., propranolol, cause negative inotropy by binding beta-adrenoceptors inhibiting the stimulation.

The elevated intracellular calcium concentration and increased energy consumption caused by many inotropes are linked to adverse effects including arrythmias and myocardial ischemia (Hasenfuss and Teerlink 2011; Kaplinsky and Mallarkey 2018). Myosin activators and inhibitors, and calcium sensitizers target the myofilaments without affecting the cytosolic calcium concentration. For example, the myosin activator omecamtiv mecarbil binds to myosin increasing the speed of ATP hydrolysis and thus, the number of myosin heads bounding to actin. This increases the force production and systole duration (Kaplinsky and Mallarkey 2018). The calcium sensitizer levosimendan increases the calcium affinity of troponin C (Hasenfuss and Teerlink 2011).

3 AIMS OF THE STUDY

Aims of this study were to develop a cardiac tissue model for routine testing of cardiac effects, and to develop a technology for measuring cardiac contraction forces in the cardiac tissue model.

1. to develop a functional human cell -based standardised cardiac tissue model that mimics the adult human myocardium structure, gene expression, and function (**study I**)

2. to develop a contraction force measurement technology that can be used for measuring the contraction forces in the cardiac tissue model (**studies II-IV**)

3. to confirm the functionality of the cardiac tissue model and contraction force measurement technology by known inotropic drug exposures (**study IV**)

4 MATERIALS AND METHODS

4.1 Ethical considerations

This study conforms to the principles of the Declaration of Helsinki. Human adipose tissues were obtained from surgical operations and human umbilical cords from scheduled caesarean sections from Tampere University Hospital, Tampere, Finland. An individual written informed consent was obtained from each tissue donor. The use of human adipose stromal cells (hASC) and human umbilical vein endothelial cells (HUVEC) was approved by the Ethics Committee of Pirkanmaa Hospital District (permit numbers R03058 and R15161 for hASC, R08028 and R15033 for HUVEC).

4.2 Cardiac tissue model

4.2.1 Cells

The cardiac tissue models contain a vascular-like network and cardiomyocytes in co-culture. The vascular-like networks are formed from hASCs and HUVECs. The hASC and the HUVEC lines were tested negative for mycoplasma contamination.

The hASCs were isolated from donated adipose tissue samples using a mechanical and enzymatic dissociation method (Sarkanen et al. 2012). The cells were cultured in DMEM/F12 (Gibco, 21331) supplemented with 10% Human Serum (Biowest, S4190) and 1% L-glutamine (Gibco, 25030) (Sarkanen et al. 2012; Toimela et al. 2017). They were maintained in a humidified incubator at 37°C, 5% CO_2, and the medium was refreshed every 2–3 days. The identity of the hASC lines was confirmed positive for CD90, CD73 and CD105 by flow cytometry. Passage 2 was used.

The HUVECs were isolated from umbilical cords enzymatically (Sarkanen et al. 2012). The HUVECs were cultured in EBM-2 with EGM-2 SingleQuots

supplements (Lonza, CC-3162) (Sarkanen et al. 2012; Toimela et al. 2017). The cells were maintained in a humidified incubator at +37°C, 5% CO_2. The HUVEC lines that were used had passed a tube formation test. Passage 4 was used.

In the **studies I**, **III**, and **IV**, commercial cardiomyocytes iCell Cardiomyocytes^2 from Cellular Dynamics were used. They were thawed directly before use following the manufacturer's instructions. In **study II**, the cardiomyocytes were differentiated from hiPSCs as follows. First, the differentiation was initiated using Cardiomyocyte Differentiation Medium A (Gibco, A29209-01). Two days later, the medium was replaced by Cardiomyocyte Differentiation Medium B (Gibco, A29210-01). Three days later, the medium was replaced by Cardiomyocyte Maintenance Medium (Gibco, A29208-01). Media were refreshed every 1–3 days. By two weeks the cells had started beating and they could be used for experiments.

4.2.2 Fibrin

Fibrin was used to improve the long-term attachment and stability of the model. In the studies, fibrin was used either as a thin coating to improve cell attachment (**studies I-II**) or as a thicker coating (**study III**) and a hydrogel (**study IV**) that provided elastic culture surface for the contracting cells. Fibrin was prepared by mixing 1:1 a solution containing 5.5 mg/ml fibrinogen (Sigma Aldrich, F3879) with 38 μg/ml aprotinin (Sigma Aldrich, A1153) and a solution of 2.75 UN/ml thrombin (Sigma Aldrich, T7009), followed by incubation at 37°C 30–90 min to accelerate the polymerization. Moreover, fibrin coating without aprotinin was used in the coating of force sensor tips (**studies II-IV**).

4.2.3 Vascular networks

The hASC-HUVEC co-cultures were established to produce vascular-like network bases for cardiac tissue models. First, hASCs were seeded on fibrin coating 20,000 cells/cm^2 in EBM-2 with EGM-2 SingleQuots supplements (Lonza, CC-3162). Then HUVECs were seeded at 4,000 cells/cm^2 on top of the hASC culture 1–4 hours later. The next day, angiogenesis stimulation was initiated using a serum-free stimulation medium (SFSM) consisting of DMEM/F12, 2.56 mM L-glutamine, 0.1 nM 3,3',5-triiodo-L-thyronine sodium salt, ITS™ Premix: 1.15 μM: 6.65 μg/ml insulin, 6.65 μg/ml transferrin, 6.65 ng/ml selenious acid, 1% bovine serum albumin,

2.8 mM sodium pyruvate, 200 μg/ml ascorbic acid, 0.5 μg/ml heparin, 2 μg/ml hydrocortisone, 10 ng/ml vascular endothelial growth factor (VEGF), and 1 ng/ml basic fibroblast growth factor (FGF-β) (Huttala et al. 2015). The vascular networks were formed in one week of hASC-HUVEC co-culture and could be used as the base for the cardiac tissue models.

The cells in the hASC-HUVEC vascular networks continue to proliferate in the culture. To prevent the overgrowth of the hASC-HUVEC vascular bases in long term cultures, two options were tested i.e., decellularized vascular networks and growth-arrested vascular networks as bases for the cardiac tissue models.

4.2.3.1 Decellularized vascular network

Decellularization of vascular networks was performed as described by Huttala et al. (2022) one week after initiating the hASC-HUVEC coculture to allow the vascular network structures to form. The cultures were first washed twice with phosphate-buffered saline (PBS). The cells were treated with Decellularization solution A containing 0.5% Triton X-100 (Electran, 437002A) in 0.02 M NH_4OH (Honeywell Fluka) with 0.5 × Complete Protease inhibitor (Roche, 11836153001) for 5 minutes in 37°C followed by washing twice with PBS. Next the cells were treated with Decellularization solution B containing 30 U/mL DNase (Biolabs, M3035), 1.25 mM $MgCl_2$ (Sigma, M8266), and 0.5 × Complete Protease inhibitor in 1 × DNAse Buffer (New England Biolabs) 30 min in 37°C. Finally, the cells were washed 3 times with PBS. The last PBS was left in the wells. They were ready to be used as vascular bases.

4.2.3.2 Growth-arrested vascular network

An optimization study was performed to select the suitable concentration, duration, and timing for the Mitomycin C treatment. Mitomycin C is a deoxyribonucleic acid (DNA) cross-linker that inhibits DNA synthesis and mitosis but does not affect much ribonucleic acid (RNA) or protein synthesis (Chugh et al. 2016). Mitomycin C is used for growth-arrest of feeder cell layers in stem cell cultures (Chugh et al. 2016; Ponchio et al. 2000). For the optimization study, hASC-HUVEC cocultures were established on 48-well plates (Nunc) and treated with Mitomycin C (Sigma, M7949) after 4 or 7 days in culture for 1 or 2 hours. Mitomycin concentrations were 1, 5, 10, 20, 50 μg/ml. The cultures were analysed on day 1 and day 14 after Mitomycin C

treatment. Viability of the cells was studied using WST-1 assay, and number of mitotic cells were analysed by immunofluorescence staining against the proliferation marker Ki67 with the endothelial marker von Willebrand factor (vWf) to analyse the formation of vascular-like networks. The aim was to select treatment parameters that would impair the mitotic activity enough to prevent at least a portion of the cell proliferation and diminish the metabolic rate of the cocultures but not to kill the cells and allow formation of vascular tubule network.

Taking into account the results of the optimization study, growth-arrested vascular networks were produced by treating the hASC-HUVEC co-cultures with 1 μg/ml Mitomycin C (Millipore, 47589/Sigma, M7949) for 1.5 hours on day 7 after initiating the hASC-HUVEC co-culture to impair their mitotic activity in **studies I**, **III**, and **IV**.

4.2.4 Adding the cardiomyocytes

Cardiomyocytes were seeded on top of the vascular networks to produce cardiac tissue cultures. The commercial iCell Cardiomyocytes² (Cellular Dynamics) were seeded in iCell Cardiomyocytes Plating Medium (Cellular Dynamics, M1001). The plating medium was replaced with 1:1 iCell Cardiomyocytes Maintenance Medium (Cellular Dynamics, M1003) and SFSM 4 hours later. The self-differentiated cardiomyocytes were seeded in 1:1 Cardiomyocyte Maintenance Medium (Gibco Invitrogen, A209208) and SFSM. The media were refreshed every second or third day.

For **study I**, the iCell cardiomyocyte concentration was 156,000 cells/cm² as recommended by the supplier. For the contraction force measurement **studies III** and **IV**, the iCell cardiomyocyte cell density was 312,000 cells/cm² to ensure cardiomyocyte-cardiomyocyte contacts and synchronous beating of the entire construct. The cardiac tissue cultures were allowed to form and mature one week after seeding the iCell cardiomyocytes before using them in experiments. In **study I**, the iCell cardiomyocytes were cultured also as a monoculture at 156,000 cells/cm² in Cardiomyocytes Plating Medium. The medium was replaced by iCell Cardiomyocytes Maintenance Medium 4 hours later.

In **study II**, hiPSC-CMs were enzymatically and mechanically detached from the culture dishes. First, the cultures were treated with 0.5 U/ml EDTA (ATCC, ACS-

3010) for 7 min. Then the detachment was aided by scraping the cells from the culture dish. The cell suspension was pipetted a few times back and forth to break the large cell aggregates. The cells were seeded as small aggregates on the vascular network bases in 1:1 Cardiomyocyte Maintenance Medium (Gibco Invitrogen, A209208) and SFSM. The media were refreshed every second or third days. The cultures were used for measurements in four weeks.

4.2.5 Cell culture platforms

In **study I**, the cells were cultured in well plates, in chambered coverslips (ibidi, 80826), and in 24-well and 96-well MEA plates (Multi Channel Systems, 24W700/100F-288 and 96W700/100F-288).

For the contraction force measurement applications, certain requirements for the culture platforms needed to be considered. Because there was a limited amount of space under the microscope, the force sensor design determined the dimensions of the culture platforms. Moreover, the measuring of the contraction movement impaired on rigid culture substrates.

4.2.5.1 Polydimethylsiloxane

Polydimethylsiloxane (PDMS) sheets were utilised in **studies II** and **III**. Initially, a single axis sensor design required a large contact angle with the cardiac tissue construct to fit under the microscope. Therefore, the culture dish needed to be relatively large and have low walls. However, to decrease the required number of cells and possibly allow more throughput for the method, polydimethylsiloxane moulds were used to create smaller cell constructs in the larger dishes in **study II**. In the **study II**, the cardiac tissues were cultured into fibrin-coated 5 mm diameter perforations in a PDMS (Sylgard 184, Dow Corning, USA) sheet reversibly bonded to a cell culture dish (d=60 mm). Five days after cardiomyocyte seeding, the PDMS sheets were removed to leave the vascularized cardiac tissue constructs to form spontaneously. This process also detached the edges of the cardiac tissue constructs which provided attachment points to the force measurement cantilever.

4.2.5.2 Lift-off culture method

Because the spontaneous growth in a cell culture dish was not controllable enough, a lift-off culture method was developed and used in **study III**. Perforated PDMS sheets were used for culturing transferable cardiac tissue models in the **study III**. The PDMS sheets were approximately 1 mm thick and had 3 mm diameter circular perforations. The sheets were reversibly bonded to temperature-responsive cell culture dishes (Nunc UpCell #174904, ThermoFisher Scientific) to form small 3 mm diameter wells. A fibrin coating was applied to the PDMS walls and culture dish bottom of the wells. Cells were cultured in these wells in the PDMS sheets. After six days the PDMS sheets with the cardiac tissue constructs were detached from the temperature-responsive culture dishes by first lowering the temperature to change the hydrophobicity of the surface, and then lifting the PDMS sheets manually by tweezers. The PDMS sheets were placed on top of PDMS holders to produce off-lifted cardiac tissue constructs that were attached to the PDMS walls and not attached to the bottom of a 35-mm diameter cell culture dish. This allowed freer movement of the contracting tissues for the force measurement.

4.2.5.3 Hydrogel culture method

After developing an L-shaped dual axis sensor, the cell culture dish dimension requirements lessened and allowed a more simple and efficient culture method with flexible fibrin hydrogel substrates in standard 96-well plates (**study IV**). In **study IV**, a fibrin hydrogel was formed by mixing 50 µl fibrinogen and 50 µl thrombin solutions into wells of 96-well plates. The cells were seeded on top of the fibrin hydrogel. This produced thick and elastic hydrogels that allowed the contraction movement of the cardiac tissue constructs.

4.3 Characterization of cardiac tissue model

4.3.1 Immunofluorescence

Immunofluorescence was used for determining specific cell types in the cultures and for examining the cardiomyocyte structures and organization, and formation of vascular-like networks. The cells were fixed with 70% ethanol or 4% formaldehyde

for 20 minutes. The cells were stained with primary antibodies monoclonal mouse anti-Troponin T antibody (1:100, Invitrogen, MA5-12960), monoclonal mouse anti-α-Actinin (1:100, Sigma, A7732), and polyclonal rabbit anti-vWf (1:100, Dako, A0082) at +4°C overnight. Secondary antibodies anti-mouse IgG Alexa Fluor 488 (1:400, Invitrogen, A21202) and anti-rabbit IgG Alexa Fluor 594 (1:400, Invitrogen, A21207) or anti-mouse fluorescein isothiocyanate (FITC) (1:100, Sigma Aldrich, F4143) and anti-mouse tetramethyl rhodamine isothiocyanate (TRITC) (1:50, Sigma Aldrich, T6778) were incubated for 45 minutes at room temperature. The cells were imaged using Nikon Eclipse TiS microscope with a 20x objective (**study I**), Olympus IX51 Inverted Fluorescence Microscope with a 10x objective (**study III**-**IV**) or Zeiss Laser Scanning Confocal Microscope LSCM 780 with a 25x and a 63x objectives (**study I**).

For comparison of different vascular bases (unpublished study), cardiac tissue models on decellularized, growth-arrested, and untreated vascular networks were stained with primary antibody chicken anti-Troponin T antibody (1:50, Sanovo Biotech A/S, SBT0107) and secondary antibody anti-chicken IgY (IgG) aminomethylcoumarin acetate (AMCA) (1:50, Jackson ImmunoResearch, 103-155-155). The cells were imaged using Olympus IX51 Inverted Fluorescence Microscope with a 10x objective.

4.3.2 Transmission electron microscopy

Transmission electron microscopy (TEM) was used for analysing the intracellular structures of the different cell types in the cardiac tissue model and for comparing the cardiomyocyte in cardiac tissue model and cardiomyocyte monoculture in **study I**. The cardiac tissue models and cardiomyocyte monocultures were fixed for 60 minutes with 4% paraformaldehyde +1% glutaraldehyde in 0.1 M phosphate buffer. Samples were taken 1 day and 1 week after cardiomyocyte seeding to study the development and maturing of the cultures. The cells were carefully removed from the dishes and pelleted. Fixed cell pellets were postfixed in 1% osmiumtetroxide, dehydrated in acetone and embedded in Epon LX 112 (Ladd Research Industries). Thin sections (70 nm) were cut with a Leica Ultracut UCT ultramicrotome, stained in uranyl acetate and lead citrate, and examined in a Tecnai G2 Spirit transmission electron microscope (FEI Europe). Images were captured by a Quemesa CCD camera and analysed using iTEM software (Olympus Soft Imaging Solutions GMBH).

4.3.3 Gene expression

The gene expression in cardiac tissue models was analysed one day and one week after cardiomyocyte seeding and compared to that of cardiomyocyte monocultures in **study I**. The total RNA was collected from the samples using a PureLink RNA Mini Kit (Life Technologies, 12183018A). The messenger RNA (mRNA) samples quality was analysed with Agilent 2100 Bioanalyzer. Initial bioinformatics were performed by Novogene CO Ltd. (Beijing, China). They performed RNA sequencing including complementary DNA (cDNA) library preparation and sequencing (20 M clean reads/sample) using Illumina PE150 (Q30≥80%) equipment.

The initial quality control for the results was done using FastQC (Andrews 2010). Then, raw reads were mapped to GRCh38 (GENCODE comprehensive annotation v29) using STAR v2.7.1 (Dobin et al. 2013). The resulting Binary Alignment Map (.bam) files were sorted and indexed using SAMtools v1.9 (Li et al. 2009). Lastly, the gene counts were accessed using featureCounts v2.0.1 (Liao et al. 2014) on hg38 (GENCODE basic annotation v34) and filtered for protein coding genes using biomaRt v2.40.5 (Durinck et al. 2009).

The samples were plotted on a two-dimensional graph using dimensionality reduction through principal components to select suitable replicates for downstream expression analysis. Differential expression analysis was performed using DESeq2 v1.24.0 (Love et al. 2014). Changes in gene expression between the days were determined using the "contrast" function on DESeq2. Significant differentially expressed genes (DEGs) were filtered using a Benjamini-Hochberg adjusted p-value (BH p-value) of <0.05 and an absolute log2-fold-change of >1 as thresholds. The resulting gene lists were used for enrichment analysis using the g:GOSt functional profiling tool (Raudvere et al. 2019) and a significance threshold of a BH p-value <0.01. Gene Ontology biological processes (GO:BP, ENSEMBL 99 release 2020-01-01) excluding evidence Inferred from Electronic Annotation (IEA) and KEGG pathways (KEGG FTP release 2020-02-03) were used as databases (Kanehisa 1996). In case a gene symbol matched multiple ENSEMBL ids, the one with the most GO annotations was used. The annotated genes for the heatmaps were selected from the DEGs ($p \leq 0.05$) found under the significant GO terms including words "heart" and "cardiac" as well as genes that are expressed primarily in cardiomyocytes (Jiang et al. 2018; Karbassi et al. 2020; Ronaldson-Bouchard et al. 2018). The gene

expression of the samples was also compared to mature heart tissue RNA sequencing data from the Genotype-Tissue Expression (GTEx) (Lonsdale et al. 2013) as a positive control.

4.3.4 Electrophysiology

Electrophysiological measurements were performed in **study I**. Extracellular field potentials were recorded using micro electrode arrays (MEA). The cardiac tissue models were cultured on 24- and 96-well MEA plates (Multi Channel Systems, 24W700/100F-288 and 96W700/100F-288). The electrical activity was recorded with Multiwell-Screen software (Multi Channel Systems) with a 20 kHz sampling frequency on days 8–9 after cardiomyocyte seeding and analysed with Multiwell-Analyzer software (Multi Channel Systems). The temperature was set at 37°C and the cells were supplied with 5% CO_2 during the measurements. First, spontaneous baseline activity was recorded for two minutes. The ½ logarithmic cumulative concentration series from 300 pM to 10 μM were added with 8-minute wash-in periods and 2-minute recordings. The baseline measurement was thus followed by 11 measurements with the cumulative concentrations resulting in approximately 2-hour exposure from the first concentration to the end of the measurements. The data from electrodes that showed clear beating patterns, sodium spike voltage change >70 μV, and a detectable T-wave were averaged in each well. The ratio of test compound-induced changes was calculated against the recorded baseline from the same well. For each compound, we analysed the effects on field potential durations (FPD), beat rate and peak amplitude. The FPD values were corrected against the changes in beating frequency using the Fridericia formula $\mathrm{cFPD} = \mathrm{FPD}/\sqrt[3]{\mathrm{RR}}$, where RR is the RR interval.

For comparison of different vascular bases (unpublished study), cardiac tissue models on decellularized, growth-arrested, and untreated vascular networks were cultured in 6-well MEAs (Multi Channel Systems). Activity was recorded using MEA2100 System (Multi Channel Systems) and analysed using Cardiomyocyte MEA Data Analysis (CardioMDA) software (Pradhapan et al. 2013).

In **study I**, 29 drugs with known effects on heart and three negative controls known to have no effects on cardiac function were tested on MEA. Hydrophobic compounds were solubilized in dimethyl sulfoxide (DMSO) as 10 mM stocks and water-soluble compounds in distilled water as 1 mM stocks. These stocks were

diluted to the exposure medium (DMEM/F12 + 2.56 mM L-glutamine, 0.1 nM 3,3',5-Triiodo-L-thyronine sodium salt, ITS™ Premix: 1.15 µM: 6.65 µg/ml insulin, 6.65 µg/ml transferrin, 6.65 ng/ml selenious acid, 1% bovine serum albumin, 2.8 mM sodium pyruvate).

4.4 Contraction force measurement setup

In **studies II**, **III** and **IV**, the contraction force measurements were performed on a microscope (Zeiss Primovert).

4.4.1 Force measurement sensors and data acquisition

Piezoelectric materials are commonly used as sensors and actuators because of their ability for mechanical to electrical and electrical to mechanical conversion (Surbhi and Sukesha 2020). The contraction force measurement sensor types i.e., single axis, and dual axis cantilever sensors, are presented in Figure 6. The single-axis piezoelectric cantilever sensor (**study II** and **III**) consisted of a metallic cantilever attached to one end of a lead zirconate titanate (PZT) piezoelectric disc which was attached to a fixed attachment point at the other end. The dual-axis piezoelectric cantilever sensor (**studies III** and **IV**) had two piezoelectric discs perpendicular to each other forming an L-shape. The location of the measurement point between the force sensor cantilever tip and the cardiac cultures was adjusted with a 3-axis linear micromanipulator (Newport Corporation). The measurement locations were manually selected favouring wells with strong and regular beating.

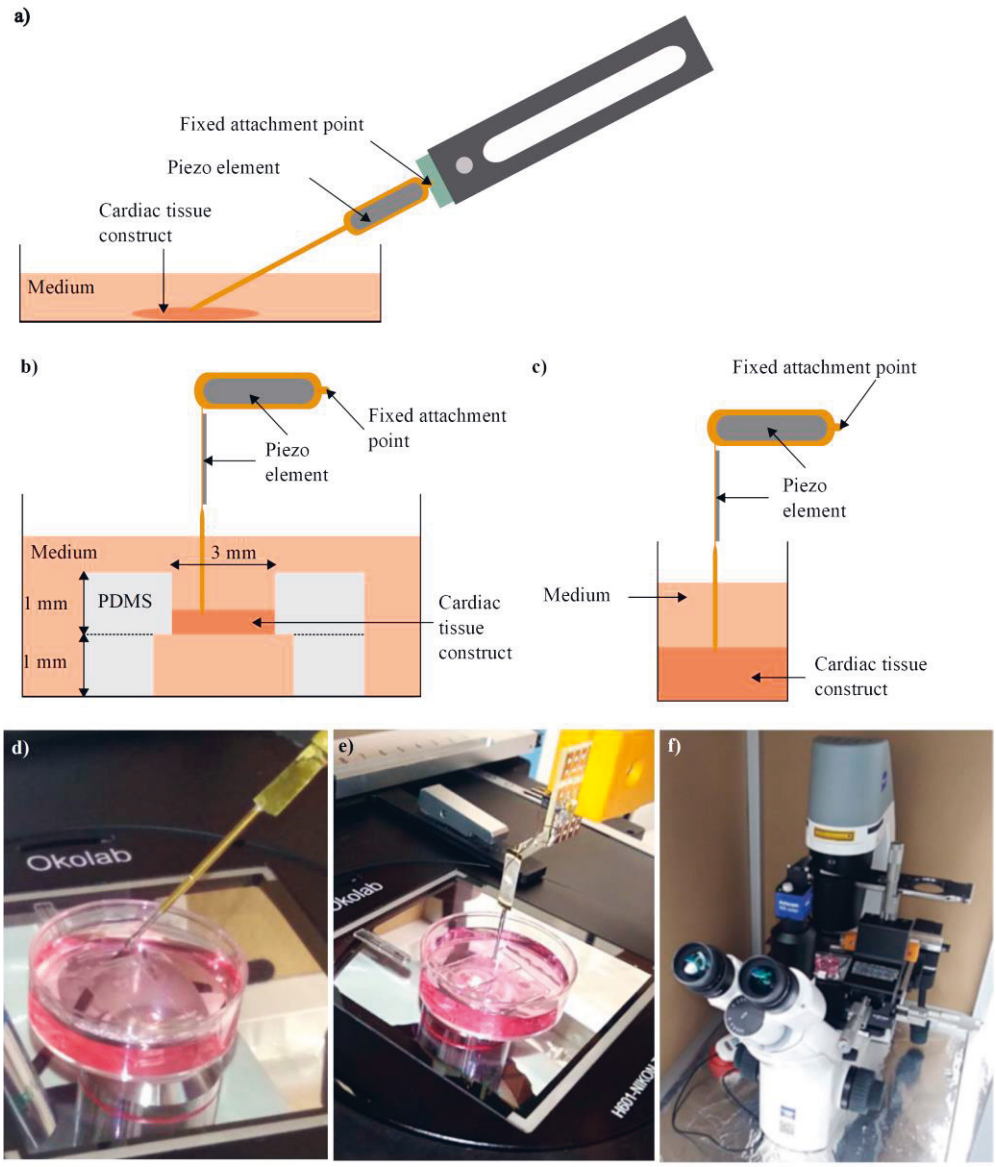

Figure 6. a) Schematic figure of the measurement setup cross section in **study II**. The single axis cantilever sensor is connected in approximately 30° angle to the cardiac tissue construct that is cultured in a wide culture dish. The sensor is attached to an arm that connects it to the micromanipulator. b) Cross section of the measurement setup in **study III** with a dual axis cantilever sensor and a lift-off cardiac construct. c) The measurement setup **in study IV** with a dual axis sensor and a cardiac tissue construct in 96-well plate. d) Single axis and e) dual axis sensors. f) Measurement setup with microscope in a faraday cage (figures d-f from **study III**, © 2021 IEEE).

The piezoelectric discs converted the mechanical strain of the cantilever to an electric form which was directed to a buffer amplifier (AD8691, Analog Devices Inc.). The amplified signal was read and processed with Arduino Due analog-to-digital converter (**study II**) or Teensy 3.6 board (PJRC.COM LLC.) (**studies III-IV**) with final 50 Hz sampling rate. Finally, the data was sent to LabVIEW software on a personal computer for data collection.

4.4.1.1 Parylene coating

The dual-axis sensor design was used in **study IV** in which it was further developed to better sustain the humid measurement environment by coating the sensor with parylene. Parylene is a common polymer coating material with inherent biocompatibility, biostability and conformal nature of deposited film (Kuppusami and Oskouei 2015; Zeniieh et al. 2013). The connectors of the sensors were taped before the coating process to prevent the coating materials from getting inside the connectors. A 10 μm parylene coating was deposited on the sensor in a vacuum chamber using a Para Tech Lab Top Parylene Coater (Model 3000). In short, 10 g of a raw powder called dimer (Dichloro-p-cyclophane, $C_{16}H_{14}Cl_2$) was fed in the heating tube of the coater. First, the dimer was heated up in the vacuum atmosphere vaporizing it as the dimeric gas. Next, the dimeric gas was pyrolyzed to the monomeric form of the dimer, and the gas was deposited on the surface of the sample in the vacuum chamber held at room temperature.

4.4.1.2 Sensor calibration

The force sensors were calibrated using a texture analyser Stable Micro Systems TA.XTPlus (Stable Micro Systems Ltd, Surrey, United Kingdom). Comparing the force needed for a displacement, measured by the texture analyser, with the cantilever sensor output data we determined the convergence factors for each sensor for calculating the absolute forces measured from the cardiac tissue constructs.

4.4.2 Environmental control during force measurements

The following adjustments were used in **studies III** and **IV**. Before the force measurements, the CO_2-dependent sodium bicarbonate buffered cell culture

medium was replaced with serum-free Leibovitz's L-15 medium (Gibco, 11415) which is buffered by phosphates and free base amino acids to maintain its pH outside the CO_2 incubators. If the temperature differs from the optimal 37°C, cardiomyocytes change their beating behaviour (Laurila et al. 2016). During the measurements, the cell culture vessels were placed on a heater plate (Okolab, H601-NIKON-TS2R-GLASS) on the microscope to keep them at 37°C. Moreover, the microscope was placed inside a custom-made faraday cage that also prevented airflow and light from disturbing the measurements (Figure 6f).

4.4.3 Inotropic drug exposures

In **study IV**, positive inotropes isoproterenol (Sigma Aldrich, I5627), milrinone (Tocris, 1504) and omecamtiv mecarbil (Adooq Biosciences, A11206), and negative inotropes verapamil (Tocris, 0654) and propranolol (Sigma Aldrich, P0884) were tested. The drug solutions were prepared freshly before use. Isoproterenol and verapamil were solubilized in distilled water (Gibco, 15230-071) as 10 mM stock. Propranolol and omecamtiv mecarbil were solubilized in DMSO (Sigma, D2650) as 10 mM, and milrinone as 50 mM stock. They were diluted in serum-free L-15 medium (Gibco, 11415). During the measurements, the test compounds were administered in 5 µl volumes directly into the wells diluting them to the final concentrations. The well volume was initially 200 µl and after the final, third administration 215 µl. The amount of DMSO in the final concentrations of omecamtiv mecarbil and propranolol did not exceed 0.003%. For milrinone, the amounts of DMSO in the final concentrations were 0.002%, 0.02% and 0.2%.

During the force measurements in **study IV**, a 3-min baseline activity was measured first, followed by administration of the first concentration of the test drug from the cumulative concentration series of three increasing concentrations. The activity was measured 10 min after adding each drug concentration.

4.5 Force measurement data analysis

The force measurement data were analysed using Octave software (GNU Octave) (**studies II-IV**).

In **study III**, the 60-second raw data recordings were first filtered with a bandpass Butterworth filter. For the dual-axis sensor data, the total force was calculated using both x- and y-channels and their rotation angle. The upward peaks were detected by finding the local maxima above a threshold value that was set to 0.4 of the one highest data point in the measurement file. Beating rate was calculated from the peak intervals. The displacement was calculated from the forces and spring constant of the sensor in both x- and y-axes.

In **study IV**, two-minute periods of the recordings were selected for the analyses so that 2 min was taken from the end of the (approximately 3-minute long) baseline measurements, and 2 min was taken between 8–10 min after the administration of each drug concentration (>10 min recordings). The data were first filtered using a moving average filter with a window size of 2 s. The filtered data were then used for peak detection. The upward and downward peaks were detected separately by finding the local maxima above an adaptive threshold that was set to include 4–10% of the highest force value data points in the filtered data. The threshold percentage 4–10% was selected based on the beating frequency and total peak count in the 2 min recordings. The peak pairs were formed by selecting the closest upward and downward peaks. The peak pairs were used for calculating the peak-to-peak (P-P) amplitudes from the unfiltered data. Beating frequency was calculated from the peak intervals. For each well, the results from either x or y channel of the dual axis sensor were selected based on peak detection success i.e., more detected peaks. The same channel was selected from the four consecutive measurements (baseline and three increasing drug concentrations) of the same well to enable comparison between them. The effects of the drugs were normalized for comparison among different wells by calculating the percentage change from the baseline activity of the same well.

4.6 Statistical analyses

For electrophysiology results (**study I**), the p-values were calculated using Student's two-tailed t-test in Excel (Microsoft), and half maximal effective concentration (EC_{50}) and half maximal inhibitory concentration (IC_{50}) values were calculated using non-linear fit four-parameters logistic equation Prism version 5.0. (GraphPad). The correlation between EC_{50} values and clinical plasma concentrations was calculated using Pearson r and Goodness of fit was expressed as R^2. To test the statistical

significance cell and myofibril circular variances, independent samples Mann-Whitney U test was performed in IBM SPSS Statistics 27.

In **study IV**, statistical analyses were performed in IBM SPSS Statistics 27. Kruskal-Wallis test with Bonferroni correction was used to test the statistical significance of the changes in beat frequency and peak-to-peak force amplitudes in different drug concentrations and baseline measurements. The p-values <0.05 were considered statistically significant.

5 SUMMARY OF THE RESULTS

5.1 Cardiac tissue model

To select a vascular base for the cardiac tissue model, three different vascular bases and cardiomyocyte monoculture were compared. The decellularized vascular base, growth-arrested vascular base and untreated hASC-HUVEC vascular base promoted cardiomyocyte alignment compared to monocultured cardiomyocytes (Figure 7a and b, Figure 8). Both vascular bases containing hASC-HUVEC layer under the cardiomyocytes i.e., growth-arrested vascular base and untreated vascular base, attenuated extracellular field potentials on MEA and resulted in lower signal-to-noise ratio (SNR) compared to decellularized vascular base or cardiomyocyte monoculture (Figure 7c and d). The active electrodes are defined as electrodes that give a reliable beat rate result. This depends on the actual electrical activity of the cardiomyocytes but also on the quality of the signal which needs to be sufficient for the analysis i.e., regularity of the beating and synchronicity of the cells in the proximity of the electrode, and SNR. The synchronicity of the beating increases from day 3 to day 10. However, the percentage of active electrodes did not increase in the untreated vascular base group likely due to the growth of the vascular base which acts as an insulating layer between the cardiomyocytes and the electrodes and possibly between cardiomyocytes inhibiting direct cell-cell contacts between cardiomyocytes. Therefore, the growth-arrested vascular base was superior to the untreated hASC-HUVEC vascular base regarding the percentage of active electrodes. Moreover, the recorded peak-to-peak amplitudes of the sodium peaks were higher from the cardiomyocyte monoculture and decellularized vascular base groups compared to the vascular bases containing hASC-HUVEC layer under the cardiomyocytes i.e., growth-arrested vascular base and untreated vascular base (unpublished results).

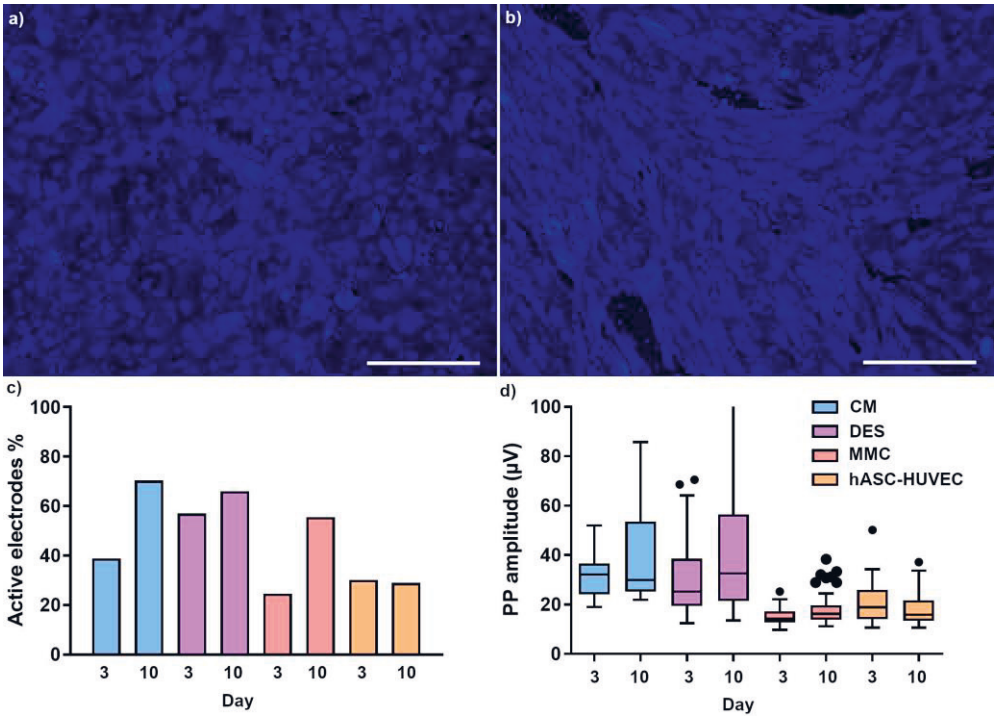

Figure 7. Cardiac troponin T (cTnT) positive cardiomyocytes a) in cardiomyocyte monoculture and b) on decellularized vascular base 13 days after cardiomyocyte seeding. Scale bar 200 µm. c) The percentage of active electrodes and d) peak-to-peak amplitudes from MEA recordings of cardiac cultures with the different vascular bases and monoculture (number of parallel wells n = 6 in CM, n = 18 in DES, MMC and hASC-HUVEC). CM = cardiomyocyte monoculture, DES = decellularized vascular base, MMC = growth-arrested vascular base, hASC-HUVEC = untreated vascular base. (unpublished results).

The growth-arrested vascular base was selected for further development including the characterisation and relevance studies of the model and comparison with monoculture (**study I**), and studies with the beating force measurement technology (**studies III–IV**) except **study II** which was done with the untreated vascular base. The selection was based on the anticipated beneficial cell-cell interaction among the different cell types of the vascular base and cardiomyocytes, and its suitability to long-term cultures unlike the untreated vascular base which tended to overgrow in longer cultures. Decreasing the amount of cell divisions in the growth-arrested vascular base prevents the overgrowth of the cells but enables the formation of vascular-like networks (unpublished results).

5.1.1 Structural characterization

The cardiac tissue model was characterized structurally using immunofluorescence and TEM imaging to study the presence of different cell types, cardiomyocyte morphology, and subcellular structures of the cells. The structure of the cardiomyocytes in the model was compared to cardiomyocyte monoculture to evaluate the anticipated beneficial effects of the vascular base. Furthermore, the structure of the model was studied to evaluate the resemblance to native myocardium.

Immunofluorescence images confirm the presence of cardiac troponin T (cTnT)- and α-actinin-positive cardiomyocytes with vWf-positive endothelial cells in the cardiac tissue model (Figure 8). The cardiomyocytes in the cardiac tissue model show more mature morphology with elongated cardiomyocytes and aligned myofibrils compared to cardiomyocyte monoculture with circular and unoriented cells. The structural characterization results are included in **study I**.

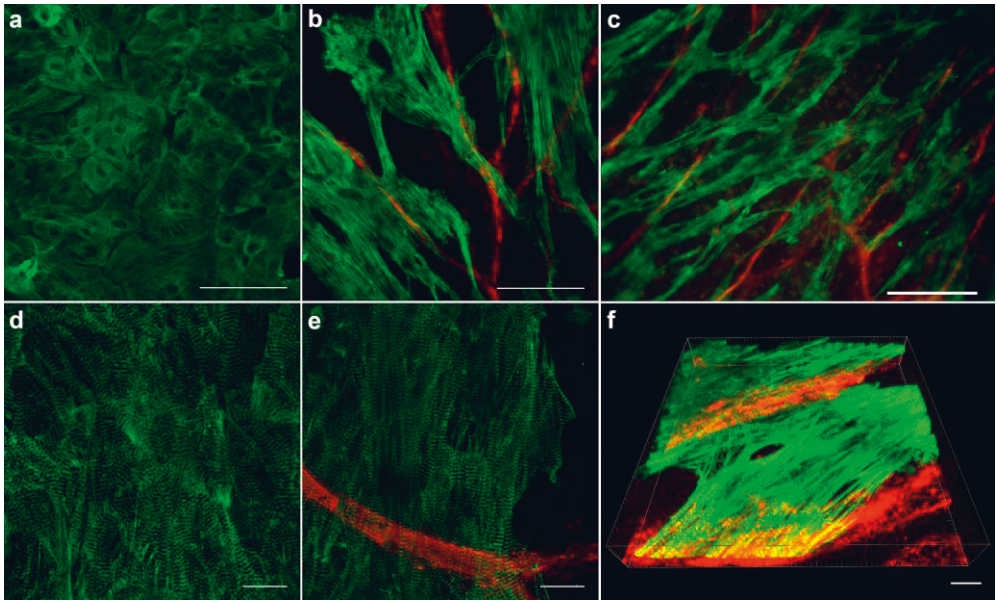

Figure 8. Cardiomyocytes in a) cardiomyocyte monoculture, b) in cardiac tissue model, and c) in cardiac tissue model cultured for force measurement application on a fibrin hydrogel. Myofibrils in d) cardiomyocyte monoculture and e) cardiac tissue model. f) 3D image of cardiac tissue model. Imaged at day 8 after cardiomyocyte seeding except c at day 9. red = vWf; green = cTnT in a-c, f; green = α-act in d-e. Scale bar 100 µm in a-b; 200 µm in c; 20 µm in d-e; 15 µm in f. Image c from publication IV, image f from publication I.

TEM images of the cardiac tissue model are presented in Figure 9. After one week in culture, cardiomyocytes with highly organized and aligned sarcomeres have connected to each other by intercalated discs and desmosomes. However, cardiomyocytes of different maturity stages are present and the number of myofilaments and mitochondria in the cells varies. In addition to cardiomyocytes, endothelial cells and myofibroblasts are present. The results are included in **study I**.

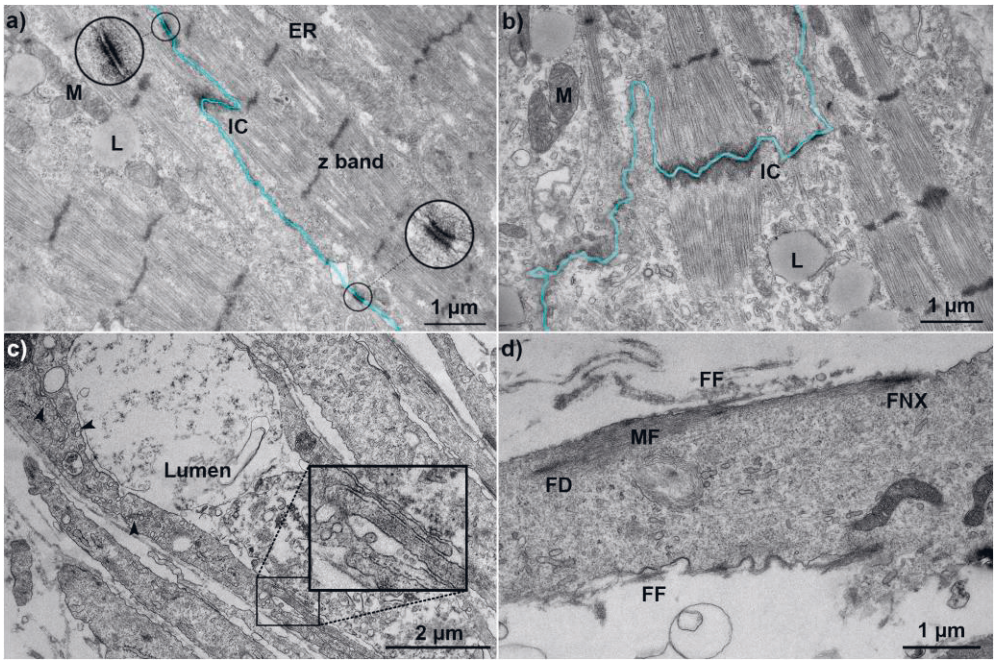

Figure 9. TEM images of cardiac tissue model. Light blue indicates the line between two adjacent cardiomyocytes with highly developed and aligned sarcomeres 6 days after cardiomyocyte seeding in (a) and (b). a) Intercalated discs (IC) and desmosome connections (circled and magnified) between cardiomyocytes. M=mitochondria, L=lipid droplet, ER=endoplasmic reticulum. b) The transverse section of an IC is located at sarcomere z band. c) Endothelial cells with transcytotic vesicles (arrow heads) have formed endothelial cell-endothelial cell junctions (magnified in the box) and a vessel lumen 1 day after cardiomyocyte seeding. d) A myofibroblast 6 days after cardiomyocyte seeding. FD=focal density, FF=fibronectin filament, FNX=fibronexus, MF=myofilament. Images a, c, d modified from publication I.

The results from the structural characterization show that the coculture with the vascular base improves the structural maturity of the cardiomyocytes. The cardiac tissue model also contains relevant cardiac cell types present in native myocardium.

5.1.2 Gene expression

The gene expression profile of the cardiac tissue model was compared to cardiomyocyte monoculture to evaluate the anticipated beneficial effects of the vascular base. The gene expression results are included in **study I**. The principal component analysis (PCA) plot using top 500 most variable genes and variance stabilizing transformation (DESeq2) is shown in Figure 10a. The cardiomyocyte monoculture and cardiac tissue model samples at the two time points are separated from each other. Comparing to the GTEx data (Lonsdale et al. 2013), the PCA results show greater similarity between the mature heart tissue and the cardiac tissue model than the mature heart tissue and the cardiomyocyte monoculture along the PC1, attributing to 68% of inter-sample variance. The 500 most variable genes were also found enriched with heart-specific genes that were previously identified from the GTEx data (Ahn et al. 2020) indicating that the PCA captures information from relevant genes.

The log2fold changes for selected genes from day 1 to day 7 are shown in Figure 10b for cardiomyocyte monoculture and cardiac tissue model. The gene expression shifted towards mature type as several foetal or immaturity markers were downregulated, and maturity markers were upregulated in the model. For example, the structural maturity markers *MYH7, MYL2, TCAP* and *TNNI3* were upregulated and the foetal/progenitor markers *CACNG7, ERBB4, HES1, SALL1*, and *SNAI1* were downregulated in the model. The gene expression results show that the cardiomyocytes in the cardiac tissue model mature more during the one-week culture compared to cardiomyocytes in monoculture. The gene expression profiles of the cardiac tissue model show characteristics of adult human heart.

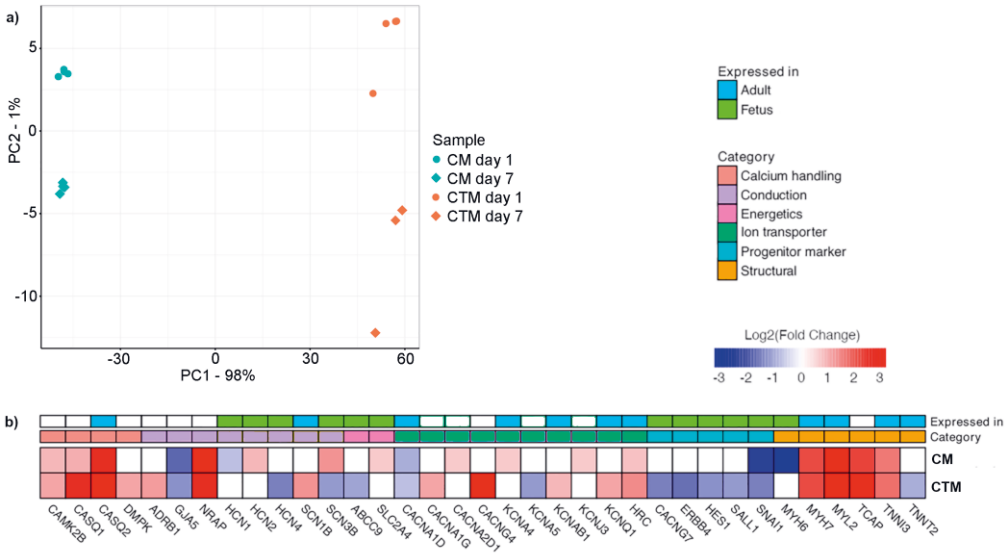

Figure 10. The gene expression results from cardiac tissue model and cardiomyocyte monoculture. a) PCA plot of cardiomyocyte monoculture (CM) and cardiac tissue model (CTM) day 1 and day 7 samples using top 500 most variable genes and variance stabilizing transformation (DESeq2). Numbers attached to the principal components correspond to the percentage of variance that is attributed to it. b) Heatmap of the log2-transformed fold changes (day 1 to day 7) of the CM and CTM samples. Pre-selected genes of interest are annotated according to category and typical site of expression. Values for genes with a statistically insignificant fold change (padj>0.05) are not reported. Image modified from publication I.

5.1.3 Functional characterization with known drugs with different mechanisms

The functionality of the cardiac tissue model was studied using known drugs with different effects on cardiac function to evaluate the suitability of the model to predict drug-induced effects on human heart. Field potential duration, beat rate, and Na^+ peak amplitude EC_{50} values of all test compounds are presented in Table 4. The results are included in **study I**.

Table 4. Field potential duration (FPD), beat rate (BPM), and Na^+ peak amplitude (Amp) EC_{50} values of all test compounds and therapeutic concentration of the compound (C therapeutic). The reported concentrations from our model are the total (nominal) concentrations, and the therapeutic concentrations from the literature are the free plasma concentrations. Table modified from publication I.

End-point	Compound	Known mechanism	Action	FPD EC_{50} (nM)	BPM EC_{50} (nM)	Amp EC_{50} (nM)	C therapeutic (nM)
FPD	Alfuzosin	QT prolonging	Na^+ channel activator, α-AR antagonist	↑3,228	↓6,775	↓6,528	56 (Guo et al. 2013)
	Haloperidol	QT prolonging	K^+ channel blocker	↑22.71	↓45.21	↓103.1	45 (Ando et al. 2017)
	Astemizole	QT prolonging	hERG blocker	↑33.12	↓1,043	↓1,274	8 (Guo et al. 2013)
	Cisapride	QT prolonging	hERG blocker	↑10.58	↓3,694	↓4,432	2.5 (Blinova et al. 2017)
	Dofetilide	QT prolonging	hERG blocker	↑1.638	↓2.085	↓3.491	2 (Ando et al. 2017)
	E-4031	QT prolonging	hERG blocker	↑5.001	↓57.38	↓50.68	8.4 (Ando et al. 2017)
	Moxifloxasin	QT prolonging	hERG blocker	↑2,431	-	-	5,600 (Ando et al. 2017)
	Sotalol	QT prolonging	hERG blocker	↑4,209	↓6,051	-	13,000 (Ando et al. 2017)
	Thioridazine	QT prolonging	hERG blocker	↑45.43	↓2,239	↓1,854	45 (Ando et al. 2017)
	Tolterodine	QT prolonging	hERG blocker	↑502.8	↓4,593	↓3,046	5
	Pimozide	QT prolonging	hERG and Ca^{2+} channel blocker	↑5.643	↓1,466	↓307	3.7 (Sirenko et al. 2013)
	Isradipine	QT shortening	L-type Ca^{2+} channel blocker	↓36.57	↑109.8	↓3,314	80 (Sirenko et al. 2013)
	Nifedipine	QT shortening	L-type Ca^{2+} channel blocker	↓89.56	↑296.9	↓7,797	190 (Ando et al. 2017)
	Verapamil	QT shortening	L-type Ca^{2+} channel blocker	↓285.3	↑103.6	↓2,633	92 (Ando et al. 2017)
BPM	Digoxin	Pos. inotropic	Na/K ATPase blocker	-	↑111.2	-	2.8 (Sirenko et al. 2013)
	Dopamine	Pos. inotropic	dopamine receptor, AR agonist	↓109.3	↑119.4	-	300 (20% increase)
	Epinephrine	Pos. inotropic	AR agonist	-	↑183.5	-	2.64 (Stratton et al. 1985)
	Isoprenaline	Pos. inotropic	AR agonist	-	↑31.53	↑33.65	0.84 (Stratton et al. 1992)
	Doxazosin	Neg. inotropic	α1-AR blocker	↑29.17	↓220.6	↓288.5	133 (Sirenko et al. 2013)
	Propranolol	Neg. inotropic	AR blocker	-	↓6,902	↓7,606	1,095 (Oh, Chia, and Taylor 1985)

Amp	Flecainide	Neg. inotropic	Na^+ channel blocker	↑162.9	↓1,297	↓1,516	1,160 (Ando et al. 2017)
	Lidocaine	Neg. inotropic	Na^+ channel blocker	-	↓4,980	↓5,157	2,500 (Blinova et al. 2017)
	Quinidine	QT prolonging	Na^+ channel blocker	↑505.9	↓5,061	↓3,701	3,240 (Ando et al. 2017)
	Ranolazine	Neg. inotropic, QT prolonging	Na^+ channel blocker, hERG blocker	-	↓8,579	↓9,709	6010 (Guo et al. 2013)
	Terfenadine	QT prolonging	hERG blocker, multi-channel blocker	↓900.2	↓1,419	↓680.4	300 (Guo et al. 2013)
	Terodiline	QT prolonging	hERG blocker, Ca^{2+} channel blocker	-	↓3,805	↓2,607	1,800 (Ando et al. 2017)
No end-point	Acetyl salicylic acid	No effect on heart function		-	-	-	-
	Hexylresorcinol	No effect on heart function		-	-	-	-
	Ibuprofen	No effect on heart function		-	-	-	-
	Doxorubicin	Apoptotic	ROS?	-	-	-	
	Levosimendan	Pos. inotropic	Ca^{2+} sensitizer	-	-	-	129 (Guo et al. 2013)
	Pentamidine	QT prolonging	Effects hERG channel transport	-	-	-	190 (Sirenko et al. 2013)

↑ = increase in the measured parameter; ↓ = decrease in the measured parameter; AR = adrenoceptor; EC50 = half maximal effective concentration; hERG = Human ether-à-go-go, voltage-gated K^+ channel Kv11.1; ROS = reactive oxygen species

Cardiac tissue model showed high predictivity in drug testing with high correlation to human data (Figure 11). The model predicted the cardiac effects with a predictive accuracy of 91%, sensitivity of 90% and specificity of 100%. The correlation between EC_{50} values and clinical i.e., therapeutic plasma peak concentrations of 26 drugs was $r = 0.852$ and the goodness of fit $R^2 = 0.726$. The three drugs with no effect on heart function i.e., acetyl salicylic acid, hexylresorcinol, and ibuprofen, were excluded from the correlation analysis as well as doxorubicin, levosimendan, and pentamidine whose effects were not detected in the study (see Chapter 6.1).

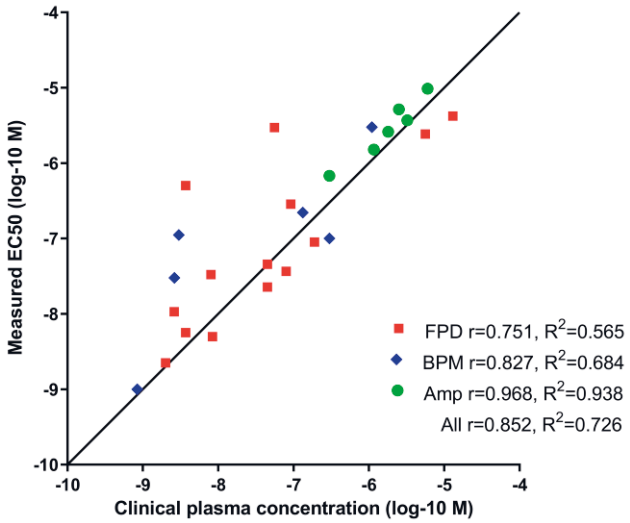

Figure 11. The correlation between measured EC_{50} values and clinical plasma concentrations of the 26 drugs with detected effects on cardiac function. Image from publication I.

The results from the functional characterization show that the cardiac tissue model can be used to test acute drug-induced effects on human heart. The cardiac tissue model mimics well the electrophysiological function of the native myocardium and the data obtained from the model is transferable to clinical setting for evaluation of drug-induced cardiac effects.

5.2 Contraction force measurements

Contraction force measurements were performed to evaluate the functionality of the measurement technology and the functionality of the cardiac tissue model. Contraction force measurements were performed in **studies II-IV**. Summary of the measurements including sensor types, culture platforms and measurement results is presented in Table 5. The **study IV** results include the baseline measurements without inotropic drug exposures. The measured contraction forces were in μN range in all measurement setups. The self-differentiated cardiomyocytes in **study II** had higher beating rate than the iCell Cardiomyocytes² in **studies III-IV**. The number of measurements in **study II** was 5 technical replicates from the same well. The number of wells in **study III** was 4 parallel wells for both sensor types, and the number of wells in **study IV** was in total 40 wells from 5 independent repeats.

Table 5. Force measurements in **studies II-IV**. The results are presented as mean and SD of beat rates and forces except the beat rate results from **study III**.

Study	Culture platform	Sensor type	Beat rate (BPM)	Contraction force (μN)	Number of
II	PDMS mould on 60-mm dish & spontaneous growth	single axis	46.1 (SD 2.3)	P-P: 13.3 (SD 3.6)	measurements: 5
III	lift-off PDMS on 35-mm dish	single axis	range 22–38	4.5 (SD 1.5)	wells: 4
		dual axis	range 19–25	10.3 (SD 0.8)	wells: 4
IV	hydrogels in 96-well plates	dual axis	21.2 (SD 7.0)	P-P: 331.0 (SD 602.2)	wells: 40

PDMS = polydimethylsiloxane; P-P = peak-to-peak force

Examples of the contraction force waveforms are presented in Figure 12. Butterworth filtering affected the single axis and dual axis waveforms from **study III** (Figure 12a and Figure 12b, respectively) while the waveform from **study IV** (Figure 12c) represents the signal without the effect of filtering.

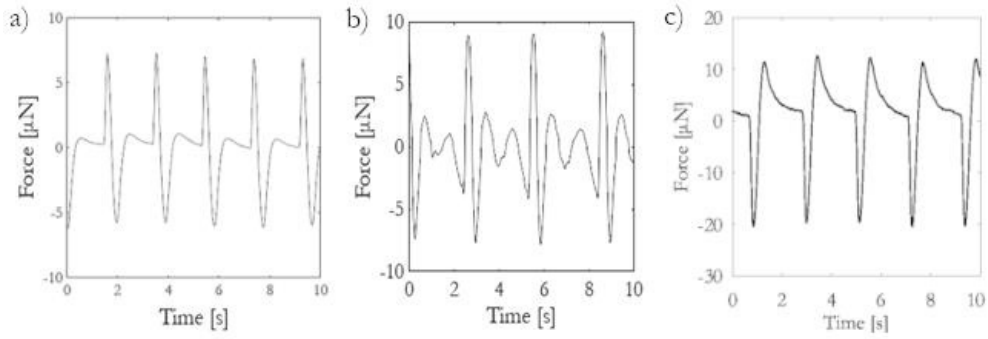

Figure 12. Example signals from a) single axis and b) dual axis measurements, and c) dual axis measurements without Butterworth filtering (a and b from **study III**, © 2021 IEEE).

The contraction force measurement results show that the piezoelectric cantilever sensors are able to detect the contraction forces of cardiac tissue models. Both single axis and dual axis sensor types were successfully used for measuring the cardiac contraction forces from different cell culture platforms.

5.2.1 Functional characterisation with known inotropes

Functional characterization was performed using known inotropic drugs to evaluate the functionality of the cardiac tissue model and the suitability of the measurement technology to detect drug-induced effects on the cardiac contraction forces. Drug-induced inotropic effects were measured in **study IV**. The beat rate and peak-to-peak contraction force amplitudes during baseline measurements and the percentage changes during the cumulative concentration series of the inotropic drugs are presented in Figure 13. The positive chronotropic effects of 30 nM and 100 nM isoprenaline (p-values 0.016 and 0.005, respectively), 100 μM milrinone (p-value >0.001), and 100 nM verapamil (p-value 0.007), and negative chronotropic effect of 300 nM propranolol (p-value 0.010) were statistically significant. Even though both positive and negative inotropic effects were observed e.g., positive trend in isoprenaline and milrinone and negative trend in verapamil, the changes in contraction force were not statistically significant for any of the tested drugs. The number of wells for isoprenaline was 3 parallel wells from 2 independent repeats (n=6), for milrinone 3 parallel wells from 3 repeats (n=9), for omacamtiv mecarbil 3–4 parallel wells from 3 repeats (n=10 wells), for propranolol 3 parallel wells from 3 repeats (n=9), and for verapamil 3 parallel wells from 2 repeats (n=6). The contraction force measurement system with the cardiac tissue model have potential to be used for testing both positive and negative drug-induced inotropic effects with different mechanisms on the cardiac function.

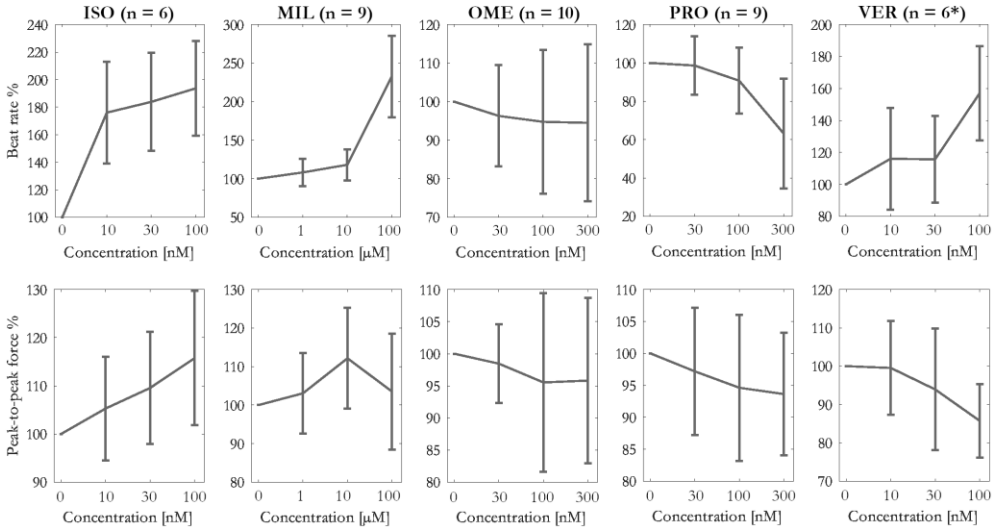

Figure 13. Percentage change of beat rate (top row) and peak-to-peak force (bottom row) in the cumulative concentrations of positive inotropes isoprenaline (ISO), milrinone (MIL), omecamtiv mecarbil (OME), and negative inotropes propranolol (PRO) and verapamil (VER) exposures. Mean and SD. *) n = 4 wells at 100 nM verapamil.

6 DISCUSSION

Drug-induced adverse cardiac effects are a major reason for discontinuations of drug development and post-approval market withdrawals (Magdy et al. 2018). The high attrition rates at clinical phases and at post-approval stage show the inadequacy of the current nonclinical cardiac safety and efficacy testing methods to predict human effects. *In vivo* testing with animal models does not sufficiently represent the human heart function (Mathur et al. 2016). Thus, there is an unmet need for models better mimicking the human biology. For this purpose, human cell -based models serve as a potential valuable tool. Because of the complexity of the heart function, *in vitro* testing would benefit from more tissue-like models instead of focusing on single cell models or testing drug-induced effects on only one vulnerable ion channel (Magdy et al. 2018).

Requirements for an adequate model are that it should be repeatable, reproducible, and relevant to predict the aimed effect in human. A model for predicting drug-induced cardiac effects should have human cardiac type electrophysiological properties, relevant ion channels (calcium, sodium, and potassium channels), cell-cell junctions enabling communication and synchronism, and exhibit measurable spontaneous (or stimulated) beating activity. A model also enabling the measurement of cardiac contraction force should also have the intracellular structures that enable the production of contraction forces (i.e., excitation contraction coupling, contraction machinery) and the intercellular structures that enable the transmission of the mechanical force. To determine drug-induced effects, the range of the measured activity needs to be large enough so that the measurement system is able to detect the drug-induced changes and determine the concentration-response relationships.

The ideal cardiac model would be a multicellular tissue model containing relevant cardiac cell types with 3D structure. It should enable contraction force measurements which allow the testing of drug-induced effects on the cardiac function in a complementary way to what electrophysiological measurements offer.

In that way the model would provide information on most critical cardiac effects and serve as a valuable tool for drug development and testing.

This PhD thesis consisted of two parts: the development of the cardiac tissue model, and the development of the contraction force measurement system as an additional feature for the cardiac tissue model.

6.1 Development of the cardiac tissue model

The cardiac tissue model developed in this work was built on previous work in our research group. The cardiac tissue model developed previously in FICAM first consisted of HUVECs with hASCs or fibroblasts, and neonatal rat cardiomyocytes (Vuorenpää et al. 2014) and later of HUVECs, fibroblasts and hPSC-derived cardiomyocytes (Vuorenpää et al. 2017). Both hASC-HUVEC and fibroblast-HUVEC vascular network bases supported the rat cardiomyocyte functionality and viability, but he hASC-HUVEC coculture formed denser vascular network compared to fibroblast-HUVEC coculture (Vuorenpää et al. 2014). The human cell -based model with fibroblast-HUVEC vascular base and hPSC-derived cardiomyocytes was stable and promoted cardiomyocyte alignment with the vasculature (Vuorenpää et al. 2017). However, hASCs as mesenchymal stromal cells bring to the model opportunities for differentiation of auxiliary cells. Therefore, even though more challenging to handle, the vascular base with hASC-HUVEC coculture was chosen for the further development in this thesis.

Continuing the work of Vuorenpää et al. (2014; 2017), the cardiac tissue model was further optimised in this thesis for the drug development and chemical testing purposes. As an additional new feature, a contraction force measurement technology was developed to be added to the cardiac tissue model. Another upgrade of the model was the adding of a functional coating. The cardiac model of Vuorenpää et al. (2017) was implemented without a biomaterial coating. This approach functioned well with the fibroblast-HUVEC vascular base because it remained relatively well attached to the bottom of the well even with beating cardiomyocytes, while the hASC-HUVEC base detached easily (Vasaramäki 2014). Functional coating material was not easy to find since the contraction forces of beating cardiomyocytes tended to tear the tissue model off the substrate when testing several different coating materials. The coating that finally worked well was fibrin. Fibrin is a natural polymer

that is formed by polymerization of fibrinogen in the presence of thrombin. Fibrin form a highly elastic, three-dimensional fibrous network that contains a large proportion of water, forming a hydrogel. The mechanical properties of fibrin depend on the polymerisation conditions (Janmey et al. 2009). After adding the fibrin coating, the stability and the attachment of the cardiac tissue model with hASC-HUVEC vascular base was improved and allowed also long-term (several weeks) cultures.

In addition to improving the long-term attachment of the model, the addition of fibrin enabled the production of measurable contraction movement in the force measurement applications. When using MEA as the culture substrate, the coating should not be too thick because it acts as an insulator layer between the recording electrodes and the measured cells. The amplitude of the measured signal depends on the proximity of the cells to the measuring electrode (Obien et al. 2015). On the other hand, in the force measurement applications, it was beneficial to allow the movement of the cardiomyocyte contraction using an elastic culture substrate instead of a rigid one. A thicker fibrin layer provided a more elastic culture substrate for the contracting cells compared to the rigid bottom of traditional cell culture plates.

The hASC-HUVEC vascular base has been previously characterized by Huttala et al. (2015). The co-culture of hASC and HUVEC was shown to develop into a vascular-like network with a lumen, a basement membrane, and adherence junctions. In addition to mature endothelial cells, the coculture also contained pericytes and smooth muscle cells adjacent to the vessels (Huttala et al. 2015). In an intra-laboratory validation, the hASC-HUVEC coculture model was found reproducible and repeatable (Toimela et al. 2017). In **study I**, the TEM images revealed the presence of endothelial cells and myofibroblasts in the cardiac tissue model. These cell types are normally present in the healthy myocardium (Zhou and Pu 2016), except the myofibroblasts that are typically present in fibrosis because they produce large amounts of the extracellular matrix proteins. This is a logical process because at the beginning of the culture the matrix consists of fibrin and the cells are remodelling their environment by producing relevant ECM components. Myofibroblasts can arise from fibroblast-to- myofibroblast transition (D'Urso and Kurniawan 2020), which would suggest the presence of also fibroblasts in the cardiac tissue model. The heterogenous cell population of hASCs that is used for the producing the vascular-like network bases also likely contains fibroblasts. However,

they are difficult to reliably identify without specific fibroblast markers. Fibroblasts, endothelial cells, and perivascular cells participate in cell-cell communication between different cell types and together they regulate cellular organization, differentiation, viability, and function in the heart (Zamani et al. 2018).

The different cell types of the hASC-HUVEC coculture develop during the first week of culture before cardiomyocyte seeding as shown by Huttala et al. (2015) and in **study I**. According to literature, the cardiomyocyte maturation benefits from preformed vasculature more than simultaneous seeding with endothelial cells (Narmoneva et al. 2004; Iyer et al. 2009). The effect could be due to a more favourable culture environment for the cardiomyocytes (Munawar and Turnbull 2021). The formation of vascular-like networks prior to cardiomyocyte seeding also allowed the possibility to treat the vascular base with Mitomycin C without affecting the cardiomyocytes. The treatment of the vascular bases with mitomycin at day 6 was included to the protocol to prevent overgrowth of the cells in the vascular base. This growth arrest of the vascular base enables also longer culture time which is beneficial for cardiomyocyte maturation (Lewandowski et al. 2018) and would enable the testing of longer drug exposure times.

The cardiomyocytes used in the cardiac tissue model were hiPSC-CMs. They were chosen because of their human origin which makes them more suitable for modelling the human heart than animal-derived cells. As pluripotent stem cells, hiPSCs are capable of self-renewal, which makes them a good cell source. They also do not have the ethical issue related to hESCs. The hiPSC-CMs show several relevant functions including cardiac action potential and contractility. Because they express several relevant ion channels, hiPSC-CMs can be used for detecting drug-induced effects on the electrophysiology and heart function (Blinova et al. 2017).

The cardiomyocytes were differentiated from hiPSCs in **study II**. The gain of the differentiation protocol was high, but repeatability should had been improved. The differentiation process depends on multiple parameters such as cell density and exact timing of the differentiation phases. The optimization of the cardiomyocyte differentiation protocol was not included in the scope of this dissertation. To get standardized quality and sufficient amounts of hiPSC-CMs we decided to use cells from commercial sources in the **studies I** and **III**-**IV**. The commercial cells were also optimised for a fast recovery from the cryopreservation. In comparison, the recovery of the self-differentiated cardiomyocytes from the dissociation and

replating into the cocultures should had been improved. In addition, forming the single cell suspension from the self-differentiated cardiomyocytes was challenging and likely resulted in inaccuracies in the replated cardiomyocyte numbers in the cocultures. Using the commercial cardiomyocytes enabled more accurate control over the quality and amount of cardiomyocytes in the cocultures.

The structural characterization and gene expression results in **study I** indicate improved maturation of the cardiomyocytes in coculture with the hASC-HUVEC vascular networks compared to cardiomyocytes in monoculture. The pre-formed vascular-like network added and promoted the appearance of relevant cell types in our model compared to only cardiomyocyte monoculture, as shown in **study I**. The cell-cell crosstalk among these cell types and with the extracellular matrix seems to be important for the maturation of cardiomyocytes. For example, the endothelial cell-cardiomyocyte paracrine signalling is important for cardiac tissue growth and remodelling (Talman and Kivelä 2018). The localisation of cardiomyocytes next to at least one capillary ensures adequate oxygen and nutrient supply for the cardiomyocytes in the native myocardium. Moreover, the close cardiomyocyte-endothelial cell localisation enables vesicle transport and local communication between the cell types (Hsieh et al. 2006). Both of these cell types express gap junction forming connexins which may play a role in the cardiomyocyte-endothelial cell interaction (Talman and Kivelä 2018; Colliva et al. 2020). Gap junctions are also expressed in fibroblasts that participate in the electrical signalling between cardiomyocytes (Zamani et al. 2018). The mature cardiomyocyte morphology may also be mediated by cardiomyocyte-ECM connections which induce the elongated cardiomyocyte phenotype during development and enhance the structural integrity of the heart (Howard and Baudino 2014).

The cardiomyocytes continue to mature in the coculture model more compared to the cardiomyocyte monoculture. The results from the RNA sequencing and functional testing in **study I** show that the cardiomyocytes in the cardiac tissue model express relevant ion channels to produce proper electrophysiological properties to recapitulate the function of the heart for drug testing purposes.

The functional characterization with known drugs showed the functional similarity between the electrophysiology and drug responses of the cardiac tissue model and the human heart. The high goodness of fit ($R^2 = 0.726$) and correlation ($r = 0.852$) between measured IC_{50} values from the cardiac tissue model and the clinical peak

plasma concentration in **study I** showed the capability of the model to recapitulate relevant cardiac function for drug testing. These results also indicate that the model could be used for predicting concentration levels in addition to the cardiac effects. The model can be used for detecting many types of mechanisms that affect the cardiac function. The results were especially good for the compounds affecting the amplitude i.e., sodium channel blockers ($r = 0.968$, $R^2 = 0.938$). This could be due to the adult like expression of sodium channels SCN1B and SCN3B in the cardiac tissue model as SCN1B, which is predominantly expressed in adult heart, was upregulated while SCN3B, which is predominantly expressed in foetal heart, was downregulated.

The EC_{50} values of digoxin and propranolol, that affect the heart rate, differed from the clinical concentrations more than tenfold. Propranolol has been reported to block also cardiac NaV1.5 sodium channels (Wang et al. 2010), which could be responsible for the negative chronotropic effect instead of blocking β-adrenoceptors in the absence of adrenergic stimulation in the model. Digoxin increases the intracellular calcium level by inhibiting the Na^+/K^+ pump in the cell membrane. This increases the contractility but also the risk of tachycardia. The distribution of digoxin in human is slow (approximately 6 hours) which causes inaccurate results in the serum concentration if they are measured less than six hours after the last dose. Moreover, several conditions can increase sensitivity to digoxin e.g., hypokalaemia, hypomagnesaemia, hypercalcaemia, or myocardial ischaemia (Pincus 2016). These conditions are not present in the model in which the drug distribution is also fast.

The EC_{50} values of QT-prolonging drugs alfuzosin and tolterodine were more than tenfold above the clinical plasma concentrations. Alfuzosin has been reported to cause a mild QT increase in patients at high doses (100 nM), and significantly prolong the QT interval *in vitro* at 300 nM (Lacerda et al. 2008). A statistically significant 20% increase in FPD was detected in the cardiac tissue model at 300 nM (**study I**). Tolterodine does not have a QT prolonging effect in clinical use (Malhotra et al. 2007), and *in vitro*, the QT-prolonging effect has been reported only with a very high concentration. The QT prolonging effects of alfuzosin and tolterodine have been reported clinically in plasma concentrations above the normal plasma concentration, which is supported by our data. Therefore, it is logical that the measured EC_{50} values would not precisely correlate with the reported clinical concentrations. This also suggests that our model could be used for predicting the safety margins of the drugs.

The effects of doxorubicin, levosimendan, and pentamidine were not detected in the test in **study I**. The cumulative exposure time from the beginning of the exposure with increasing concentrations in every 10 minutes was 2 hours at the end of the last measurement. It was likely too short for doxorubicin-induced apoptotic effects which have been reported in hiPSC-CMs after two days of exposure (Louisse et al. 2017). The positive inotropic effect of levosimendan could not be detected using MEA recordings which measures the extracellular field potentials. Levosimendan increases the calcium affinity of troponin (Hasenfuss and Teerlink 2011), which does not affect the MEA parameters. The pentamidine-induced FPD prolongation by blocking of the transport of hERG channels to the cardiomyocyte plasma membrane (Kuryshev et al. 2005) was likely not detected because the half-life of hERG channels is 2.8 hours (Osterbur Badhey et al. 2017) and the pentamidine concentration exceeded the clinical plasma concentration only for 50 minutes in the test in **study I**. The exposure and measurement protocol used in the study allowed only the detection of acute effects on the cardiomyocyte electrophysiology. Extending the exposure time would better enable the detection of effects that require longer time to emerge such as doxorubicin-induced apoptotic effects or effects on the channel transport.

The QT-prolonging effects of terfenadine and terodiline were not detected in our test in **study I**. For terfenadine we instead detected FPD shortening after a non-significant 10% increase in FPD similar to Mehta et al. (2013). Terfenadine is a multichannel blocker (Ming and Nordin 1995) with reported IC_{50} values to calcium channels at 185 nM (Hove-Madsen et al. 2006), hERG channel at 350 nM (Roy et al. 1996), and sodium channels at 930 nM in canine atrial myocytes (Lu and Wang 1999), which could explain the unexpected result in the cardiac tissue model. In the test, terfenadine-induced blocking of sodium channels appeared to be the major effect. This effect has also been previously reported in cardiomyocyte monocultures (Mehta et al. 2013). For terodiline, we detected cardiotoxic effects on amplitude with an EC_{50} value close to the reported toxic plasma concentration for terodiline in humans (Andersson 1984). The optical isomers R- and S-terodiline, which were present in the racemic terodiline used in the test, have different cardiac effects. R-terodiline causes FPD prolongation (Hartigan-Go et al. 1996) while S-terodiline causes blocking of calcium channels (Hayashi et al. 1997). The FPD shortening effect of S-terodiline likely concealed the FPD prolonging effect of R-terodiline.

The negative controls acetyl salicylic acid, hexylresorcinol and ibuprofen did not affect the measured MEA parameters, as expected. This further indicates the relevance of the model in mimicking the functionality of the human heart.

6.2 Comparison of cardiac tissue models

Table 6 presents the cardiac tissue model developed in this thesis compared with other advanced cardiac models structurally, in gene expression, and if they were characterized functionally, and whether the models were combined with a direct or indirect contraction force measurement method.

Table 6. Comparison of cardiac models. The + symbols describe the maturity level of the model in structural and gene expression levels, and functionally, i.e., correct detection of drug-induced cardiac effects, or the extensivity of testing in the study.

Coculture model	Structure	Gene expression	Functionality	Force measurement	Reference
hiPSC-CM + hASC + HUVEC	++	++	+++	direct	(this work)
hiPSC-CM + FB	+++	++	+	direct	(Ronaldson-Bouchard et al. 2018; 2019)
hiPSC-CM + FB	+	+	NA	NA	(Beauchamp et al. 2020)
hiPSC-CM + FB + EC	+++	++	+	indirect	(Giacomelli et al. 2020)
hiPSC-CM	++	+	+++	indirect	(Mannhardt et al. 2016; 2017)

EC = endothelial cell; FB = fibroblast; hASC = human adipose stromal cells; hiPSC-CM = human induced pluripotent cell -derived cardiomyocyte; HUVEC = human umbilical cord vein endothelial cell; NA = not available

Advanced cardiac tissue models including the coculture of hiPSC-CM and fibroblast were developed by Ronaldson-Bouchard et al. (2018; 2019) and Beauchamp et al. (2020). The cardiac model of Ronaldson-Bouchard et al. (2018; 2019) consisted of cardiomyocytes and dermal fibroblasts encapsulated in a fibrin hydrogel. The cardiac construct was attached between flexible pillars for passive mechanical stretching and electrical stimulation was applied. The passive stretching between the pillars induced cardiomyocyte elongation and alignment. Moreover, the tissues contracted against the load of the pillars mimicking physiological auxotonic contractions. Their method enhanced the cardiomyocyte maturity including adult-like gene expression profiles,

improved intracellular structure such as physiological sarcomere length (2.2 μm), high density of mitochondria (30%), oxidative metabolism, a positive force–frequency relationship and functional calcium handling. They reported the presence of transverse tubules which we did not detect in our cardiac tissue model. The longer (4-week) culture time in their model compared to the 1-week culture time in our model and the application of mechanical stretching and electrical stimulation during the culture likely enhanced these cardiomyocyte features in their model. They measured the direct contraction force using an organ bath and force transducers and obtained physiological responses to isoproterenol in their model but did not test other cardioactive compounds. They reported positive force-frequency relationship like in mature cardiomyocytes. They reported changes in the gene expression including decreased *HCN4* (adult-like conduction), increased *MYH7* and *TNNI3* (ultrastructure) similar to our model. They reported also increase in *GJA5* (connexin 40) which was decreased in our model. However, the gene expression was not completely comparable to the adult stage. For example, the gene expression of the adult type of sodium channel SCN1B was not induced (Ronaldson-Bouchard et al. 2018) as it was in our model.

Beauchamp et al. (2020) developed cardiac spheroids of hiPSC-CM and fibroblast coculture. Their method improved the cardiomyocyte maturity compared to 2D and 3D cardiomyocyte monocultures after a 30-day culture time. They reported some degree of cardiomyocyte alignment on the outer layer of the spheroids. They reported the presence of myofibrils, mitochondria, and cell-cell contact structures including adherens junctions and desmosomes reminiscent of intercalated discs in their 3D cardiac spheroids (Beauchamp et al. 2020). However, these structures did not seem as well developed as in our model with well-organised and aligned sarcomeres with regular z-bands and the transverse section of intercalated discs located at the sarcomere z-bands. The gene expression results showed that the expression of *TNNI3* (cardiac troponin) was higher than the expression of *TNNI1* (skeletal troponin) (Beauchamp et al. 2020), as it was also in our model.

Giacomelli et al. (2020) developed 3D cardiac microtissue cocultures of hiPSC-CM, cardiac fibroblasts, and cardiac endothelial cells. After the culture time of 21 days, they reported improved cardiomyocytes structural maturity with well-organized sarcomeres like in our model, but we did not detect transverse tubules like they did. They did not report alignment of cardiomyocytes in their spheroids. The gene expression levels of cardiac sarcomeric genes were higher in their model compared

to 2D cardiomyocyte monoculture. For example, the structural markers *TNNT2, MYL2, TNNI3* and *TCAP* were upregulated. These genes were also upregulated in our model during the 7-day culture period except for *TNNT2*. In the coculture model, Giacomelli et al. (2020) reported enhanced contractility, which they studied using video imaging, enhanced mitochondrial respiration, and electrophysiology, which was measured using sharp electrodes after cutting the cardiac constructs to smaller pieces and using patch clamp after dissociating the cardiac constructs to single cells and culturing for one more week. The reported physiological responses to the inotropic drugs verapamil and Bay-K8644 (Giacomelli et al. 2020).

The cardiac model of Mannhardt et al. (2016; 2017) consisted of hiPSC-CMs in Matrigel-fibrin hydrogels that were attached between elastic pillars whose deflection was video-imagined for force measurement purpose. This setup also allows the cardiomyocytes to perform physiological auxotonic contractile work against the elastic pillars. Even though their cardiac model consisted only of hiPSC-CMs with 60%–90% purity without added cardiac cell types, the cells showed well-developed sarcomere organization and alignment, and frequent mitochondria after 30–35 days of culture. In addition, they reported high degree of cardiomyocyte alignment. However, the cells did not reach the level of mature cardiomyocytes (Mannhardt et al. 2016). The reported cardiomyocyte morphology results are comparable to our model. The gene expression in their model showed transition from an *MLC2a*$^{+}$/*MLC2v*$^{-}$ to an *MLC2a*$^{-}$/*MLC2v*$^{+}$ population in the model. The gene expression of the ventricular form *MLC2v*$^{-}$ *(i.e., MYL2)* was upregulated also in our model.

Mannhardt et al. (2016) tested the functionality of the model with drugs affecting the pacemaker mechanism, physiological and pharmacological regulators of inotropy, modulators of cardiac ion channels, and proarrhythmic compounds. The results showed expected effects in the cells. Instead of measuring cardiac action potentials, they measured the contractility of their 3D engineered heart tissues (EHTs) and showed that the relaxation time can be used for estimating effects on the cardiac repolarization. With engineered cardiac tissues formed from commercial Cor.4U and iCell cardiomyocytes they reported comparable results to ion channel modulators. Mannhardt et al. (2020) tested the differences between cardiomyocytes from different hPSC-lines in the EHT setup. The spontaneous baseline contractility (e.g., contraction frequency and force) of the different cell lines and differentiation

batches varied considerably. Despite the baseline variability, mainly canonical responses to inotropic drugs were obtained from the different EHTs.

The cardiac tissue model developed in this thesis is compatible with standard MEA technology for the analysis of the cardiomyocyte electrophysiological functionality in contrast to the above-mentioned cardiac tissue models which have more 3D structures and are thus not well suited for MEAs. The MEA technology is less labour-intensive than patch clamp measurements from tissue spheroids or dissociated cells. Patch clamp was used e.g., in the work of Ronaldson-Bouchard et al. (2018) after dissociating the cardiac tissue constructs to single cells and in the work of Beauchamp et al. (2020) for the spheroids. Moreover, the culture time after adding the cardiomyocytes was shorter and the culture method less complicated in our model compared to these studies (Ronaldson-Bouchard et al. 2018; Giacomelli et al. 2020; Beauchamp et al. 2020; Mannhardt et al. 2016).

Even though all the features in our model were not developed as mature as in some other models e.g., we did not detect T-tubules, the functionality of our model that was extensively tested with the different compounds in **study I** shows the suitability of the model for testing cardiotoxicity and efficacy of acute drug-induced effects on human heart. The applicability limitations to the predictivity of the model that were found in **study I** included compounds that would have required longer time to cause an effect than the maximal exposure time of 2 hours in the study (doxorubicin and pentamidine) as well as levosimendan which increases the Ca^{2+} affinity of troponin and cannot be detected with MEA.

6.3 Contraction force measurements

In the second part of this work, a contraction force measurement technology was developed and applied to the cardiac tissue model. The culture method and the cardiac tissue model were also slightly modified for the use in force measurement application. The requirements for the model with the added contraction force measurement method include synchronized contractions i.e., electrical coupling among the cardiomyocytes, mechanical coupling, alignment of the cardiomyocytes, well-developed and aligned sarcomeres, and elastic culture substrate to allow the contraction movements. The alignment of the cells and myofibrils was critical for producing the measurable contraction forces. The measured contraction force

amplitudes need also be high enough so that drug-induced changes, both increase and decrease, can be detected with the measurement system.

The immunofluorescence and TEM imaging showed the development of well-organized sarcomeres and alignment of neighbouring cardiac cells. The cultures were able to produce contraction forces in locally aligned directions. Moreover, the cardiomyocytes were electrically connected and contracted in synchrony which enabled the use of measurement system that measured the combined effect of multiple cardiomyocytes.

The development of the piezoelectric force measurement system from the single axis sensor to the dual axis sensor presented different requirements for the sample dimensions. Initially, the cultures needed to be implemented on wide cell culture dishes to fit under the microscope with the sensor. Due to the sensor design, wide contact angle was needed between the sensor tip and the cardiac tissue construct, which required wide cell culture dishes with low walls.

The PDMS moulds were used for decreasing the sample size on these culture dishes. The lift-off method in **study III** with temperature responsive cell culture dishes improved to controllability of the sample growth compared to **study II**. The lift-off culture method also allowed more contraction movement of the cardiac tissues as the cultures were not attached to a rigid cell culture plastic. This method improved the repeatability of the culture. However, the method contained phases of manual work that required a skilled operator e.g., transferring the PDMS sheets with the cells from the temperature responsive culture dishes onto PDMS holds on other dishes.

The development of the dual axis sensor that could fit under the microscope while approaching the sample from above, opened the possibility to utilise standard cell culture wells for culturing the cardiac tissue constructs. The hydrogel cell culture method in **study IV** was considerable simpler and more repeatable than the lift-off culture method in **study III**. In addition to enabling simpler cell culture methods, the dual-axis sensor approach avoided the need to find the optimal contact orientation between the contraction direction and the cantilever measurement direction in the measurement spot because the dual axis sensor could measure the force in the dual-axis plane.

The dual axis force measurement technology does not require a specialized cell culture platform. The cells can be cultured in standard cell culture well plates with

applying an elastic hydrogel under the cells to enable the contraction movement. In many other cardiac force measurement technologies, the cells are cultured directly on of the force measurement sensor e.g., CellDrum technology (Linder et al. 2010), microcantilevers (Park et al. 2005; Kim et al. 2008), on different kind of pillars and post arrays (Mannhardt et al. 2016; Kajzar et al. 2008; Rodriguez et al. 2014). However, there are also benefits to use nonstandard culture ware. For example, culturing the cardiac tissues e.g., between flexible pillars introduces passive stretching to the tissue aligning the cardiomyocytes, and creates physiologic auxotonic contraction conditions (Mannhardt et al. 2016).

The piezoelectric cantilever sensors are a direct force measurement method that does not need accompany an advanced video imaging equipment. The imaging-based force measurement methods require a high sampling speed (>300 fps) to accurately detect the cardiomyocyte transient kinetics (van Meer et al. 2019), which poses criteria for the imaging system.

Both single axis and dual axis sensors were able to measure cardiac contraction forces in micronewton range. Higher forces were measured with the dual axis sensor. This could be due to nonoptimal alignment of the single axis measurement direction and the contraction direction of the measurement location. Another aspect is that the spring constant of the single axis probe was approximately 1 N/m while the spring constant of the dual axis probe was approximately 5 or 9 N/m depending on the orientation of the probe. The lower spring constant may have been too small for loading sufficiently the cardiac construct at the cantilever tip contact. In this case, the single axis measurement may have been more displacement measurement than force measurement (Virtanen 2020).

The force measurement data analysis was changed after the **study III** for **study IV** to enable the comparison of the drug effects. The contraction force measurement data was filtered for reliable peak detection. The selected filter needed to have a flat amplitude frequency response because drug-induce or other changes in the beating frequency between consecutive measurements might distort the comparison of the filtered data between altered beating rates. Even though designed to have maximally flat frequency response curve (Thompson 2014), the Butterworth filter used in **study II** affected the force amplitudes depending on the beating frequency. This was not acceptable for comparing the drug-induced effects in cumulative concentration series especially for drugs that changed markedly the beating rate e.g., isoprenaline.

Moreover, the Butterworth filtering changed the data waveforms. Therefore, the filter was replaced by a moving average filter that did not change the waveforms. This method enabled matching the peak locations in the filtered data to the peak locations in the raw data, and the unfiltered data could be used for determining the peak amplitude to remove any effect of filtering on the amplitudes. Because the measurement data contained background wandering, the force amplitudes were determined as peak-to-peak values.

The background wandering even after filtering caused the need to also change the method for the determining of the peak detection threshold. Instead of basing the threshold to one highest value in the measurement, the peak detection threshold was set to include a portion of the highest data points. This method was also less sensitive to occasional artefacts in the data.

Another change in the data analysis was to use only one of the channels of the dual-axis sensors instead of calculating the total force in **study IV**. This change was due to inconsistency in the working of both channels simultaneously. Piezoelectric sensors are sensitive to humidity (Surbhi and Sukesha 2020), which likely interfered their performance in the measurement spot where the wells of filled with media on the heater plate are located under the piezoelectric discs even after applying the protective parylene coating in **study IV**.

The adequacy of the contraction force measurement technology to predict human effects was tested with inotropic drugs (**study IV**). The results indicated the suitability of the system for measuring drug-induced cardiac effects. Both positive and negative inotropic effects could be measured. However, the repeatability of the results should be improved. The variability among different cardiac constructs was high. Causes for the variation in the absolute contraction forces include differences between the hand-made sensors, different contraction strength and location of the strongest beating in the cardiac constructs, differences in contact point between the sensor tip and the cardiac construct, and the orientation of the beating relative to the sensor elements.

The measured positive chronotropic and inotropic effects of β-adrenoceptor agonist isoprenaline in **study IV** are well in line with previous studies. These effects have been previously reported in hiPSC-CMs (Saleem et al. 2020; Mannhardt et al. 2016), in hiPSC-CM and fibroblasts cocultures (Huebsch et al. 2016), and in hiPSC-CM, fibroblasts and endothelial cell cocultures (Arai et al. 2020).

The positive inotropic effect of PDE3 inhibitor milrinone has been previously reported in electrically stimulated engineered cardiac tissues containing cardiomyocytes and fibroblasts (Feric et al. 2019), and in cardiac triculture microtissues containing endothelial cells and fibroblasts (Ravenscroft et al. 2016). However, milrinone has also been reported to lack the effect in hPSC-derived cardiomyocytes (Ravenscroft et al. 2016; Mannhardt et al. 2016; Saleem et al. 2020). The lack of effect may be due to lower expression of PDE3 in immature cardiomyocytes (Saleem et al. 2020). Even though the inotropic effect was not consistent in **study IV**, it indicates improved maturity of the cardiac tissue model developed in this study.

The inotropic effects of cardiac myosin activator omecamtiv mecarbil greatly varied among the cardiac constructs in **study IV**. Inconsistencies in the inotropic effects of the drug have been reported also in other studies. Ballan et al. (2020) reported positive inotropy in hiPSC-CMs at 100 nM but negative inotropy at higher doses. Ribeiro et al. (2017), reported positive inotropy immediately after exposure but negative inotropy 5 min later possibly due to myofibril damage. The anticipated positive inotropic effects were reported in cardiomyocyte-fibroblast cocultures with an EC_{50} of 370 nM (Feric et al. 2019). Rhoden et al. (2022) studied the effects of omecamtiv mecarbil on hiPSC-EHTs in isometric and auxotonic conditions. They detected positive inotropic responses in preload-controlled isometric conditions but not in auxotonic conditions. The Ca^{2+} sensitivity depends on muscle length (Fuchs and Smith 2001), which could explain the differences in the results between the experimental setups. The inotropic effect in isometric conditions was biphasic increasing the contraction force until 3 μM with maximal effect at 1 μM but decreasing the force at 10 μM. They also studied the effects of omecamtiv mecarbil on neonatal rat-EHTs and obtained negative inotropic effect at 3 μM unlike in the hiPSC-EHTs indicating species-dependency of the effects (Rhoden et al. 2022).

The β-adrenoceptor antagonist propranolol would not be expected to cause negative inotropic effects in the absence of adrenergic stimulation. However, the drug has been reported to also inhibit sodium channels (Wang et al. 2010), which could explain the negative chronotropic effects in the **study IV**.

Negative chronotropic and inotropic effects of verapamil have been previously reported in hiPSC-CMs (Morimoto et al. 2016) and cardiac constructs consisting of hiPSC-CM, fibroblasts, and endothelial cells (Arai et al. 2020). The L-type calcium

channel inhibitor verapamil has been reported to cause negative inotropy in engineered cardiac tissue (Mannhardt et al. 2016) and hiPSC-CMs (Goßmann et al. 2016) similar to the trend of the negative inotropy observed in **study IV**.

6.4 Future directions

The cardiac tissue model aims to mimic the human heart tissue. This cardiac tissue model does not fully recapitulate the structure of the heart but rather the layer of the heart wall containing the force-producing cardiomyocytes, the myocardium. The model shows many features of the native myocardium. The cardiomyocytes are locally aligned, electrically and mechanically connected with each other forming a synchronously beating network. Moreover, the myofibrils are organised into sarcomeres. These features are included in the criteria for a cardiac *in vitro* model. The model should contain relevant ion channels and exhibit electrophysiological properties similar to human heart. These features are present in the cardiac tissue model developed in this thesis. The electrical activity is measurable with MEA technology while the mechanical behaviour and contraction forces are measurable with the cantilever sensor system. The testing with cardioactive drugs showed good resemblance to the drug-induced responses in heart. In addition to the cardiomyocytes, the developed model contains also a vascular-like network formed by endothelial cells, as well as perivascular cells and (myo)fibroblasts. Thus, the cell composition of the developed model includes many cell types present in the native myocardium.

Even though the coculture with the vascular-like network enables cell-cell communication among the different cell types enhancing the cardiomyocyte maturation, the model does not fully reach the adult state of the human heart tissue. The cardiomyocyte structure does not match with the adult cardiomyocytes completely. For example, the presence of T-tubules and the relative proportion of sarcomeres and mitochondria in the intracellular space. Moreover, the gene expression of the cardiac model, although closer than the monoculture, did not reach at the adult cardiomyocyte level. Similar to many other hiPSC-CM -based *in vitro* cardiac models, the maturity of the cardiomyocytes could still be improved to reach the maturity state of cardiomyocytes of the adult human heart. Additional methods could include electrical or mechanical stimulation during the culture (Ronaldson-

Bouchard et al. 2018). Further enhancing the maturity of the cardiomyocytes would be beneficial to increase the model's resemblance to the adult human heart.

The model also has no connections with nerve stimulation. Considering the testing of drug-induces heart effects, cardioactive compounds whose mechanisms depend on affecting the signals from autonomic nervous system e.g., blocking of the adrenergic stimulation, do not function in the model. Cardiac autonomic nervous system has important role in heart function modulating cardiac contractility, relaxation, beating rate, conduction velocity and cardiomyocyte cohesion (Fedele and Brand 2020). The cardiac tissue model also does not include immune cells which are present in the myocardium (Zamani et al. 2018). The immune cells play roles in both maintaining the cardiac homeostasis and in pathological conditions (Koc and Cagavi 2021). For example, resident macrophages participate in electrical coupling, mechanosensing, and maintaining cardiomyocyte homeostasis (Steffens et al. 2021).

The current study design allows testing of acute short-term effects of the compounds. Extending the exposure times would be needed for measuring possible cardiac effects that require longer time to develop or chronic exposures. Furthermore, the model measures only the direct effects of the parent drugs because the metabolic activity in cardiomyocytes is weak. The inclusion of liver metabolism in the model using organ-on-a-chip (OoC) technology combining the cardiac tissue model with a functional liver tissue model in the chip would enable the measurement of the cardiac effects of the parent drug as well as possible active drug metabolites (Marx et al. 2020). The OoC technology would also enable more precise control of the culture microenvironment, monitoring of electrical and mechanical behaviour with embedded microsensors, and introduce physiological shear stress to the cells (Leung et al. 2022).

This cardiac tissue model aims to mimic the function of the healthy human heart. However, especially for testing the efficacy of cardiac drugs, it could be beneficial to also model the diseased myocardium. For example, genetic cardiac diseases could be modelled by replacing the healthy cardiomyocytes in the model with hiPSC-CMs carrying a genetic cardiac disease e.g., long QT syndrome or dilated cardiomyopathy (Parrotta et al. 2020). Another example of creating a cardiac disease model could be exposing the healthy cells to hypoxic conditions to model myocardial infarction (Ma et al. 2021).

The repeatability, reproducibility, and relevancy of the cardiac tissue model with the MEA measurements were shown and are suitable for using the model in standardised testing of drug-induced cardiac effects. The variation of the results was small and concentration-response curves were obtained for the different cardioactive drugs. However, repeatability and throughput of the force measurements would need further optimisation. The concentration-response curves for the inotropes were not always obtained and the variation among parallel wells and among the repeats was high.

In the force measurements, the selecting of the measured wells and measurement locations was manual and preferred cultures with strong and regular beating. Increasing the similarity of cardiac constructs for example with guiding the cell orientation and the direction of the contraction might be beneficial. The contraction force measurement system would also benefit from a more robust drug administration during the consecutive measurements. Manually pipetting the amount of drug to the well was susceptible for interference the critical contact point between sensor tip and cells. The measurement technique in its current form is time consuming and laborious because only one well can be measured at a time. Increasing the throughput would be needed to enable better usability of the method.

7 CONCLUSIONS

The aim of this study was to develop a functional human cell -based cardiac tissue model mimicking the healthy adult human heart and combine it with a contraction force measurement system for testing drug-induced cardiac effects. The main conclusions of this work can be drawn as follows:

- The coculture with the pre-formed hASC-HUVEC vascular-like networks supports the hiPSC-CM organization and maturation including improved cardiomyocyte alignment and morphology, well-developed contractile machinery, and cell-cell-connections. Furthermore, the gene expression profiles of the cardiac tissue model show characteristics of the adult human heart.

- The cardiac tissue model was shown to be repeatable, reproducible, and relevant for testing cardiotoxicity and efficacy of acute drug-induced effects on human heart. The cardiomyocytes in the model develop electrophysiological properties that mimic accurately the function of the heart as shown in functional characterization with the positive and negative reference compounds compared to the respective clinical data. Although some applicability limitations were discovered, the results show that the data gained from the cardiac tissue model are transferable to the clinical setting for the evaluation of cardiac effects including acute cardiotoxicity.

- The piezoelectric cantilever sensor system can be used for measuring the contraction force of cardiac tissue model constructs including single and dual axis sensor designs and various cell culture platforms.

- The functionality of the cardiac tissue model with the contraction force measurement system was shown in a proof-of-concept level. The piezoelectric cantilever sensor with the human cell -based cardiac tissue constructs have potential to be used for testing both positive and negative

drug-induced inotropic effects with different mechanisms on the cardiac function.

REFERENCES

Abulaiti, Mosha, Yaxiaer Yalikun, Kozue Murata, Asako Sato, Mustafa M. Sami, Yuko Sasaki, Yasue Fujiwara, et al. 2020. “Establishment of a Heart-on-a-Chip Microdevice Based on Human IPS Cells for the Evaluation of Human Heart Tissue Function.” *Scientific Reports* 10 (1): 19201. https://doi.org/10.1038/s41598-020-76062-w.

Ahn, Jinsoo, Huiguang Wu, and Kichoon Lee. 2020. “Integrative Analysis Revealing Human Heart-Specific Genes and Consolidating Heart-Related Phenotypes.” *Frontiers in Genetics* 11. https://www.frontiersin.org/article/10.3389/fgene.2020.00777.

Akiyama, Hirokazu, Akira Ito, Masanori Sato, Yoshinori Kawabe, and Masamichi Kamihira. 2010. “Construction of Cardiac Tissue Rings Using a Magnetic Tissue Fabrication Technique.” *International Journal of Molecular Sciences* 11 (8): 2910–20. https://doi.org/10.3390/ijms11082910.

Andersson, K. E. 1984. “Clinical Pharmacology of Terodiline.” *Scandinavian Journal of Urology and Nephrology* 87 (Journal Article): 13–20. https://www.ncbi.nlm.nih.gov/pubmed/6599419.

Ando, Hiroyuki, Takashi Yoshinaga, Wataru Yamamoto, Keiichi Asakura, Takaaki Uda, Tomohiko Taniguchi, Atsuko Ojima, et al. 2017. “A New Paradigm for Drug-Induced Torsadogenic Risk Assessment Using Human IPS Cell-Derived Cardiomyocytes.” *Journal of Pharmacological and Toxicological Methods* 84 (Journal Article): 111–27. https://doi.org/10.1016/j.vascn.2016.12.003.

Andrews, Simon. 2010. “FastQC: A Quality Control Tool for High Throughput Sequence Data.” http://www.bioinformatics.babraham.ac.uk/projects/fastqc/.

Arackal, Anita, and Khalid Alsayouri. 2022. “Histology, Heart.” In *StatPearls*. Treasure Island (FL): StatPearls Publishing. http://www.ncbi.nlm.nih.gov/books/NBK545143/.

Arai, Kenichi, Daiki Murata, Shoko Takao, Anna Nakamura, Manabu Itoh, Takahiro Kitsuka, and Koichi Nakayama. 2020. “Drug Response Analysis for Scaffold-Free Cardiac Constructs Fabricated Using Bio-3D Printer.” *Scientific Reports* 10 (June): 8972. https://doi.org/10.1038/s41598-020-65681-y.

Arrowsmith, John, and Philip Miller. 2013. “Phase II and Phase III Attrition Rates 2011–2012.” *Nature Reviews Drug Discovery* 12 (8): 569–569. https://doi.org/10.1038/nrd4090.

Ballan, Nimer, Naim Shaheen, Gordon M. Keller, and Lior Gepstein. 2020. “Single-Cell Mechanical Analysis of Human Pluripotent Stem Cell-Derived Cardiomyocytes for Drug Testing and Pathophysiological Studies.” *Stem Cell Reports* 15 (3): 587–96. https://doi.org/10.1016/j.stemcr.2020.07.006.

Barnett, Vincent A. 2009. “Cellular Myocytes.” In *Handbook of Cardiac Anatomy, Physiology, and Devices*, edited by Paul A. Iaizzo, 147–58. Totowa, NJ: Humana Press. https://doi.org/10.1007/978-1-60327-372-5_10.

Beauchamp, Philippe, Christopher B. Jackson, Lijo Cherian Ozhathil, Irina Agarkova, Cristi L. Galindo, Douglas B. Sawyer, Thomas M. Suter, and Christian Zuppinger. 2020. “3D Co-Culture of HiPSC-Derived Cardiomyocytes With Cardiac Fibroblasts Improves Tissue-Like Features of Cardiac Spheroids.” *Frontiers in Molecular Biosciences* 7: 14. https://doi.org/10.3389/fmolb.2020.00014.

Bers, Donald M. 2002. “Cardiac Excitation–Contraction Coupling.” *Nature* 415 (6868): 198–205. https://doi.org/10.1038/415198a.

Bers, Donald M. 2008. “Calcium Cycling and Signaling in Cardiac Myocytes.” *Annual Review of Physiology* 70: 23–49. https://doi.org/10.1146/annurev.physiol.70.113006.100455.

Blinova, K., J. Stohlman, J. Vicente, D. Chan, L. Johannesen, M. P. Hortigon-Vinagre, V. Zamora, et al. 2017. “Comprehensive Translational Assessment of Human-Induced Pluripotent Stem Cell Derived Cardiomyocytes for Evaluating Drug-Induced Arrhythmias.” *Toxicological Sciences : An Official Journal of the Society of Toxicology* 155 (1): 234–47. https://doi.org/10.1093/toxsci/kfw200.

Boudou, Thomas, Wesley R. Legant, Anbin Mu, Michael A. Borochin, Nimalan Thavandiran, Milica Radisic, Peter W. Zandstra, Jonathan A. Epstein, Kenneth B. Margulies, and Christopher S. Chen. 2012. “A Microfabricated Platform to Measure and Manipulate the Mechanics of Engineered Cardiac Microtissues.” *Tissue Engineering Part A* 18 (9–10): 91–919. https://doi.org/10.1089/ten.tea.2011.0341.

Bowes, Joanne, Andrew J. Brown, Jacques Hamon, Wolfgang Jarolimek, Arun Sridhar, Gareth Waldron, and Steven Whitebread. 2012. “Reducing Safety-Related Drug Attrition: The Use of in Vitro Pharmacological Profiling.” *Nature Reviews. Drug Discovery* 11 (12): 909–22. https://doi.org/10.1038/nrd3845.

Burridge, Paul W, Scott A Metzler, Karina H Nakayama, Oscar J Abilez, Chelsey S Simmons, Marc A Bruce, Yuka Matsuura, et al. 2014. “Multi-Cellular Interactions Sustain Long-Term Contractility of Human Pluripotent Stem Cell-Derived Cardiomyocytes.” *American Journal of Translational Research* 6 (6): 724–35. https://www.ncbi.nlm.nih.gov/pmc/articles/PMC4297340/.

Chang, Wei-Tien, David Yu, Yu-Cheng Lai, Kuen-You Lin, and Ian Liau. 2013. “Characterization of the Mechanodynamic Response of Cardiomyocytes

with Atomic Force Microscopy." *Analytical Chemistry* 85 (3): 1395–1400. https://doi.org/10.1021/ac3022532.

Chugh, Rishi Man, Madhusudan Chaturvedi, and Lakshmana Kumar Yerneni. 2016. "Exposure Cell Number during Feeder Cell Growth-Arrest by Mitomycin C Is a Critical Pharmacological Aspect in Stem Cell Culture System." *Journal of Pharmacological and Toxicological Methods* 80 (Journal Article): 68–74. https://doi.org/10.1016/j.vascn.2016.05.006.

CiPA. 2019. "About CIPA – CIPA." 2019. https://cipaproject.org/about-cipa/.

Colatsky, Thomas, Bernard Fermini, Gary Gintant, Jennifer B. Pierson, Philip Sager, Yuko Sekino, David G. Strauss, and Norman Stockbridge. 2016. "The Comprehensive in Vitro Proarrhythmia Assay (CiPA) Initiative — Update on Progress." *Journal of Pharmacological and Toxicological Methods*, Focused Issue on Safety Pharmacology, 81 (September): 15–20. https://doi.org/10.1016/j.vascn.2016.06.002.

Colliva, Andrea, Luca Braga, Mauro Giacca, and Serena Zacchigna. 2020. "Endothelial Cell–Cardiomyocyte Crosstalk in Heart Development and Disease." *The Journal of Physiology* 598 (14): 2923–39. https://doi.org/10.1113/JP276758.

Dehne, Eva-Maria, Tobias Hasenberg, and Uwe Marx. 2017. "The Ascendance of Microphysiological Systems to Solve the Drug Testing Dilemma." *Future Science OA* 3 (2): FSO185. https://doi.org/10.4155/fsoa-2017-0002.

Dobin, Alexander, Carrie A. Davis, Felix Schlesinger, Jorg Drenkow, Chris Zaleski, Sonali Jha, Philippe Batut, Mark Chaisson, and Thomas R. Gingeras. 2013. "STAR: Ultrafast Universal RNA-Seq Aligner." *Bioinformatics* 29 (1): 15–21. https://doi.org/10.1093/bioinformatics/bts635.

Dou, Wenkun, Manpreet Malhi, Qili Zhao, Li Wang, Zongjie Huang, Junhui Law, Na Liu, Craig A. Simmons, Jason T. Maynes, and Yu Sun. 2022. "Microengineered Platforms for Characterizing the Contractile Function of in Vitro Cardiac Models." *Microsystems & Nanoengineering* 8 (1): 1–22. https://doi.org/10.1038/s41378-021-00344-0.

Dunn, Kaitlin K., Isabella M. Reichardt, Aaron D. Simmons, Gyuhyung Jin, Martha E. Floy, Kelsey M. Hoon, and Sean P. Palecek. 2019. "Coculture of Endothelial Cells with Human Pluripotent Stem Cell-Derived Cardiac Progenitors Reveals a Differentiation Stage-Specific Enhancement of Cardiomyocyte Maturation." *Biotechnology Journal* 14 (8): e1800725. https://doi.org/10.1002/biot.201800725.

Dupre, Anthony, Sarah Vieau, and Paul A. Iaizzo. 2009. "Basic ECG Theory, 12-Lead Recordings and Their Interpretation." In *Handbook of Cardiac Anatomy, Physiology, and Devices*, edited by Paul A. Iaizzo, 257–69. Totowa, NJ: Humana Press. https://doi.org/10.1007/978-1-60327-372-5_17.

Durinck, Steffen, Paul T. Spellman, Ewan Birney, and Wolfgang Huber. 2009. "Mapping Identifiers for the Integration of Genomic Datasets with the

R/Bioconductor Package BiomaRt." *Nature Protocols* 4 (8): 1184–91. https://doi.org/10.1038/nprot.2009.97.

D'Urso, Mirko, and Nicholas A. Kurniawan. 2020. "Mechanical and Physical Regulation of Fibroblast–Myofibroblast Transition: From Cellular Mechanoresponse to Tissue Pathology." *Frontiers in Bioengineering and Biotechnology* 8. https://www.frontiersin.org/articles/10.3389/fbioe.2020.609653.

Eisner, David A., Jessica L. Caldwell, Kornél Kistamás, and Andrew W. Trafford. 2017. "Calcium and Excitation-Contraction Coupling in the Heart." *Circulation Research* 121 (2): 181–95. https://doi.org/10.1161/CIRCRESAHA.117.310230.

EMEA. 2006. "ICH S7B The Nonclinical Evaluation of the Potential for Delayed Ventricular Repolarization (QT Interval Prolongation) by Human Pharmaceuticals." European Medicines Agency. https://www.ema.europa.eu/en/ich-s7b-non-clinical-evaluation-potential-delayed-ventricular-repolarization-qt-interval.

Eschenhagen, Thomas, Christine Fink, Ute Remmers, Hasso Scholz, Jens Wattchow, Joachim Weil, Wolfram Zimmermann, et al. 1997. "Three-Dimensional Reconstitution of Embryonic Cardiomyocytes in a Collagen Matrix: A New Heart Muscle Model System." *FASEB Journal : Official Publication of the Federation of American Societies for Experimental Biology* 11 (8): 683–394.

FDA. 2020. "The Drug Development Process." FDA. FDA. February 20, 2020. https://www.fda.gov/patients/learn-about-drug-and-device-approvals/drug-development-process.

Fedele, Laura, and Thomas Brand. 2020. "The Intrinsic Cardiac Nervous System and Its Role in Cardiac Pacemaking and Conduction." *Journal of Cardiovascular Development and Disease* 7 (4): 54. https://doi.org/10.3390/jcdd7040054.

Feng, Zhonggang, Tatsuo Kitajima, Tadashi Kosawada, Takao Nakamura, Daisuke Sato, and Mitsuo Umezu. 2014. "Dynamic Analysis of Circular Engineered Cardiac Tissue to Evaluate the Active Contractile Force." In *Life System Modeling and Simulation*, edited by Shiwei Ma, Li Jia, Xin Li, Ling Wang, Huiyu Zhou, and Xin Sun, 461:198–208. Communications in Computer and Information Science. Berlin, Heidelberg: Springer Berlin Heidelberg. https://doi.org/10.1007/978-3-662-45283-7_21.

Feric, Nicole T, Isabella Pallotta, Rishabh Singh, Danielle R Bogdanowicz, Marietta M Gustilo, Khuram W Chaudhary, Robert N Willette, et al. 2019. "Engineered Cardiac Tissues Generated in the Biowire II: A Platform for Human-Based Drug Discovery." *Toxicological Sciences* 172 (1): 89–97. https://doi.org/10.1093/toxsci/kfz168.

Feyen, Dries A. M., Wesley L. McKeithan, Arne A. N. Bruyneel, Sean Spiering, Larissa Hörmann, Bärbel Ulmer, Hui Zhang, et al. 2020. "Metabolic Maturation Media Improve Physiological Function of Human IPSC-Derived

Cardiomyocytes." *Cell Reports* 32 (3): 107925. https://doi.org/10.1016/j.celrep.2020.107925.

Fitzgerald, Kevin, Robert F. Wilson, and Paul A. Iaizzo. 2009. "Autonomic Nervous System." In *Handbook of Cardiac Anatomy, Physiology, and Devices*, edited by Paul A. Iaizzo, 177–89. Totowa, NJ: Humana Press. https://doi.org/10.1007/978-1-60327-372-5_12.

Fuchs, Franklin, and Stephen H. Smith. 2001. "Calcium, Cross-Bridges, and the Frank-Starling Relationship." *Physiology* 16 (1): 5–10. https://doi.org/10.1152/physiologyonline.2001.16.1.5.

Gaitas, Angelo, Ricky Malhotra, Tao Li, Todd Herron, and José Jalife. 2015. "A Device for Rapid and Quantitative Measurement of Cardiac Myocyte Contractility." *The Review of Scientific Instruments* 86 (3): 034302. https://doi.org/10.1063/1.4915500.

Garzoni, Luciana R., Maria Isabel D. Rossi, Ana P. D. N. de Barros, Virgínia Guarani, Michelle Keramidas, Luciene B. L. Balottin, Daniel Adesse, et al. 2009. "Dissecting Coronary Angiogenesis: 3D Co-Culture of Cardiomyocytes with Endothelial or Mesenchymal Cells." *Experimental Cell Research* 315 (19): 3406–18. https://doi.org/10.1016/j.yexcr.2009.09.016.

Giacomelli, Elisa, Milena Bellin, Luca Sala, Berend J. van Meer, Leon G. J. Tertoolen, Valeria V. Orlova, and Christine L. Mummery. 2017. "Three-Dimensional Cardiac Microtissues Composed of Cardiomyocytes and Endothelial Cells Co-Differentiated from Human Pluripotent Stem Cells." *Development (Cambridge, England)* 144 (6): 1008–17. https://doi.org/10.1242/dev.143438.

Giacomelli, Elisa, Viviana Meraviglia, Giulia Campostrini, Amy Cochrane, Xu Cao, Ruben W.J. van Helden, Ana Krotenberg Garcia, et al. 2020. "Human-IPSC-Derived Cardiac Stromal Cells Enhance Maturation in 3D Cardiac Microtissues and Reveal Non-Cardiomyocyte Contributions to Heart Disease." *Cell Stem Cell* 26 (6): 862-879.e11. https://doi.org/10.1016/j.stem.2020.05.004.

Gintant, Gary. 2011. "An Evaluation of HERG Current Assay Performance: Translating Preclinical Safety Studies to Clinical QT Prolongation." *Pharmacology & Therapeutics* 129 (2): 109–19. https://doi.org/10.1016/j.pharmthera.2010.08.008.

Gordan, Richard, Judith K Gwathmey, and Lai-Hua Xie. 2015. "Autonomic and Endocrine Control of Cardiovascular Function." *World Journal of Cardiology* 7 (4): 204–14. https://doi.org/10.4330/wjc.v7.i4.204.

Goßmann, Matthias, Ralf Frotscher, Peter Linder, Stephan Neumann, Robin Bayer, Matthias Epple, Manfred Staat, Ayşegül (Temiz) Artmann, and Gerhard M. Artmann. 2016. "Mechano-Pharmacological Characterization of Cardiomyocytes Derived from Human Induced Pluripotent Stem Cells."

Cellular Physiology and Biochemistry 38 (3): 1182–98. https://doi.org/10.1159/000443124.

Grant, Augustus O. 2009. "Cardiac Ion Channels." *Circulation: Arrhythmia and Electrophysiology* 2 (2): 185–94. https://doi.org/10.1161/CIRCEP.108.789081.

Gray, GA, IS Toor, RFP Castellan, M Crisan, and M Meloni. 2018. "Resident Cells of the Myocardium: More than Spectators in Cardiac Injury, Repair and Regeneration." *Current Opinion in Physiology*, Cardiac physiology from inside to out, 1 (February): 46–51. https://doi.org/10.1016/j.cophys.2017.08.001.

Guo, L., L. Coyle, R. M. Abrams, R. Kemper, E. T. Chiao, and K. L. Kolaja. 2013. "Refining the Human IPSC-Cardiomyocyte Arrhythmic Risk Assessment Model." *Toxicological Sciences : An Official Journal of the Society of Toxicology* 136 (2): 581–94. https://doi.org/10.1093/toxsci/kft205.

Guth, Brian D., Michael Engwall, Sandy Eldridge, C. Michael Foley, Liang Guo, Gary Gintant, John Koerner, et al. 2019. "Considerations for an In Vitro , Cell-Based Testing Platform for Detection of Adverse Drug-Induced Inotropic Effects in Early Drug Development. Part 1: General Considerations for Development of Novel Testing Platforms." *Frontiers in Pharmacology* 10 (Journal Article): 884. https://doi.org/10.3389/fphar.2019.00884.

Hansen, Arne, Alexandra Eder, Marlene Bönstrup, Marianne Flato, Marco Mewe, Sebastian Schaaf, Bülent Aksehirlioglu, Alexander Schwoerer, June Uebeler, and Thomas Eschenhagen. 2010. "Development of a Drug Screening Platform Based on Engineered Heart Tissue." *Circulation Research* 107 (1): 35–44. https://doi.org/10.1161/CIRCRESAHA.109.211458.

Haraguchi, Yuji, Tatsuya Shimizu, Masayuki Yamato, and Teruo Okano. 2010. "Electrical Interaction between Cardiomyocyte Sheets Separated by Non-Cardiomyocyte Sheets in Heterogeneous Tissues." *Journal of Tissue Engineering and Regenerative Medicine* 4 (4): 291–99. https://doi.org/10.1002/term.241.

Hartigan-Go, K., D. N. Bateman, A. K. Daly, and S. H. Thomas. 1996. "Stereoselective Cardiotoxic Effects of Terodiline." *Clinical Pharmacology and Therapeutics* 60 (1): 89–98.

Hasenfuss, Gerd, and John R. Teerlink. 2011. "Cardiac Inotropes: Current Agents and Future Directions." *European Heart Journal* 32 (15): 1838–45. https://doi.org/10.1093/eurheartj/ehr026.

Hayashi, S., T. Natsukawa, C. Suma, Y. Ukai, Y. Yoshikuni, and K. Kimura. 1997. "Cardiac Electrophysiological Actions of NS-21 and Its Active Metabolite, RCC-36, Compared with Terodiline." *Naunyn-Schmiedeberg's Archives of Pharmacology* 355 (5): 651–58. https://doi.org/10.1007/pl00004997.

Hazeltine, Laurie B., Chelsey S. Simmons, Max R. Salick, Xiaojun Lian, Mehmet G. Badur, Wenqing Han, Stephanie M. Delgado, et al. 2012. “Effects of Substrate Mechanics on Contractility of Cardiomyocytes Generated from Human Pluripotent Stem Cells.” *International Journal of Cell Biology* 2012: 1–13. https://doi.org/10.1155/2012/508294.

Heinonen, Tuula. 2015. “Better Science with Human Cell-Based Organ and Tissue Models.” *Alternatives to Laboratory Animals: ATLA* 43 (1): 29–38. https://doi.org/10.1177/026119291504300107.

Helle, Emmi, Minna Ampuja, Alexandra Dainis, Laura Antola, Elina Temmes, Erik Tolvanen, Eero Mervaala, and Riikka Kivelä. 2021. “HiPS-Endothelial Cells Acquire Cardiac Endothelial Phenotype in Co-Culture With HiPS-Cardiomyocytes.” *Frontiers in Cell and Developmental Biology* 9. https://www.frontiersin.org/articles/10.3389/fcell.2021.715093.

Hirt, Marc N, Jasper Boeddinghaus, Alice Mitchell, Sebastian Schaaf, Christian Börnchen, Christian Müller, Herbert Schulz, et al. 2014. “Functional Improvement and Maturation of Rat and Human Engineered Heart Tissue by Chronic Electrical Stimulation.” *Journal of Molecular and Cellular Cardiology* 74 (Journal Article): 151–61. https://doi.org/10.1016/j.yjmcc.2014.05.009.

Hove-Madsen, L., A. Llach, C. E. Molina, C. Prat-Vidal, J. Farre, S. Roura, and J. Cinca. 2006. “The Proarrhythmic Antihistaminic Drug Terfenadine Increases Spontaneous Calcium Release in Human Atrial Myocytes.” *European Journal of Pharmacology* 553 (1–3): 215–21. https://doi.org/10.1016/j.ejphar.2006.09.023.

Howard, Catherine M., and Troy A. Baudino. 2014. “Dynamic Cell–Cell and Cell–ECM Interactions in the Heart.” *Journal of Molecular and Cellular Cardiology*, Myocyte - Fibroblast Signalling in Myocardium, 70 (May): 19–26. https://doi.org/10.1016/j.yjmcc.2013.10.006.

Hsieh, Patrick C.H., Michael E. Davis, Laura K. Lisowski, and Richard T. Lee. 2006. “Endothelial-Cardiomyocyte Interactions in Cardiac Development and Repair.” *Annual Review of Physiology* 68: 51–66. https://doi.org/10.1146/annurev.physiol.68.040104.124629.

Huebsch, Nathaniel, Peter Loskill, Nikhil Deveshwar, C. Ian Spencer, Luke M. Judge, Mohammad A. Mandegar, Cade B. Fox, et al. 2016. “Miniaturized IPS-Cell-Derived Cardiac Muscles for Physiologically Relevant Drug Response Analyses.” *Scientific Reports* 6 (1): 24726. https://doi.org/10.1038/srep24726.

Huttala, Outi, Desiree Loreth, Synnöve Staff, Minna Tanner, Harriet Wikman, and Timo Ylikomi. 2022. “Decellularized In Vitro Capillaries for Studies of Metastatic Tendency and Selection of Treatment.” *Biomedicines* 10 (2): 271. https://doi.org/10.3390/biomedicines10020271.

Huttala, Outi, Hanna Vuorenpää, Tarja Toimela, Jukka Uotila, Hannu Kuokkanen, Timo Ylikomi, Jertta-Riina Sarkanen, and Tuula Heinonen. 2015. “Human Vascular Model with Defined Stimulation Medium - a Characterization Study.” *ALTEX* 32 (2): 125–36. https://doi.org/10.14573/altex.1411271.

Iwamiya, Takahiro, Katsuhisa Matsuura, Shinako Masuda, Tatsuya Shimizu, and Teruo Okano. 2016. “Cardiac Fibroblast-Derived VCAM-1 Enhances Cardiomyocyte Proliferation for Fabrication of Bioengineered Cardiac Tissue.” *Regenerative Therapy* 4 (June): 92–102. https://doi.org/10.1016/j.reth.2016.01.005.

Iyer, Rohin K., Loraine L. Y. Chiu, and Milica Radisic. 2009. “Microfabricated Poly(Ethylene Glycol) Templates Enable Rapid Screening of Triculture Conditions for Cardiac Tissue Engineering.” *Journal of Biomedical Materials Research Part A* 89A (3): 616–31. https://doi.org/10.1002/jbm.a.32014.

Janmey, Paul A, Jessamine P Winer, and John W Weisel. 2009. “Fibrin Gels and Their Clinical and Bioengineering Applications.” *Journal of The Royal Society Interface* 6 (30): 1–10. https://doi.org/10.1098/rsif.2008.0327.

Jiang, Yanqing, Peter Park, Sang-Min Hong, and Kiwon Ban. 2018. “Maturation of Cardiomyocytes Derived from Human Pluripotent Stem Cells: Current Strategies and Limitations.” *Molecules and Cells* 41 (7): 613–21. https://doi.org/10.14348/molcells.2018.0143.

Kajzar, A., C. M. Cesa, N. Kirchgeßner, B. Hoffmann, and R. Merkel. 2008. “Toward Physiological Conditions for Cell Analyses: Forces of Heart Muscle Cells Suspended Between Elastic Micropillars.” *Biophysical Journal* 94 (5): 1854–66. https://doi.org/10.1529/biophysj.107.115766.

Kanehisa, M. 1996. “Toward Pathway Engineering: A New Database of Genetic and Molecular Pathways.” *Science & Technology Japan* 59: 34–38.

Kaplinsky, Edgardo, and Gordon Mallarkey. 2018. “Cardiac Myosin Activators for Heart Failure Therapy: Focus on Omecamtiv Mecarbil.” *Drugs in Context* 7 (April): 212518. https://doi.org/10.7573/dic.212518.

Karbassi, Elaheh, Aidan Fenix, Silvia Marchiano, Naoto Muraoka, Kenta Nakamura, Xiulan Yang, and Charles E. Murry. 2020. “Cardiomyocyte Maturation: Advances in Knowledge and Implications for Regenerative Medicine.” *Nature Reviews. Cardiology* 17 (6): 341–59. https://doi.org/10.1038/s41569-019-0331-x.

Kijlstra, Jan David, Dongjian Hu, Nikhil Mittal, Eduardo Kausel, Peter van der Meer, Arman Garakani, and Ibrahim J. Domian. 2015. “Integrated Analysis of Contractile Kinetics, Force Generation, and Electrical Activity in Single Human Stem Cell-Derived Cardiomyocytes.” *Stem Cell Reports* 5 (6): 1226–38. https://doi.org/10.1016/j.stemcr.2015.10.017.

Kim, Jinseok, Jongoh Park, Jungyul Park, Sukho Park, Kyounghwan Na, Sungwook Yang, Jeongeun Baek, et al. 2008. “Quantitative Evaluation of Cardiomyocyte Contractility in a 3D Microenvironment.” *Journal of*

Biomechanics 41 (11): 2396–2401. https://doi.org/10.1016/j.jbiomech.2008.05.036.

Koc, Arzuhan, and Esra Cagavi. 2021. “Cardiac Immunology: A New Era for Immune Cells in the Heart.” In *Cell Biology and Translational Medicine, Volume 11: Stem Cell Therapy - Potential and Challenges*, edited by Kursad Turksen, 75–95. Advances in Experimental Medicine and Biology. Cham: Springer International Publishing. https://doi.org/10.1007/5584_2020_576.

Koenig, Andrew L., Irina Shchukina, Junedh Amrute, Prabhakar S. Andhey, Konstantin Zaitsev, Lulu Lai, Geetika Bajpai, et al. 2022. “Single-Cell Transcriptomics Reveals Cell-Type-Specific Diversification in Human Heart Failure.” *Nature Cardiovascular Research* 1 (3): 263–80. https://doi.org/10.1038/s44161-022-00028-6.

Kuppusami, Sushmitha, and Reza H. Oskouei. 2015. “Parylene Coatings in Medical Devices and Implants: A Review.” *Universal Journal of Biomedical Engineering* 3 (2): 9–14. https://doi.org/10.13189/ujbe.2015.030201.

Kuryshev, Y. A., E. Ficker, L. Wang, P. Hawryluk, A. T. Dennis, B. A. Wible, A. M. Brown, et al. 2005. “Pentamidine-Induced Long QT Syndrome and Block of HERG Trafficking.” *The Journal of Pharmacology and Experimental Therapeutics* 312 (1): 316–23. https://doi.org/10.1124/jpet.104.073692.

Kussauer, Sophie, Robert David, and Heiko Lemcke. 2019. “HiPSCs Derived Cardiac Cells for Drug and Toxicity Screening and Disease Modeling: What Micro-Electrode-Array Analyses Can Tell Us.” *Cells* 8 (11): 1331. https://doi.org/10.3390/cells8111331.

Lacerda, Antonio E., Yuri A. Kuryshev, Yuan Chen, Renganathan, Heather Eng, Sanjay J. Danthi, James W. Kramer, Tianen Yang, and Arthur M. Brown. 2008. “Alfuzosin Delays Cardiac Repolarization by a Novel Mechanism.” *Journal of Pharmacology and Experimental Therapeutics* 324 (2): 427–33. https://doi.org/10.1124/jpet.107.128405.

Laske, Timothy G., Maneesh Shrivastav, and Paul A. Iaizzo. 2009. “The Cardiac Conduction System.” In *Handbook of Cardiac Anatomy, Physiology, and Devices*, edited by Paul A. Iaizzo, 159–75. Totowa, NJ: Humana Press. https://doi.org/10.1007/978-1-60327-372-5_11.

Lasser, Karen E., Paul D. Allen, Steffie J. Woolhandler, David U. Himmelstein, Sidney M. Wolfe, and David H. Bor. 2002. “Timing of New Black Box Warnings and Withdrawals for Prescription Medications.” *JAMA* 287 (17): 2215–20. https://doi.org/10.1001/jama.287.17.2215.

Laurila, Eeva, Antti Ahola, Jari Hyttinen, and Katriina Aalto-Setälä. 2016. “Methods for in Vitro Functional Analysis of IPSC Derived Cardiomyocytes — Special Focus on Analyzing the Mechanical Beating Behavior.” *Biochimica et Biophysica Acta (BBA) - Molecular Cell Research*, Cardiomyocyte Biology: Integration of Developmental and Environmental Cues in the Heart, 1863 (7, Part B): 1864–72. https://doi.org/10.1016/j.bbamcr.2015.12.013.

Laverty, HG, C. Benson, EJ Cartwright, MJ Cross, C. Garland, T. Hammond, C. Holloway, et al. 2011. “How Can We Improve Our Understanding of Cardiovascular Safety Liabilities to Develop Safer Medicines?” *British Journal of Pharmacology* 163 (4): 675–93. https://doi.org/10.1111/j.1476-5381.2011.01255.x.

Leung, Chak Ming, Pim de Haan, Kacey Ronaldson-Bouchard, Ge-Ah Kim, Jihoon Ko, Hoon Suk Rho, Zhu Chen, et al. 2022. “A Guide to the Organ-on-a-Chip.” *Nature Reviews Methods Primers* 2 (1): 1–29. https://doi.org/10.1038/s43586-022-00118-6.

Lewandowski, Jarosław, Natalia Rozwadowska, Tomasz J. Kolanowski, Agnieszka Malcher, Agnieszka Zimna, Anna Rugowska, Katarzyna Fiedorowicz, et al. 2018. “The Impact of in Vitro Cell Culture Duration on the Maturation of Human Cardiomyocytes Derived from Induced Pluripotent Stem Cells of Myogenic Origin.” *Cell Transplantation* 27 (7): 1047–67. https://doi.org/10.1177/0963689718779346.

Li, Daxiang, Jian Wu, Yan Bai, Xiaochen Zhao, and Lijun Liu. 2014. “Isolation and Culture of Adult Mouse Cardiomyocytes for Cell Signaling and in Vitro Cardiac Hypertrophy.” *Journal of Visualized Experiments : JoVE*, no. 87 (May): 51357. https://doi.org/10.3791/51357.

Li, Heng, Bob Handsaker, Alec Wysoker, Tim Fennell, Jue Ruan, Nils Homer, Gabor Marth, Goncalo Abecasis, and Richard Durbin. 2009. “The Sequence Alignment/Map Format and SAMtools.” *Bioinformatics* 25 (16): 2078–79. https://doi.org/10.1093/bioinformatics/btp352.

Li, Junjun, Ying Hua, Shigeru Miyagawa, Jingbo Zhang, Lingjun Li, Li Liu, and Yoshiki Sawa. 2020. “HiPSC-Derived Cardiac Tissue for Disease Modeling and Drug Discovery.” *International Journal of Molecular Sciences* 21 (23): 8893. https://doi.org/10.3390/ijms21238893.

Li, Xichun, Rui Zhang, Bin Zhao, Christoph Lossin, and Zhengyu Cao. 2016. “Cardiotoxicity Screening: A Review of Rapid-Throughput in Vitro Approaches.” *Archives of Toxicology* 90 (8): 1803–16. https://doi.org/10.1007/s00204-015-1651-1.

Li, Yanzhen, Huda Asfour, and Nenad Bursac. 2017. “Age-Dependent Functional Crosstalk between Cardiac Fibroblasts and Cardiomyocytes in a 3D Engineered Cardiac Tissue.” *Acta Biomaterialia* 55 (June): 120–30. https://doi.org/10.1016/j.actbio.2017.04.027.

Liao, Yang, Gordon K. Smyth, and Wei Shi. 2014. “FeatureCounts: An Efficient General Purpose Program for Assigning Sequence Reads to Genomic Features.” *Bioinformatics (Oxford, England)* 30 (7): 923–30. https://doi.org/10.1093/bioinformatics/btt656.

Linder, P., J. Trzewik, M. Rüffer, G. Artmann, I. Digel, R. Kurz, A. Rothermel, A. Robitzki, and A. Temiz Artmann. 2010. “Contractile Tension and Beating Rates of Self-Exciting Monolayers and 3D-Tissue Constructs of Neonatal

Rat Cardiomyocytes." *Medical & Biological Engineering & Computing* 48 (1): 59–65. https://doi.org/10.1007/s11517-009-0552-y.
Litviňuková, Monika, Carlos Talavera-López, Henrike Maatz, Daniel Reichart, Catherine L. Worth, Eric L. Lindberg, Masatoshi Kanda, et al. 2020. "Cells of the Adult Human Heart." *Nature* 588 (7838): 466–72. https://doi.org/10.1038/s41586-020-2797-4.
Liu, Jianwei, Ning Sun, Marc A. Bruce, Joseph C. Wu, and Manish J. Butte. 2012. "Atomic Force Mechanobiology of Pluripotent Stem Cell-Derived Cardiomyocytes." *PLoS ONE* 7 (5): e37559. https://doi.org/10.1371/journal.pone.0037559.
Lonsdale, John, Jeffrey Thomas, Mike Salvatore, Rebecca Phillips, Edmund Lo, Saboor Shad, Richard Hasz, et al. 2013. "The Genotype-Tissue Expression (GTEx) Project." *Nature Genetics* 45 (6): 580–85. https://doi.org/10.1038/ng.2653.
Louch, William E., Katherine A. Sheehan, and Beata M. Wolska. 2011. "Methods in Cardiomyocyte Isolation, Culture, and Gene Transfer." *Journal of Molecular and Cellular Cardiology* 51 (3): 288–98. https://doi.org/10.1016/j.yjmcc.2011.06.012.
Louisse, Jochem, Rob C. I. Wüst, Francesca Pistollato, Taina Palosaari, Manuela Barilari, Peter Macko, Susanne Bremer, and Pilar Prieto. 2017. "Assessment of Acute and Chronic Toxicity of Doxorubicin in Human Induced Pluripotent Stem Cell-Derived Cardiomyocytes." *Toxicology in Vitro* 42 (Journal Article): 182–90. https://doi.org/10.1016/j.tiv.2017.04.023.
Love, Michael I., Wolfgang Huber, and Simon Anders. 2014. "Moderated Estimation of Fold Change and Dispersion for RNA-Seq Data with DESeq2." *Genome Biology* 15 (12): 550. https://doi.org/10.1186/s13059-014-0550-8.
Lu, Y., and Z. Wang. 1999. "Terfenadine Block of Sodium Current in Canine Atrial Myocytes." *Journal of Cardiovascular Pharmacology* 33 (3): 507–13. https://doi.org/10.1097/00005344-199903000-00023.
Ma, Qingming, Haixia Ma, Fenglan Xu, Xinyu Wang, and Wentao Sun. 2021. "Microfluidics in Cardiovascular Disease Research: State of the Art and Future Outlook." *Microsystems & Nanoengineering* 7 (1): 1–19. https://doi.org/10.1038/s41378-021-00245-2.
MacDonald, James S., and Richard T. Robertson. 2009. "Toxicity Testing in the 21st Century: A View from the Pharmaceutical Industry." *Toxicological Sciences* 110 (1): 40–46. https://doi.org/10.1093/toxsci/kfp088.
Magdy, Tarek, Adam J.T. Schuldt, Joseph C. Wu, Daniel Bernstein, and Paul W. Burridge. 2018. "Human Induced Pluripotent Stem Cell (HiPSC)-Derived Cells to Assess Drug Cardiotoxicity: Opportunities and Problems." *Annual Review of Pharmacology and Toxicology* 58 (January): 83–103. https://doi.org/10.1146/annurev-pharmtox-010617-053110.

Malhotra, B. K., P. Glue, K. Sweeney, R. Anziano, J. Mancuso, and P. Wicker. 2007. "Thorough QT Study with Recommended and Supratherapeutic Doses of Tolterodine." *Clinical Pharmacology & Therapeutics* 81 (3): 377–85. https://doi.org/10.1038/sj.clpt.6100089.

Mannhardt, Ingra, Kaja Breckwoldt, David Letuffe-Brenière, Sebastian Schaaf, Herbert Schulz, Christiane Neuber, Anika Benzin, et al. 2016. "Human Engineered Heart Tissue: Analysis of Contractile Force." *Stem Cell Reports* 7 (1): 29–42. https://doi.org/10.1016/j.stemcr.2016.04.011.

Mannhardt, Ingra, Alexandra Eder, Berengere Dumotier, Maksymilian Prondzynski, Elisabeth Krämer, Martin Traebert, Klaus-Dieter Söhren, et al. 2017. "Blinded Contractility Analysis in HiPSC-Cardiomyocytes in Engineered Heart Tissue Format: Comparison With Human Atrial Trabeculae." *Toxicological Sciences* 158 (1): 164–75. https://doi.org/10.1093/toxsci/kfx081.

Mannhardt, Ingra, Umber Saleem, Diogo Mosqueira, Malte F. Loos, Bärbel M. Ulmer, Marc D. Lemoine, Camilla Larsson, et al. 2020. "Comparison of 10 Control HPSC Lines for Drug Screening in an Engineered Heart Tissue Format." *Stem Cell Reports* 15 (4): 983–98. https://doi.org/10.1016/j.stemcr.2020.09.002.

Marsano, Anna, Chiara Conficconi, Marta Lemme, Paola Occhetta, Emanuele Gaudiello, Emiliano Votta, Giulia Cerino, Alberto Redaelli, and Marco Rasponi. 2016. "Beating Heart on a Chip: A Novel Microfluidic Platform to Generate Functional 3D Cardiac Microtissues." *Lab on a Chip* 16 (3): 599–610. https://doi.org/10.1039/C5LC01356A.

Marx, Uwe, Takafumi Akabane, Tommy B. Andersson, Elizabeth Baker, Mario Beilmann, Sonja Beken, Susanne Brendler-Schwaab, et al. 2020. "Biology-Inspired Microphysiological Systems to Advance Patient Benefit and Animal Welfare in Drug Development." *ALTEX - Alternatives to Animal Experimentation* 37 (3): 365–94. https://doi.org/10.14573/altex.2001241.

Mastikhina, Olya, Byeong-Ui Moon, Kenneth Williams, Rupal Hatkar, Dakota Gustafson, Omar Mourad, Xuetao Sun, et al. 2020. "Human Cardiac Fibrosis-on-a-Chip Model Recapitulates Disease Hallmarks and Can Serve as a Platform for Drug Testing." *Biomaterials* 233 (March): 119741. https://doi.org/10.1016/j.biomaterials.2019.119741.

Mathews, Grant, Claus Sondergaard, Angela Jeffreys, William Childs, Bao Linh Le, Amrit Sahota, Skender Najibi, Jan Nolta, and Ming-Sing Si. 2012. "Computational Analysis of Contractility in Engineered Heart Tissue." *IEEE TRANSACTIONS ON BIOMEDICAL ENGINEERING* 59 (5): 1429–35. https://doi.org/10.1109/TBME.2012.2187899.

Mathur, Anurag, Zhen Ma, Peter Loskill, Shaheen Jeeawoody, and Kevin E. Healy. 2016. "In Vitro Cardiac Tissue Models: Current Status and Future Prospects." *Advanced Drug Delivery Reviews*, Tissue engineering of the

heart: from in vitro models to regenerative solutions, 96 (January): 203–13. https://doi.org/10.1016/j.addr.2015.09.011.

Matsuura, Katsuhisa, Shinako Masuda, Yuji Haraguchi, Noriko Yasuda, Tatsuya Shimizu, Nobuhisa Hagiwara, Peter W. Zandstra, and Teruo Okano. 2011. "Creation of Mouse Embryonic Stem Cell-Derived Cardiac Cell Sheets." *Biomaterials* 32 (30): 7355–62. https://doi.org/10.1016/j.biomaterials.2011.05.042.

Meer, Berend J. van, Ana Krotenberg, Luca Sala, Richard P. Davis, Thomas Eschenhagen, Chris Denning, Leon G. J. Tertoolen, and Christine L. Mummery. 2019. "Simultaneous Measurement of Excitation-Contraction Coupling Parameters Identifies Mechanisms Underlying Contractile Responses of HiPSC-Derived Cardiomyocytes." *Nature Communications* 10 (1): 1–9. https://doi.org/10.1038/s41467-019-12354-8.

Mehta, Ashish, YingYing Chung, Glen Lester Sequiera, Philip Wong, Reginald Liew, and Winston Shim. 2013. "Pharmacoelectrophysiology of Viral-Free Induced Pluripotent Stem Cell-Derived Human Cardiomyocytes." *Toxicological Sciences : An Official Journal of the Society of Toxicology* 131 (2): 458–69. https://doi.org/10.1093/toxsci/kfs309.

Meyer, Thomas, Karl-Heinz Boven, Elke Günther, and Michael Fejtl. 2004. "Micro-Electrode Arrays in Cardiac Safety Pharmacology." *Drug Safety* 27 (11): 763–72. https://doi.org/10.2165/00002018-200427110-00002.

Millard, Daniel, Qianyu Dang, Hong Shi, Xiaou Zhang, Chris Strock, Udo Kraushaar, Haoyu Zeng, et al. 2018. "Cross-Site Reliability of Human Induced Pluripotent Stem Cell-Derived Cardiomyocyte Based Safety Assays Using Microelectrode Arrays: Results from a Blinded CiPA Pilot Study." *Toxicological Sciences* 164 (2): 550–62. https://doi.org/10.1093/toxsci/kfy110.

Mills, Richard J., Drew M. Titmarsh, Xaver Koenig, Benjamin L. Parker, James G. Ryall, Gregory A. Quaife-Ryan, Holly K. Voges, et al. 2017. "Functional Screening in Human Cardiac Organoids Reveals a Metabolic Mechanism for Cardiomyocyte Cell Cycle Arrest." *Proceedings of the National Academy of Sciences* 114 (40): E8372–81. https://doi.org/10.1073/pnas.1707316114.

Ming, Z., and C. Nordin. 1995. "Terfenadine Blocks Time-Dependent Ca2+, Na+, and K+ Channels in Guinea Pig Ventricular Myocytes." *Journal of Cardiovascular Pharmacology* 26 (5): 761–69. https://doi.org/10.1097/00005344-199511000-00013.

Morimoto, Y., S. Mori, F. Sakai, and S. Takeuchi. 2016. "Human Induced Pluripotent Stem Cell-Derived Fiber-Shaped Cardiac Tissue on a Chip." *Lab on a Chip* 16 (12): 2295–2301. https://doi.org/10.1039/C6LC00422A.

Munawar, Sadek, and Irene C. Turnbull. 2021. "Cardiac Tissue Engineering: Inclusion of Non-Cardiomyocytes for Enhanced Features." *Frontiers in Cell*

and Developmental Biology 9. https://www.frontiersin.org/articles/10.3389/fcell.2021.653127.

Nanion Technologies. 2023. "FLEXcyte 96." Nanion Technologies. 2023. https://www.nanion.de/products/flexcyte-96/.

Narmoneva, Daria A., Rada Vukmirovic, Michael E. Davis, Roger D. Kamm, and Richard T. Lee. 2004. "Endothelial Cells Promote Cardiac Myocyte Survival and Spatial Reorganization." *Circulation* 110 (8): 962–68. https://doi.org/10.1161/01.CIR.0000140667.37070.07.

Nichol, Jason W., George C. Engelmayr, Mingyu Cheng, and Lisa E. Freed. 2008. "Co-Culture Induces Alignment in Engineered Cardiac Constructs via MMP-2 Expression." *Biochemical and Biophysical Research Communications* 373 (3): 360–65. https://doi.org/10.1016/j.bbrc.2008.06.019.

Obergrussberger, Alison, Søren Friis, Andrea Brüggemann, and Niels Fertig. 2021. "Automated Patch Clamp in Drug Discovery: Major Breakthroughs and Innovation in the Last Decade." *Expert Opinion on Drug Discovery* 16 (1): 1–5. https://doi.org/10.1080/17460441.2020.1791079.

Obien, Marie Engelene J., Kosmas Deligkaris, Torsten Bullmann, Douglas J. Bakkum, and Urs Frey. 2015. "Revealing Neuronal Function through Microelectrode Array Recordings." *Frontiers in Neuroscience* 8 (Journal Article). https://doi.org/10.3389/fnins.2014.00423.

Oh, VM, BL Chia, and EA Taylor. 1985. "Effects of Long-acting Propranolol on Blood Pressure and Heart Rate in Hypertensive Chinese." *British Journal of Clinical Pharmacology* 20 (2): 144–47. https://doi.org/10.1111/j.1365-2125.1985.tb05046.x.

Osterbur Badhey, Marika L., Alexander C. Bertalovitz, and Thomas V. McDonald. 2017. "Express with Caution: Epitope Tags and CDNA Variants Effects on HERG Channel Trafficking, Half-Life and Function." *Journal of Cardiovascular Electrophysiology* 28 (9): 1070–82. https://doi.org/10.1111/jce.13259.

Overgaard, Christopher B., and Vladimír Džavík. 2008. "Inotropes and Vasopressors." *Circulation* 118 (10): 1047–56. https://doi.org/10.1161/CIRCULATIONAHA.107.728840.

Paloschi, Valentina, Maria Sabater-Lleal, Heleen Middelkamp, Aisen Vivas, Sofia Johansson, Andries van der Meer, Maria Tenje, and Lars Maegdefessel. 2021. "Organ-on-a-Chip Technology: A Novel Approach to Investigate Cardiovascular Diseases." *Cardiovascular Research* 117 (14): 2742–54. https://doi.org/10.1093/cvr/cvab088.

Park, Jungyul, Jaewook Ryu, Seung Kyu Choi, Eunseok Seo, Jae Min Cha, Seokchang Ryu, Jinseok Kim, Byungkyu Kim, and Sang Ho Lee. 2005. "Real-Time Measurement of the Contractile Forces of Self-Organized Cardiomyocytes on Hybrid Biopolymer Microcantilevers." *Analytical Chemistry* 77 (20): 6571–80. https://doi.org/10.1021/ac0507800.

Parrotta, Elvira Immacolata, Valeria Lucchino, Luana Scaramuzzino, Stefania Scalise, and Giovanni Cuda. 2020. “Modeling Cardiac Disease Mechanisms Using Induced Pluripotent Stem Cell-Derived Cardiomyocytes: Progress, Promises and Challenges.” *International Journal of Molecular Sciences* 21 (12): 4354. https://doi.org/10.3390/ijms21124354.

Peña, Brisa, Mostafa Adbel-Hafiz, Maria Cavasin, Luisa Mestroni, and Orfeo Sbaizero. 2022. “Atomic Force Microscopy (AFM) Applications in Arrhythmogenic Cardiomyopathy.” *International Journal of Molecular Sciences* 23 (7): 3700. https://doi.org/10.3390/ijms23073700.

Pillekamp, Frank, Michael Reppel, Olga Rubenchyk, Kurt Pfannkuche, Matthias Matzkies, Wilhelm Bloch, Narayanswami Sreeram, Konrad Brockmeier, and Jürgen Hescheler. 2007. “Force Measurements of Human Embryonic Stem Cell-Derived Cardiomyocytes in an In Vitro Transplantation Model.” *STEM CELLS* 25: 174–80.

Pincus, M. 2016. “Management of Digoxin Toxicity.” *Australian Prescriber* 39 (1): 18–20. https://doi.org/10.18773/austprescr.2016.006.

Ponchio, L., L. Duma, B. Oliviero, N. Gibelli, P. Pedrazzoli, and G. Robustelli della Cuna. 2000. “Mitomycin C as an Alternative to Irradiation to Inhibit the Feeder Layer Growth in Long-Term Culture Assays.” *Cytotherapy* 2 (4): 281–86. https://doi.org/10.1080/146532400539215.

Pradhapan, Paruthi, Jukka Kuusela, Jari Viik, Katriina Aalto-Setälä, and Jari Hyttinen. 2013. “Cardiomyocyte MEA Data Analysis (CardioMDA) – A Novel Field Potential Data Analysis Software for Pluripotent Stem Cell Derived Cardiomyocytes.” *PLOS ONE* 8 (9): e73637. https://doi.org/10.1371/journal.pone.0073637.

Radisic, Milica, Hyoungshin Park, Timothy P. Martens, Johanna E. Salazar-Lazaro, Wenliang Geng, Yadong Wang, Robert Langer, Lisa E. Freed, and Gordana Vunjak-Novakovic. 2008. “Pre-Treatment of Synthetic Elastomeric Scaffolds by Cardiac Fibroblasts Improves Engineered Heart Tissue.” *Journal of Biomedical Materials Research. Part A* 86 (3): 713–24. https://doi.org/10.1002/jbm.a.31578.

Raudvere, Uku, Liis Kolberg, Ivan Kuzmin, Tambet Arak, Priit Adler, Hedi Peterson, and Jaak Vilo. 2019. “G:Profiler: A Web Server for Functional Enrichment Analysis and Conversions of Gene Lists (2019 Update).” *Nucleic Acids Research* 47 (W1): W191–98. https://doi.org/10.1093/nar/gkz369.

Ravenscroft, Stephanie M., Amy Pointon, Awel W. Williams, Michael J. Cross, and James E. Sidaway. 2016. “Cardiac Non-Myocyte Cells Show Enhanced Pharmacological Function Suggestive of Contractile Maturity in Stem Cell Derived Cardiomyocyte Microtissues.” *Toxicological Sciences* 152 (1): 99–112. https://doi.org/10.1093/toxsci/kfw069.

Rhoden, Alexandra, Thomas Schulze, Niels Pietsch, Torsten Christ, Arne Hansen, and Thomas Eschenhagen. 2022. “Comprehensive Analyses of the

Inotropic Compound Omecamtiv Mecarbil in Rat and Human Cardiac Preparations." *American Journal of Physiology-Heart and Circulatory Physiology* 322 (3): H373–85. https://doi.org/10.1152/ajpheart.00534.2021.

Ribeiro, Alexandre J. S., Brian D. Guth, Michael Engwall, Sandy Eldridge, C. Michael Foley, Liang Guo, Gary Gintant, et al. 2019. "Considerations for an In Vitro, Cell-Based Testing Platform for Detection of Drug-Induced Inotropic Effects in Early Drug Development. Part 2: Designing and Fabricating Microsystems for Assaying Cardiac Contractility With Physiological Relevance Using Human IPSC-Cardiomyocytes." *Frontiers in Pharmacology* 10 (Journal Article). https://doi.org/10.3389/fphar.2019.00934.

Ribeiro, Alexandre J.S., Olivier Schwab, Mohammad A. Mandegar, Yen-Sin Ang, Bruce R. Conklin, Deepak Srivastava, and Beth L. Pruitt. 2017. "Multi-Imaging Method to Assay the Contractile Mechanical Output of Micropatterned Human IPSC-Derived Cardiac Myocytes." *Circulation Research* 120 (10): 1572–83. https://doi.org/10.1161/CIRCRESAHA.116.310363.

Ribeiro, Marcelo C., Leon G. Tertoolen, Juan A. Guadix, Milena Bellin, Georgios Kosmidis, Cristina D'Aniello, Jantine Monshouwer-Kloots, et al. 2015. "Functional Maturation of Human Pluripotent Stem Cell Derived Cardiomyocytes in Vitro - Correlation between Contraction Force and Electrophysiology." *Biomaterials* 51 (Journal Article): 138–50.

Robertson, Claire, David D. Tran, and Steven C. George. 2013. "Concise Review: Maturation Phases of Human Pluripotent Stem Cell-Derived Cardiomyocytes." *STEM CELLS* 31 (5): 829–37. https://doi.org/10.1002/stem.1331.

Rodriguez, Marita L., Brandon T. Graham, Lil M. Pabon, Sangyoon J. Han, Charles E. Murry, and Nathan J. Sniadecki. 2014. "Measuring the Contractile Forces of Human Induced Pluripotent Stem Cell-Derived Cardiomyocytes with Arrays of Microposts." *Journal of Biomechanical Engineering* 136 (5): 051005. https://doi.org/10.1115/1.4027145.

Ronaldson-Bouchard, Kacey, Stephen P. Ma, Keith Yeager, Timothy Chen, LouJin Song, Dario Sirabella, Kumi Morikawa, Diogo Teles, Masayuki Yazawa, and Gordana Vunjak-Novakovic. 2018. "Advanced Maturation of Human Cardiac Tissue Grown from Pluripotent Stem Cells." *Nature* 556 (7700): 239–43. https://doi.org/10.1038/s41586-018-0016-3.

Ronaldson-Bouchard, Kacey, Keith Yeager, Diogo Teles, Timothy Chen, Stephen Ma, LouJin Song, Kumi Morikawa, et al. 2019. "Engineering of Human Cardiac Muscle Electromechanically Matured to an Adult-like Phenotype." *Nature Protocols* 14 (10): 2781–2817. https://doi.org/10.1038/s41596-019-0189-8.

Roy, M., R. Dumaine, and A. M. Brown. 1996. “HERG, a Primary Human Ventricular Target of the Nonsedating Antihistamine Terfenadine.” *Circulation* 94 (4): 817–23. https://doi.org/10.1161/01.cir.94.4.817.

Sadeghi, Amir Hossein, Su Ryon Shin, Janine C. Deddens, Giuseppe Fratta, Serena Mandla, Iman K. Yazdi, Gyan Prakash, et al. 2017. “Engineered 3D Cardiac Fibrotic Tissue to Study Fibrotic Remodeling.” *Advanced Healthcare Materials* 6 (11). https://doi.org/10.1002/adhm.201601434.

Saenz Cogollo, Jose, Mariateresa Tedesco, Sergio Martinoia, and Roberto Raiteri. 2011. “A New Integrated System Combining Atomic Force Microscopy and Micro-Electrode Array for Measuring the Mechanical Properties of Living Cardiac Myocytes.” *Biomedical Microdevices* 13 (4): 613–21. https://doi.org/10.1007/s10544-011-9531-9.

Saini, Harpinder, Ali Navaei, Alison Van Putten, and Mehdi Nikkhah. 2015. “3D Cardiac Microtissues Encapsulated with the Co-Culture of Cardiomyocytes and Cardiac Fibroblasts.” *Advanced Healthcare Materials* 4 (13): 1961–71. https://doi.org/10.1002/adhm.201500331.

Saleem, Umber, Djemail Ismaili, Ingra Mannhardt, Hans Pinnschmidt, Thomas Schulze, Torsten Christ, Thomas Eschenhagen, and Arne Hansen. 2020. “Regulation of ICa,L and Force by PDEs in Human-induced Pluripotent Stem Cell-derived Cardiomyocytes.” *British Journal of Pharmacology* 177 (13): 3036–45. https://doi.org/10.1111/bph.15032.

Sands, Gregory B., Bruce H. Smaill, and Ian J. LeGrice. 2008. “Virtual Sectioning of Cardiac Tissue Relative to Fiber Orientation.” *Annual International Conference of the IEEE Engineering in Medicine and Biology Society. IEEE Engineering in Medicine and Biology Society. Annual International Conference* 2008: 226–29. https://doi.org/10.1109/IEMBS.2008.4649131.

Santana, Luis F., Edward P. Cheng, and W. Jonathan Lederer. 2010. “How Does the Shape of the Cardiac Action Potential Control Calcium Signaling and Contraction in the Heart?” *Journal of Molecular and Cellular Cardiology* 49 (6): 901–3. https://doi.org/10.1016/j.yjmcc.2010.09.005.

Sarkanen, J. R., H. Vuorenpaa, O. Huttala, B. Mannerstrom, H. Kuokkanen, S. Miettinen, T. Heinonen, and T. Ylikomi. 2012. “Adipose Stromal Cell Tubule Network Model Provides a Versatile Tool for Vascular Research and Tissue Engineering.” *Cells, Tissues, Organs* 196 (5): 385–97. https://doi.org/10.1159/000336679.

Sasaki, Daisuke, Katsuhisa Matsuura, Hiroyoshi Seta, Yuji Haraguchi, Teruo Okano, and Tatsuya Shimizu. 2018. “Contractile Force Measurement of Human Induced Pluripotent Stem Cell-Derived Cardiac Cell Sheet-Tissue.” *PLOS ONE* 13 (5): e0198026. https://doi.org/10.1371/journal.pone.0198026.

Schaaf, Sebastian, Aya Shibamiya, Marco Mewe, Alexandra Eder, Andrea Stöhr, Marc N. Hirt, Thomas Rau, et al. 2011. “Human Engineered Heart Tissue as

a Versatile Tool in Basic Research and Preclinical Toxicology." *PLoS One* 6 (10): e26397. https://doi.org/10.1371/journal.pone.0026397.

Schaefer, Jeremy A., and Robert T. Tranquillo. 2016. "Tissue Contraction Force Microscopy for Optimization of Engineered Cardiac Tissue." *Tissue Engineering Part C: Methods* 22 (1): 76–83. https://doi.org/10.1089/ten.tec.2015.0220.

Schwan, Jonas, Andrea T. Kwaczala, Thomas J. Ryan, Oscar Bartulos, Yongming Ren, Lorenzo R. Sewanan, Aaron H. Morris, Daniel L. Jacoby, Yibing Qyang, and Stuart G. Campbell. 2016. "Anisotropic Engineered Heart Tissue Made from Laser-Cut Decellularized Myocardium." *Scientific Reports* 6 (Journal Article): 32068. https://doi.org/10.1038/srep32068.

Segev, Amir, Francisco Garcia-Oscos, and Saïd Kourrich. 2016. "Whole-Cell Patch-Clamp Recordings in Brain Slices." *Journal of Visualized Experiments : JoVE*, no. 112 (June): 54024. https://doi.org/10.3791/54024.

Sekine, Hidekazu, Tatsuya Shimizu, Kyoko Hobo, Sachiko Sekiya, Joseph Yang, Masayuki Yamato, Hiromi Kurosawa, Eiji Kobayashi, and Teruo Okano. 2008. "Endothelial Cell Coculture within Tissue-Engineered Cardiomyocyte Sheets Enhances Neovascularization and Improves Cardiac Function of Ischemic Hearts." *Circulation* 118 (14 Suppl): S145-152. https://doi.org/10.1161/CIRCULATIONAHA.107.757286.

Sirenko, O., C. Crittenden, N. Callamaras, J. Hesley, Y. W. Chen, C. Funes, I. Rusyn, B. Anson, and E. F. Cromwell. 2013. "Multiparameter in Vitro Assessment of Compound Effects on Cardiomyocyte Physiology Using IPSC Cells." *Journal of Biomolecular Screening* 18 (1): 39–53. https://doi.org/10.1177/1087057112457590.

Smith, Alec S. T., Jesse Macadangdang, Winnie Leung, Michael A. Laflamme, and Deok-Ho Kim. 2017. "Human IPSC-Derived Cardiomyocytes and Tissue Engineering Strategies for Disease Modeling and Drug Screening." *Biotechnology Advances* 35 (1): 77–94. https://doi.org/10.1016/j.biotechadv.2016.12.002.

Sondergaard, Claus Svane, Grant Mathews, Lianguo Wang, Angela Jeffreys, Amrit Sahota, Moira Wood, Crystal M. Ripplinger, and Ming-Sing Si. 2012. "Contractile and Electrophysiologic Characterization of Optimized Self-Organizing Engineered Heart Tissue." *The Annals of Thoracic Surgery* 94 (4): 1241–49. https://doi.org/10.1016/j.athoracsur.2012.04.098.

Steffens, Sabine, Matthias Nahrendorf, and Rosalinda Madonna. 2021. "Immune Cells in Cardiac Homeostasis and Disease: Emerging Insights from Novel Technologies." *European Heart Journal* 43 (16): 1533–41. https://doi.org/10.1093/eurheartj/ehab842.

Stoehr, Andrea, Christiane Neuber, Christina Baldauf, Ingra Vollert, Felix W. Friedrich, Frederik Flenner, Lucie Carrier, et al. 2014. "Automated Analysis of Contractile Force and Ca2+ Transients in Engineered Heart Tissue."

American Journal of Physiology. Heart and Circulatory Physiology 306 (9): H1353–63. https://doi.org/10.1152/ajpheart.00705.2013.

Stratton, J. R., M. D. Cerqueira, R. S. Schwartz, W. C. Levy, R. C. Veith, S. E. Kahn, and I. B. Abrass. 1992. "Differences in Cardiovascular Responses to Isoproterenol in Relation to Age and Exercise Training in Healthy Men." *Circulation* 86 (2): 504–12. https://doi.org/10.1161/01.CIR.86.2.504.

Stratton, J. R., M. A. Pfeifer, J. L. Ritchie, and J. B. Halter. 1985. "Hemodynamic Effects of Epinephrine: Concentration-Effect Study in Humans." *Journal of Applied Physiology* 58 (4): 1199–1206. https://doi.org/10.1152/jappl.1985.58.4.1199.

Sung, Jong Hwan, Ying I. Wang, Narasimhan Narasimhan Sriram, Max Jackson, Christopher Long, James J. Hickman, and Michael L. Shuler. 2019. "Recent Advances in Body-on-a-Chip Systems." *Analytical Chemistry* 91 (1): 330–51. https://doi.org/10.1021/acs.analchem.8b05293.

Surbhi and Sukesha. 2020. "Response of Piezoelectric Materials to the External Temperature, Electric Field and Humidity." *Materials Today: Proceedings*, International Conference on Aspects of Materials Science and Engineering, 28 (January): 1951–54. https://doi.org/10.1016/j.matpr.2020.05.555.

Sutanto, Henry, Aurore Lyon, Joost Lumens, Ulrich Schotten, Dobromir Dobrev, and Jordi Heijman. 2020. "Cardiomyocyte Calcium Handling in Health and Disease: Insights from in Vitro and in Silico Studies." *Progress in Biophysics and Molecular Biology*, Evaluation of Data in Cellular Electrophysiology, 157 (November): 54–75. https://doi.org/10.1016/j.pbiomolbio.2020.02.008.

Sweeney, Mark, and Gabor Foldes. 2018. "It Takes Two: Endothelial-Perivascular Cell Cross-Talk in Vascular Development and Disease." *Frontiers in Cardiovascular Medicine* 5. https://www.frontiersin.org/article/10.3389/fcvm.2018.00154.

Takahashi, Kazutoshi, Koji Tanabe, Mari Ohnuki, Megumi Narita, Tomoko Ichisaka, Kiichiro Tomoda, and Shinya Yamanaka. 2007. "Induction of Pluripotent Stem Cells from Adult Human Fibroblasts by Defined Factors." *Cell* 131 (5): 861–72. https://doi.org/10.1016/j.cell.2007.11.019.

Takahashi, Kazutoshi, and Shinya Yamanaka. 2006. "Induction of Pluripotent Stem Cells from Mouse Embryonic and Adult Fibroblast Cultures by Defined Factors." *Cell* 126 (4): 663–76. https://doi.org/10.1016/j.cell.2006.07.024.

Takeda, Maki, Shigeru Miyagawa, Satsuki Fukushima, Atsuhiro Saito, Emiko Ito, Akima Harada, Ryohei Matsuura, et al. 2018. "Development of In Vitro Drug-Induced Cardiotoxicity Assay by Using Three-Dimensional Cardiac Tissues Derived from Human Induced Pluripotent Stem Cells." *Tissue Engineering Part C: Methods* 24 (1): 56–67. https://doi.org/10.1089/ten.tec.2017.0247.

Talman, Virpi, and Riikka Kivelä. 2018. “Cardiomyocyte—Endothelial Cell Interactions in Cardiac Remodeling and Regeneration.” *Frontiers in Cardiovascular Medicine* 5: 101. https://doi.org/10.3389/fcvm.2018.00101.

Thompson, Marc T. 2014. “Chapter 14 - Analog Low-Pass Filters.” In *Intuitive Analog Circuit Design (Second Edition)*, edited by Marc T. Thompson, 531–83. Boston: Newnes. https://doi.org/10.1016/B978-0-12-405866-8.00014-0.

Tirziu, Daniela, Frank J. Giordano, and Michael Simons. 2010. “Cell Communications in the Heart.” *Circulation* 122 (9): 928–37. https://doi.org/10.1161/CIRCULATIONAHA.108.847731.

Toimela, T., O. Huttala, E. Sabell, M. Mannerström, J. R. Sarkanen, T. Ylikomi, and T. Heinonen. 2017. “Intra-Laboratory Validated Human Cell-Based in Vitro Vasculogenesis/Angiogenesis Test with Serum-Free Medium.” *Reproductive Toxicology* 70 (Journal Article): 116–25. https://doi.org/10.1016/j.reprotox.2016.11.015.

Tsukamoto, Yoshinari, Takami Akagi, and Mitsuru Akashi. 2020. “Vascularized Cardiac Tissue Construction with Orientation by Layer-by-Layer Method and 3D Printer.” *Scientific Reports* 10 (1): 5484. https://doi.org/10.1038/s41598-020-59371-y.

Tucker, Nathan R., Mark Chaffin, Stephen J. Fleming, Amelia W. Hall, Victoria A. Parsons, Kenneth C. Bedi, Amer-Denis Akkad, et al. 2020. “Transcriptional and Cellular Diversity of the Human Heart.” *Circulation* 142 (5): 466–82. https://doi.org/10.1161/CIRCULATIONAHA.119.045401.

Turnbull, Irene C., Ioannis Karakikes, Gregory W. Serrao, Peter Backeris, Jia-Jye Lee, Chaoqin Xie, Grant Senyei, et al. 2014. “Advancing Functional Engineered Cardiac Tissues toward a Preclinical Model of Human Myocardium.” *FASEB Journal : Official Publication of the Federation of American Societies for Experimental Biology* 28 (2): 644–54. https://doi.org/10.1096/fj.13-228007.

Varzideh, Fahimeh, Elena Mahmoudi, and Sara Pahlavan. 2019. “Coculture with Noncardiac Cells Promoted Maturation of Human Stem Cell–Derived Cardiomyocyte Microtissues.” *Journal of Cellular Biochemistry* 120 (10): 16681–91. https://doi.org/10.1002/jcb.28926.

Vasaramäki, Sanna-Kaisa. 2014. “Ihmissolupohjaisen sydänmallin alustapinnoitukset eri materiaaleilla.” Fi=AMK-opinnäytetyö|sv=YH-examensarbete|en=Bachelor’s thesis|, Tampereen ammattikorkeakoulu. http://www.theseus.fi/handle/10024/76160.

Virtanen, Juhani. 2020. *Development of Measurement Concepts for Canine Dry Electrode Electrocardiogram and Human Cardiac Construct Contraction Force Measurements*. Tampere University. https://trepo.tuni.fi/handle/10024/122635.

Vunjak-Novakovic, Gordana, Thomas Eschenhagen, and Christine Mummery. 2014. "Myocardial Tissue Engineering: In Vitro Models." *Cold Spring Harbor Perspectives in Medicine* 4 (3): a014076. https://doi.org/10.1101/cshperspect.a014076.

Vunjak-Novakovic, Gordana, Nina Tandon, Amandine Godier, Robert Maidhof, Anna Marsano, Timothy P. Martens, and Milica Radisic. 2010. "Challenges in Cardiac Tissue Engineering." *Tissue Engineering Part B: Reviews* 16 (2): 169–87. https://doi.org/10.1089/ten.teb.2009.0352.

Vuorenpää, Hanna, Liisa Ikonen, Kirsi Kujala, Outi Huttala, Jertta-Riina Sarkanen, Timo Ylikomi, Katriina Aalto-Setälä, and Tuula Heinonen. 2014. "Novel in Vitro Cardiovascular Constructs Composed of Vascular-like Networks and Cardiomyocytes." *In Vitro Cellular & Developmental Biology - Animal* 50 (4): 275–86. https://doi.org/10.1007/s11626-013-9703-4.

Vuorenpää, Hanna, Kirsi Penttinen, Tuula Heinonen, Mari Pekkanen-Mattila, Jertta-Riina Sarkanen, Timo Ylikomi, and Katriina Aalto-Setälä. 2017. "Maturation of Human Pluripotent Stem Cell Derived Cardiomyocytes Is Improved in Cardiovascular Construct." *Cytotechnology* 69 (5): 785–800. https://doi.org/10.1007/s10616-017-0088-1.

Wagner, Julian Uwe Gabriel, Minh Duc Pham, Luka Nicin, Marie Hammer, Katharina Bottermann, Ting Yuan, Rahul Sharma, et al. 2020. "Dissection of Heterocellular Cross-Talk in Vascularized Cardiac Tissue Mimetics." *Journal of Molecular and Cellular Cardiology* 138 (January): 269–82. https://doi.org/10.1016/j.yjmcc.2019.12.005.

Wang, Dao W., Akshitkumar M. Mistry, Kristopher M. Kahlig, Jennifer A. Kearney, Jizhou Xiang, and Alfred R. George. 2010. "Propranolol Blocks Cardiac and Neuronal Voltage-Gated Sodium Channels." *Frontiers in Pharmacology* 1. https://doi.org/10.3389/fphar.2010.00144.

Weinhaus, Anthony J., and Kenneth P. Roberts. 2009. "Anatomy of the Human Heart." In *Handbook of Cardiac Anatomy, Physiology, and Devices*, edited by Paul A. Iaizzo, 59–85. Totowa, NJ: Humana Press. https://doi.org/10.1007/978-1-60327-372-5_5.

WHO. 2021. "Cardiovascular Diseases." 2021. https://www.who.int/news-room/fact-sheets/detail/cardiovascular-diseases-(cvds).

Xi, Jiaoya, Markus Khalil, Nava Shishechian, Tobias Hannes, Kurt Pfannkuche, Huamin Liang, Azra Fatima, et al. 2010. "Comparison of Contractile Behavior of Native Murine Ventricular Tissue and Cardiomyocytes Derived from Embryonic or Induced Pluripotent Stem Cells." *FASEB Journal : Official Publication of the Federation of American Societies for Experimental Biology* 24 (8): 2739–51. https://doi.org/10.1096/fj.09-145177.

Yang, Qingzhen, Zhanfeng Xiao, Xuemeng Lv, Tingting Zhang, and Han Liu. 2021. "Fabrication and Biomedical Applications of Heart-on-a-Chip."

International Journal of Bioprinting 7 (3): 370. https://doi.org/10.18063/ijb.v7i3.370.

Yin, Shizhuo, Xueqian Zhang, Chun Zhan, Juntao Wu, Jinchao Xu, and Joseph Cheung. 2005. "Measuring Single Cardiac Myocyte Contractile Force via Moving a Magnetic Bead." *Biophysical Journal* 88 (2): 1489–95. https://doi.org/10.1529/biophysj.104.048157.

Zamani, Maedeh, Esra Karaca, and Ngan F. Huang. 2018. "Multicellular Interactions in 3D Engineered Myocardial Tissue." *Frontiers in Cardiovascular Medicine* 5. https://www.frontiersin.org/article/10.3389/fcvm.2018.00147.

Zeniieh, D., A. Bajwa, and F. Olcaytug. 2013. "Parylene-C Thin Film for Biocompatible Encapsulations with Very Strong Adhesion and Superior Barrier Properties." In . Cairns Convention Centre, Queensland, Australia. https://www.semanticscholar.org/paper/PARYLENE-C-THIN-FILM-FOR-BIOCOMPATIBLE-WITH-VERY-Zeniieh-Bajwa/a134089d3c6865a0038df655648159eccfb511ac.

Zhang, Feng, Kai-Yun Qu, Bin Zhou, Yong Luo, Zhen Zhu, De-Jing Pan, Chang Cui, Yue Zhu, Ming-Long Chen, and Ning-Ping Huang. 2021. "Design and Fabrication of an Integrated Heart-on-a-Chip Platform for Construction of Cardiac Tissue from Human IPSC-Derived Cardiomyocytes and in Situ Evaluation of Physiological Function." *Biosensors and Bioelectronics* 179 (May): 113080. https://doi.org/10.1016/j.bios.2021.113080.

Zhou, Bingying, Xun Shi, Xiaoli Tang, Quanyi Zhao, Le Wang, Fang Yao, Yongfeng Hou, et al. 2022. "Functional Isolation, Culture and Cryopreservation of Adult Human Primary Cardiomyocytes." *Signal Transduction and Targeted Therapy* 7 (1): 1–16. https://doi.org/10.1038/s41392-022-01044-5.

Zhou, Pingzhu, and William T. Pu. 2016. "Recounting Cardiac Cellular Composition." *Circulation Research* 118 (3): 368–70. https://doi.org/10.1161/CIRCRESAHA.116.308139.

Zhou, Z., Q. Gong, B. Ye, Z. Fan, J. C. Makielski, G. A. Robertson, and C. T. January. 1998. "Properties of HERG Channels Stably Expressed in HEK 293 Cells Studied at Physiological Temperature." *Biophysical Journal* 74 (1): 230–41. https://doi.org/10.1016/S0006-3495(98)77782-3.

Zimmermann, W. -H, K. Schneiderbanger, P. Schubert, M. Didie, F. Munzel, J. F. Heubach, S. Kostin, W. L. Neuhuber, and T. Eschenhagen. 2002. "Tissue Engineering of a Differentiated Cardiac Muscle Construct." *Circulation Research* 90 (2): 223–30. https://doi.org/10.1161/hh0202.103644.

ORIGINAL PUBLICATIONS

PUBLICATION I

Functional human cell-based vascularised cardiac tissue model for biomedical research and testing

Koivisto M, Tolvanen TA, Toimela T, Miinalainen I, Kiviaho A, Kesseli J, Nykter M, Eklund L and Heinonen T

Scientific Reports 12(1):13459 (2022)
DOI: 10.1038/s41598-022-17498-0

scientific reports

Check for updates

OPEN

Functional human cell-based vascularised cardiac tissue model for biomedical research and testing

Maria Koivisto[1]✉, Tuomas A. Tolvanen[1], Tarja Toimela[1], Ilkka Miinalainen[2], Antti Kiviaho[3], Juha Kesseli[3], Matti Nykter[3], Lauri Eklund[4] & Tuula Heinonen[1]

Cardiomyocytes derived from human induced pluripotent stem cells (hiPSC) are widely used in in vitro biomedical research and testing. However, fully matured, adult cardiomyocyte characteristics have not been achieved. To improve the maturity and physiological relevance of hiPSC-derived cardiomyocytes, we co-cultured them with preconstructed vascular-like networks to form a functional, human cell-based cardiac tissue model. The morphology and gene expression profiles indicated advanced maturation in the cardiac tissue model compared to those of a cardiomyocyte monoculture. The cardiac tissue model's functionality was confirmed by measuring the effects of 32 compounds with multielectrode array and comparing results to human data. Our model predicted the cardiac effects with a predictive accuracy of 91%, sensitivity of 90% and specificity of 100%. The correlation between the effective concentration (EC50) and the reported clinical plasma concentrations was 0.952 (R^2 = 0.905). The developed advanced human cell-based cardiac tissue model showed characteristics and functionality of human cardiac tissue enabling accurate transferability of gained in vitro data to human settings. The model is standardized and thus, it would be highly useful in biomedical research and cardiotoxicity testing.

The adverse cardiac effects of drugs are a major cause of drug attrition during drug development and post-approval market withdrawal[1,2]. The cardiotoxicity screening of new drugs typically includes in vitro non-myocyte-based cell assays and in vivo animal testing. The reliability of animal studies suffers from intrinsic electrophysiological differences between different species and humans[3]. The humanised cardiac ion channels in vitro models have been used in detecting compounds causing Torsades de Pointes arrythmia but their benefit for assessment of other cardiotoxic mechanisms as well as for efficacy screening is poor[4]. One reason is that drug-induced adverse cardiac effects can occur in multiple ion channels, structures and functions of the cardiovascular system[5]. Therefore, in vitro models comprising tissue type structure would be needed[4]. The use of human induced pluripotent stem cells (hiPSC)-derived cardiomyocytes in cardiotoxicity testing is proposed to be a more reliable screening platform for cardiac effects than the non-myocyte-based cell assay because hiPSC-derived cardiomyocytes resemble more accurately native human cardiomyocytes including the relevant ion channels[6].

Even though effective protocols for cardiomyocyte differentiation in vitro have been developed[7,8], maturation of the cardiomyocytes has remained a challenge. In their structure and function, the presently available hiPSC-derived cardiomyocytes more closely resemble embryonic or foetal cardiomyocytes than adult cardiomyocytes. These in vitro differentiated cardiomyocytes are typically circular, have irregularly arranged myofibrils and use glycolysis for ATP production, while adult cardiomyocytes are rod-shaped, have highly organized sarcomeres and utilize the oxidative phosphorylation of fatty acids for energy production[9,10]. For example, the sarcomere length and organization of hiPSC-derived cardiomyocytes is comparable to neonatal cardiomyocytes[11]. Immature and mature cardiomyocytes also have differences in, e.g., ion channel expression, calcium handling and electrophysiology[9,10]. Improving the maturity of the hiPSC-derived cardiomyocytes would increase their resemblance to the native adult myocardium and hence the predictivity of the results obtained using these test models[12]. Slight improvements have been obtained using approaches such as increased culture time, 3D culture methods and co-culture with non-myocytes[10,13].

[1]Faculty of Medicine and Health Technology, Tampere University, Arvo Ylpön katu 34, 33520 Tampere, Finland. [2]Biocenter Oulu Electron Microscopy Core Facility, University of Oulu, Oulu, Finland. [3]Computational Biology, Faculty of Medicine and Health Technology, Tampere University, Tampere, Finland. [4]Oulu Centre for Cell-Matrix Research, Faculty of Biochemistry and Molecular Medicine, Biocenter Oulu, University of Oulu, Oulu, Finland. ✉email: maria.koivisto@tuni.fi

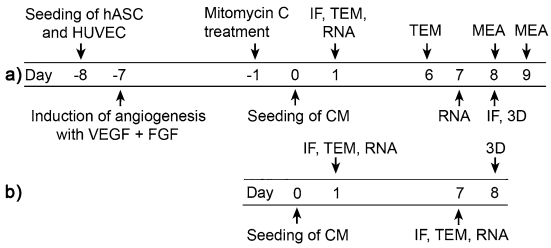

Figure 1. Cell culturing procedure. Cell culturing procedure for (**a**) the cardiac tissue model and (**b**) the cardiomyocyte monoculture. Time points for immunofluorescence (IF), immunofluorescence 3D images (3D), transmission electron microscopy (TEM), gene expression analyses (RNA) and electrophysiological measurements (MEA).

In the native human myocardium, the most abundant non-myocytes are fibroblasts, endothelial cells and perivascular cells. These cells have important functions in supporting normal heart homeostasis and in adaptation to pathological stimuli[14]. The role of the fibroblasts is to maintain the myocardial structure by secreting extracellular matrix components. They also mediate cardiomyocyte function by cell–cell interactions and paracrine factors[15]. Furthermore, fibroblasts can undergo phenotype conversion to proliferative myofibroblasts when augmentation of the matrix production is needed[16]. In the myocardium, endothelial cells form the capillaries that are essential for providing the cardiomyocytes with oxygen and nutrients in vivo. They also mediate cardiomyocyte spatial organization, contraction, survival and function. The physiological relevance of in vitro cardiac tissues could benefit from utilization of these complex and dynamic interactions between the different cell types as well as between the cells and the matrix[15].

Previously we have shown that hASC-HUVEC co-culture produces a vascular network containing a lumen, and including different cell types such as endothelial cells, pericytes and smooth muscle cells[17,18]. In this paper, we present a cardiac tissue model that develops from a co-culture of a vascular-like network and hiPSC-derived cardiomyocytes under laboratory conditions to form a functional cardiac tissue model. We show the characteristics of the model on the structural and gene expression levels compared to a cardiomyocyte monoculture. The relevance of the model to predict human effects was verified by a set of known positive and negative substances, i.e., drugs with human data.

Results

Cardiomyocyte structural maturity improves when co-cultured with vascular-like networks. Cardiac tissue models and cardiomyocyte monocultures were established as presented in Fig. 1. The co-culturing of cardiomyocytes with the vascular-like networks affected the cardiomyocyte morphology remarkably, making it different from cardiomyocyte monocultures (Fig. 2). Already one day after the seeding, the shape of the cardiomyocytes was elongated in the cardiac tissue model, resembling their phenotype in cardiac tissues, whereas the cardiomyocytes in the monoculture were mainly circular. The difference further increased when the cardiomyocytes developed a connected network of aligned cardiomyocytes in the cardiac tissue model after one week. In the same time, the cardiomyocyte monoculture conserved the immature morphology and isotropic cell orientation. The orientation of myofibrils followed the cell shape and alignment. The myofibrils were highly oriented along the longitudinal direction of the cardiomyocytes in the cardiac tissue model (Fig. 2f), while in the monoculture, they oriented in multiple directions (Fig. 2c). The mean circular variance of cell orientation in cardiomyocyte monocultures was 0.90 (SD 0.06; N = 6) while the cardiomyocytes in cardiac tissue models were clearly more aligned with mean circular variance of 0.54 (SD 0.07; N = 15). The mean circular variance of myofilament orientation in a few neighbouring cardiomyocytes in the monoculture was 0.90 (SD 0.07; N = 3) and in the cardiac tissue model 0.61 (SD 0.08; N = 9). The improved alignment was statistically significant for both cell and myofilament orientation with $p < 0.001$ and $p = 0.009$, respectively.

Transmission electron microscopy (TEM) micrographs show that the monocultured cardiomyocytes were circular or slightly elongated on day 1. In the elongated cardiomyocytes, some aligned myofibrils were detected, and some of the myofibrils had arranged into sarcomere structures (Fig. 3a). Cell–cell connections had started to form. The cardiomyocytes in the cardiac tissue model were also immature on day 1 (Fig. 3b). After a week, the monocultured cardiomyocytes had developed well-formed sarcomeres (Fig. 3c). In the cardiac tissue model, sarcomeres with regular z-bands were highly aligned in adjacent cardiomyocytes six days after cardiomyocyte seeding (Fig. 3d). Intercalated discs connected cardiomyocytes, and transverse sections were located at the sarcomere z-bands. On the lateral side, desmosomes connected neighbouring cardiomyocytes, in contrast to the monocultured cardiomyocytes, which displayed immature intercalated discs and junctions. In the cardiac tissue model, the endoplasmic reticulum (ER) was also found near the sarcomere z-band. In the cardiac tissue model, the mitochondria appeared to be located in between and along the sarcomeres. Lipid droplets were located near the mitochondria and sarcomeres in the cardiomyocytes in the cardiac tissue model. Lipid droplets were not detected in the monocultured cardiomyocytes after one week. Although a large portion of the cardiomyocytes in the cardiac tissue models had developed many mature cardiomyocyte characteristics, some of the cells still displayed immature characteristics after one week. The number of myofilaments and mitochondria in the cytosol

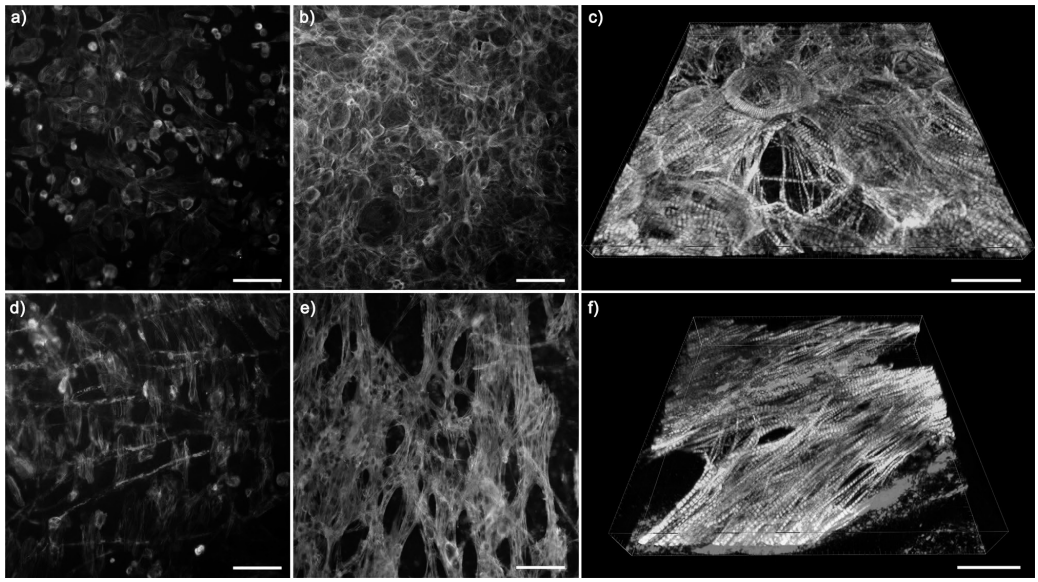

Figure 2. Immunofluorescence staining showed improved structural maturity of cardiomyocytes in cardiac tissue model compared to cardiomyocyte monoculture. (**a**) Immunofluorescence staining of the cardiomyocyte monoculture on day 1 and (**b**) day 7. (**c**) 3D-confocal microscopy image of the cardiomyocyte monoculture on day 8. (**d**) Immunofluorescence staining of the cardiac tissue model on day 1 and (**e**) day 8. (**f**) 3D-confocal microscopy image of the cardiac tissue model on day 8. Green: cardiac troponin T, red: von Willebrandt factor. Scale bar 100 µm (**a**,**b**, **d**, **e**), scale bar 30 µm (**c**, **f**). The experiment was repeated three times.

varied greatly between the cardiomyocytes. The cells that contained less of the regular myofilaments also had fewer intercalated disc connections to adjacent cardiomyocytes.

In addition to cardiomyocytes, numerous endothelial cells and myofibroblasts were found in the cardiac tissue model (Supplementary Fig. S1). Both cell types were present already one day after cardiomyocyte seeding. There were no significant changes in the gene expression levels of endothelial cell markers *PECAM1*, *CDH5*, and *VWF* between day 1 and 7 in the cardiac tissue model. However, these markers were clearly more expressed in the model compared to the monoculture at day 7. Endothelial cells are probably the remains of HUVECs but the myofibroblasts have developed in the model. Myofibroblasts can derive from endothelial cells via epithelial-mesenchymal transition or from mesenchymal cells via mesenchymal-epithelial transition. To reveal the origin of these myofibroblasts further studies are needed.

Cardiomyocyte gene expression profile reached a more mature state in cardiac tissue model than in monocultured cardiomyocytes. To further confirm differences in the maturation of the monocultured cardiomyocytes and cardiac tissue model, we compared the gene expression patterns on day 1 and day 7 post cardiomyocyte seeding. Principal component analysis (PCA) of both the monocultured cardiomyocytes and cardiac tissue model show the day 1 and day 7 samples to be separated into their own clusters (Fig. 4a). Furthermore, we found that external RNA expression data from adult heart samples clustered closer to the cardiac tissue model samples than monocultured cardiomyocytes samples in the PCA space (Supplementary Fig. S2). Some 604 genes were significantly differentially expressed ($p \leq 0.05$ and fold difference ≥ 1) in the monocultured cardiomyocyte samples, compared to 579 genes in the cardiac tissue model samples. In the monocultured cardiomyocyte samples, a positive log2 fold change (log2FC) was observed in 419 genes and a negative log2FC was observed in 185 genes. The corresponding counts for the cardiac tissue model samples were 237 positive log2FC genes and 342 negative log2FC genes (see the full lists of genes in Supplementary Table S1).

The RNA sequencing revealed that both the monocultured cardiomyocytes and cardiomyocytes in the cardiac tissue model were maturing during the seven days of culture (Supplementary Fig. S3, Supplementary Table S1), as the structural and ion channel coding genes were differentially expressed between days 1 and 7 (Fig. 4b). For example, the markers of myofibril maturation *MYH7*, *MYL2* and *TNNI3* were upregulated in both cardiac tissue model and cardiomyocyte monoculture. However, on day 7, the cardiac tissue model was more mature compared to the monocultured cardiomyocytes (Fig. 4c). The expression levels of sodium channel subunits *SCN1B*, predominantly expressed in the adult heart, and *SCN3B*, highly expressed in the embryonic heart and iPSC-derived cardiomyocytes[19], shifted toward a more adult heart-like expression pattern in the cardiac tissue model, but not in the monocultured cardiomyocytes (Fig. 4c). Genes expressed in foetal heart and cardiomyocyte progenitor

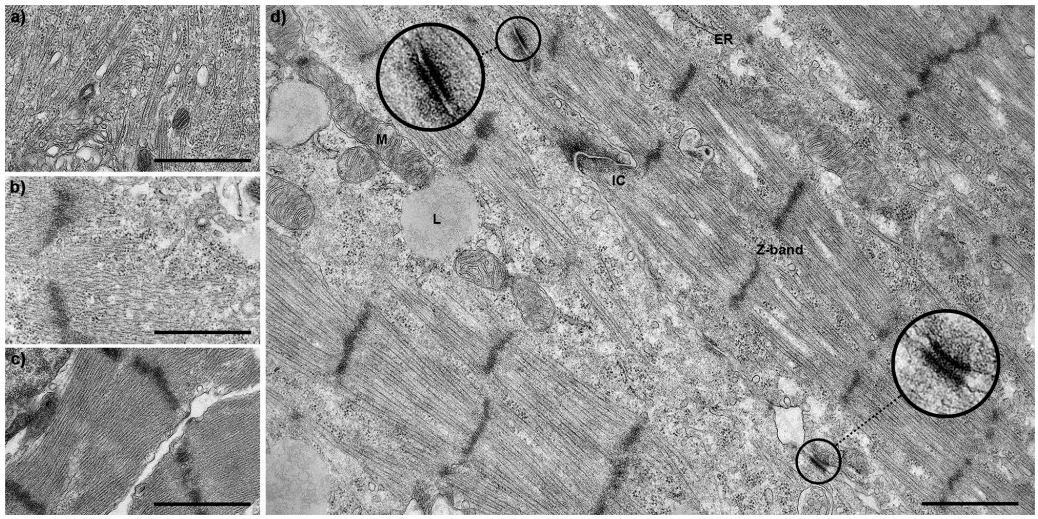

Figure 3. Transmission electron microscopy showed improved structural maturity of cardiomyocytes in cardiac tissue model compared to cardiomyocyte monoculture. Immature cardiomyocytes in (**a**) the cardiomyocyte monoculture and (**b**) the cardiac tissue model contain unorganized myofibrils on day 1. (**c**) Monocultured cardiomyocytes have developed organized sarcomeres by day 7. (**d**) Two adjacent cardiomyocytes with highly developed and aligned sarcomeres show intercalated discs (IC) and desmosome connections (circled and magnified) in the cardiac tissue model on day 6. Light blue indicates the line between two adjacent cardiomyocytes. ER = endoplasmic reticulum, M = mitochondria, L = lipid droplet. Scale bar 1 µm. The experiment was performed with one well from CM day 1, two parallel wells from CTM day 1, two parallel wells from CM day 7, and two parallel wells from CTM day 6.

cells, such as *ABCC9*, *SALL1*, *HES1*, *CACNG7*, *SNAI1* and *ERBB4*, were significantly downregulated in the cardiac tissue model, but not in the monocultured cardiomyocytes (Fig. 4b). The monocultured cardiomyocytes also had an increased expression of *CACNA2D* and *KCNJ3*, genes coding the ion channels mainly expressed in the atrium. In contrast, *KCNA5*, an atrial ion channel, and *HCN4*, mainly expressed in the sinoatrial node, were significantly downregulated in the cardiac tissue model but not in the monocultured cardiomyocytes (Fig. 4b). Full lists of the differentially expressed genes and enriched GO terms are presented in the Supplementary Table S1.

Cardiac tissue model yielded high predictivity in drug testing with high correlation to human data. To investigate how the more mature morphology and gene expression profile affect electrophysiology, we measured the baseline electrophysiological characteristics of the cardiac tissue model with a microelectrode array (MEA). The baseline field potential duration (FPD) was 441 ms (SD 42 ms) and the beating frequency was 45 (SD 4) beats per minute (BPM). To test the applicability of the cardiac tissue model to identify cardiac effects, we exposed the model to 29 substances with known effects on cardiac function and three negative controls known to have no effect (see Table 1 for the compounds and their known mechanisms). We used the multiwell format of MEA, which allows medium throughput capacity with a 96-well plate. As the selected test substances covered many different mechanisms of action, we analysed beating frequency and sodium spike amplitude in addition to the regularly analysed FPD. Table 1 presents the measured EC_{50} values for each parameter and Δ_{20} value, which represents the first concentration that caused a change over 20% to the parameter compared to the baseline. The biological significance level of 20% change was chosen based on preceding literature[20–22]. We found that 26 out of the 29 positive reference compounds presented activity characteristics that have been previously reported in literature. The concentration-dependent effects of these 26 study compounds are presented in Supplementary Fig. S4. None of the three negative controls (Acetyl salicylic acid, Hexylresorcinol and Ibuprofen) showed signs of cardio activity or toxicity. This yielded a predictive accuracy of 91%, sensitivity of 90% and specificity of 100%. Compounds that were not recognized or expected to cause the clinically known effect in our test setting were doxorubicin, levosimendan and pentamidine. The correlation of the measured EC_{50} values to the reported clinical plasma concentrations was for all the compounds 0.852, with $R^2 = 0.725$ (Fig. 5a). With epinephrine, isoprenaline and propranolol the Δ_{20} value was used for the calculation of the correlations as the clinical concentrations of these drugs alter the beating frequency about 20%. Our model gave excellent prediction for the drugs with the amplitude as the endpoint, with a correlation of 0.968 ($R^2 = 0.938$). The substances with an over tenfold difference between the measured EC_{50} value and the clinically relevant plasma concentration were alfuzosin, digoxin, and tolterodine. The detected effects of these three drugs are clinically observed only in overdose and thus can be excluded from the correlation, leading to a correlation of 0.952, with $R^2 = 0.905$ (Fig. 5b).

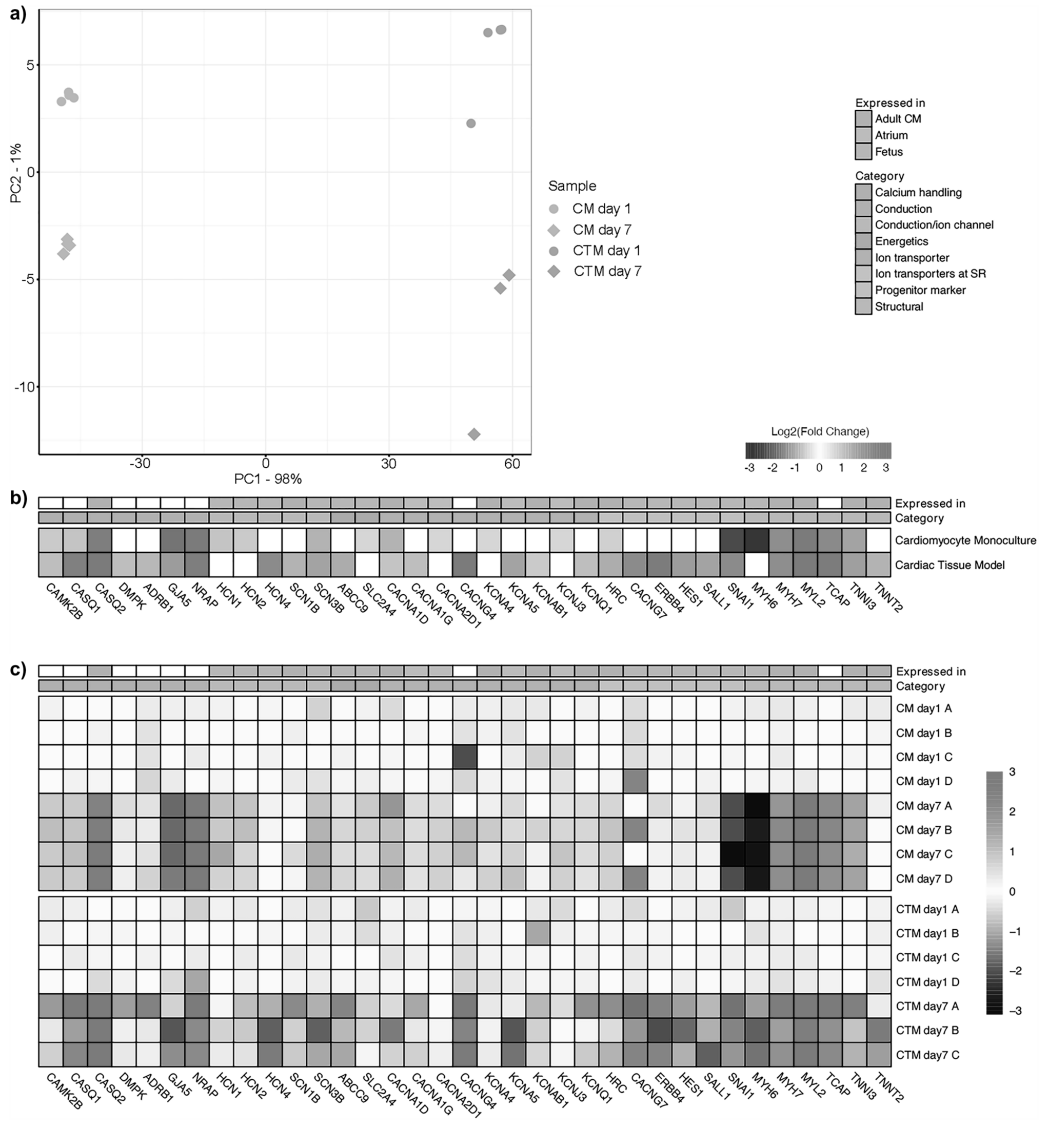

Figure 4. Cardiomyocyte gene expression profile reached a more mature state in cardiac tissue model than in monocultured cardiomyocytes. (**a**) PCA plot of cardiomyocyte monoculture (CM day 1 & CM day 7) and cardiac tissue model (CTM day 1 & CTM day 7) samples using top 500 most variable genes and variance stabilizing transformation (DESeq2). Numbers attached to the principal components correspond to the percentage of variance that is attributed to it. (**b**) Heatmap of the log2-transformed fold changes (day 1 to day 7) of the cardiomyocyte monoculture and cardiac tissue model samples. Pre-selected genes of interest are annotated according to category and typical site of expression. Values for genes with a statistically insignificant fold change (padj > 0.05) are not reported. (**c**) Heatmap of expression changes per gene for each sample. The DESeq2-normalized count of each gene was additionally normalized against the mean of the day 1 expression of each gene. Day 1 normalization was done separately for CM and CTM, followed by a log2 transformation. Genes and their annotations correspond to those of (**b**). Number of replicates from two repeats n = 4 for CTM day 1, CM day 1 and CM day 7; n = 3 for CTM day 7. The heatmaps were created in R 3.6.0 using pheatmap v1.0.12 (https://github.com/raivokolde/pheatmap).

Compound	Known mechanism	Action	End point	FPD Δ_{20} (nM)	FPD EC_{50} (nM)	BPM Δ_{20} (nM)	BPM EC_{50} (nM)	Amp Δ_{20} (nM)	Amp EC_{50} (nM)	Therapeutic concentration (nM)
Alfuzosin	QT prolonging	Na + channel activator alfa-AR antagonist	FPD	↑300	↑3,228	↓10,000	↓6,775	↓10,000	↓6,528	56[21]
Haloperidol	QT prolonging	K + channel blocker	FPD	↑3	↑22.71	↓10	↓45.21	↓30	↓103.1	45[60]
Astemizole	QT prolonging	hERG blocker	FPD	↑30	↑33.12	↓100	↓1,043	↓100	↓1,274	8[21]
Cisapride	QT prolonging	hERG blocker	FPD	↑3	↑10.58	↓300	↓3,694	↓3,000	↓4,432	2.5[29]
Dofetilide	QT prolonging	hERG blocker	FPD	↑1	↑1.638	↓3	↓2.085	↓10	↓3.491	2[60]
E-4031	QT prolonging	hERG blocker	FPD	↑3	↑5.001	↓30	↓57.38	↓30	↓50.68	8.4[60]
Moxifloxasin	QT prolonging	hERG blocker	FPD	↑10,000	↑2,431	–	–	–	–	5600[60]
Sotalol	QT prolonging	hERG blocker	FPD	↑1,000	↑4,209	↓30,000	↓6,051	–	–	13,000[60]
Thioridazine	QT prolonging	hERG blocker	FPD	↑300	↑45.43	↓3,000	↓2,239	↓1,000	↓1,854	45[60]
Tolterodine	QT prolonging	hERG blocker	FPD	↑100	↑502.8	↓3,000	↓4,593	↓3,000	↓3,046	5
Pimozide	QT prolonging	hERG and Ca2 + channel blocker	FPD	↑10	↑5.643	↓30	↓1,466	↓100	↓307	3.7[61]
Isradipine	QT shortening	L-type Ca2 + channel blocker	FPD	↓10	↓36.57	↑10	↑109.8	↓3,000	↓3,314	80[61]
Nifedipine	QT shortening	L-type Ca2 + channel blocker	FPD	↓30	↓89.56	↑30	↑296.9	↓10,000	↓7,797	190[60]
Verapamil	QT shortening	L-type Ca2 + channel blocker	FPD	↓100	↓285.3	↑10	↑103.6	↓3,000	↓2,633	92[60]
Digoxin	Positive inotropic	Na/K ATPase blocker	BPM	–	–	↑100	↑111.2	–	–	2.8[61]
Dopamine	Positive inotropic	dopamine receptor, AR-receptor agonist	BPM	↓300	↓109.3	↑100	↑119.4	–	–	300 (20% increase)
Epinephrine	Positive inotropic	AR agonist	BPM	–	–	↑30	↑183.5	–	–	2.64[62]
Isoprenaline	Positive inotropic	AR agonist	BPM	–	–	↑1	↑31.53	↑100	↑33.65	0.84[63]
Doxazosin	Negative inotropic	alfa1-AR blocker	BPM	↑300	↑29.17	↓100	↓220.6	↓300	↓288.5	133[61]
Propranolol	Negative inotropic	AR blocker	BPM	–	–	↓3,000	↓6,902	↓3,000	↓7,606	1095[64]
Flecainide	Negative inotropic	Na + channel blocker	Amp	↑300	↑162.9	↓1,000	↓1,297	↓1,000	↓1,516	1160[60]
Lidocaine	Negative inotropic	Na + channel blocker	Amp	–	–	↓3,000	↓4,980	↓3,000	↓5,157	2500[29]
Quinidine	QT prolonging	Na + channel blocker	Amp	↑300	↑505.9	↓1,000	↓5,061	↓1,000	↓3,701	3240[60]
Ranolazine	Negative inotropic, QT prolonging	Na + channel blocker, hERG blocker	Amp	–	–	↓30,000	↓8,579	↓10,000	↓9,709	6010[21]
Terfenadine	QT prolonging	hERG blocker, multi-channel blocker	Amp	↓1,000	↓900.2	↓1,000	↓1,419	↓300	↓680.4	300[21]
Terodiline	QT prolonging	hERG blocker, Ca2 + channel blocker	Amp	–	–	↓3,000	↓3,805	↓1,000	↓2,607	1800[60]
Acetyl salicylic acid	No effect on heart function		–	–	–	–	–	–	–	–
Hexylresorcinol	No effect on heart function		–	–	–	–	–	–	–	–
Ibuprofen	No effect on heart function		–	–	–	↑30,000	–	–	–	–
Doxorubicin	apoptotic	ROS?	–	–	–	–	–	–	–	
Levosimendan	Positive inotropic	Ca2 + sensitizer	–	–	–	–	–	–	–	129[21]
Pentamidine	QT prolonging	Effects hERG channel transport	–	–	–	↑30,000	–	↑300	–	190[61]

Table 1. Field potential duration (FPD), beats per minute (BPM), and Na^+ peak amplitude (Amp) Δ_{20} and EC_{50} values of all test compounds and therapeutic concentration of the compound. The symbol ↑ indicates an increase and the symbol ↓ indicates a decrease in the measured parameter. The reported concentrations from our model are the total (nominal) concentrations, and the therapeutic concentrations from the literature are the free plasma concentrations.

Discussion

The results of the structural characterization together with the RNA sequencing imply that the cardiomyocytes develop further when cultured with in vitro constructed tubular network. The vascular-like network that was included in this cardiac tissue model has been characterized previously[17,18]. The hASC-HUVEC co-culture forms a tubular network of endothelial cells with perivascular and smooth muscle cells in six days[17]. In the cardiac tissue model, the endothelial cells and myofibroblasts were found one day after cardiomyocyte seeding. These cell types are normally present in the healthy myocardium[14], except the myofibroblasts, whose presence typically indicates remodeling of the extracellular matrix[23].

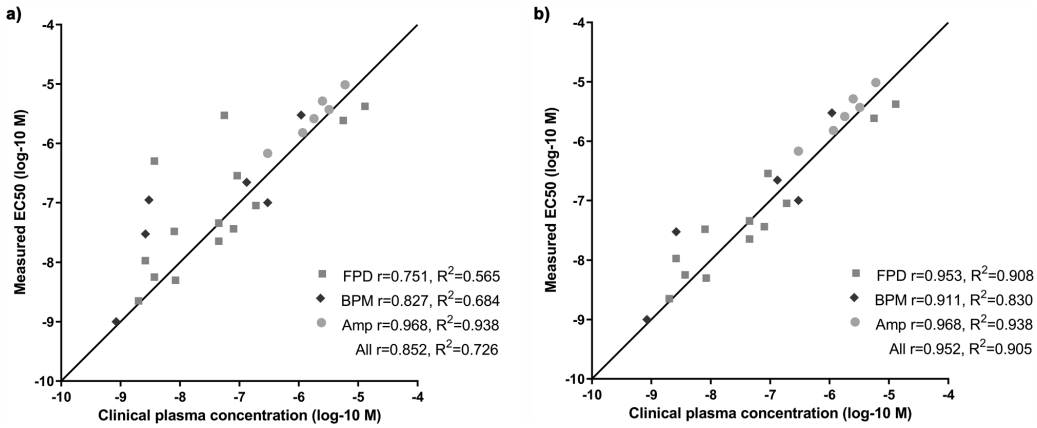

Figure 5. Cardiac tissue model yielded high predictivity in drug testing with high correlation to human data. Correlation between measured EC_{50} values and clinical plasma concentrations of (**a**) 26 study compounds (drugs) and (**b**) without alfuzosin, digoxin and tolterodine. Correlation scores for the groups are calculated using Pearson r. Goodness of fit is expressed as R^2. Number of replicates n = 4–8 per repeat depending on MEA well format, repeated three times.

A previously reported in vitro cardiac tissue, cultured with supporting dermal fibroblasts within an artificial scaffold and with electrical stimulation, has been shown to mimic well the cardiomyocytes of an adult heart[24]. Our method to produce a mature cardiac tissue model is technically less challenging and composed of commercially available cell lines. In our model, the co-cultured cells develop into a cardiac tissue-mimicking construct in vitro without artificial scaffolds or external stimulation. This model presents reliable and cost-effective tool for screening acute cardiac effects of drugs.

Morphological differences between the cardiac tissue model and monocultured cardiomyocytes indicate that the crosstalk between the different cell types and contact with the extracellular matrix are crucial for the maturation of cardiomyocytes. This can be mediated by endothelial cell-cardiomyocyte paracrine signalling which plays an important role in cardiac tissue growth and remodelling[25], and by cardiomyocyte-extracellular matrix connections which induce the rod-shaped phenotype of cardiomyocytes during development and contribute the structural integrity of the heart[26]. In the native myocardium, each cardiomyocyte is located next to at least one capillary, which ensures the adequate oxygen and nutrient supply in vivo but also enables vesicle transport and local communication between cardiomyocytes and endothelial cells[27]. Moreover, both cardiomyocytes and endothelial cells express connexins, that form gap junctions which may play a role in the cardiomyocyte—endothelial cell interaction[25,28]. The presence of lipid droplets next to the sarcomeres and mitochondria in the cardiomyocytes in our cardiac tissue model (Fig. 3d) suggests the transfer of energy metabolism from foetal glycolysis to the oxidation of phospholipids[24]. Moreover, the improved organization and alignment of cardiomyocytes (Fig. 2e) and sarcomeres (Fig. 3d) in the cardiac tissue model indicates advanced maturation compared to the cardiomyocyte monoculture (Fig. 2b)[10]. The sarcomeres of mature adult cardiomyocytes are longer, approximately 1.7–2.2 µm depending on contraction stage, than the sarcomeres of immature cardiomyocytes[11,13]. We did not notice longer sarcomeres in cardiac tissue models compared to cardiomyocyte monocultures. However, for a reliable comparison of the sarcomere lengths in the cardiac tissue model and cardiomyocyte monoculture we would have needed a greater number of images in this study.

As the cardiomyocytes used for the RNA sequencing were from two differentiation batches, the batches caused some variance between them (Fig. 4c). The results show that both the monocultured cardiomyocytes and cardiomyocytes in the cardiac tissue model matured during the seven days of the culture. However, the monocultured cardiomyocytes were still expressing more genes present in the cardiac progenitor cells and in the atrium on day 7 compared to the cardiac tissue model (Fig. 4b). Interestingly, 18 of the 131 GO terms enriched in the cardiac tissue samples contain 'heart' or 'cardiac' in their name, compared to only 2 out of the 91 for the monocultured cardiomyocyte samples (Supplementary Table S1). This suggests that the cardiomyocytes in our cardiac tissue model are more mature and more of the homogenously ventricular type of cardiomyocytes.

Monocultured iCell cardiomyocytes have been previously reported to have an FPD of 468 ms (SD 42) and a BPM of 38 (SD 2.5)[29], while in humans, QT times ≤ 420 ms and a heart rate of 60 BPM are considered normal. In our cardiac tissue model, the FPD of 441 ms (SD 42) and beat rate of 45 BPM (SD 4) were closer to the physiological values of the human heart compared to the monocultured cardiomyocytes.

The high goodness of fit ($R^2 = 0.938$) and correlation (r = 0.963) between observed IC50 values and the clinical plasma concentration of the sodium channel blockers are likely due to the more adult-like expression pattern of the sodium channels (SCN1B vs SCN3B) in our cardiac tissue model. SCN1B is predominantly expressed in adult heart and SCN3B in foetal heart[19]. Culturing cardiomyocytes with supporting dermal fibroblasts within an

artificial scaffold and with electrical stimulation was not sufficient to induce SCN1B expression[24]. Thus, it seems that the addition of stromal cells (hASC), which can differentiate into multiple different cell types and create a more natural environment, enhances the maturation of the cardiomyocytes. The IC50 values for flecainide, lidocaine and quinidine were closer to the therapeutic concentrations than previously reported IC50 values from hiPSC-derived cardiomyocytes[30].

Of the QT-prolonging compounds, the measured FPD-prolonging EC50 values of alfuzosin and tolterodine were more than tenfold above the clinical plasma concentrations. At high doses (100 nM), alfuzosin is reported to cause a mild QT increase in patients and significantly prolong the QT interval in vitro at a concentration of 300 nM[31]. At 300 nM, we detected a statistically significant 20% increase in FPD. Tolterodine does not prolong the QT interval in clinical use[32], and the QT-prolonging effect has been reported only with a very high concentration in vitro (corresponding to a 340 nM concentration in vivo). These QT prolongations are identified adverse effects for both drugs, and they have been reported with plasma concentrations above the normal clinical plasma concentrations, which is supported by our data. This also suggests that our model could be used to predict safety margins for the drugs. In addition, the EC/IC50 values from our model were closer to the therapeutic concentrations than previously reported values for e.g., nifedipine[33,34], isradipine[35], sotalol[34], and verapamil[35]. For other compounds, such as E-4031[33,35], the previously reported EC/IC50 values were already close to the therapeutic concentrations.

Of the compounds affecting heart rate, the measured EC50 values for digoxin and propranolol differed from their clinical plasma concentrations more than tenfold. Tachycardia is an adverse effect of a mild overdose of digoxin. Thus, the higher concentration needed in our model for BPM changes compared to the situation in the clinical setting for digoxin is likely to be explained by the slow distribution of digoxin shown in humans[36]. The EC50 values were closer to the therapeutic concentrations than previously reported values for e.g., isoprenaline[34].

Doxorubicin is reported not to affect FPD or beat rate during short exposures, but to increase the apoptosis of hiPSC-derived cardiomyocytes after two days of exposure[37]. As we expected, we could not detect any doxorubicin-induced changes to FPD, BPM or amplitude in our short-term experiments. Doxorubicin appears not to affect the electrophysiology of cardiomyocytes during short exposures up to 2 h. Levosimendan is a positive inotrope which increases the beating force of the cardiomyocytes by binding to troponin C in a calcium-dependent manner[38]. Using MEA, it is not possible to measure beating force. Therefore, we did not expect levosimendan to show any effect in MEA. Pentamidine has been reported to block the transport of hERG channels to the cardiomyocyte plasma membrane[39]. As the half-life of hERG channels is 2.8 h[40], we could not detect any significant FPD prolongation in our test setting where pentamidine concentration exceeds the clinical plasma concentration only for 50 min.

Terfenadine is clinically shown to prolong QT time. However, we detected terfenadine-induced FPD shortening. We also detected a non-significant 10% increase in FPD, similarly as reported by Mehta et al.[41], before the shortening of FPD initiated. Terfenadine acts as an unspecific multi-channel blocker and not only as a hERG blocker[42], with reported IC50 to calcium channels at 185 nM[43], hERG at 350 nM[44] and sodium channels at 930 nM in canine atrial myocytes[45]. These multi-channel effects might explain the unexpected results obtained with terfenadine. In our model, the blocking of sodium channels appears to be the major effect of terfenadine, which is also in line with the previously reported results of terfenadine in monocultured cardiomyocytes[41].

We did not detect the expected FPD prolongation of terodiline. However, we could detect its cardiotoxicity based on its effects on beating amplitude. Terodiline has two optical isomers, R- and S-terodiline, which were both present in the racemic terodiline used in our experiments. R-terodiline shows high anticholinergic properties, responsible for the prolongation of FPD[46], whereas S-terodiline shows calcium antagonist properties[47]. It is likely that the FPD shortening effect of calcium antagonist S-terodiline concealed the FPD prolongation effect of R-terodiline. The reported toxic plasma concentration for terodiline in humans is 2.1 μM[48], which is very close to the amplitude EC50 concentration (2.6 μM) detected in our experiments. This together with the results from terfenadine emphasizes the importance of monitoring not only the FPD changes but also BPM and amplitude, which are measured by default while using MEA, to better detect the cardiotoxic effects of the compounds.

This cardiac tissue model aims to mimic human heart tissue. Despite improvements in the cardiac tissue maturation, it does not fully recapitulate the adult state of the human heart tissue. The cardiac tissue model also does not recapitulate the structure of the whole human heart. For example, the tissue model does not have connections with nerve stimulation. Furthermore, the model measures only the direct effects of the parent drugs as the cardiomyocytes present only weak drug metabolism. MEA measurements are useful to detect many types of drug effects. However, certain drugs mechanisms of actions remain undetected with this method. For example, MEA cannot detect changes in the beating force of the cardiomyocytes, so the inotropic effects are missed if they do not affect the beating frequency e.g., levosimendan. Moreover, only acute short-term effects of the compounds were measured in this study. For effects requiring longer time to develop, culture and exposure times could be extended. Cardioactive drugs that require longer time to affect e.g., pentamidine, were not recognized. In addition, the balance between positive (29) and negative (3) test substances could impact the determination of the sensitivity, specificity and accuracy values in this study.

In this research, we have shown that hiPSC-derived cardiomyocytes cultured together with a vascular-like network form a functional cardiac tissue-mimicking construct in vitro. The morphology and gene expression levels of our cardiac tissue model show the characteristics of an adult heart, and the maturation of the cardiomyocytes is more advanced when compared to cardiomyocyte monocultures. The functional characterization with the positive and negative reference compounds compared with human data shows that the data gained from our model are transferable to the clinical setting for the evaluation of cardiac effects, including acute cardiotoxicity.

Methods

Human cell-based cardiac tissue model. This study conforms to the principles outlined in the Declaration of Helsinki. The use of human adipose stromal cells (hASCs) obtained from surgical operations and the use of human umbilical vein endothelial cells (HUVECs) from scheduled caesarean sections was approved by the Ethics Committee of Pirkanmaa Hospital District (permit numbers R15161 and R15033, respectively). Informed consent was received from the tissue donors prior the study. The hASCs and HUVECs were isolated and propagated as previously described[17,49]. They were maintained in a humidified incubator at + 37 °C, 5% CO_2, and the medium was refreshed every 2–3 days. The hASC lines were confirmed CD90, CD73 and CD105 positive by flow cytometry as previously described[49], and passage 2 was used in cultures. The HUVEC lines passed a tube formation test as previously described[49], and passage 4 was used in cultures. The hASC and HUVEC lines were tested negative for mycoplasma contamination.

To improve the long-term attachment of the cells, a thin fibrin coating was applied to the cell culture wells by mixing a 1:1 solution containing 5.5 mg/ml fibrinogen (Sigma Aldrich, F3879) with 38 µg/ml aprotinin (Sigma Aldrich, A1153) and a solution of 2.75 UN/ml thrombin (Sigma Aldrich, T7009). Excess solution was removed prior to incubation for 45 min at + 37 °C.

To produce the vascular-like networks, hASCs were seeded in the fibrin-coated wells at 20,000 cells/cm^2 and HUVECs were seeded on top of them at 4000 cells/cm^2 1–4 h later in EBM-2 with EGM-2 SingleQuots supplements (Lonza, CC-3162) as previously described[49]. The next day, angiogenesis stimulation was initiated using a serum-free stimulation medium (SFSM) consisting of DMEM/F12, 2.56 mM L-glutamine, 0.1 nM 3,3′,5-Triiodo-L-thyronine sodium salt, ITS™ Premix: 1.15 µM: 6.65 µg/ml insulin, 6.65 µg/ml Transferrin, 6.65 ng/ml selenious acid, 1% Bovine serum albumin, 2.8 mM Sodium pyruvate, 200 µg/ml Ascorbic acid, 0.5 µg/ml Heparin, 2 µg/ml Hydrocortisone, 10 ng/ml VEGF, and 1 ng/ml FGF-β as described earlier[18]. On day 4, the SFSM was refreshed. After seven days of co-culture, the cells were treated with 1 µg/ml Mitomycin C (Millipore, 47,589) for 1.5 h to impair their mitotic activity. Co-cultures were washed three times with warm PBS before the administration of fresh SFSM. On the next day, hiPSC-derived cardiomyocytes (iCell^2, Cellular Dynamics) were seeded on top of the vascular-like networks at 156,000 cells/cm^2 in iCell Cardiomyocytes Plating Medium (Cellular Dynamics, M1001). The plating medium was replaced with 1:1 SFSM and iCell Cardiomyocytes Maintenance Medium (Cellular Dynamics, M1003) 4 h later. The cells were maintained in a humidified incubator at + 37 °C, 5% CO_2, and the medium was refreshed every second day.

Cardiomyocyte monoculture. Cardiomyocyte monocultures were established by seeding iCell^2 cardiomyocytes in fibrin-coated wells at 156,000 cells/cm^2 in Cardiomyocytes Plating Medium. The medium was replaced by iCell Cardiomyocytes Maintenance Medium 4 h later. Cardiomyocytes were maintained in a humidified incubator at + 37 °C, 5% CO_2, and the medium was refreshed every second day.

Immunocytochemistry. For immunocytochemistry, the cells were seeded in chambered coverslips. The cells were fixed with 70% ethanol or 4% formaldehyde (3D images) for 20 min on day 1 and day 7 or 8 after cardiomyocyte seeding (time points are presented in Fig. 1). The cells were stained with monoclonal mouse anti-Troponin T antibody (1:100, Invitrogen, MA5-12,960, lot TK2667027) and polyclonal rabbit anti-von Willebrand factor (1:100, Dako, A0082, lot 20,030,046 and 20,067,357) at + 4 °C overnight. Secondary antibodies anti-mouse IgG Alexa Fluor 488 (Invitrogen, A21202, lot 2,018,296) and anti-rabbit IgG Alexa Fluor 594 (Invitrogen, A21207, lot 2,066,086) or FITC (Sigma Aldrich, F4143, lot 018M4797V and 045M4881V) and TRITC (Sigma Aldrich, T6778, lot 036M4785V) (3D images) were incubated for 45 min at RT. The cells were imaged using a Nikon Eclipse TiS with a 20 × objective and a Zeiss Laser Scanning Confocal Microscope LSCM 780 with a 63 × objective (3D images). Images were prepared with Photoshop CC (Adobe) except the 3D images which were prepared with Imaris software (Bitplane, Zürich, Switzerland). Cardiomyocyte and myofilament orientation analyses was performed using CytoSpectre 1.2 software (http://www.tut.fi/cytospectre)[50]. The software calculates the orientation of image components based on spectral analysis. The variance of image structure orientation is described as circular variance on a scale from 0 (perfect alignment) to 1 (perfect isotropy). In the software, mixed component mode was used, and spectral resolution/noise was set to balanced. Images taken with 20 × or 25 × objective were used for cardiomyocyte orientation analysis, and confocal images taken with 63 × objective were used for myofilament orientation analysis.

Electron microscopy. Cardiac tissue constructs and cardiomyocyte monocultures were fixed for 60 min with 4% paraformaldehyde + 1% glutaraldehyde in 0.1 M phosphate buffer on day 1 and day 6 (cardiac tissue model) or day 7 (cardiomyocyte monoculture) after cardiomyocyte seeding. The cells were carefully removed from the dishes and pelleted. Fixed cell pellets were postfixed in 1% osmiumtetroxide, dehydrated in acetone and embedded in Epon LX 112 (Ladd Research Industries). Thin Sects. (70 nm) were cut with a Leica Ultracut UCT ultramicrotome, stained in uranyl acetate and lead citrate, and examined in a Tecnai G2 Spirit transmission electron microscope (FEI EuropeImages were captured by a Quemesa CCD camera and analysed using iTEM software (Olympus Soft Imaging Solutions GMBH).

Gene expression. Gene expression was analysed by RNA sequencing from four replicate cultures of the cardiac tissue model from day 1 and from three replicate cultures from day 7, and from four samples per time point for the cardiomyocyte monoculture. The total RNA was collected using a PureLink RNA Mini Kit (Life Technologies, 12183018A) following the manufacturer's protocol on days 1 and 7 after cardiomyocyte seeding. The quality of the mRNA samples was verified with Agilent 2100 Bioanalyzer and RNA sequencing, and the

initial bioinformatics were performed by Novogene CO Ltd. (Beijing, China). RNA sequencing included cDNA library preparation and sequencing (20 M clean reads/sample) using Illumina PE150 (Q30 ≥ 80%) equipment.

Initial quality control was done using FastQC[51], after which raw reads were mapped to GRCh38 (GENCODE comprehensive annotation v29) using STAR v2.7.1[52]. The resulting Binary Alignment Map (.bam) files were sorted and indexed using SAMtools v1.9[53]. Gene counts were accessed using featureCounts v2.0.1[54] on hg38 (GENCODE basic annotation v34) and filtered for protein coding genes using biomaRt v2.40.5[55].

To determine suitable replicates for downstream expression analysis, each sample was plotted on a two-dimensional graph using dimensionality reduction through principal components. Differential expression analysis was performed using DESeq2 v1.24.0[56]. Day-specific differences in gene expression were determined using the "contrast" function on DESeq2. Significant differentially expressed genes were filtered using a Benjamini–Hochberg adjusted p-value (BH *p*-value) of less than 0.05 and an absolute log2-fold-change of more than 1 as thresholds. Enrichment analysis was performed on the resulting gene lists using the g:GOSt functional profiling tool[57] and a significance threshold of a BH p-value less than 0.01. Gene Ontology biological processes (GO:BP, ENSEMBL 99 release 2020–01-01) excluding evidence Inferred from Electronic Annotation (IEA) and KEGG pathways (KEGG FTP release 2020–02-03) were used as databases[58]. If a gene symbol in the query matched multiple ENSEMBL ids, the one with the most GO annotations was used. The annotated genes for the heatmaps were selected from the DEGs ($p \leq 0.05$) found under the significant GO terms including words "heart" and "cardiac" and from previous publications[10,13,24]. The genes were chosen based on their expression primarily in cardiomyocytes[10,13,24].

Preparation of stock solutions used in electrophysiology. Hydrophobic compounds were solubilized in DMSO as 10 mM stocks. The water-soluble compounds were solubilized in distilled water as 1 mM stocks. These stocks were diluted to the exposure medium (DMEM/F12 + 2.56 mM L-glutamine, 0.1 nM 3,3′,5-Triiodo-L-thyronine sodium salt, ITS™ Premix: 1.15 µM: 6.65 µg/ml insulin, 6.65 µg/ml Transferrin, 6.65 ng/ml selenious acid, 1% Bovine serum albumin, 2.8 mM Sodium pyruvate).

Electrophysiology. For the electrophysiological measurements, the cardiac tissue models were cultured in 24-well or 96-well multielectrode array (MEA) plates (Multi Channel Systems, 24W700/100F-288 or 96W700/100F-288). Extracellular field potentials were recorded using a Multiwell-MEA-System (Multi Channel Systems) with a 20 kHz sampling frequency on days 8–9 after cardiomyocyte seeding. The temperature was set at 37 °C and the cells were supplied with 5% CO_2 during the measurements. Two-minute recordings were obtained as spontaneous baseline beating, after which the cardiac tissue models were exposed to a ½ logarithmic cumulative concentration series spanning from 300 to 30 µM of the test compounds. With 24-well plates four replicate wells and with 96-well plates eight replicate wells were used for each compound. The wash-in period between administration of the test compounds and 2-min recording was 8 min. The field potentials were recorded with Multiwell-Screen software (Multi Channel Systems) and analysed with Multiwell-Analyzer software (Multi Channel Systems). The data from the electrodes showing clear beating patterns, sodium spike voltage change over 70 µV, and a detectable T-wave were used for the analyses. Data obtained from the electrodes of one well were averaged. In the analyses, each well was treated as an individual and (the ratio of) test compound-induced changes were calculated against the recorded baseline from the same well. The data was normalized only against the baseline values, not against the vehicle control. All the field potential durations (FPD) were corrected against the changes in beating frequency using the Fridericia formula $cFPD = FPD/\sqrt[3]{RR}$, where RR is the RR interval.

For each compound, we analysed the effects on FPD, beat rate and amplitude. We selected one MEA parameter based on their mechanism of action. FPD, that corresponds to the QT interval[59], was selected for compounds that are known to affect the QT time e.g., by targeting hERG or Ca^{2+} channels. Beat rate was selected for compounds that target adrenergic receptors. The strong transient spike in the MEA data results from Na + influx[59], and the amplitude was selected for compounds targeting the Na^+ channel.

Quantification and statistical analysis. For the electrophysiology measurements, the chosen sample size was either 4 when using 24-well MEA plates with 12 electrodes per well and 8 when using 96-well MEA plates with 3 electrodes per well. The reported n stands for the number of wells (cardiac tissue models) per repetition of the study. Each test was repeated 3 times using 4–8 parallels in each concentration. Excel (Microsoft) was used for to calculate the p-values using Student's two-tailed t-test. EC_{50} and IC_{50} values were calculated using non-linear fit four-parameters logistic equation Prism version 5.0. (GraphPad). The baseline values were used as E_{min}. Because determination of E_{max} was shown to be case sensitive, the second plateau of the sigmoidal curve was taken as E_{max}, except in case the plateau was not reached at the maximal concentration of 30 µM, the effect seen at this concentration was selected as E_{max}. The data from electrodes that did not show clear beating patterns, sodium spike voltage changes over 70 µV and a detectable T-wave, were excluded from the analyses. On average approximately 15% of the wells had to be excluded from the experiment, if less than 3 wells out of 8 well per compound did pass the above-mentioned criteria the whole compound was excluded from the analysis of that experiment.

Gene expression (RNAseq) was performed for samples acquired from two replications the expression pattern of majority of the genes were similar for both replications according to sample clustering after principal component analysis (PCA). One sample was excluded from each timepoint for both culture types (cardiac tissue model and cardiomyocyte monoculture). The exclusion was done based on sample clustering after PCA. The excluded samples originated from the same cardiomyocyte culture batch. Benjamini–Hochberg procedure was applied for the data as described above.

Immunofluorescence and electrophysiology studies were replicated at least 3 valid times. Electron microscopy was performed once for each sample type with the 1–2 replicate wells indicating similar results. Independent

samples Mann–Whitney U test was performed in IBM SPSS Statistics 27 to test the statistical significance of the cell and myofibril circular variances in monoculture and cardiomyocyte model.

Data availability

A gene count matrix with corresponding metadata has been included in supplementary data.

Code availability

Open-source and commercial codes and software that were used in this study are specified in the Methods. No custom codes or software were used.

Received: 21 December 2021; Accepted: 26 July 2022
Published online: 05 August 2022

References

1. Lasser, K. E. *et al.* Timing of new black box warnings and withdrawals for prescription medications. *JAMA* **287**, 2215–2220 (2002).
2. Li, X., Zhang, R., Zhao, B., Lossin, C. & Cao, Z. Cardiotoxicity screening: a review of rapid-throughput in vitro approaches. *Arch. Toxicol.* **90**, 1803–1816 (2016).
3. Takeda, M. *et al.* Development of in vitro drug-induced cardiotoxicity assay by using three-dimensional cardiac tissues derived from human induced pluripotent stem cells. *Tissue Eng. Part C Methods* **24**, 56–67 (2018).
4. Fritsche, E. *et al.* Stem cells for next level toxicity testing in the 21st century. *Small* **17**, 2006252 (2021).
5. Weaver, R. J. & Valentin, J.-P. Today's challenges to de-risk and predict drug safety in human "mind-the-gap". *Toxicol. Sci.* **167**, 307–321 (2019).
6. Bernstein, D. Induced pluripotent stem cell-derived cardiomyocytes: A platform for testing for drug cardiotoxicity. *Prog. Pediatr. Cardiol.* **46**, 2–6 (2017).
7. Tabar, V. & Studer, L. Pluripotent stem cells in regenerative medicine: challenges and recent progress. *Nat. Rev. Genet.* **15**, 82–92 (2014).
8. Burridge, P. W., Holmström, A. & Wu, J. C. Chemically defined culture and cardiomyocyte differentiation of human pluripotent stem cells. *Curr. Protoc. Hum. Genet.* **87**, 21.3.1-21.315 (2015).
9. Robertson, C., Tran, D. D. & George, S. C. Concise review: Maturation phases of human pluripotent stem cell-derived cardiomyocytes. *STEM CELLS* **31**, 829–837 (2013).
10. Jiang, Y., Park, P., Hong, S.-M. & Ban, K. Maturation of cardiomyocytes derived from human pluripotent stem cells: Current strategies and limitations. *Mol. Cells* **41**, 613–621 (2018).
11. Lemcke, H., Skorska, A., Lang, C. I., Johann, L. & David, R. Quantitative evaluation of the sarcomere network of human hiPSC-derived cardiomyocytes using single-molecule localization microscopy. *Int. J. Mol. Sci.* **21**, 2819 (2020).
12. Mills, R. J. & Hudson, J. E. Bioengineering adult human heart tissue: How close are we?. *APL Bioeng.* **3**, 010901 (2019).
13. Karbassi, E. *et al.* Cardiomyocyte maturation: advances in knowledge and implications for regenerative medicine. *Nat. Rev. Cardiol.* **17**, 341–359 (2020).
14. Zhou, P. & Pu, W. Recounting cardiac cellular composition. *Circ. Res.* **118**, 368–370 (2016).
15. Zamani, M., Karaca, E. & Huang, N. F. Multicellular interactions in 3D engineered myocardial tissue. *Front. Cardiovasc. Med.* **5**, 147 (2018).
16. Gray, G. A., Toor, I. S., Castellan, R., Crisan, M. & Meloni, M. Resident cells of the myocardium: more than spectators in cardiac injury, repair and regeneration. *Curr. Opin. Physiol.* **1**, 46–51 (2018).
17. Sarkanen, J. R. *et al.* Adipose stromal cell tubule network model provides a versatile tool for vascular research and tissue engineering. *Cells Tissues Organs* **196**, 385–397 (2012).
18. Huttala, O. *et al.* Human vascular model with defined stimulation medium - a characterization study. *Altex* **32**, 125–136 (2015).
19. Okata, S. *et al.* Embryonic type Na(+) channel beta-subunit, SCN3B masks the disease phenotype of Brugada syndrome. *Sci. Rep.* **6**, 34198 (2016).
20. Doherty, K. R. *et al.* Structural and functional screening in human induced-pluripotent stem cell-derived cardiomyocytes accurately identifies cardiotoxicity of multiple drug types. *Toxicol. Appl. Pharmacol.* **285**, 51–60 (2015).
21. Guo, L. *et al.* Refining the human iPSC-cardiomyocyte arrhythmic risk assessment model. *Toxicol. Sci. Off. J. Soc. Toxicol.* **136**, 581–594 (2013).
22. Koci, B. *et al.* An impedance-based approach using human iPSC-derived cardiomyocytes significantly improves in vitro prediction of in vivo cardiotox liabilities. *Toxicol. Appl. Pharmacol.* **329**, 121–127 (2017).
23. Kim, J. *et al.* Quantitative evaluation of cardiomyocyte contractility in a 3D microenvironment. *J. Biomech.* **41**, 2396–2401 (2008).
24. Ronaldson-Bouchard, K. *et al.* Advanced maturation of human cardiac tissue grown from pluripotent stem cells. *Nature* **556**, 239–243 (2018).
25. Talman, V. & Kivelä, R. Cardiomyocyte—endothelial cell interactions in cardiac remodeling and regeneration. *Front. Cardiovasc. Med.* **5**, 101 (2018).
26. Howard, C. M. & Baudino, T. A. Dynamic cell-cell and cell-ECM interactions in the heart. *J. Mol. Cell. Cardiol.* **70**, 19–26 (2014).
27. Hsieh, P. C. H., Davis, M. E., Lisowski, L. K. & Lee, R. T. Endothelial-cardiomyocyte interactions in cardiac development and repair. *Annu. Rev. Physiol.* **68**, 51–66 (2006).
28. Colliva, A., Braga, L., Giacca, M. & Zacchigna, S. Endothelial cell–cardiomyocyte crosstalk in heart development and disease. *J. Physiol.* **598**, 2923–2939 (2020).
29. Blinova, K. *et al.* Comprehensive translational assessment of human-induced pluripotent stem cell derived cardiomyocytes for evaluating drug-induced arrhythmias. *Toxicol. Sci. Off. J. Soc. Toxicol.* **155**, 234–247 (2017).
30. Lee, H.-A., Hyun, S.-A., Byun, B., Chae, J.-H. & Kim, K.-S. Electrophysiological mechanisms of vandetanib-induced cardiotoxicity: Comparison of action potentials in rabbit Purkinje fibers and pluripotent stem cell-derived cardiomyocytes. *PLoS ONE* **13**, e0195577 (2018).
31. Lacerda, A. E. *et al.* Alfuzosin delays cardiac repolarization by a novel mechanism. *J. Pharmacol. Exp. Ther.* **324**, 427–433 (2008).
32. Malhotra, B. K. *et al.* Thorough QT study with recommended and supratherapeutic doses of tolterodine. *Clin. Pharmacol. Ther.* **81**, 377–385 (2007).
33. Harris, K. *et al.* Comparison of electrophysiological data from human-induced pluripotent stem cell-derived cardiomyocytes to functional preclinical safety assays. *Toxicol. Sci.* **134**, 412–426 (2013).
34. Navarrete, E. G. *et al.* Screening drug-induced arrhythmia using human induced pluripotent stem cell-derived cardiomyocytes and low-impedance microelectrode arrays. *Circulation* **128**, S3–S13 (2013).
35. McKeithan, W. L. *et al.* An automated platform for assessment of congenital and drug-induced arrhythmia with hiPSC-derived cardiomyocytes. *Front. Physiol.* **8**, 766 (2017).
36. Pincus, M. Management of digoxin toxicity. *Aust. Prescr.* **39**, 18–20 (2016).

37. Louisse, J. *et al.* Assessment of acute and chronic toxicity of doxorubicin in human induced pluripotent stem cell-derived cardiomyocytes. *Toxicol. In Vitro* **42**, 182–190 (2017).
38. Haikala, H., Levijoki, J. & Linden, I. B. Troponin C-mediated calcium sensitization by levosimendan accelerates the proportional development of isometric tension. *J. Mol. Cell. Cardiol.* **27**, 2155–2165 (1995).
39. Kuryshev, Y. A. *et al.* Pentamidine-induced long QT syndrome and block of hERG trafficking. *J. Pharmacol. Exp. Ther.* **312**, 316–323 (2005).
40. Osterbur Badhey, M. L., Bertalovitz, A. C. & McDonald, T. V. Express with caution: Epitope tags and cDNA variants effects on hERG channel trafficking, half-life and function. *J. Cardiovasc. Electrophysiol.* **28**, 1070–1082 (2017).
41. Mehta, A. *et al.* Pharmacoelectrophysiology of viral-free induced pluripotent stem cell-derived human cardiomyocytes. *Toxicol. Sci. Off. J. Soc. Toxicol.* **131**, 458–469 (2013).
42. Ming, Z. & Nordin, C. Terfenadine blocks time-dependent Ca2+, Na+, and K+ channels in guinea pig ventricular myocytes. *J. Cardiovasc. Pharmacol.* **26**, 761–769 (1995).
43. Hove-Madsen, L. *et al.* The proarrhythmic antihistaminic drug terfenadine increases spontaneous calcium release in human atrial myocytes. *Eur. J. Pharmacol.* **553**, 215–221 (2006).
44. Roy, M., Dumaine, R. & Brown, A. M. HERG, a primary human ventricular target of the nonsedating antihistamine terfenadine. *Circulation* **94**, 817–823 (1996).
45. Lu, Y. & Wang, Z. Terfenadine block of sodium current in canine atrial myocytes. *J. Cardiovasc. Pharmacol.* **33**, 507–513 (1999).
46. Hartigan-Go, K., Bateman, D. N., Daly, A. K. & Thomas, S. H. Stereoselective cardiotoxic effects of terodiline. *Clin. Pharmacol. Ther.* **60**, 89–98 (1996).
47. Hayashi, S. *et al.* Cardiac electrophysiological actions of NS-21 and its active metabolite, RCC-36, compared with terodiline. *Naunyn. Schmiedebergs Arch. Pharmacol.* **355**, 651–658 (1997).
48. Andersson, K. E. Clinical pharmacology of terodiline. *Scand. J. Urol. Nephrol.* **87**, 13–20 (1984).
49. Toimela, T. *et al.* Intra-laboratory validated human cell-based in vitro vasculogenesis/angiogenesis test with serum-free medium. *Reprod. Toxicol. Elmsford N* **70**, 116–125 (2017).
50. Kartasalo, K. *et al.* CytoSpectre: a tool for spectral analysis of oriented structures on cellular and subcellular levels. *BMC Bioinf.* **16**, 344 (2015).
51. Andrews, S. FastQC: A quality control tool for high throughput sequence data. (2010).
52. Dobin, A. *et al.* STAR: Ultrafast universal RNA-seq aligner. *Bioinformatics* **29**, 15–21 (2013).
53. Li, H. *et al.* The sequence alignment/map format and SAMtools. *Bioinformatics* **25**, 2078–2079 (2009).
54. Liao, Y., Smyth, G. K. & Shi, W. featureCounts: An efficient general purpose program for assigning sequence reads to genomic features. *Bioinforma. Oxf. Engl.* **30**, 923–930 (2014).
55. Durinck, S., Spellman, P. T., Birney, E. & Huber, W. Mapping identifiers for the integration of genomic datasets with the R/Bioconductor package biomaRt. *Nat. Protoc.* **4**, 1184–1191 (2009).
56. Love, M. I., Huber, W. & Anders, S. Moderated estimation of fold change and dispersion for RNA-seq data with DESeq2. *Genome Biol.* **15**, 550 (2014).
57. Raudvere, U. *et al.* g:Profiler: A web server for functional enrichment analysis and conversions of gene lists (2019 update). *Nucleic Acids Res.* **47**, W191–W198 (2019).
58. Kanehisa, M. Toward pathway engineering: A new database of genetic and molecular pathways. *Sci. Technol. Jpn.* **59**, 34–38 (1996).
59. Kussauer, S., David, R. & Lemcke, H. hiPSCs derived cardiac cells for drug and toxicity screening and disease modeling: What micro- electrode-array analyses can tell us. *Cells Basel Switz.* **8**, 1331 (2019).
60. Ando, H. *et al.* A new paradigm for drug-induced torsadogenic risk assessment using human iPS cell-derived cardiomyocytes. *J. Pharmacol. Toxicol. Methods* **84**, 111–127 (2017).
61. Sirenko, O. *et al.* Multiparameter in vitro assessment of compound effects on cardiomyocyte physiology using iPSC cells. *J. Biomol. Screen.* **18**, 39–53 (2013).
62. Stratton, J. R., Pfeifer, M. A., Ritchie, J. L. & Halter, J. B. Hemodynamic effects of epinephrine: Concentration-effect study in humans. *J. Appl. Physiol.* **58**, 1199–1206 (1985).
63. Stratton, J. R. *et al.* Differences in cardiovascular responses to isoproterenol in relation to age and exercise training in healthy men. *Circulation* **86**, 504–512 (1992).
64. Oh, V., Chia, B. & Taylor, E. Effects of long-acting propranolol on blood pressure and heart rate in hypertensive Chinese. *Br. J. Clin. Pharmacol.* **20**, 144–147 (1985).

Acknowledgements

This work was supported by Business Finland [grant number 6785/31/2017]; Academy of Finland [grant number 310527]; Pirkanmaa Cultural Foundation [grant number 50211545]; Ministry of Agriculture and Forestry [grant number 1149/03.02.05.02/2019]; Juliana von Wendt foundation; and Ministry of Education and Culture. The authors acknowledge the Biocenter Finland (BF), Tampere Imaging Facility (TIF) and Biocenter Oulu (BCO) Electron Microscopy Core Facilities for research infrastructure services.

Author contributions

M.K., T.A.T., T.T. and T.H. designed the experiments. M.K. and T.A.T. performed the experiments excluding the TEM imaging, which was performed by I.M. M.K. and T.A.T. analyzed the immunofluorescence images and functionality results. The TEM images were analyzed by I.M. and L.E. The RNA sequencing results were analyzed by A.K., J.K. and M.N. M.K. and T.A.T. wrote the manuscript, to which T.T., T.H., I.M., L.E., A.K., J.K. and M.N. gave comments.

Competing interests

The authors affiliated to Tampere University, MK, TAT, TT, AK, JK, MN, and TH, may have a conflict of interest due to the patent E2723853: "In vitro cardiovascular model" that is owned by Tampere University. IL and LE declare no competing interests.

Additional information

Supplementary Information The online version contains supplementary material available at https://doi.org/10.1038/s41598-022-17498-0.

Correspondence and requests for materials should be addressed to M.K.

PUBLICATION II

Direct measurement of contraction force in human cardiac tissue model using piezoelectric cantilever sensor technique

Virtanen J, Toivanen M, Toimela T, Heinonen T and Tuukkanen S

Current Applied Physics 20(1):155-160 (2020)
DOI: 10.1016/j.cap.2019.10.020

Current Applied Physics 20 (2020) 155–160

Contents lists available at ScienceDirect

Current Applied Physics

journal homepage: www.elsevier.com/locate/cap

Direct measurement of contraction force in human cardiac tissue model using piezoelectric cantilever sensor technique

J. Virtanen[a], M. Toivanen[b], T. Toimela[b], T. Heinonen[b], S. Tuukkanen[a,*]

[a] Faculty of Medicine and Health Technology, Tampere University, Tampere, Finland
[b] FICAM (Finnish Center for Alternative Methods), Faculty of Medicine and Health Technology, Tampere University, Finland

ARTICLE INFO

Keywords:
Cardiomyocyte
Piezoelectric sensor
Cantilever
Contraction force

ABSTRACT

A proof-of-concept method for measuring cardiac tissue contraction force using an in-house-developed piezoelectric cantilever sensor system is demonstrated. Contracting forces of 7.2–16.6 μN (n = 5) were measured from a human cardiac tissue construct. Beating cardiac tissue constructs were monitored in-situ under a microscope during the contraction force measurements. Development of the measurement method allows very low forces such as the ones that appear in biological small scale systems to be determined.

1. Introduction

Cardiotoxicity is one of the leading causes for drug attrition during a drug development process and for post-approval drug withdrawal [1,2]. Animal experiments are poor predictors of drug-induced toxicity in humans [3]. Human stem cell-based tissue and organ models would be more reliable and ethical than experiments on animals [4]. The development of a functional cardiac tissue model requires advanced and controlled cell culture techniques combined with highly sensitive measuring technology. The generation of the contraction force is a key element in the functioning of the heart, so drugs affecting the contraction function of cardiomyocytes pose a potentially high risk for cardiac safety [5]. Therefore, there is an urgent need for a reliable method to measure the contraction force in cardiomyocytes. At present, there are only a few reports in the literature describing varying approaches to overcome this issue [6–10].

Our highly sensitive force sensors were constructed from a metallic cantilever attached to a piezoelectric sensor, which was connected to in-house-built dedicated hardware and a user interface plate. The measurement system was a further development from a previous study [11].

In this paper, we demonstrate a proof-of-concept technique for directly measuring the contraction force of a human cardiac tissue model in-situ under microscope. The measurement method is based on the fact that the piezoelectric sensor detects the movement of the cantilever when it is brought into contact with the cardiac tissue construct.

2. Materials and methods

2.1. Cardiac tissue construct fabrication

The use of human umbilical vein endothelial cells (HUVECs) from scheduled caesarean sections and human adipose stromal cells (hASCs) obtained from surgical operations was approved by the Ethics Committee of the Pirkanmaa Hospital District (permit numbers R08028 and R03058, respectively).

The human-induced pluripotent stem cells (ATCC-BXS0116 hiPSC) were differentiated into cardiomyocytes using a PSC Cardiomyocyte Differentiation Kit (Gibco Invitrogen, A2921201). The cells were maintained at 37 °C and 5% CO_2 in a humidified incubator, and the medium was replaced every 2–3 days.

The cardiac tissue constructs were fabricated by a technique adapted from previous work [12,13]. A punched polydimethylsiloxane (PDMS, Sylgard 184, Dow Corning, USA) sheet was reversibly bonded to a cell culture dish and the holes (d = 5 mm) were coated with fibrinogen (Sigma Aldrich, F3879). The hASCs and HUVECs were propagated separately and a co-culture was formed in the PDMS holes to produce vascular-like networks as previously described in Ref. [14]. Two days later, hiPSC-derived cardiomyocytes were seeded on top of the vascular structures. After cardiomyocyte seeding, a serum-free stimulation medium (SFSM) consisting of DMEM/F12, 2.56 mM L-glutamine, 0.1 nM 3,3′,5-Triiodo-L-thyronine sodium salt, ITS™ Premix: 1.15 μM: 6.65 μg/ml insulin, 6.65 μg/ml Transferrin, 6.65 ng/ml selenious acid, 1% Bovine serum albumin, 2.8 mM Sodium pyruvate, 200 μg/ml Ascorbic acid, 0.5 μg/ml Heparin, 2 μg/ml Hydrocortisone,

* Corresponding author.
E-mail address: sampo.tuukkanen@tuni.fi (S. Tuukkanen).

https://doi.org/10.1016/j.cap.2019.10.020
Received 23 August 2019; Received in revised form 15 October 2019; Accepted 25 October 2019
Available online 28 October 2019

10 ng/ml VEGF, and 1 ng/ml FGF-β as described in Ref. [15] was replaced by a 1:1 Cardiomyocyte maintenance medium (Gibco Invitrogen, A209208) and SFSM. A few days later, the cardiomyocytes regained their contracting function and the PDMS sheets were removed to allow the vascularized cardiac tissue constructs to form spontaneously. This process also detached the edges of the tissue constructs which provided attachment points to the force measurement cantilever. The beating cardiac tissue constructs remained functional over 21 days.

2.2. Piezoelectric cantilever sensors

A piezoelectric cantilever sensor was used to measure the force of the cardiac cell contraction. A cantilever sensor has linear elastic behaviour and is characterized by a spring constant. A piezoelectric sensor element in the cantilever then converts the cantilever strain to electric energy. The operation of the piezoelectric sensor element was first simulated with a finite element method and later the simulation results were verified with actual measurements from the cantilever sensor prototype. The frequency response of the cantilever measurement system was obtained via impulse response measurements. These showed a very good fit with the theoretical computations. Labview software was used to control and capture the results of the measurements obtained with the measurement hardware. The measurement hardware itself consisted of an AD8691 (Analog Devices inc, Norwood, USA), operational amplifier circuit as a buffer amplifier with a voltage amplification of 1. This amplified signal was read with an Arduino Due analog-to-digital converter and then sent through a serial communication link to Labview software [11] for further processing and analysis.

2.3. Finite element simulation of the cantilever

The functionality of the piezoelectric cantilever sensor was simulated with a COMSOL (Comsol AB, Stockholm, Sweden) multiphysics finite element method (FEM) simulator. Both linear elastic and piezoelectric models were used in conjunction with each other in the simulation. In the static simulation a 200 μN force was applied to the tip while the other end was fixed. The total displacement of the tip with this 200 μN load was 192 μm. This represents a cantilever spring constant of 0.96 N/m. In addition, the electric potential field was computed with the simulator on the piezoelectric material. The material parameters were taken from the Lead Zirconate Titanate (PZT) library material. The bottom electrode was fixed to zero electric potential and the electric potential as computed on the top of the piezoelectric element. This potential strength varied between 0.14 and 0.68 V along the piezo material depending on the stress produced when the 200 μN force was applied to the cantilever tip. Furthermore, to obtain the electric potential of the top electrode an average potential over this layer was computed. This average potential was 308 mV and represented the simulated output voltage of the cantilever sensor under a 200 μN load. Thus, the simulated sensitivity was 1.55 kV/N. The deflection of the cantilever beam under the load is illustrated in Fig. 1 a) while the electric field is shown in Fig. 1 b). The simulated and measured sensitivities and spring constants are listed in Table 1.

The piezoelectric cantilever frequency response was also simulated with FEM and later an analytical transfer function model was constructed to model both the mechanical and electrical behaviour of the cantilever measurement system. The modeled and measured frequency response graphs were then compared.

2.4. The prototype cantilever sensor

This sensor element was constructed in-house by soldering a 33 mm long test probe pin (P100-D2-1.5 mm) to a 15 mm diameter circular piezo disc with brass plate thickness of 70 μm and PZT –layer thickness of 50 μm thus a total thickness was 130 μm (Farnell P/N 2667639). The top electrode was located on top of the PZT layer. The piezo disc was

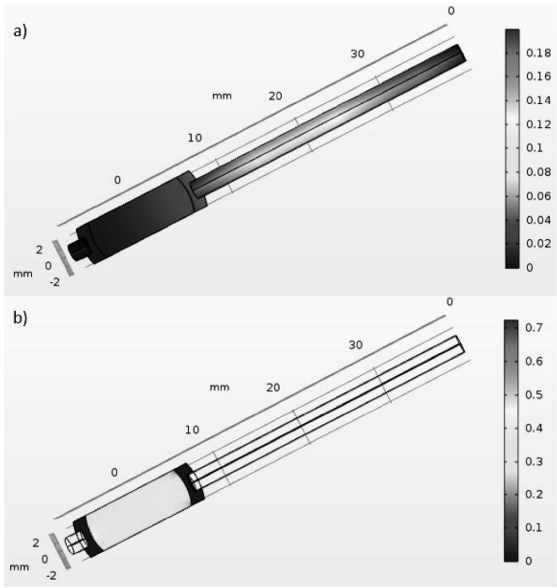

Fig. 1. A FEM computed response with a 200 μN stationary load at the cantilever tip a) total displacement in mm b) electric potential field in Volts.

Table 1
Simulation and calibration results for the cantilever sensor sensitivity.

	Simulated	Measured
Sensitivity	1.55 kV/N	1.97 kV/N
Spring constant	0.96 N/m	0.78 N/m

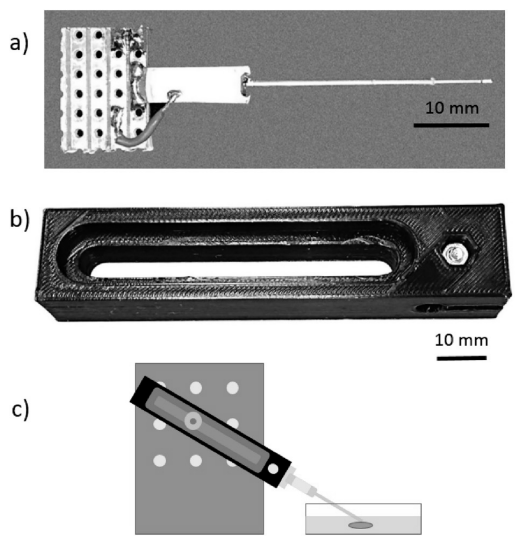

Fig. 2. a) Piezoelectric cantilever sensor probe used in the measurements. b) A 3d-printed mounting fixture for the sensor probe. c) The probe and the arm in the measurement setup.

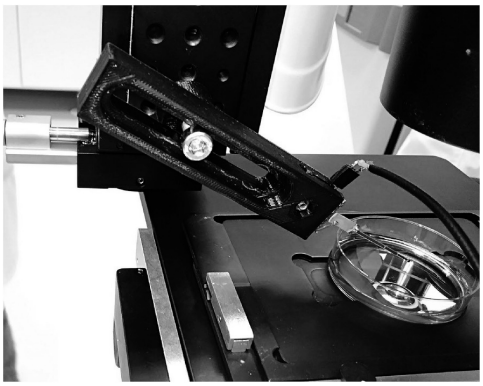

Fig. 3. Cantilever sensor probe attached into the 3-axis micromanipulator to in-situ microscope measurement setup.

further narrowed with a diamond blade cutter to a 5 mm width perpendicular to the orientation of the probe. The cantilever sensor probe prototype is shown in Fig. 2a. The other side of the narrowed piezo disc (ground electrode) was attached to a prototyping wiring board with a solder joint. This formed a fixed point for the cantilever and was also an attachment point to a 3d-printed fixture arm, which is shown in Fig. 2b. This structure was finally attached to a 3-axis linear micro manipulator (Newport Corporation, Irvine, USA) to enable accurate alignment of the probe tip during the measurements (see Figs. 2c and 3). The probe was set to 30° angle to the cultivation dish and the tip was put into the medium as shown in Fig. 2c.

2.5. Cantilever sensor sensitivity measurements

The voltage versus force sensitivities for the prepared cantilever sensors were measured using texture analyser Stable Micro Systems TA. XTPlus (Stable Micro Systems Ltd, Surrey, United Kingdom). In the calibration procedure a 1 Hz sinewave force excitation with 200 µm amplitude was applied to the cantilever tip and the sensor output was measured. This calibration method and data analysis are described in more detail in our previous study [11]. Here, the amplitude of the sensitivity measurement force was 157.5 µN, which yielded a 200 µm displacement and a 329 mV peak voltage reading in the sensor output. Thus, the measured sensitivity of the sensor was 1.97 kV/N and the spring constant of the cantilever 0.78 N/m. The sensor sensitivities from both the simulations and the calibration measurements are summarized in Table 1.

The differences in the simulated and measured sensitivities of the cantilever sensor may be caused by the piezoelectric material's parameters. In the specification sheet for the piezo disc there was no detailed information of the piezoelectric material, so the parameters in our simulation may not be accurate. However this was not a problem since the actual sensor operation was carefully measured.

The standard deviation in the force measurements during calibration was 2.11 µN. This was computed from the deviation from the sinusoidal excitation signal used in the calibration procedure. This is illustrated in Fig. 4a, in which the continuous line represents the excitation signal and the stars show the measurement observations. In Fig. 4b a calibration curve of the sensor is shown. Furthermore, the distribution of the measurement error is shown in Fig. 4c. This shows that the average error (AVG) is 0.47 µN and the standard deviation of the error (STD) is 2.11 µN.

2.6. Impulse response measurement of the cantilever sensor

The impulse response measurement of the system was conducted to ensure that the cantilever measurement was operating in the right frequency range and that the sensitivity measurements could be interlinked in the frequency domain. The impulse response was measured by knocking the sensor element and measuring the time-domain response. This time-domain impulse response is shown in Fig. 5a. The frequency response of the cantilever sensor was then computed by performing a fourier transform on the impulse response data. The comparison of the modeled and measured frequency responses of the measurement system is shown in Fig. 5b. There, the measured and computed responses show that the usable frequency band is ~0.5 Hz–10 Hz with a resonance peak at ~15 Hz.

2.7. In-situ contraction force measurement setup

An optical microscope (Zeiss Primovert, Carl Zeiss AG, Oberkochen, Germany) was used for in-situ characterization of the cardiac tissue constructs during the force measurements. The use of in-situ microscopy was crucial, both for maneuvering the cantilever into its desired position in the selected cardiac tissue constructs, and also for quantifying the synchronised movement of the cantilever and the cardiac tissue construct. The in-situ microscope setup with the cantilever sensor and cell culture dish are shown in Fig. 6.

The contraction force of the cardiac tissue constructs was measured by placing the cell culture dish under the microscope and preparing the sensor probe tip with fibrin coating to enhance its adhesion to the cardiac tissue construct. The coating procedure was to dip the tip into a 5.5 mg/ml fibrinogen solution 5 times and then let it dry for 60 s. Non-coated and PDMS-coated probe tips were also tried, but they did not give reliable measurement results. Altogether, 5 measurements were conducted using this probe measurement system on the cardiac tissue constructs.

3. Results and discussion

3.1. Microscopic analysis of cardiac tissue constructs

Fig. 7 shows an example of a cardiac tissue construct on a cell culture dish 2 weeks after cardiomyocyte seeding. The cardiac tissue construct has not become partially detached from the cell culture dish like the cardiac tissue construct that was used in the measurements. The diameter of the beating cardiac construct was approximately 5 mm and had a circular shape and the contact area of the tip is marked with amber circle.

3.2. In-situ imaging during force measurement

Fig. 8 shows an example of the images captured from one of the videos (in Supplementary material) filmed during the contraction force measurements. There, the cantilever tip and part of a cardiac tissue construct is shown. The contact area of the cantilever tip and the cell construct is approximately 1 mm^2. Furthermore, the supplementary video material shows the synchronous movement of the probe tip and the cell contraction.

Supplementary video related to this article can be found at https://doi.org/10.1016/j.cap.2019.10.020.

The beating frequency computed from the measured data varied between 43 and 49 beats per minute. This corresponds to beating frequencies of between 0.71 and 0.81 Hz, and thus the measurements fall into the usable range of the cantilever frequency band.

3.3. Contraction force measurements

Fig. 9 shows all the 5 force measurements in a time domain with a 5 s period for the measurements. There are systematic beating patterns for the cardiac tissue constructs. Fig. 10 shows individual plots of the measurements where the contracting and relaxing phases of the cardiac

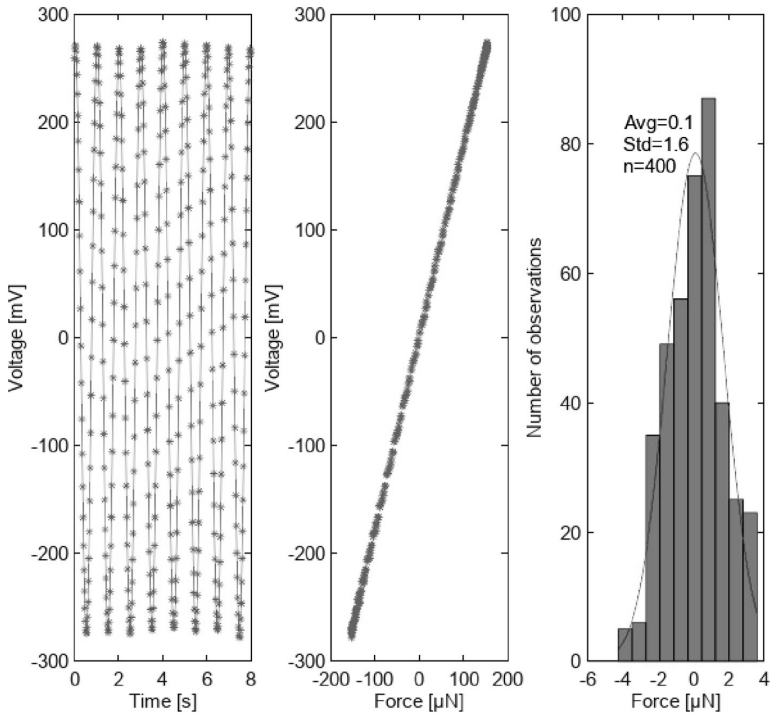

Fig. 4. a) Measurement data fitted to the sinusoidal excitation signal. B) Calibration curve c) Force measurement error distribution.

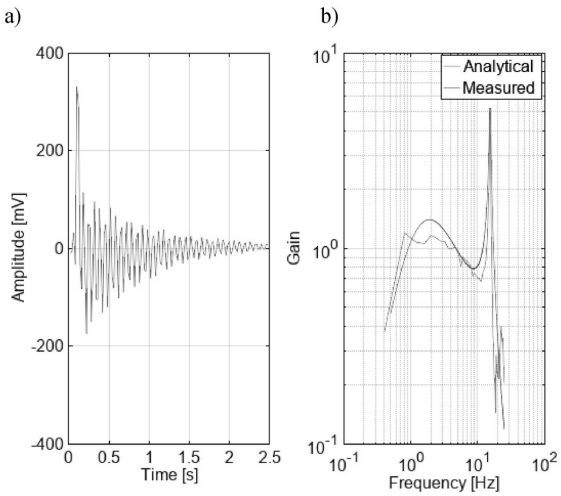

Fig. 5. a) Time domain impulse response of the cantilever measurement system. b) Computed and measured frequency response of the cantilever sensor system in frequency domain.

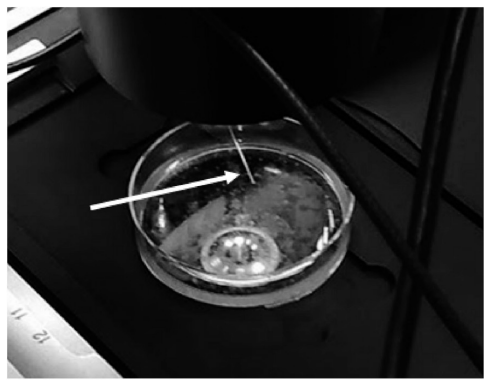

Fig. 6. In-situ measurement setup with a cell culture dish containing the cardiac tissue construct. The measurement cantilever is visible above the Petri dish and marked with the white arrow.

activity can be seen. These stable periodical signals suggest that the fibrin coating enables a good attachment between the tip of the measurement probe and the cardiac tissue construct so that the contracting force is transferred to the probe tip. The beating force from peak to peak of the cardiac tissue construct varied between 7.2 μN and 16.6 μN over the 5 measurements. These values are listed in Table 2 according to the order in which the measurements were taken. As the force measurement results can be considered to be reliable by themselves it should be noted that a biological organism itself may induce variation to the force measurement results. For example the cantilever tip location in the cell construct may be critical in the actual force measurement.

The obtained contraction force measurement results are in line with the previously reported data. Although much higher reported contraction forces have been reported, such as over 1 mN by Sasaki et al. it should be noted that with engineered tissue the total contraction force is a function of the size of the cell population [10]; the larger the cell population, the larger the forces. Accordingly, much lower contraction forces have been recorded right down to the single-cell scale. Such

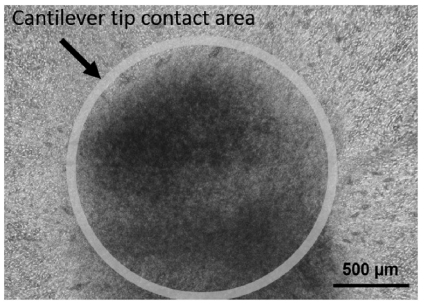

Fig. 7. An example of a cardiac tissue construct 2 weeks after cardiomyocyte seeding with cantilever tip contact area marked with amber circle.

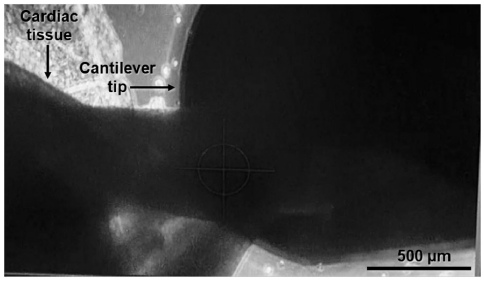

Fig. 8. Microscope image of the cardiac tissue construct and the cantilever during the contraction force measurements. This image is a still from the in-situ video, which is available in the supplementary material.

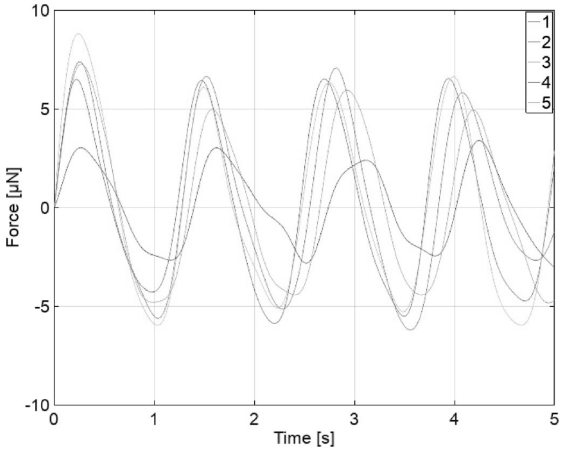

Fig. 9. Contraction force measurement in time domain (all measurements).

small-scale measurements, however, may require cell cultivation directly onto an Atomic Force Microscope (AFM) tip, for example, or onto a dedicated mechanical structure, as described by Linder et al. and Kim et al. [6,9].

In this study, one consideration for the development of this approach is the very concept of force measurement itself. As the elastic force measurement principle combines a force and a displacement measurement, it is important to account for how much the displacement reflects the force measurement readings. This issue is common to any application of this measurement principle, regardless of the scale of the measurement. For example, if the cantilever is very elastic the

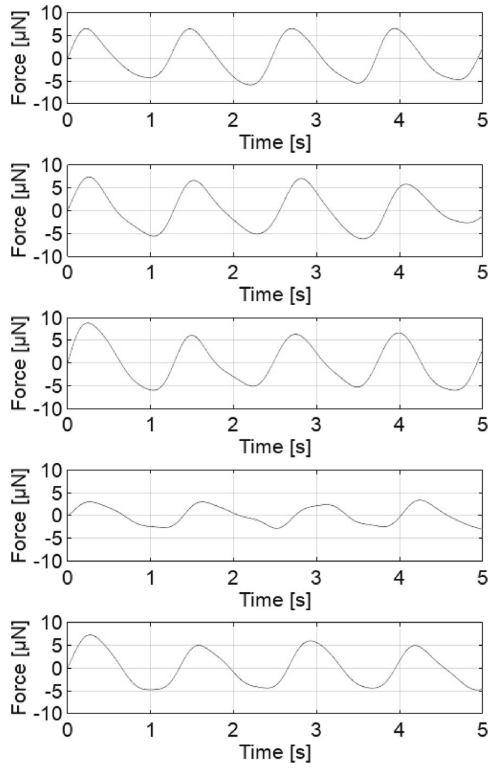

Fig. 10. Individual beating waveforms where the contracting and relaxing phases can be seen.

system may not show the maximum force production, if that is point of interest. Instead, it may more or less measure only the displacement or the movement of the tissue structure. On the other hand, if the probe arrangement is very stiff it may not give any force readings at all as the tissue is too weak to cause any measurable displacement to the tip. Therefore, the role of the spring constant, or the elasticity of the sensor element, become critical. In theory, they need to be tuned to the right range or value to obtain the desired force measurement results. One possibility is to construct a variable load mechanism on the sensor element. With piezoelectric devices, it should be possible to combine a piezoelectric actuator and sensor to provide such a variable load. On the other hand the force measurement probe could be used along with existing force measurement concepts. For example the linear elastic wire video monitoring based measurement (Sidorov et al.) could be replaced with the probe. Potentially simplifying the measurement arrangement. for Nevertheless this is an interesting prospect for the future development of piezoelectric cantilever biomeasurement systems.

The practical arrangements for the force measurement system also require attention. For example, how can the measurements' repeatability be ensured. There are a number of factors that can raise significant challenges for this, not just the sensor itself, but also the mechanism used for attachment to the cells and the properties of the engineered tissue. Repeatability requires standardisation of the cardiac tissue construct itself and its cultivation. Although these challenges have not been much addressed here, it is willingly acknowledged that these are all important considerations if the system is to be applied in, for example, toxicity studies or personalised medicinal applications.

Table 2
Peak To Peak Contraction Force And Recorded Beats per Minute for the 5 Measurements. The Standard Deviation Of The Measurement Error Is 2.11 μN.

Measurement	Peak to peak contraction force [μN]	Beats per minute	Beating frequency [Hz]
1	13.9	48.9	0.81
2	15.2	47.0	0.78
3	16.6	46.9	0.78
4	7.24	43.0	0.71
5	13.6	44.5	0.74

4. Conclusions

In this study we have shown that it is possible to measure cardiac tissue construct contraction forces with a direct force measurement apparatus. The measurements were done with relatively simple devices in a straightforward measurement setup. As this aim of this work was just to prove the concept, there are still many issues to be resolved before this technology reaches its final form. For example, at this stage the method has proved to be suitable only for a multiple cell construct, and is not yet sensitive enough to measure single-cell contraction forces.

However, in this proof-of-concept paper we have demonstrated that a fibrin-coated cantilever connected to a piezoelectric plate sensor can be utilised for measuring cardiac tissue contraction force. The fibrin coating proved itself able to produce reliable force readings, and the measurements of the cells' beating frequency were consistent with the beating frequency obtained from the video (see Supplementary material). The measured cardiac tissue contraction forces from peak to peak ranged from 7.2 to 16.6 μN in amplitude.

Declaration of competing interest

The authors declare that they have no known competing financial interests or personal relationships that could have appeared to influence the work reported in this paper.

Acknowledgement

The authors acknowledge the project funding from the Academy of Finland (grant numbers: 310347 and 310527).

Appendix A. Supplementary data

Supplementary data to this article can be found online at https://doi.org/10.1016/j.cap.2019.10.020.

References

[1] K.E. Lasser, P.D. Allen, S.J. Woolhandler, D.U. Himmelstein, S.M. Wolfe, D.H. Bor, Timing of new black box warnings and withdrawals for prescription medications, J. Am. Med. Assoc. 287 (17) (2002) 2215–2220, https://doi.org/10.1001/jama.287.17.2215.

[2] X. Li, R. Zhang, B. Zhao, C. Lossin, Z. Cao, Cardiotoxicity screening: a review of rapid-throughput in vitro approaches, Arch. Toxicol. 90 (8) (2016) 1803–1816, https://doi.org/10.1007/s00204-015-1651-1.

[3] H. Olson, G. Betton, D. Robinson, K. Thomas, A. Monro, G. Kolaja, P. Lilly, J. Sanders, G. Sipes, W. Bracken, M. Dorato, K. Van Deun, P. Smith, B. Berger, A. Heller, Concordance of the toxicity of pharmaceuticals in humans and in animals, Regul. Toxicol. Pharmacol. 32 (1) (2000) 56–67, https://doi.org/10.1006/rtph.2000.1399.

[4] T.C. Stummann, M. Beilmann, G. Duker, B. Dumotier, J.M. Fredriksson, R.L. Jones, M. Hasiwa, Y.J. Kang, C.-F. Mandenius, T. Meyer, G. Minotti, Y.J.-P. Valentin, B.J. Zünkler, S. Bremer, Report and recommendations of the workshop of the European centre for the validation of alternative methods for drug-induced cardiotoxicity, Cardiovasc. Toxicol. 9 (2009) 107–125, https://doi.org/10.1007/s12012-009-9045-3.

[5] R. Wallis, M. Gharanei, H. Maddock, Predictivity of in vitro non-clinical cardiac contractility assays for inotropic effects in humans — a literature search, J. Pharmacol. Toxicol. Methods 75 (2015) 62–69, https://doi.org/10.1016/j.vascn.2015.05.009.

[6] P. Linder, J. Trzewik, M. Rüffer, G.M. Artmann, I. Digel, R. Kurz, A. Rothermel, A. Robitzki, A. Temiz Artmann, Contractile tension and beating rates of self-exciting monolayers and 3D-tissue constructs of neonatal rat cardiomyocytes, Med. Biol. Eng. Comput. 48 (1) (2010) 59, https://doi.org/10.1007/s11517-009-0552-y.

[7] M.L. Rodriguez, B.T. Graham, L.M. Pabon, S.J. Han, C.E. Murry, N.J. Sniadecki, Measuring the contractile forces of human induced pluripotent stem cell-derived cardiomyocytes with arrays of microposts, J. Biomech. Eng. 136 (5) (2014) 051005, https://doi.org/10.1115/1.4027145.

[8] V. Vyas, N. Nagarajan, P. Zorlutuna, B.D. Huey, Nanostethoscopy: atomic force microscopy probe contact force versus measured amplitude of cardiomyocytic contractions, J. Bionanoscience 11 (4) (2017) 319–322, https://doi.org/10.1166/jbns.2017.1441.

[9] D.-S. Kim, Y.-J. Jeong, B.-K. Lee, A. Shanmugasundaram, D.-W. Lee, Piezoresistive sensor-integrated PDMS cantilever: a new class of device for measuring the drug-induced changes in the mechanical activity of cardiomyocytes, Sens. Actuators B Chem. 240 (2017) 566–572, https://doi.org/10.1016/j.snb.2016.08.167.

[10] D. Sasaki, K. Matsuura, H. Seta, Y. Haraguchi, T. Okano, Tatsuya Shimizu, Contractile force measurement of human induced pluripotent stem cell-derived cardiac cell sheet-tissue, PLoS One 13 (5) (2018) e0198026, , https://doi.org/10.1371/journal.pone.0198026.

[11] J. Virtanen, V. Sariola, S. Tuukkanen, Piezoelectric cantilever force sensor sensitivity measurements, J. Phys. Conf. Ser. 1065 (2018) 042005, , https://doi.org/10.1088/1742-6596/1065/4/042005.

[12] H. Vuorenpää, L. Ikonen, K. Kujala, O. Huttala, J. Sarkanen, T. Ylikomi, K. Aalto-Setälä, T. Heinonen, Novel in vitro cardiovascular constructs composed of vascular-like networks and cardiomyocytes, In Vitro Cell. Dev. Biol. Anim. 50 (2014) 275–286, https://doi.org/10.1007/s11626-013-9703-4.

[13] H. Vuorenpää, K. Penttinen, T. Heinonen, M. Pekkanen-Mattila, J. Sarkanen, T. Ylikomi, K. Aalto-Setälä, Maturation of human pluripotent stem cell derived cardiomyocytes is improved in cardiovascular construct, Cytotechnology 69 (2017) 785–800, https://doi.org/10.1007/s10616-017-0088-1.

[14] T. Toimela, O. Huttala, E. Sabell, M. Mannerström, J.R. Sarkanen, T. Ylikomi, T. Heinonen, Intra-laboratory validated human cell-based in vitro vasculogenesis/angiogenesis test with serum-free medium, Reprod. Toxicol. 70 (2017) 116–125, https://doi.org/10.1016/j.reprotox.2016.11.015.

[15] O. Huttala, H. Vuorenpää, T. Toimela, J. Uotila, H. Kuokkanen, T. Ylikomi, J. Sarkanen, T. Heinonen, Human vascular model with defined stimulation medium - a characterization study, ALTEX 32 (2) (2015) 125–136, https://doi.org/10.14573/altex.1411271.

PUBLICATION III

Direct measurement of contraction force in cardiac tissue construct in 2D-plane using dual axis cantilever sensor

Virtanen J, Koivisto M, Toimela T, Vehkaoja A, Heinonen T and Tuukkanen S

IEEE Sensors Journal 21(3):2702–2711 (2021)
DOI: 10.1109/JSEN.2020.3027857

Direct measurement of contraction force in cardiac tissue construct in 2D- plane using dual axis cantilever sensor

Juhani Virtanen[1,†], Maria Koivisto[2,†], Tarja Toimela[2], Antti Vehkaoja (Member IEEE)[1], Tuula Heinonen[2], Sampo Tuukkanen[1,*]
[1]Faculty of Medicine and Health Technology (MET) and [2]FICAM (Finnish Center for Alternative Methods), at Tampere University (TAU), Tampere, Finland.

[†]Equal contribution by authors JV and MK.
*Corresponding author email: sampo.tuukkanen@tuni.fi.

Abstract— **In this work, we present a technique for a dual axis contraction force measurement of human cell based cardiac tissue constructs. The cardiac tissue constructs consist of a vascular-like network and induced pluripotent stem cell derived cardiomyocytes. Before the force measurements, the cardiac tissue constructs were detached from the culture substrate to allow less restricted contraction. The in-house prepared force sensors are composed of piezoelectric sensing elements and a metallic cantilever for contacting the cardiac tissue constructs. A dedicated measurement platform with embedded signal processing software is used for data acquisition from the sensors. Dual axis force sensor results are compared with our previously developed single axis force sensor technique. Additionally, the proposed dual axis force measurement system can measure two-dimensional displacement trajectories of the cantilever probe tip. We propose a pattern matching method for classification of the captured cardiac contraction cycle patterns and for extracting anomalies in the measured cycles. We demonstrate both single and dual axis peak cardiac construct contraction force measurement results in the ranges of 3.4 - 6.7 µN and 9.4 - 10.6 µN, respectively. The relative standard deviation of the peak contraction force results varied between 1.0 and 4.1% in eight captured 60 second measurement sequences.**

Keywords—Contraction force measurement, Data processing, hiPSC, Cardiac construct, Pattern matching

I. Introduction

Cardiotoxicity is one of the main reasons for discontinuation of drug development processes and for post approval market withdrawals [1,2]. In addition to ethical issues, the use of animal models is not optimal for predicting drug effects in humans [3]. Human induced pluripotent stem cell (hiPSC) based cardiac in vitro models have been under active research as a potential path to more accurate test systems. The cardiotoxicity of drugs can be studied in hiPSC-derived cardiomyocytes by using, for example, patch clamp, microelectrode array (MEA), impedance and calcium dynamics measurements [3]. While they are valuable tools for measuring the electrophysiology and contractility of the cardiomyocytes in toxicity studies, they cannot directly measure the contraction force of cardiomyocytes. The direct contraction force measurement would provide more useful information about the contraction force which cannot be obtained by action potential measurements.

Various approaches to cardiac cell and tissue contraction force measurements have been proposed. Direct force measurements, where the force signal is obtained by a force measurement system, have been reported using atomic force microscope [4-6]. A flexible sheet approach, where cardiac cells are cultured on an elastic sheet and the cardiac contraction is measured from the deflection of the sheet during contraction, has been proposed by Linder *et al.* [7], while Kim *et al.* used piezoresistive sensor integrated on elastic PDMS cantilevers which bend due to cell contraction forces [8]. Contraction force measurement can also be conducted indirectly using video imaging. Balaban *et al*. proposed a microstructured substrate with elastic properties used with video imaging [9]. Mannhardt *et al.* proposed using cardiac construct cultures on bending pillars and obtaining the reactive contraction force by video imaging [10]. Imaging techniques can also be applied to cantilever-based force measurement approaches [11, 12]. Sugiura *et al*. have proposed a method where mechanical properties of a carbon fibre are used in the measurement by observing the displacement of the carbon fibre with video imaging and obtaining the force from this information [11].

In this paper, we present an improved technique compared to our previously reported single axis force measurement setup [13]. We demonstrate a piezoelectric dual axis cantilever force sensor, which allows the direct contraction force measurement of cardiac tissue constructs in x- and y- directions simultaneously. In addition, this measurement concept does not need imaging devices and therefore is not limited to the diffraction limit of optical microscopy. In order to avoid

potential phototoxicity effects [14, 15] the measurements with this approach can be carried out in complete darkness. Moreover, many drugs are light-sensitive [16], and darkness is required when their effects are studied. Our cardiac tissue constructs consist of vascular-like networks and hiPSC-derived cardiomyocytes. Our approach utilizes a perforated silicone sheet and a detachment procedure in the cardiac tissue construct fabrication. The detachment enables less restricted contraction of the cardiac tissue construct, as it is not attached to the culture substrate. We present in vitro contraction force measurement results on both single axis and dual axis approaches and compare their results.

This manuscript first explains the sensor design procedure, the used measurement system. and the culture of the measured cardiac constructs. Then we present the measurement system calibration and the *in vitro* contraction force measurements of cardiac constructs in both our new dual axis and our previously proposed single axis measurement systems. Finally, the results and the conclusions drawn in this study are presented.

II. Materials and Methods

A. Force sensor design

The single axis force measurements were carried out with a previously studied single axis force measurement probe consisting of a single piezoelectric sensor element attached to a metal probe to form a cantilever force sensor. The sensor design and measurement setup are described in more detail in [13].

A dual axis piezoelectric cantilever force sensor with two lead zirconate titanate (PZT) sensing elements was developed and studied in this work. The sensor itself consists of a brass plate coated with PZT sensor material. Dual axis sensing capability is achieved by assembling two piezoelectric sensor elements perpendicular to each other, forming a L- shaped structure. While the end of one sensor plate is used as a fixed attachment point of the sensor, the other plate is attached to a rigid cantilever beam, whose tip is used for contacting the measured cardiac tissue construct. The operation of the sensing element is based on the linear elastic behaviour of the brass plate coated with the PZT. The dynamic characteristic of the sensor is determined by the mass, its location in the sensor and the spring constant of the cantilever, as well as piezoelectric properties of the PZT material. When force is applied to the cantilever probe tip, the piezoelectric material converts the resulting stress to electrical signal. The sensor design was optimised using COMSOL Multiphysics (Comsol AB, Stockholm, Sweden) finite element method (FEM) simulations. The simulations provide information about the expected charge-output/force-input behaviour for certain sensor dimensions and assembly.

A hand-made prototype of the cantilever sensor was fabricated with a similar method to the one reported previously [13]. Commercial piezo discs were used as the sensing elements and their shape was tailored by cutting to match the simulated design. The L- shaped sensor structure and electrical contacts were soldered to form an electrically connected dual axis force sensor. An example of a prepared dual axis force sensor is shown in Fig. 1(a) and 1(b). A schematic drawing of the sensor concept is shown in Fig. 1(c).

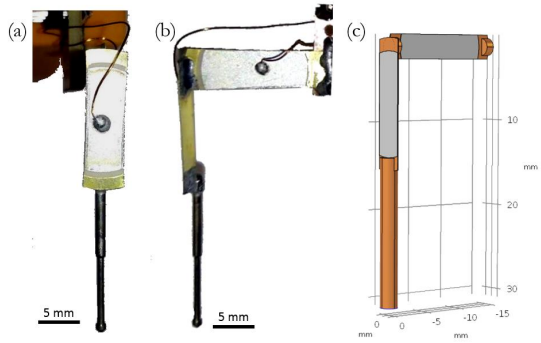

Fig. 1. The L- shaped sensor construction. Front view and side view are shown in panels (a) and (b), respectively. Panel (c) shows a dimensioned drawing of the sensor prototype.

It is necessary to have the cantilever sensor spring constant at an appropriate level to measure force instead of only displacement. Furthermore, the spring constant should not be too high, in order to avoid affecting cardiac construct contractility behaviour. The spring constant value of the sensor was thus set as the main design parameter, with a target value of 5 N/m, in order to study the effect of larger (> 1 N/m) spring constant (i.e. more restriction to the movement of the cells) on the cardiac contraction force measurement results. Another aim was to have a higher resonant frequency margin compared to our previous single axis measurement probe, which has a natural frequency of approximately 14 Hz (Virtanen *et al*. 2020).

The calibration of the sensor was carried out using a texture analyser Stable Micro Systems TA.XTPlus (Stable Micro Systems Ltd, Surrey, United Kingdom). The calibration procedure has been presented in detail previously in [13, 17, 18]. Briefly, the sensor was loaded with a sine wave sweep that has a defined displacement amplitude. Here the used displacement sweep amplitude was 100 µm and the implied force was recorded with both the texture analyser and with the proposed sensor. This procedure was performed with both of the axes. After the calibration measurements, the axial tilt or distortion in the sensor output was corrected with software to fit the data on x- and y- axes.

The impulse response measurement was carried out for both of the axes in order to ensure a suitable frequency response band in the measurement system. The impulse excitation was done by manually tapping the sensor probe tip. The frequency response was then obtained by Fourier transforming the impulse response data.

B. Data acquisition platform

The measurement hardware and embedded signal processing software is similar to our previous work [17], except that the embedded part of the digital electronics was implemented using a Teensy 3.6 board (PJRC.COM LLC., Sherwood, USA)

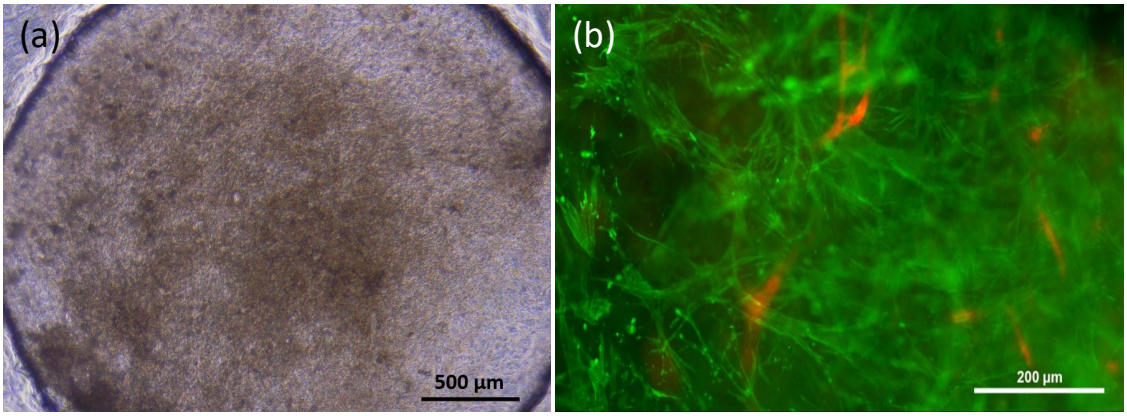

Fig. 2. (a) A detached cardiac tissue construct in a PDMS hole 10 days after cardiomyocyte seeding. (b) Immunofluorescence stained cardiac tissue construct where cardiomyocytes (green) and von Willebrand factor positive endothelial cells (red).

instead of Arduino Due, which was used previously. The measurement electronics consists of a buffer amplifier with a gain of 1 and input impedance of 50 MΩ. The main difference affecting the measurement results between the Arduino Due and Teensy 3.6 is the analog to digital conversion resolution, which is 12- bits in Arduino Due and 16- bits in Teensy 3.6. The functionality of the software was retained and the program was only recompiled and programmed to Teensy 3.6 hardware. The embedded system first samples the sensor signal at 6 kHz for each of the two channels. After the sampling, a seventh order digital filter is applied to the signal in order to limit the bandwidth and remove powerline interference and its harmonics. The signals are then averaged to reduce the sampling rate to 50 Hz. Finally, data are transferred to a personal computer via a Universal Serial Bus (USB). As with the previous demonstration, the data is moved from the Teensy 3.6 platform to a LabVIEW user interface and data collection software. The signal processing methodology is described in more detail in [17].

C. Fabrication of cardiac tissue constructs

The use of human adipose stromal cells (hASCs) obtained from surgical operations and human umbilical vein endothelial cells (HUVECs) from scheduled caesarean sections was approved by the Ethics Committee of the Pirkanmaa Hospital District (permit numbers R03058 and R08028, respectively).

The cardiac tissue constructs were fabricated by a technique, which was adapted from previous work [13, 19, 20]. A polydimethylsiloxane (PDMS, Sylgard 184, Dow Corning, USA) sheet (h = 1 mm) containing punched holes (d = 3 mm) was reversibly bonded to a temperature responsive cell culture dish (Nunc UpCell, Thermo Scientific). A fibrin gel was formed in the PDMS holes by mixing 1:1 an excess of a solution containing 5.5 mg/ml fibrinogen (Sigma Aldrich, F3879), 38 µg/ml aprotinin (Sigma Aldrich, A1153) and an excess of thrombin (Sigma Aldrich, T7009), and leaving 5 µl of the mixture in each hole for polymerization at +37 °C. This method ensured that the fibrin was properly attached to the walls of the PDMS holes.

To produce a vascular-like network base for cardiac tissue constructs, hASCs and HUVECs were propagated separately before seeding them as a co-culture onto the fibrin as previously described in [21]. The vascular-like network was allowed to form for 7 days in a serum-free stimulation medium (SFSM) consisting of DMEM/F12, 2.56 mM L-glutamine, 0.1 nM 3,3′,5-Triiodo-L-thyronine sodium salt, ITS™ Premix: 1.15 µM: 6.65 µg/ml insulin, 6.65 µg/ml Transferrin, 6.65 ng/ml selenious acid, 1% Bovine serum albumin, 2.8 mM Sodium pyruvate, 200 µg/ml Ascorbic acid, 0.5 µg/ml Heparin, 2 µg/ml Hydrocortisone, 10 ng/ml VEGF, and 1 ng/ml FGF-β as described in [22]. On day 8, hiPSC-derived cardiomyocytes (iCell², Cellular Dynamics) were seeded on top of the vascular-like network at 312000 cardiomyocytes/cm² in iCell Cardiomyocytes Plating Medium (Cellular Dynamics, M1001). After cardiomyocyte seeding, 1:1 iCell Cardiomyocytes Maintenance Medium (Cellular Dynamics, M1003) and SFSM were used. Cells were maintained in a humidified incubator at +37°C, 5% CO_2 and the medium was refreshed every 2 days.

The PDMS sheets containing the cardiac tissue constructs were detached from the original cell culture substrates 6 days after the cardiomyocyte seeding (Fig. 2a). The PDMS sheets were placed onto PDMS stands in a new cell culture dish. This resulted in a setup where the cardiac tissue is attached to the walls of the PDMS hole and is not in direct contact with the cell culture substrate anymore. This allows the tissue to contract more freely than when attached to the bottom of a cell culture dish. Contraction force measurements were performed 9 - 14 days after cardiomyocyte seeding. Leibovitz's L-15 Medium (Gibco, 11415) was used during the measurements.

To confirm the formation and differentiation of the cardiac tissue type, we characterized the constructs by immunofluorescence imaging (Fig. 2b). The cells were fixed 15 after cardiomyocyte seeding using 70 % EtOH. Cardiomyocyte specific mouse anti-Troponin T antibody (1:100, Invitrogen, MA5-12960) and endothelial cell specific rabbit von

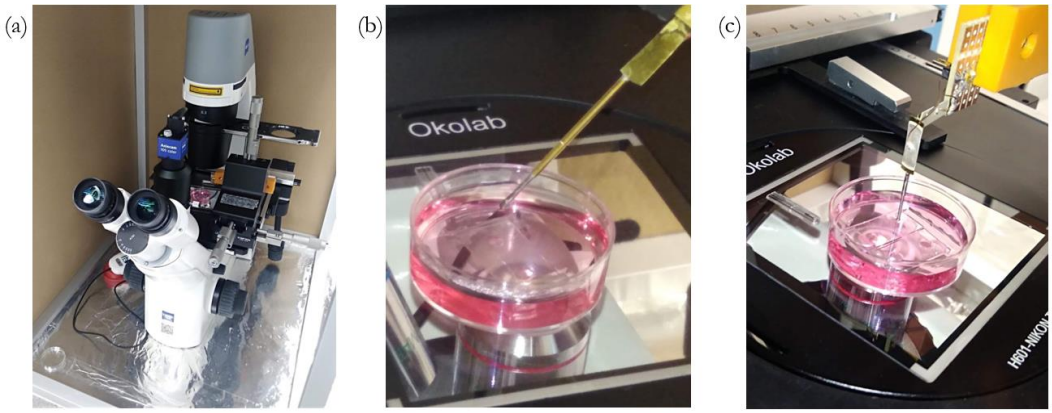

Fig. 3. (a) The measurement setup under microscope in (b) a single axis cantilever and (c) dual axis cantilever cases, showing the approach to the cardiac tissue with the sensor probes. The single axis sensor probe was used in approximately 30- degree tilt angle while the dual axis sensor probe was placed vertically to the cardiac tissue construct.

Willebrand Factor antibody (1:100, Dako, A0082) with secondary antibodies anti-mouse A488 (1:400, Invitrogen, A21202) and anti-rabbit A568 (1:400, Invitrogen, A11011) were used. The samples were imaged using Olympus IX51 inverted fluorescence microscope.

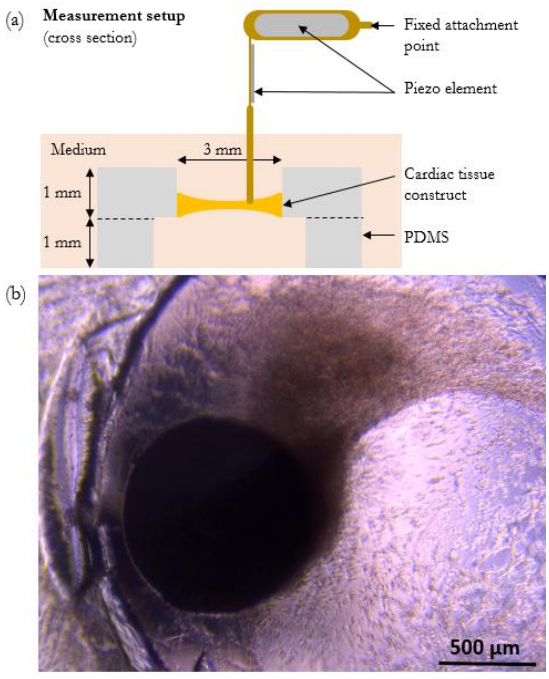

Fig. 4. (a) Cross section of the detached cardiac tissue construct on a PDMS stand and the force measurement probe. (b) The force measurement cantilever tip is in contact with the cardiac tissue construct during dual axis force measurement. The diameter of the tip shown in the figure is 0.9 mm.

D. Contraction force measurements

For contraction force measurements, the cell culture dishes were placed on a heater plate set to +37 °C on an optical microscope (Zeiss Primovert, Carl Zeiss AG, Oberkochen, Germany). To improve the attachment between the force measurement cantilever tip and the cells, the cantilever tip was coated with 5.5 mg/ml fibrinogen and contacted with the cardiac tissue construct using a 3- axis linear micromanipulator (Newport Corporation, Irvine, USA) as previously described in (Virtanen *et al*. 2020). The measurement setup is illustrated in Fig. 3 for single (b) and dual axis (c) measurements. The angle between the cardiac tissue and the cantilever was approximately 30 degrees for the single axis probe, while the dual axis probe contacted the cardiac tissue vertically. Fig. 4 describes schematically the side-view of dual axis cantilever in contact with the cardiac tissue construct and shows the microscopy view during the measurement. The probe tip location relative to the construct was selected using the microscope view. The aim was to locate the tip such that the movement amplitude was as large as possible in the microscope view.

Cardiac tissue construct contraction force measurements were carried out with both previously presented single axis [13] and the new L- shaped dual axis force measurement probe. For the comparison of the two force measurement approaches, four force measurements were carried out with both force measurement probes. Contraction force was recorded for 60 seconds during each of the eight measurements.

In the data processing, the dual axis force measurement x- and y- force components were converted to show the measurement probe tip displacement trajectory. In addition, a total force magnitude curve was computed, in order to have a comparable force representation with the single axis force measurement. This was carried out by first computing the magnitude and rotation angle of the reactive force and then projecting the force onto the main axis where the zero level corresponded the zero value in the force magnitude. As the

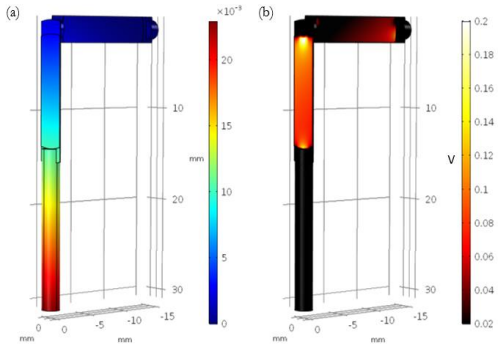

Fig. 5. FEM simulation results (a) displacement [mm], (b) electric potential [V].

measured force signals were clean of artefacts and had high signal-to-noise ratio, a simple method of finding local maxima above an adaptive threshold was sufficient for locating the cycles with 100% sensitivity and specificity. The peak location data were used to obtain the beat rate of the cardiac tissue construct by computing a time interval between consecutive peaks.

E. Cardiac contraction cycle pattern matching

We propose the use of a pattern matching approach for further processing the measurement data. This is used to divide the measured cardiac cycles in two groups: the cycles closely resembling each other and the ones that contain any type of disturbance, either originating from the cell contraction itself or caused by the environment, e.g. vibration or percussion. The purpose of dividing the data is twofold: 1. to enhance the precision of the peak force measurement by removing cardiac cycles containing random variation and noise and 2. to automatically identify the cycles containing anomalies and separate them for further investigation. This method is principally presented in our previous work [23] and has been further developed with the addition of peak detection and pattern template forming. Briefly, first the maximum force peaks are identified by differentiating the measured force signal from the 60 second data. Two consecutive peaks then locate a cardiac contraction cycles, which are then used to compute a pointwise average or median curve to be used as a template for the pattern matcher. In this work a median template was chosen.

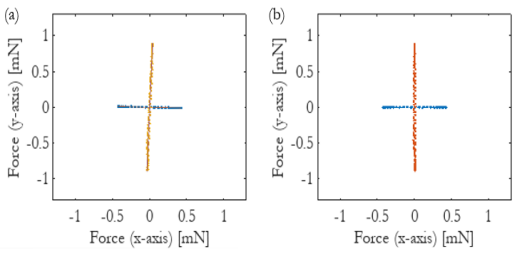

Fig. 6. x- and y- axis calibration measurement results before tilt correction (a) and after tilt correction (b).

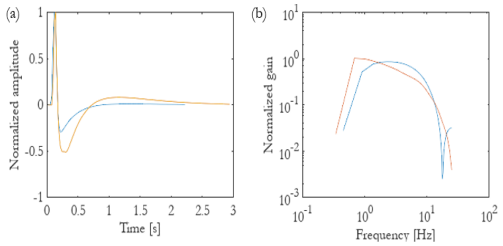

Fig. 7. Normalised impulse (a) and frequency (b) responses of the x-channel (blue) and the y- channel (red).

Since the identified peak does not initiate a cardiac cycle, a certain offset was added to the template to represent a complete cycle.

Cardiac cycle data are then compared to the template by first normalising them with the maximum value of one cardiac cycle. Then a squared sum of differences between the template and each data point represents a distance to the template. Here the thresholding level for the pattern matcher was heuristically obtained from a particularly successful sample set such that the thresholding would cause all the cycles in this dataset to be interpreted as matching cycles. Finally, the decision with the other cycle sets of either matching or discarding cycles was done by thresholding the computed distance values.

III. Results

A. Dual axis FEM and calibration measurement results

The sensitivity and spring constant values of the dual axis probe were obtained both with FEM modeling and calibration measurements. The results obtained with modeling are listed in Table 1 along with the measured results. The spring constants of 8.8 N/m and 5.1 N/m were obtained in the simulation for the bending mode (corresponding to x- axis measurement) and twisting mode (corresponding to y- axis measurement), respectively. These spring constant values are comparable to the measured calibration values which were 8.8 N/m and 4.3 N/m for x- and y- axis, respectively. Similarly, the sensitivity values of 890 V/N in x- axis and 322 V/N in y- axis were obtained from the FEM computations. Calibration measurements show slightly different values of 863 V/N and 464 V/N for x- and y- axis, respectively. The FEM computing results of the displacement and electric potential in the piezoelectric material with 0.1 mN load are illustrated in Fig. 5(a) and 5(b), respectively.

TABLE I. Spring constant and Sensitivity results FEM and calibration.

	x- axis (bend mode)		**y- axis (twist mode)**	
	FEM	**Measured**	**FEM**	**Measured**
Spring constant	8.8	8.8	5.1	4.3
Sensitivity [V/N]	890	863	322	464

Due to the hand-fabricated sensor the axes were not orthogonally aligned and there was a tilt error in both axes,

which can be seen in Fig. 6(a). The sensor calibration tilt error was corrected by rotating both axes according to the calibration data. The root mean square error (RMS) with respect to the corrected axis was then computed. The results of calibration performed with sine wave excitation are presented in Fig. 6. The RMS error after the axial tilt correction was 3.0 µN in the x-direction (0 degrees rotation) and 4.4 µN in the y-direction (90 degrees rotation). These represent relative errors of 0.6% and 0.5% of the full sweep amplitude in the x- and y- axes, respectively.

B. Impulse and frequency response of the dual axis cantilever

In order to ensure that the frequency range of the dual axis measurement system is applicable, an impulse response measurement was carried out in both x- and y- directions. This was done by manually inducing an impulse excitation to the sensor and recording the consequent response. The impulse response measurement result is shown in Fig. 7(a) and the corresponding frequency response in Fig. 7(b). The passband of the frequency response is at the desired range of 0.5 - 10 Hz in both directions. The frequency response of the single axis and dual axis sensor measurement systems have similar usable frequency range, however the single axis probe has the first natural frequency at approximately 14 Hz.

C. Single axis contraction force measurements

Peak forces from the single axis contraction force measurements ranged from 3.4 to 6.7 µN between the cardiac tissue construct samples. The coefficient of variation (relative standard deviation, CV) ranged between 3.3% and 4.1%. The values of each measurement are listed in Table 2. The recorded beat rate was stable in each measurement and ranged between 22 and 38 beats per minute. The illustration of a recorded waveform is shown in Fig. 8(a). The recorded peak force and beat rate as a function of time are shown in Fig. 8 (b) and 8(c), respectively. Finally, the cardiac contraction cycles were stacked, and this plot is shown in Fig. 9 1-4 for all of the four cardiac tissue samples.

D. Dual axis contraction force measurements

The proposed L- shaped probe was used in *in vitro* measurements and the results were compared with the measurements done with a previously presented single axis force measurement probe. The trajectory of the L- shaped force measurement probe tip was computed using the x- and y-direction spring constants and the measured sensor output signals. The peak force measurement results for each measurement are shown in Table 2. The peak forces ranged between 9.4 and 10.6 µN while the CV of the peak force ranged between 1.0% and 3.2%. An exemplary shape of a measured total force curve and its corresponding trajectory curve are shown in Fig. 10 (a) and 10 (b), respectively. The displacement of the probe tip was approximately ±1 µm in x- direction and ±0.5 µm in y- direction. The trajectory loops in Fig. 8 (e) appear as smaller and larger loops, where the larger loop corresponds to the maximum contraction force peak, which can be seen from Fig. 8 (d). The recorded peak force and the beat rate as a function of time are shown in Fig. 8 (f) and 8 (g), respectively.

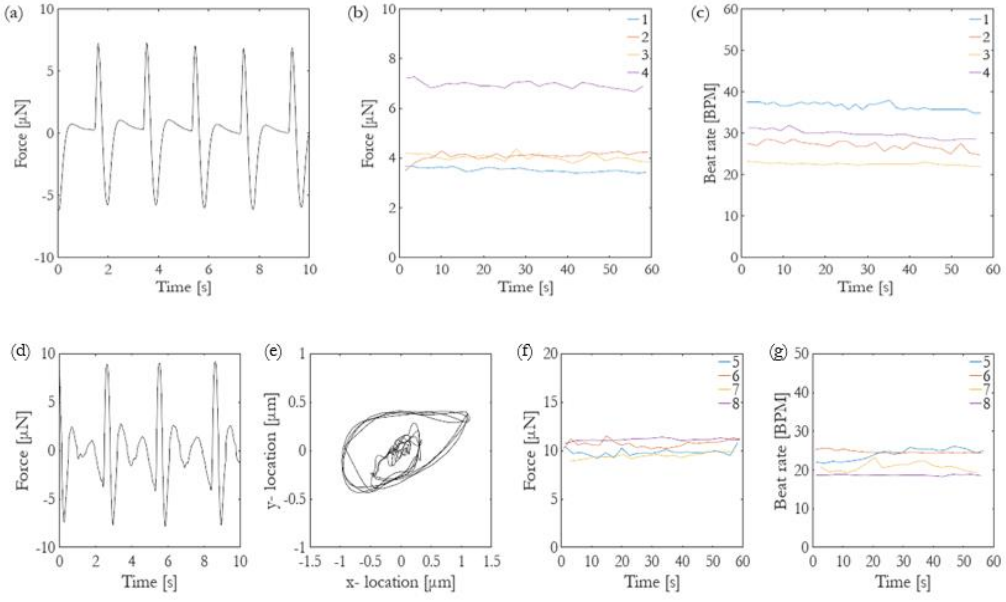

Fig. 8. Single axis cantilever contraction force measurement results in-vitro 10 s excerpt of raw measurement signal is shown in panel (a). Panel (b) shows the peak contraction force of all measured cycles for the four cases and panel (c) shows the calculated beat rates which were measured with the single axis probe A dual axis 10 s excerpt of raw measurement data presented as total force magnitude signal (d) and the dual axis probe tip location trajectory curve (d) computed from force measurement data using the spring constant values. The peak contraction force of all measured cycles for the dual axis cases (f) and the respective calculated beat rates (g).

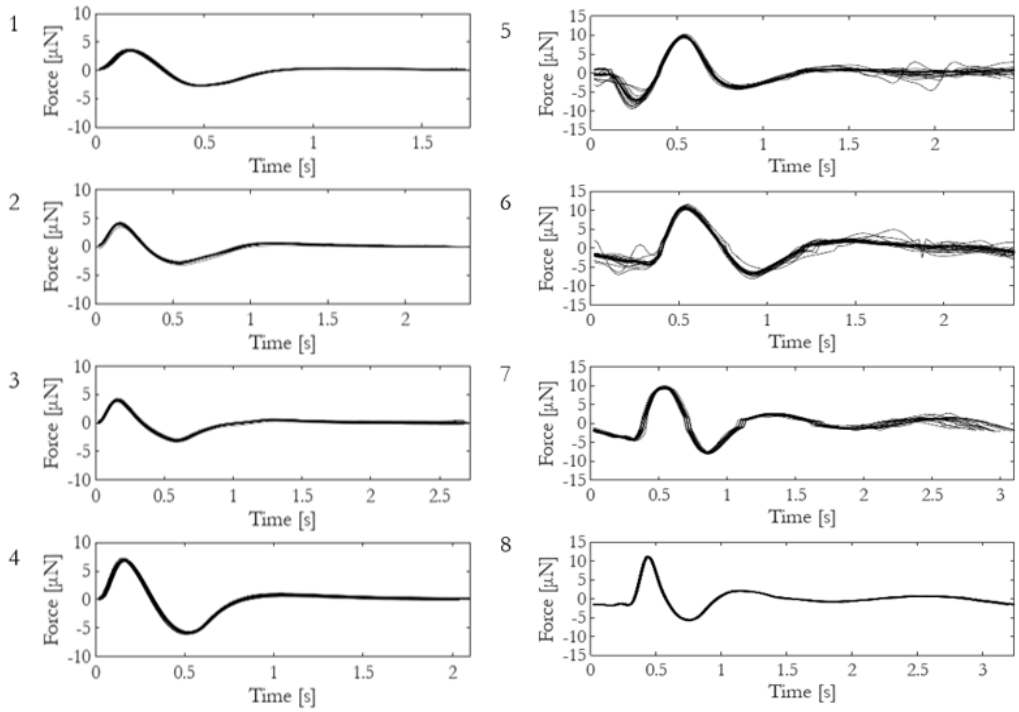

Fig. 9. Single axis cantilever stacked time domain force plots for the 60 s measurements with four different cardiac tissue populations (measurements 1-4). Beat-by-beat force magnitude cycles of four 60-second recordings measured with the dual axis probe stacked together (measurements 5-8).

The beat rate varied approximately between 19 and 25 beats per minute (BPM). Finally, the cardiac contraction cycles were stacked, and this plot is shown in Fig. 9 5-8 for all of the four cardiac tissue populations.

TABLE II. Single axis peak force measurement results. CV = coefficient of variation.

Measurement	1	2	3	4	5	6	7	8
Mean peak force [µN]	3.4	4.0	3.9	6.7	9.7	10.7	9.5	11.2
Peak force STD [µN]	0.13	0.16	0.14	0.22	0.24	0.35	0.25	0.11
CV %	3.8	4.1	3.6	3.3	2.5	3.2	2.6	1.0

E. Pattern matching and cycle analysis

The threshold level for the pattern matcher was obtained from a particularly successful or 'golden' measurement, which in this case was considered to be cycle set obtained from measurement 8. All the cycles in this 'golden' cycle group are considered to be acceptable or matching. The resulting threshold value was 2.80 (normalised units), which was then used in the method. Cardiac cycles of measurement 5 was further processed with the pattern matching technique. All the identified cycles were split into two categories based on how closely they resembled the median template using the threshold level above. This is illustrated in Fig. 10, where (a) illustrates a 60 second measurement with identified force peak locations marked with an asterisk, (b) shows the computed and normalised median curve which is used as the template for the pattern matcher and (c) shows a stacked plot of all cycles. Fig. 10 (d) also shows the 60 second cycle set, but now only the matching peaks are marked with the asterisk. Finally, (e) and (f) show stacked plots of the matching and discarded cardiac cycles respectively.

Mean and median force plots from cycle set 5, from Fig. 9, with 95% confidence levels are shown in Fig. 11(a). In Fig. 11(b) the same data are shown for the matching cycles, while (c) shows the discarded cycles, respectively. The standard deviation and the coefficient of variation (CV) computed pointwise from the force curves of these three cases are listed in Table 4. The CV of the matching cycles was 2.4% while the discarded set had CV of 5.0%. CV of all the cycles was 4.6%. The main deviations of the cardiac cycle curves are concentrated at the bottom peak at the start and at the end of the cardiac cycle, while there is little variation at the maximum force peaks.

TABLE III. Pattern matcher parameters calculated from the data presented in Fig. 12.

Cycles	All	Matching	Discarded
Mean [µN]	0.00	0.00	0.00
Standard deviation [µN]	0.51	0.26	0.56
CV %	4.6	2.4	5.0
95% Confidence limit [µN]	±1.0	±0.5	±1.1

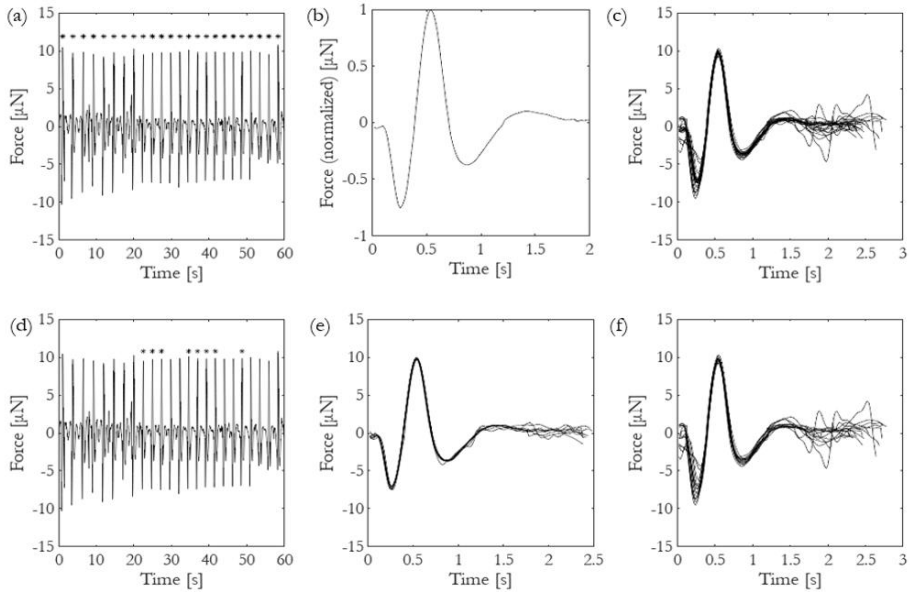

Fig. 10. Processing of a cell culture force measurement data with the proposed method. (a) all cycles with peaks identified, (b) normalised template (median waveform), (c) all cycles stacked together, (d) closely matching cycles identified, (e) only matching cycles stacked, and (f) discarded cycles stacked.

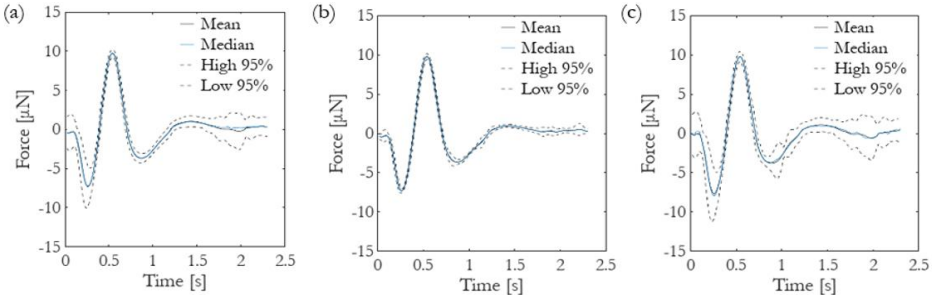

Fig. 11. Mean and median cardiac cycle from the measurement set S5 together with its 95% confidence levels. All cycles are plotted in panel (a) and the closely matching and the discarded cycles in panels (b) and (c), respectively.

IV. Discussion

Based on the results, both single and dual axis force measurement methods are capable of measuring contraction forces of cardiac tissue constructs with adequate capability at the desired force range. The novelty of the force measurement method presented in this paper compared to the other approaches which were presented in the introduction [9-12] is the ability to carry out the contraction force measurement without light. Therefore, if desired, measurement can be carried out in a darkness. This minimizes the phototoxic effects on the observed cardiac constructs during the measurement. Moreover, the potential decomposition of drug molecules during the measurements is also avoided. These properties are desirable when the drug molecule toxicity effects on humans are studied.

Regarding the overall performance of the measurement system the coefficient of variation of the peak force was found to be relatively small within all test cases. With the single axis measurements, the CV values varied between 3.3 and 4.1% while the CV values in the dual axis measurement varied between 1.0 and 3.2%, which indicates the dual axis method to be slightly more accurate. Exact quantitative estimation of the effect of the measurement setup itself on the variation is difficult. It is not possible to know how large the actual peak contraction force variation is in the 60 s measurements. It should be emphasized that other variation sources exist for the differences between the cardiac tissue samples, for example different peak contraction force capability of different tissue constructs. Despite the fact that all the measured cell populations originated from the same cell batches and were cultured with the same procedure, the size, location and

orientation of the contracting tissue differ between populations.

The recorded peak forces were higher in the dual axis measurements than in the single axis measurements. This may be partially explained by the difference in the measurement days since the single axis measurements were performed on day 9 while the dual axis measurements were performed on days 10 and 14. In addition, the location and orientation of the cantilever tip attached to the cardiac tissue construct is likely to have an effect on the measurement results, especially in the case of the single axis measurements. The main contraction component of the construct is not necessarily aligned to the cantilever sensing orientation. And even if it is aligned, more uncertainty may be induced by a non-linear contraction trajectory. In this work we have shown that with the proposed dual axis force measurement concept the tip displacement trajectory has a circular shape, thus the movement and force caused by cell contraction is not in just one direction. The dual axis probe tip displacement trajectory curve presented in this paper appears to have two different sized circles or ellipses. Moreover, the mechanical properties of the measurement probes may influence the results, especially the spring constant of the measurement probe, which was approximately 1 N/m in the single axis cantilever probe compared to the dual axis probe having spring constant of approximately 5 or 9 N/m, depending on the orientation. An excessively small spring constant may have caused the single axis measurement to be more of a displacement measurement than a force measurement if the cardiac tissue construct is not able to move with large enough amplitude.

During one cardiac cycle, cardiomyocyte contraction and relaxation occur once. In the dual axis force measurements, the force curve appears to have two after-peaks. The after-peaks may result from contraction and relaxation of cardiac tissue that is not immediately at the cantilever contact site from which the predominant peak originates. The contraction of the cardiac tissue may be conveyed along the tissue to the cantilever contact site where it causes the measured after-peaks.

The measured contraction forces ranging 3.4 - 6.7 µN for the single axis measurements and 9.4 - 10.6 µN for the dual axis measurements fit to the wide range of contraction forces obtained from hiPSC-derived cardiomyocytes using various methods. Rodriguez *et al.* measured contraction force of approximately 15 nN from single cardiomyocytes using a micropost array [24], Mannhardt *et al.* obtained contraction forces of 152 µN from their strip format engineered heart tissues [10], and Sasaki *et al.* measured contraction forces of approximately 1 mN from their cardiomyocyte sheets [25]. Possible factors affecting the different contraction force include *e.g.* the number of measured cardiomyocytes, maturity of the cells and cell orientation. Large variation in the measured contraction forces in the literature are associated with the culturing techniques of the cells. This affects the contraction force measurement system design, which has to be tailored in the right force range in each occasion.

V. Conclusion

We have demonstrated a dual axis force measurement sensor which is capable of direct contraction force measurement from human cell based cardiac tissue constructs in the range of 1 - 10 µN. The sensor element is composed of a metallic cantilever probe connected to two piezoelectric force sensor elements. This approach allows observation of the force generation direction and the displacement of a particular point in the construct in the xy- plane. The measurement results are critically analysed and compared with the results obtained with a previously developed single axis force sensor. The force measurements were performed on cardiac tissue constructs composed of a vascular-like network and induced pluripotent stem cell derived cardiomyocytes. The detachment of the cardiac tissue constructs from the culture substrate enabled less restricted contraction in the force measurements. The proposed technique allows an accurate analysis of the behaviour of human cardiac tissue constructs, for example under drug exposure, and can help enable more accurate medicine development compared to conventional methods.

Acknowledgement

The authors acknowledge the project funding from the Academy of Finland (grant numbers: 310347 and 310527).

References

[1] Lasser, K. E., Allen, P. D., Woolhandler, S. J., Himmelstein, D. U., Wolfe, S. M., & Bor, D. H. (2002). Timing of new black box warnings and withdrawals for prescription medications. Jama, 287(17), 2215-2220.

[2] Li, X., Zhang, R., Zhao, B., Lossin, C., & Cao, Z. (2016). Cardiotoxicity screening: a review of rapid-throughput in vitro approaches. Archives of toxicology, 90(8), 1803-1816.

[3] Olson, H., Betton, G., Robinson, D., Thomas, K., Monro, A., Kolaja, G., ... & Dorato, M. (2000). Concordance of the toxicity of pharmaceuticals in humans and in animals. Regulatory Toxicology and Pharmacology, 32(1), 56-67.

[4] Cogollo, J. F. S., Tedesco, M., Martinoia, S., & Raiteri, R. (2011). A new integrated system combining atomic force microscopy and micro-electrode array for measuring the mechanical properties of living cardiac myocytes. Biomedical microdevices, 13(4), 613-621.

[5] Mathur, A. B., Collinsworth, A. M., Reichert, W. M., Kraus, W. E., & Truskey, G. A. (2001). Endothelial, cardiac muscle and skeletal muscle exhibit different viscous and elastic properties as determined by atomic force microscopy. Journal of biomechanics, 34(12), 1545-1553.

[6] Vyas, V., Nagarajan, N., Zorlutuna, P., & Huey, B. D. (2017). Nanostethoscopy: atomic force microscopy probe contact force versus measured amplitude of cardiomyocytic contractions. Journal of Bionanoscience, 11(4), 319-322.

[7] Linder, P., et al. "Contractile tension and beating rates of self-exciting monolayers and 3D-tissue constructs of neonatal rat cardiomyocytes." Medical & biological engineering & computing 48.1 (2010): 59.

[8] Kim, D. S., Jeong, Y. J., Lee, B. K., Shanmugasundaram, A., & Lee, D. W. (2017). Piezoresistive sensor-integrated PDMS cantilever: A new class of device for measuring the drug-induced changes in the mechanical activity of cardiomyocytes. Sensors and Actuators B: Chemical, 240, 566-572.

[9] Balaban, N. Q., Schwarz, U. S., Riveline, D., Goichberg, P., Tzur, G., Sabanay, I., ... & Geiger, B. (2001). Force and focal adhesion assembly: a close relationship studied using elastic micropatterned substrates. Nature cell biology, 3(5), 466.

[10] Mannhardt, I., Breckwoldt, K., Letuffe-Brenière, D., Schaaf, S., Schulz, H., Neuber, C., ... & Klampe, B. (2016). Human engineered heart tissue: analysis of contractile force. Stem cell reports, 7(1), 29-42.

[11] Sugiura, Seiryo, et al. "Carbon fiber technique for the investigation of single-cell mechanics in intact cardiac myocytes." Nature protocols 1.3 (2006): 1453.

[12] Myachina, T., et al. "An Approach for Improvement of Carbon Fiber Technique to Study Cardiac Cell Contractility." IOP Conference Series: Materials Science and Engineering. Vol. 350. No. 1. IOP Publishing, 2018.

[13] Virtanen, J., Toivanen, M., Toimela, T., Heinonen, T., & Tuukkanen, S. (2020). Direct measurement of contraction force in human cardiac tissue model using piezoelectric cantilever sensor technique. Current Applied Physics, 20(1), 155-160.
[14] Wäldchen, S., Lehmann, J., Klein, T., Van De Linde, S., & Sauer, M. (2015). Light-induced cell damage in live-cell super-resolution microscopy. Scientific reports, 5, 15348.
[15] Kim, K., Park, H., & Lim, K. M. (2015). Phototoxicity: Its mechanism and animal alternative test methods. Toxicological research, 31(2), 97-104.
[16] Ahmad, I., Ahmed, S., Anwar, Z., Sheraz, M.A., Sikorski, M. (2016). Photostability and Photostabilization of Drugs and Drug Products. International Journal of Photoenergy, 2016, 8135608.
[17] Virtanen, J., Pammo, A., Vehkaoja, A., & Tuukkanen, S. (2019). Piezoelectric dual axis cantilever force measurement probe. IEEE Sensors Journal.
[18] Virtanen, J., Sariola, V., & Tuukkanen, S. (2018, August). Piezoelectric cantilever force sensor sensitivity measurements. In Journal of Physics: Conference Series (Vol. 1065, No. 4, p. 042005). IOP Publishing.
[19] Vuorenpää, H., Ikonen, L., Kujala, K., Huttala, O., Sarkanen, J. R., Ylikomi, T., ... & Heinonen, T. (2014). Novel in vitro cardiovascular constructs composed of vascular-like networks and cardiomyocytes. In Vitro Cellular & Developmental Biology-Animal, 50(4), 275-286.
[20] Vuorenpää, H., Penttinen, K., Heinonen, T., Pekkanen-Mattila, M., Sarkanen, J. R., Ylikomi, T., & Aalto-Setälä, K. (2017). Maturation of human pluripotent stem cell derived cardiomyocytes is improved in cardiovascular construct. Cytotechnology, 69(5), 785-800.
[21] Toimela, T., Huttala, O., Sabell, E., Mannerström, M., Sarkanen, J. R., Ylikomi, T., & Heinonen, T. (2017). Intra-laboratory validated human cell-based in vitro vasculogenesis/angiogenesis test with serum-free medium. Reproductive Toxicology, 70, 116-125.
[22] Huttala, O., Vuorenpää, H., Toimela, T., Uotila, J., Kuokkanen, H., Ylikomi, T., ... & Heinonen, T. (2015). Human vascular model with defined stimulation medium-a characterization study.
[23] Virtanen, J., Somppi, S., Törnqvist, H., Jeyhani, V., Fiedler, P., Gizatdinova, Y., ... & Tuukkanen, S. (2018). Evaluation of dry electrodes in canine heart rate monitoring. Sensors, 18(6), 1757.
[24] Rodriguez, M. L., Graham, B. T., Pabon, L. M., Han, S. J., Murry, C. E., & Sniadecki, N. J. (2014). Measuring the contractile forces of human induced pluripotent stem cell-derived cardiomyocytes with arrays of microposts. Journal of biomechanical engineering, 136(5).
[25] Sasaki, D., Matsuura, K., Seta, H., Haraguchi, Y., Okano, T., & Shimizu, T. (2018). Contractile force measurement of human induced pluripotent stem cell-derived cardiac cell sheet-tissue. PloS one, 13(5).

Juhani Virtanen received his M.Sc. (Tech) degree electronics and telecommunications engineering from Tampere University of Technology, Tampere, Finland in 1994. He has 20 years of industrial work experience in various positions. He is currently a doctoral student with research interests in sensor technology, measurements, physiological measurements and signal processing. He has 11 authored internationally peer reviewed articles and 7 internationally granted patents.

Maria Koivisto obtained her M.Sc. (Tech.) degree at the Tampere University of Technology in 2016 where she studied Tissue Engineering in the Biotechnology Programme. Currently, she works as a Ph.D. Student at FICAM, Tampere University. Her research topic is in vitro heart model.

Tarja Toimela, PhD, obtained her MSc degree in University of Jyväskylä cell biology as her Major. She obtained her PhD degree at University of Tampere, in Medical School in the field of in vitro toxicology (2004). Tarja Toimela has wide expertise in cell and tissue culturing and cell analysis techniques and in in vitro toxicology methods. She acts as study director in FICAM's GLP organization.

Antti Vehkaoja received his D.Sc. (Tech.) degree in automation science and engineering from Tampere University of Technology, Tampere, Finland in 2015. He has authored more than 70 scientific articles. He is currently an assistant professor (tenure tract) of sensor technology and biomeasurements at Tampere University. His research interests include development of embedded measurement technologies for physiological monitoring and related signal processing and data analysis methods with a focus on the assessment of vascular condition.

Tuula Heinonen, Professor, is an European Registered toxicologist having deep theoretical education and over 25 years´ practical experience in toxicology in industry and academia. Before joining to Tampere university 2007 she worked in pharmaceutical industry for 17 years in various senior positions covering toxicology, project management and R&D. She was responsible to set up Finnish Center for Alternative methods, FICAM (2008) and is acting as its director. FICAM develops validated tissue and organ models to supplement and replace animal experiments, educate scientists and share information. FICAM is an OECD GLP and EURL-ECVAM NETVAL laboratory. Heinonen´s publications cover toxic risk assessment of chemicals, testing strategies, molecular mechanisms and development and validation of new in vitro tests. She is past president of ecopa, SSCT, Fincopa and the Finnish Society of Toxicology and a member of the Finnish toxicology register board.

Sampo Tuukkanen received his Ph.D. in Applied physics from Department of Physics, University of Jyväskylä, Finland, in 2006. He is currently working as Associate Professor (tenure track) at Tampere University, Finland. His research interests are biomeasurements and bio-based devices. He has authored over 60 articles and has a h-index 20.

PUBLICATION IV

Direct Contraction Force Measurements of Engineered Cardiac Tissue Constructs with Inotropic Drug Exposure

Koivisto M, Mosallaei M, Toimela T, Tuukkanen S, Heinonen T

Frontiers in Pharmacology 13:871569 (2022)
DOI: 10.3389/fphar.2022.871569

frontiers | Frontiers in Pharmacology

ORIGINAL RESEARCH
published: 03 May 2022
doi: 10.3389/fphar.2022.871569

Direct Contraction Force Measurements of Engineered Cardiac Tissue Constructs With Inotropic Drug Exposure

Maria Koivisto[1]*, *Milad Mosallaei*[2], *Tarja Toimela*[1], *Sampo Tuukkanen*[2] and *Tuula Heinonen*[2]

[1]FHAIVE (Finnish Hub for Development and Validation of Integrated Approaches), Faculty of Medicine and Health Technology, Tampere University, Tampere, Finland, [2]Faculty of Medicine and Health Technology, Tampere University, Tampere, Finland

Contractility is one of the most crucial functions of the heart because it is directly related to the maintenance of blood perfusion throughout the body. Both increase and decrease in contractility may cause fatal consequences. Therefore, drug discovery would benefit greatly from reliable testing of candidate molecule effects on contractility capacity. In this study, we further developed a dual-axis piezoelectric force sensor together with our human cell–based vascularized cardiac tissue constructs for cardiac contraction force measurements. The capability to detect drug-induced inotropic effects was tested with a set of known positive and negative inotropic compounds of isoprenaline, milrinone, omecamtiv mecarbil, propranolol, or verapamil in different concentrations. Both positive and negative inotropic effects were measurable, showing that our cardiac contraction force measurement system including a piezoelectric cantilever sensor and a human cell–based cardiac tissue constructs has the potential to be used for testing of inotropic drug effects.

Keywords: force measurement, contraction force, conformal coating, cardiac tissue model, *in vitro* model, human-induced pluripotent stem cell–derived cardiomyocytes, inotropic drug

OPEN ACCESS

Edited by:
Ricardo Gómez,
Cold Spring Harbor Laboratory,
United States

Reviewed by:
Hugo M. Vargas,
Amgen (United States), United States
Anamika Bhargava,
Indian Institute of Technology
Hyderabad, India

***Correspondence:**
Maria Koivisto
maria.koivisto@tuni.fi

Specialty section:
This article was submitted to Cardiovascular and Smooth Muscle Pharmacology, a section of the journal Frontiers in Pharmacology

Received: *08 February 2022*
Accepted: *30 March 2022*
Published: *03 May 2022*

Citation:
Koivisto M, Mosallaei M, Toimela T, Tuukkanen S and Heinonen T (2022) Direct Contraction Force Measurements of Engineered Cardiac Tissue Constructs With Inotropic Drug Exposure. Front. Pharmacol. 13:871569. doi: 10.3389/fphar.2022.871569

INTRODUCTION

Drug-induced adverse cardiac effects are one of the main reasons for discontinuations of drug development and post-approval market withdrawals (Lasser et al., 2002; Li et al., 2016). Thus, drug discovery and development would greatly benefit early detection of cardiotoxic reactions. Furthermore, an adequate cardiac tissue model would be very useful for efficacy determination and mechanistic studies. In addition to ethical concerns, extrapolation from animal studies is impeded by species-specific differences in cardiac electrophysiology (Takeda et al., 2018). Inhibition of human Ether-a-go-go–related gene (hERG) channel causing Torsades de Pointes arrythmia can be screened *in vitro*, but this ion channel is not the only vulnerable target of drug-induced adverse reactions (Weaver and Valentin, 2019). The cardiac action potential comprises ion currents from several ion channels and disturbance of any of the channels can potentially be harmful, for example, block and enhancement of sodium channel, enhancement of calcium current, and block of potassium currents also other than hERG can cause arrythmia (Jonsson et al., 2012). Therefore, *in vitro* test systems reliably mimicking the human heart tissue have great potency to improve the probability of success of drug development.

Currently, *in vitro* cardiotoxicity and efficacy testing of drugs lack standardized testing methods for drug-induced inotropic effects on cardiac cells, even though the cardiac contractility directly affects the cardiac output (Guth et al., 2019). Approaches to measure cardiac contraction force *in vitro* include different imaging-based approaches (Rodriguez et al., 2014; Mannhardt et al., 2016) and direct force measurements such as atomic force microscope (Saenz Cogollo et al., 2011), measuring the deflection of an elastic sheet (Linder et al., 2010), and piezoresistive sensor–integrated polydimethylsiloxane (PDMS) cantilever (Kim et al., 2017).

Piezoelectric materials are commonly used in engineering applications such as sensors and actuators due to their mechanical to electrical and electrical to mechanical conversion. This feature is a result of interaction between electrical and mechanical properties of piezoelectric materials (Aabid et al., 2021). The unique mechanical–electrical conversion can also be used in medical devices such as smart sensing applications (Zaszczyńska et al., 2020).

Previously, we have developed a piezoelectric cantilever sensor which can detect low forces, down to sub-μN range, in dual-axis plane directions (Virtanen et al., 2020a). We have successfully measured the contraction force of engineered cardiac tissue constructs previously using the sensor (Virtanen et al., 2020b; Virtanen et al., 2021). The challenge observed with the sensor was that the humidity in the surrounding atmosphere may be absorbed by the surface of the piezo materials and negatively affects the functionality of the materials. Water absorption decreases the mechanical quality and resistivity of the piezo materials. The humidity can also degrade the dielectric strength of the piezoelectric materials (Surbhi and Sukesha, 2020). This is especially a concern with the *in vitro* cell or tissue measurements where an aqueous cultivation medium is present. These issues can be addressed by protection of these materials against humidity, especially in environments with no humidity control. Encapsulation is one approach that is commonly used to coat the piezo materials. Depending on the service condition of the device, different encapsulation materials are used. The demand for using biofriendly encapsulation in medical devices has increased to prevent unwanted interaction of these applications with live organs (Kuppusami and Oskouei, 2015). Parylene is one of the common polymer coating materials used in biomedical applications, which has favorable characteristics including inherent biocompatibility, biostability, and conformal nature of the deposited film (Zeniieh et al., 2013; Kuppusami and Oskouei, 2015). The vacuum-deposited parylene coating can effectively protect the piezo sensors against the incursion of humidity.

Here, we have applied parylene coating to our piezoelectric cantilever sensors and tested its suitability to measure the effects of five inotropic drugs on engineered cardiac tissue contraction force *in vitro*. We could measure both positive and negative inotropic drug effects with the system along with chronotropic responses to the drugs.

MATERIALS AND METHODS

Cell Culture

The use of human adipose stromal cells (hASCs) obtained from surgical operations and the use of human umbilical vein endothelial cells (HUVECs) obtained from scheduled cesarean sections were approved by the Ethics Committee of Pirkanmaa Hospital District (permit numbers R15161 and R15033, respectively). The hASCs and HUVECs were isolated and propagated as previously described (Sarkanen et al., 2012; Toimela et al., 2017). They were maintained in a humidified incubator at +37°C and 5% CO_2, and the medium was refreshed every 2–3 days.

Cardiac tissue models were cultured using a method modified from a previous work (Virtanen et al., 2021). A fibrin hydrogel was prepared in 96-well plates by mixing 50 μL of a solution containing 5.5 mg/ml fibrinogen (Sigma Aldrich, F3879) with 38 μg/ml aprotinin (Sigma Aldrich, A1153) and 50 μL of 2.75 UN/ml thrombin (Sigma Aldrich, T7009). They were incubated for 45 min at +37°C before seeding of hASCs at 20,000 cells/cm^2 on the fibrin hydrogel. HUVECs were seeded on top of them at 4,000 cells/cm^2 and 1–4 h later in EBM-2 with EGM-2 SingleQuots supplements (Lonza, CC-3162), as previously described (Toimela et al., 2017). Angiogenesis stimulation was initiated using a serum-free stimulation medium (SFSM) comprising DMEM/F12, 2.56 mM L-glutamine, 0.1 nM 3,3′,5-triiodo-L-thyronine sodium salt, ITS™ Premix: 1.15 μM: 6.65 μg/ml insulin, 6.65 μg/ml transferrin, 6.65 ng/ml selenious acid, 1% bovine serum albumin, 2.8 mM sodium pyruvate, 200 μg/ml ascorbic acid, 0.5 μg/ml heparin, 2 μg/ml hydrocortisone, 10 ng/ml VEGF, and 1 ng/ml FGF-β on the next day, as described earlier (Huttala et al., 2015). After 7 days, the cells were treated with 1 μg/ml mitomycin C (Millipore, 47589). On the next day, hiPSC-derived cardiomyocytes (iCell^2, Cellular Dynamics, lot. 105451 and 105455) were seeded on top of the vascular-like networks at 312000 cells/cm^2 in iCell Cardiomyocytes Plating Medium (Cellular Dynamics, M1001). The plating medium was replaced with 1:1 SFSM and iCell Cardiomyocytes Maintenance Medium (Cellular Dynamics, M1003) 4 h later. The cells were maintained in a humidified incubator at +37°C and 5% CO_2, and the medium was refreshed every second day. The whole cell culture process was repeated five times.

Sensor Preparation

The dual-axis L-shaped force measurement sensors were fabricated and calibrated, as previously described (Virtanen et al., 2021). In brief, two lead zirconate titanate (PZT) piezoelectric sensing elements were cut in desired dimension and soldered together in a position of 90° against each other. One end of the L-shaped structure is attached to a printed circuit board, while the other end is soldered to a cantilever beam.

The functionality and calibration of the fabricated sensors were verified by a texture analyzer Stable Micro Systems TX.XTPlus before the actual measurement on the heart tissues. To carry out this process, 1 Hz sinusoidal displacement amplitude of 100 μm (±50 μm) was subjected to the tip of the piezo sensor for 10 cycles. The loading/unloading was applied by a probe attached to a calibrated load cell of 500 g, which provided a high-resolution force output. While the texture analyzer measured the force required for the displacement, the corresponded sensor output was measured simultaneously.

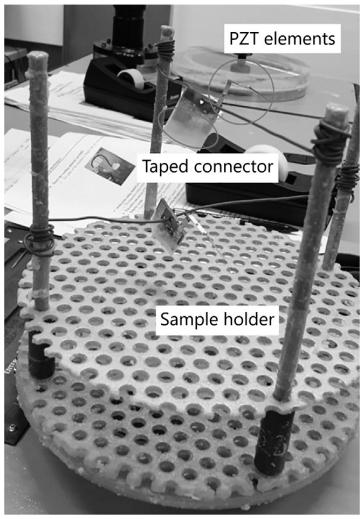

FIGURE 1 | Attachment of the sensor in the sample holder of parylene coating equipment and keeping them in a standing condition with a piece of wire for uniform coating of the polymer in all sides of the sensor during the deposition.

The output data from the texture analyzer and the sensor were then compared together to find the convergence factor in order to calculate the actual construction force of the measured heart tissue constructs.

The deposition of parylene was conducted by addition of the polymer in the vacuum chamber using a ParaTech LabTop 3000 Parylene Coater. Before the coating process, the sensors were placed in a sample holder of the parylene coater, and the connectors were taped to prevent the coating materials from getting inside the connectors, as shown in **Figure 1**. Next, the sample holder was placed inside the vacuum chamber. The procedure for making a 10-μm-thick coating was chosen from the software of the coating machine. In brief, 10 g of a raw powder called dimer (dichloro-p-cyclophane, $C_{16}H_{14}C_{l2}$) was fed in the heating tube of the coater. The dimer was first heated up in the vacuum atmosphere vaporizing the dimeric gas. Next, the dimeric gas was pyrolyzed to the monomeric form of the dimer, and the gas was deposited on the surface of the sample located in the vacuum chamber which was held at room temperature. At the end of the process, a transparent thin film of parylene was coated on the sample (Kuppusami and Oskouei, 2015).

Inotropic Drugs

Isoproterenol (ISO; Sigma Aldrich, I5627), milrinone (MIL; Tocris, 1,504), omecamtiv mecarbil (OME; Adooq Biosciences, A11206), verapamil (VER; Tocris, 0654), and propranolol (PRO; Sigma Aldrich, P0884) solutions were prepared freshly before use. Isoproterenol and verapamil were solubilized in distilled water (Gibco, 15230-071) as 10 mM stock. Propranolol and omecamtiv mecarbil were solubilized in DMSO (Sigma, D2650) as 10 mM stock and milrinone as 50 mM stock. They were diluted in L-15 medium (Gibco, 11415-049). During measurements, the test compounds were administered directly to the wells, diluting them to the final concentrations. The amount of DMSO in the final concentrations of omecamtiv mecarbil and propranolol did not exceed 0.003%. For milrinone, the amount of DMSO in the final concentrations was 0.002, 0.02, and 0.2%.

Force Measurements

The force measurement setup and data acquisition platform were similar to those in our previous work (Virtanen et al., 2021). Synchronously beating cardiac tissue constructs were measured 6–9 days after cardiomyocyte seeding. The cell culture plates with beating cardiac tissue constructs were placed on a heater plate set to +37°C on an optical microscope (Zeiss Primovert, Carl Zeiss AG, Oberkochen, Germany), as shown in **Figure 2**. The cantilever tip was coated by dipping it to 5.5 mg/ml fibrinogen (Sigma Aldrich, F3879) and 2.75 UN/ml thrombin (Sigma Aldrich, T7009) solutions, as previously described (Virtanen et al., 2020b), before contacting the tip to each cardiac tissue construct using a 3-axis linear micromanipulator (Newport Corporation, Irvine, United States). First, a 3-min baseline activity was measured, followed by administration of the first concentration of the test drug from the cumulative concentration series. The activity was measured 10 min after adding each drug concentration. In total, four individual cantilever sensors were used in the measurements.

Immunocytochemistry

Immunocytochemical staining was performed to confirm the presence of cardiomyocytes and vascular networks in the cardiac tissue constructs. The cells were fixed with 70% ethanol for 20 min on day 9 after cardiomyocyte seeding. The cells were stained with cardiomyocyte-specific monoclonal mouse anti-troponin T antibody (1:100, Invitrogen, MA5-12960, lot UF2730196) and endothelial cell–specific polyclonal rabbit anti–von Willebrand factor (1:100, Dako, A0082, lot 20067357) at +4°C overnight. Secondary antibodies anti-mouse IgG Alexa Fluor 488 (Invitrogen, A21202, lot 2018296) and anti-rabbit IgG Alexa Fluor 594 (Invitrogen, A21207, lot 2066086) were incubated for 45 min at RT. The cells were imaged using an Olympus IX51 inverted fluorescence microscope using a ×10 objective. The images were prepared with Photoshop CC (Adobe).

Data Analysis

Data were analyzed in Octave software. 2-minute periods of the recordings were included in the analyses, taking 2 min from the end of the baseline measurement and 2 min from 8 to 10 min after administration of each drug concentration in the same cardiac tissue construct. The wells with regular baseline beating were included in the analysis. Data were filtered using a moving average filter with a window size of 2 s. Filtered data were used for peak detection. The peaks were detected separately from both sides by finding the local maxima above an adaptive threshold that was set to include 4–10% of the highest force values in the filtered data. The up and down peak pairs were formed by selecting the closest peaks. Peak-to-peak amplitudes were

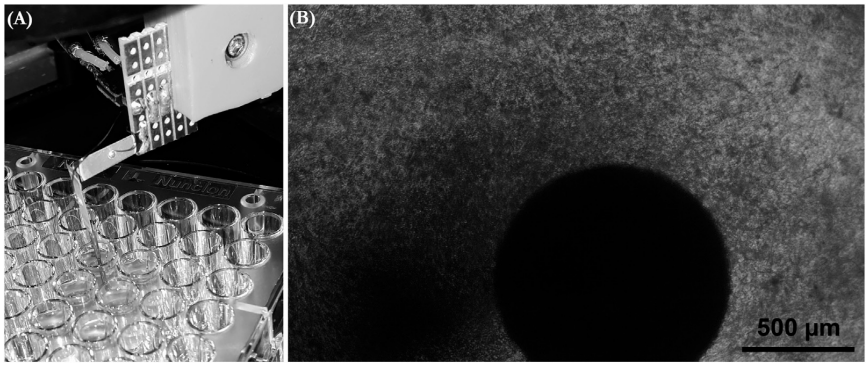

FIGURE 2 | (A) Measurement setup where the culture plate is placed on a heater plate under a microscope, and the measurement sensor is brought into contact with a cardiac tissue construct. **(B)** Microscope view of the sensor tip attached onto the cardiac tissue construct.

TABLE 1 | Mean beating rate and peak-to-peak force amplitudes from the baseline measurements and their percentage changes in the cumulative concentrations of the tested drugs normalized to the baseline measurements.

Drug	Concentration	Mean beating rate	SD	Mean peak-to-peak force	SD	Number of wells
ISO	0 nM	25.87 BPM	6.44	88.95 µN	82.15	6
	10 nM	176.05%	33.79	105.28%	9.84	6
	30 nM	183.86%	32.59	109.56%	10.62	6
	100 nM	193.72%	31.50	115.76%	12.72	6
MIL	0 µM	20.76 BPM	5.95	465.44 µN	622.6	9
	1 µM	108.13%	16.73	103.06%	9.91	9
	10 µM	118.06%	19.11	112.15%	12.38	9
	100 µM	232.67%	50.05	103.51%	14.19	9
OME	0 nM	22.22 BPM	6.77	37.45 µN	16.90	10
	30 nM	96.31%	12.49	98.45%	5.819	10
	100 nM	94.76%	17.67	95.53%	13.20	10
	300 nM	94.51%	19.36	95.81%	12.23	10
PRO	0 nM	21.47 BPM	4.856	673.27 µN	822.83	9
	30 nM	98.62%	14.43	97.18%	9.39	9
	100 nM	90.73%	16.24	94.62%	10.79	9
	300 nM	63.16%	26.93	93.63%	9.03	9
VER	0 nM	15.10 BPM	7.77	347.28 µN	645.90	6
	10 nM	116.01%	31.83	99.53%	12.20	6
	30 nM	115.62%	27.07	93.90%	15.86	6
	100 nM	157.02%	25.54	85.71%	8.26	4

calculated for the peak pairs from the unfiltered data. Beating frequency was calculated from the peak intervals. For each well, the results from either the x or y channel of the dual-axis sensor were selected based on peak detection. The channel from which more peaks were detected was selected. The same channel was selected from the four consecutive measurements of the same well. The effects of the drugs were normalized for comparison by calculating the percentage change from the baseline activity of each well.

Statistical analyses were performed in IBM SPSS Statistics 27. The nonparametric Kruskal–Wallis test with Bonferroni correction was used for testing the statistical significance of the changes in beat frequency and peak-to-peak forces in different drug concentrations and baseline measurements. The p-values <0.05 were considered statistically significant.

RESULTS

The beat rate and contraction force values of the baseline measurements together with the percentage change from the cumulative concentrations of the drugs are shown in **Table 1**. The

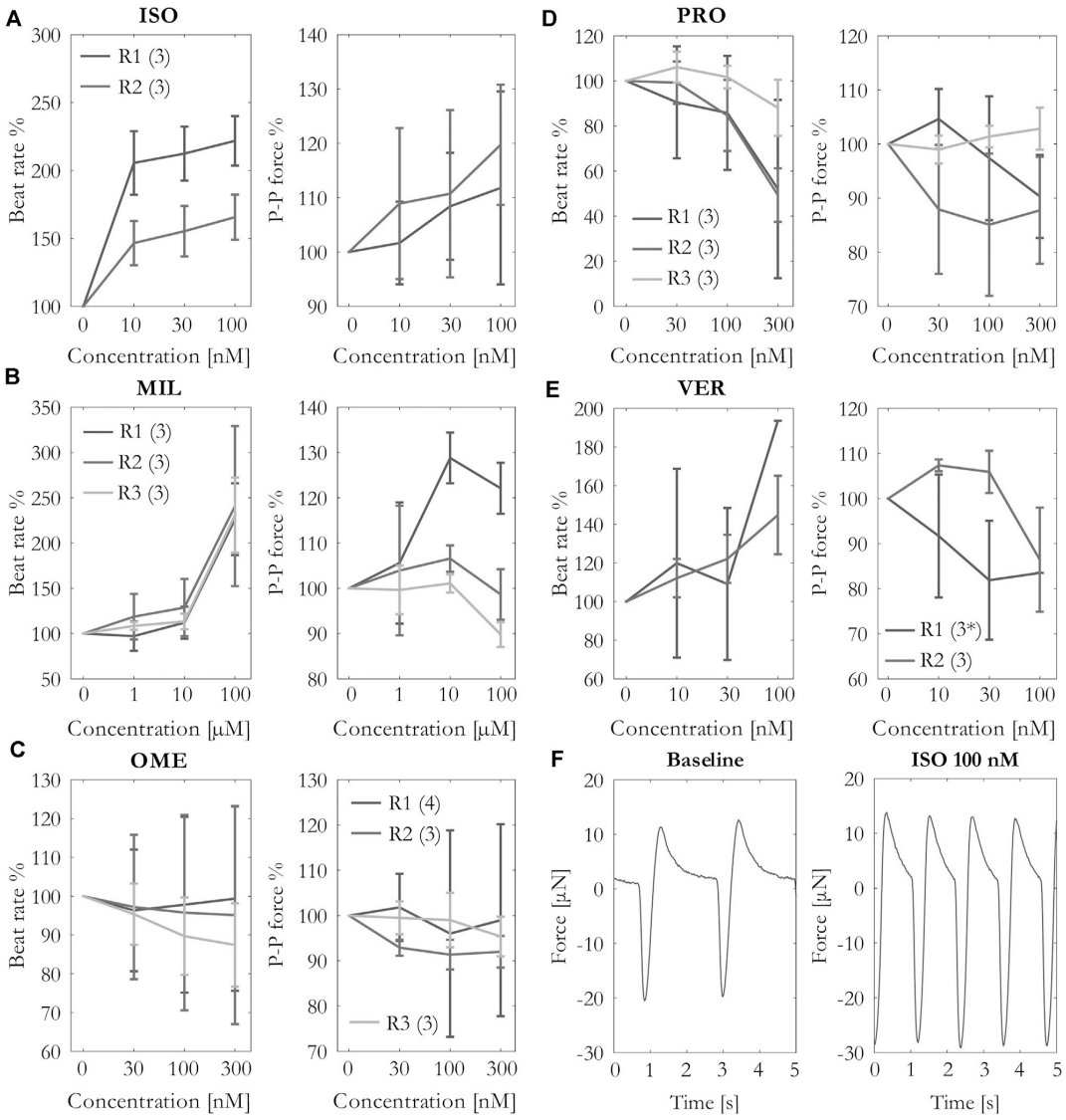

FIGURE 3 | Percentage change of the beating rate and force in the cumulative concentrations of **(A)** isoprenaline (ISO), **(B)** milrinone (MIL), **(C)** omecamtiv mecarbil (OME), **(D)** propranolol (PRO), and **(E)** verapamil (VER) exposures. Mean and SD of the beating rate and peak-to-peak amplitudes from each repeat R1–R3 (number of measurements per repeat). *N = 1 at 100 nM. **(F)** Beating from an example well during baseline and 100 nM isoprenaline force measurements.

mean beat rate was 21.2 BPM (SD 7.0) and the mean peak-to-peak contraction force amplitude 331.0 μN (SD 602.2) during the baseline measurements (N = 40 wells).

The effects of the cumulative concentrations of the tested drugs on the beat rate and contraction force are shown in **Figure 3** as percentage change from the baseline measurements. As expected, the positive chrono- and inotrope isoprenaline increased both beating rate and contraction force. However, the variation in the force results was quite high, and only the increase in the beating rate was statistically significant (p = 0.016 at 30 nM, p = 0.005 at 100 nM, N = 6).

The isoprenaline-induced change in the contraction force and beating rate is clearly visible in the example signal in **Figure 3**. The second positive inotrope, milrinone, increased the beating

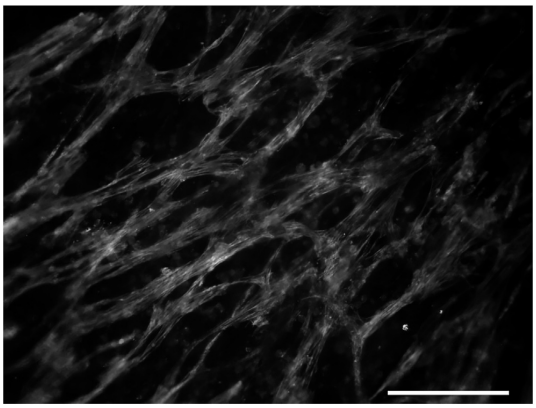

FIGURE 4 | Cardiac troponin T (green)–positive cardiomyocytes and the von Willebrand factor (red)–positive vascular network. Scale bar: 200 μm.

rate with statistical significance ($p < 0.001$ at 100 μM, N = 9). The effects of milrinone on the contraction force were incoherent among the repeats. While the drug increased the force during the repeat R1, it failed to increase it during the repeats R2 and R3.

Omecamtiv mecarbil induced nonuniform effects on the beating rate among the different wells, in some wells the effect being positive and in others negative chronotropy, causing variation to the results especially in repeats R1 and R2. In repeat R3, the trend was mainly negative chronotropy. Likewise, the results on the contraction force differed among the parallel wells in the repeat R1 from slight increase to slight decrease in force. Overall, the drug did not have an apparent effect on the contraction force. We also tested higher concentrations (600 nM and 900 nM) of omecamtiv mecarbil without a clearer effect on the force (data not shown).

Propranolol caused a statistically significant decrease in beating rate ($p = 0.003$ at 300 nM, N = 9), but the effect in contraction force was not clear. The contraction force seemed to decrease slightly in repeats R1 at the highest concentration and R2, but it did not change in repeat R3 in which also the decrease in beating rate was the smallest.

Verapamil increased the beating rate in most of the wells but decreased it in one well. Moreover, the beating rate ceased in two wells at 100 nM in repeat R1. Apart from the slight increase at 10 and 30 nM in repeat R2, the contraction force was decreased by verapamil. However, the decrease was not statistically significant.

Immunocytochemical staining confirmed the presence of cardiac troponin T–positive cardiomyocytes and the von Willebrand factor–positive vascular network in the cardiac tissue constructs (**Figure 4**). The cardiomyocytes were connected to each other and arranged into a network. The connectiveness of the cardiomyocytes was also indicated by the synchronous beating of the whole construct in each well during the force measurements.

DISCUSSION

Isoprenaline is a β-adrenergic receptor agonist and a positive inotrope. The positive inotropic effect has been previously reported in cardiac microtissues consisting of hiPSC-CM and fibroblasts (Huebsch et al., 2016) and in hiPSC-derived cardiomyocytes, for example, 51% increase in force at 10 nM (Saleem et al., 2020) and 41% increase in force at 100 nM (Mannhardt et al., 2016). Positive chrono- and inotropy at 1 μM has been reported in cardiac constructs consisting of hiPSC-CM, fibroblasts, and endothelial cells (Arai et al., 2020). Our results are well in line with those of the previous studies, although the changes were not statistically significant. The higher relative beating rates in repeat R1 can at least partly be explained by their slower baseline beating rate than those of repeat R2, which enables higher relative increases in beating rates. The chrono- and inotropic effects of isoprenaline were measurable and repeatable in our system.

Milrinone is primarily a phosphodiesterase type-3 (PDE3) inhibitor that increases intracellular calcium levels and contraction force in human heart. The drug has also been reported to lack the effect on hiPSC-derived cardiomyocytes *in vitro* (Mannhardt et al., 2017; Saleem et al., 2020), which is similar to the second and third repeats in our study. Saleem et al. (2020) concluded that the lack of inotropic effect of milrinone in their study was most likely due to the lower expression of PDE3A and PDE4A than that of human heart samples and the predominance of PDE4 isoform over PDE3 in their engineered heart tissue, which could be linked to the immaturity of the cardiomyocytes. Sube and Ertel (2017) reported higher susceptibility to PDE4 inhibition than that to PDE3 in their hiPSC-CM cultures too. In contrast, Feric et al. (2019) obtained a maximal 4.3 ± 1.2-fold increase in the contraction force at 100 μM milrinone with an EC_{50} of 1.6 μM in their engineered cardiac tissues containing cardiomyocytes and fibroblasts, and which had been electrically stimulated during the culturing to improve maturation. In the study of Ravenscroft et al. (2016), milrinone increased contraction force with EC_{50} = 83.68 μM in cardiac triculture microtissues containing endothelial cells and fibroblasts but did not have an effect on bare cardiomyocyte microtissues. Our cardiac tissue model contains several relevant cell types including endothelial cells and myofibroblasts that promote the cardiomyocyte maturation, which is further compared to monoculture of cardiomyocytes (Koivisto, M, Tolvanen, T.A, Toimela, T, Miinalainen, I, Kiviaho, A, Kesseli, J, et al. (2022). "Functional human cell–based vascularized cardiac tissue model for biomedical research and testing" [manuscript submitted for publication]). The improved maturation may enable the positive inotropic effect of milrinone in our cardiac constructs, even though it was not observed in all repeats.

Despite differences in the force results among the milrinone repeats in our study, the positive chronotropic effect was evident at the highest concentration in all repeats. The positive chronotropic effect of milrinone has been previously reported at concentrations ≥3 μM in hiPSC-CM cultures (Sube and Ertel, 2017). However, the positive chronotropic effect could also be

caused by the vehicle 0.2% DMSO at that concentration in our study because DMSO has been reported to increase the beating rate of hiPSC-CMs (Jonsson et al., 2011). The effect of DMSO could also explain the decrease of contraction force in all repeats at the highest milrinone concentration.

Omecamtiv mecarbil is a selective cardiac myosin activator that produces positive inotropy without affecting intracellular calcium levels (Planelles-Herrero et al., 2017). Positive inotropic effect has also been reported *in vitro,* for example, Feric et al. (2019) measured a maximal 2.6 ± 0.3-fold increase in contractile force in their engineered human cardiac tissue at 10 μM omecamtiv mecarbil with an EC_{50} of 370 nM. However, varying inotropic effects have also been reported. Measuring from single-cell hiPSC-CMs, Ballan et al. (2020) reported 11% increase in force at 100 nM but higher doses, 1 and 10 μM, suppressed contractility. Ribeiro et al. (2017), also measuring single-cell hiPSC-CMs, reported positive inotropy immediately after administration of 100 nM omecamtiv mecarbil. However, 5 min after the exposure, they measured negative inotropy at 10 and 100 nM, possibly due to the myofibril damage that they detected. In our study, we did not obtain a clear result in force amplitude from omecamtiv mecarbil, even though some of the wells showed positive or negative inotropic responses especially in repeat R1. Ribeiro et al. (2017) obtained positive chronotropic effects of omecamtiv mecarbil. In contrast, negative chronotropy of omecamtiv mecarbil has been reported in clinical trials (Teerlink et al., 2020). In our study, even though the beating rate seemed to decrease in repeat R3, the results from repeats R2 and R3 were inconclusive with high variation among the parallel wells, some wells showing increase and some decrease or no change in the beating rate.

Propranolol, by blocking β-adrenergic receptors, results in negative chrono- and inotropy in human heart. In the absence of adrenergic stimulation, propranolol would not be expected to cause negative inotropic effects. However, propranolol has also been reported to block cardiac NaV1.5 sodium channels (Wang et al., 2010). In our study, only the negative chronotropic effect was clear, which might result from propranolol blocking the sodium channels. The negative chronotropic and inotropic effects have been previously measured *in vitro*, for example, in hiPSC-CM constructs (Morimoto et al., 2016) and cardiac constructs consisting of hiPSC-CM, fibroblasts, and endothelial cells (Arai et al., 2020).

Verapamil is an L-type calcium channel blocker and a negative inotrope. Negative inotropy of verapamil has been reported in previous *in vitro* studies, for example, in engineered heart tissue (Mannhardt et al., 2016) and hiPSC-CMs (Gossmann et al., 2016). In our study, apart from the slight increase in force at the lowest concentrations in repeat R2, the overall trend was negative inotropy as expected. Verapamil is clinically used for slowing heart rate. However, in our study, the effect was the opposite in most of the wells. Positive chronotropy of verapamil has been previously reported in dogs (Nakaya et al., 1983). Few of the wells in our study showed decrease in the beating rate and cessation of beating at 100 nM. The beating rate in these wells was already low, that is, <10 BPM during the baseline measurements.

Overall, the beating rate of the cardiac constructs during the baseline measurements was constant among parallel wells and comparable to that of our previous force measurement study where the beating rates were in range 19–38 BPM (Virtanen et al., 2021). Variation in the beating rate can originate from the cell culture batches at different time in culture depending on the measurement days 6–9 days after cardiomyocyte seeding.

Variation in the absolute contraction force values between different measurements results from differences between the sensor elements and especially differences in calibrated amplification of the measurement channels. Although the cardiac tissues were prepared the same way for each repeat, individual cardiac tissue constructs were different in beating strength and location of the strongest beating. The sensor tip was connected with the strongest contraction point, but the direction of cardiac contraction relative to the chosen measurement channel caused variation in the absolute force values among the parallel wells. As the contact point between the cardiac tissue and sensor tip influenced the measured force amplitude, it was critical to maintain the contact point intact during the consecutive measurements of the same well to enable comparison. Because the drug administration was performed manually by pipetting the amount of the drug into the wells, it was possible that the cantilever was touched with the pipette tip, causing disturbance in the contact point between the sensor tip and cardiac tissue construct. Special attention was paid on this and when noticed, the results from the well were omitted from the analyses because the possible difference in force might not be due to the drug effect but the effect of the changed contact point. However, if it remained unnoticed, it could distort the results.

Although complex cellular models best resemble the *in vivo* situation, they are challenging to standardize. Moreover, even advanced models cannot fully represent the complexity of the *in vivo* situation. Our cardiac tissue model does not have connections with nerve stimulation and does not recapitulate the structure of the heart. Moreover, the maturity of the hiPSC-derived cardiomyocytes does not reach the level of adult human cardiomyocytes with the current techniques. Other limitations of this study include inconsistent and low number of measured wells for some of the tested drugs and high variation in the force results among parallels and among different testing times for some of the drugs. The force measurement technique used in our study is currently time-consuming and laborious because only one well can be measured at a time. Moreover, the selection of the measured wells and measurement locations in these wells is manual and prefers cultures with strong and regular beating.

As a conclusion, our cardiac contraction force measurement system including a piezoelectric cantilever sensor and a human cell–based cardiac tissue constructs has potential to be used for testing of inotropic drug effects. Even though the variation of the force results among parallel wells or repeats was relatively high for some of the tested drugs, it was possible to detect both positive and negative inotropic effects in this system.

DATA AVAILABILITY STATEMENT

The raw data supporting the conclusion of this article will be made available by the authors, without undue reservation.

ETHICS STATEMENT

The studies involving human participants were reviewed and approved by the Ethics Committee of Pirkanmaa Hospital

District. The patients/participants provided their written informed consent to participate in this study.

AUTHOR CONTRIBUTIONS

MM prepared the force sensors and performed their calibration. MK cultured the cardiac tissue constructs, and MK, MM, and TT performed the actual force measurements with drug exposure. MK analyzed the force measurement data. MK and MM wrote most parts of the manuscript. TT, ST, and TH participated in planning the experiments, commented, and reviewed the manuscript.

FUNDING

The authors acknowledge the project funding from the Academy of Finland (Grant numbers: 310347 and 310527) and Finnish Cultural Foundation, Pirkanmaa Regional fund (Grant number 50211545).

REFERENCES

Aabid, A., Raheman, M. A., Ibrahim, Y. E., Anjum, A., Hrairi, M., Parveez, B., et al. (2021). A Systematic Review of Piezoelectric Materials and Energy Harvesters for Industrial Applications. *Sensors (Basel)* 21 (12), 4145. doi:10.3390/s21124145

Arai, K., Murata, D., Takao, S., Nakamura, A., Itoh, M., Kitsuka, T., et al. (2020). Drug Response Analysis for Scaffold-free Cardiac Constructs Fabricated Using Bio-3D Printer. *Sci. Rep.* 10 (June), 8972. doi:10.1038/s41598-020-65681-y

Ballan, N., Shaheen, N., Keller, G. M., and Gepstein, L. (2020). Single-Cell Mechanical Analysis of Human Pluripotent Stem Cell-Derived Cardiomyocytes for Drug Testing and Pathophysiological Studies. *Stem Cel Rep.* 15 (3), 587–596. doi:10.1016/j.stemcr.2020.07.006

Feric, N. T., Pallotta, I., Singh, R., Bogdanowicz, D. R., Gustilo, M., Chaudhary, K., et al. (2019). Engineered Cardiac Tissues Generated in the Biowire™ II: A Platform for Human-Based Drug Discovery. *Toxicol. Sci.* 172 (1), 89–97. doi:10.1093/toxsci/kfz168

Gossmann, M., Frotscher, R., Linder, P., Neumann, S., Bayer, R., Epple, M., et al. (2016). Mechano-Pharmacological Characterization of Cardiomyocytes Derived from Human Induced Pluripotent Stem Cells. *Cell Physiol Biochem* 38 (3), 1182–1198. doi:10.1159/000443124

Guth, B. D., Engwall, M., Eldridge, S., Foley, C. M., Guo, L., Gintant, G., et al. (2019). Considerations for an *In Vitro*, Cell-Based Testing Platform for Detection of Adverse Drug-Induced Inotropic Effects in Early Drug Development. Part 1: General Considerations for Development of Novel Testing Platforms. *Front. Pharmacoljournal Article)* 10, 884. doi:10.3389/fphar.2019.00884

Huebsch, N., Loskill, P., Deveshwar, N., Spencer, C. I., Judge, L. M., Mandegar, M. A., et al. (2016). Miniaturized IPS-Cell-Derived Cardiac Muscles for Physiologically Relevant Drug Response Analyses. *Sci. Rep.* 6 (1), 24726. doi:10.1038/srep24726

Huttala, O., Vuorenpää, H., Toimela, T., Uotila, J., Kuokkanen, H., Ylikomi, T., et al. (2015). Human Vascular Model with Defined Stimulation Medium - A Characterization Study. *ALTEX* 32 (2), 125–36. doi:10.14573/altex.1411271

Jonsson, M. K., Vos, M. A., Mirams, G. R., Duker, G., Sartipy, P., de Boer, T. P., et al. (2012). Application of Human Stem Cell-Derived Cardiomyocytes in Safety Pharmacology Requires Caution beyond HERG. *J. Mol. Cel Cardiol* 52 (5), 998–1008. doi:10.1016/j.yjmcc.2012.02.002

Jonsson, M. K., Wang, Q. D., and Becker, B. (2011). Impedance-Based Detection of Beating Rhythm and Proarrhythmic Effects of Compounds on Stem Cell-Derived Cardiomyocytes. *Assay Drug Dev. Technol.* 9 (6), 589–599. doi:10.1089/adt.2011.0396

Kim, D.-S., Jeong, Y.-J., Lee, B.-K., Shanmugasundaram, A., and Lee, D.-W. (2017). Piezoresistive Sensor-Integrated PDMS Cantilever: A New Class of Device for Measuring the Drug-Induced Changes in the Mechanical Activity of Cardiomyocytes. *Sensors Actuators B: Chem.* 240 (March), 566–572. doi:10.1016/j.snb.2016.08.167

Kuppusami, S., and Oskouei, R. H. (2015). Parylene Coatings in Medical Devices and Implants: A Review. *ujbe* 3 (2), 9–14. doi:10.13189/ujbe.2015.030201

Lasser, K. E., Allen, P. D., Woolhandler, S. J., Himmelstein, D. U., Wolfe, S. M., and Bor, D. H. (2002). Timing of New Black Box Warnings and Withdrawals for Prescription Medications. *JAMA* 287 (17), 2215–2220. doi:10.1001/jama.287.17.2215

Li, X., Zhang, R., Zhao, B., Lossin, C., and Cao, Z. (2016). Cardiotoxicity Screening: A Review of Rapid-Throughput *In Vitro* Approaches. *Arch. Toxicol.* 90 (8), 1803–1816. doi:10.1007/s00204-015-1651-1

Linder, P., Trzewik, J., Rüffer, M., Artmann, G. M., Digel, I., Kurz, R., et al. (2010). Contractile Tension and Beating Rates of Self-Exciting Monolayers and 3D-Tissue Constructs of Neonatal Rat Cardiomyocytes. *Med. Biol. Eng. Comput.* 48 (1), 59–65. doi:10.1007/s11517-009-0552-y

Mannhardt, I., Breckwoldt, K., Letuffe-Brenière, D., Schaaf, S., Schulz, H., Neuber, C., et al. (2016). Human Engineered Heart Tissue: Analysis of Contractile Force. *Stem Cel Rep.* 7 (1), 29–42. doi:10.1016/j.stemcr.2016.04.011

Mannhardt, I., Eder, A., Dumotier, B., Prondzynski, M., Krämer, E., Traebert, M., et al. (2017). Blinded Contractility Analysis in HiPSC-Cardiomyocytes in Engineered Heart Tissue Format: Comparison with Human Atrial Trabeculae. *Toxicol. Sci.* 158 (1), 164–175. doi:10.1093/toxsci/kfx081

Morimoto, Y., Mori, S., Sakai, F., and Takeuchi, S. (2016). Human Induced Pluripotent Stem Cell-Derived Fiber-Shaped Cardiac Tissue on a Chip. *Lab. Chip* 16 (12), 2295–2301. doi:10.1039/C6LC00422A

Nakaya, H., Schwartz, A., and Millard, R. W. (1983). Reflex Chronotropic and Inotropic Effects of Calcium Channel-Blocking Agents in Conscious Dogs. Diltiazem, Verapamil, and Nifedipine Compared. *Circ. Res.* 52 (3), 302–311. doi:10.1161/01.RES.52.3.302

Planelles-Herrero, V. J., Hartman, J. J., Robert-Paganin, J., Malik, F. I., and Houdusse, A. (2017). Mechanistic and Structural Basis for Activation of Cardiac Myosin Force Production by Omecamtiv Mecarbil. *Nat. Commun.* 8 (1), 190. doi:10.1038/s41467-017-00176-5

Ravenscroft, S. M., Pointon, A., Williams, A. W., Cross, M. J., and Sidaway, J. E. (2016). Cardiac Non-myocyte Cells Show Enhanced Pharmacological Function Suggestive of Contractile Maturity in Stem Cell Derived Cardiomyocyte Microtissues. *Toxicol. Sci.* 152 (1), 99–112. doi:10.1093/toxsci/kfw069

Ribeiro, A. J. S., Schwab, O., Mandegar, M. A., Ang, Y. S., Conklin, B. R., Srivastava, D., et al. (2017). Multi-Imaging Method to Assay the Contractile Mechanical Output of Micropatterned Human IPSC-Derived Cardiac Myocytes. *Circ. Res.* 120 (10), 1572–1583. doi:10.1161/CIRCRESAHA.116.310363

Rodriguez, M. L., Graham, B. T., Pabon, L. M., Han, S. J., Murry, C. E., and Sniadecki, N. J. (2014). Measuring the Contractile Forces of Human Induced Pluripotent Stem Cell-Derived Cardiomyocytes with Arrays of Microposts. *J. Biomech. Eng.* 136 (5), 051005. doi:10.1115/1.4027145

Saenz Cogollo, J. F., Tedesco, M., Martinoia, S., and Raiteri, R. (2011). A New Integrated System Combining Atomic Force Microscopy and Micro-electrode Array for Measuring the Mechanical Properties of Living Cardiac Myocytes. *Biomed. Microdevices* 13 (4), 613–621. doi:10.1007/s10544-011-9531-9

Saleem, U., Ismaili, D., Mannhardt, I., Pinnschmidt, H., Schulze, T., Christ, T., et al. (2020). Regulation of ICa,L and Force by PDEs in Human-Induced Pluripotent Stem Cell-Derived Cardiomyocytes. *Br. J. Pharmacol.* 177 (13), 3036–3045. doi:10.1111/bph.15032

Sarkanen, J. R., Vuorenpää, H., Huttala, O., Mannerström, B., Kuokkanen, H., Miettinen, S., et al. (2012). Adipose Stromal Cell Tubule Network Model Provides a Versatile Tool for Vascular Research and Tissue Engineering. *Cells Tissues Organs* 196 (5), 385–397. doi:10.1159/000336679

Sube, R., and Ertel, E. A. (2017). Cardiomyocytes Derived from Human Induced Pluripotent Stem Cells: An *In-Vitro* Model to Predict Cardiac Effects of Drugs. *JBiSE* 10 (11), 527–549. doi:10.4236/jbise.2017.1011040

Surbhiand Sukesha (2020). Response of Piezoelectric Materials to the External Temperature, Electric Field and Humidity. *Mater. Today Proc.* 28 (January), 1951–1954. doi:10.1016/j.matpr.2020.05.555

Takeda, M., Miyagawa, S., Fukushima, S., Saito, A., Ito, E., Harada, A., et al. (2018). Development of *In Vitro* Drug-Induced Cardiotoxicity Assay by Using Three-Dimensional Cardiac Tissues Derived from Human Induced Pluripotent Stem Cells. *Tissue Eng. Part. C Methods* 24 (1), 56–67. doi:10.1089/ten.tec.2017.0247

Teerlink, J. R., Diaz, R., Felker, G. M., McMurray, J. J. V., Metra, M., Solomon, S. D., et al. (2020). Omecamtiv Mecarbil in Chronic Heart Failure with Reduced Ejection Fraction: Rationale and Design of GALACTIC-HF. *JACC Heart Fail.* 8 (4), 329–340. doi:10.1016/j.jchf.2019.12.001

Toimela, T., Huttala, O., Sabell, E., Mannerström, M., Sarkanen, J. R., Ylikomi, T., et al. (2017). Intra-Laboratory Validated Human Cell-Based *In Vitro* Vasculogenesis/Angiogenesis Test with Serum-free Medium. *Reprod. Toxicol.* 70, 116–125. doi:10.1016/j.reprotox.2016.11.015

Virtanen, J., Koivisto, M., Toimela, T., Vehkaoja, A., Heinonen, T., and Tuukkanen, S. (2021). Direct Measurement of Contraction Force in Cardiac Tissue Construct in 2D-Plane Using Dual Axis Cantilever Sensor. *IEEE Sensors J.* 21 (3), 2702–2711. doi:10.1109/JSEN.2020.3027857

Virtanen, J., Pammo, A., Vehkaoja, A., and Tuukkanen, S. (2020b). Piezoelectric Dual-Axis Cantilever Force Measurement Probe. *IEEE Sensors J.* 20 (4), 1786–1792. doi:10.1109/JSEN.2019.2950765

Virtanen, J., Toivanen, M., Toimela, T., Heinonen, T., and Tuukkanen, S. (2020a). Direct Measurement of Contraction Force in Human Cardiac Tissue Model Using Piezoelectric Cantilever Sensor Technique. *Curr. Appl. Phys.* 20 (1), 155–160. doi:10.1016/j.cap.2019.10.020

Wang, D. W., Mistry, A. M., Kahlig, K. M., Kearney, J. A., Xiang, J., and George, A. L. (2010). Propranolol Blocks Cardiac and Neuronal Voltage-Gated Sodium Channels. *Front. Pharmacol.* 1, 144. doi:10.3389/fphar.2010.00144

Weaver, R. J., and Valentin, J. P. (2019). Today's Challenges to De-risk and Predict Drug Safety in Human "Mind-the-Gap". *Toxicol. Sci.* 167 (2), 307–321. doi:10.1093/toxsci/kfy270

Zaszczyńska, A., Gradys, A., and Sajkiewicz, P. (2020). Progress in the Applications of Smart Piezoelectric Materials for Medical Devices. *Polymers* 12 (11), 2754. doi:10.3390/polym12112754

Zeniieh, D., Bajwa, A., and Olcaytug, F. (2013). *Parylene-C Thin Film for Biocompatible Encapsulations with Very Strong Adhesion and Superior Barrier Properties*. Queensland, Australia: Cairns Convention Centre. Available at: https://www.semanticscholar.org/paper/PARYLENE-C-THIN-FILM-FOR-BIOCOMPATIBLE-WITH-VERY-Zeniieh-Bajwa/a134089d3c6865a0038df655648159eccfb511ac.

Conflict of Interest: The authors declare that the research was conducted in the absence of any commercial or financial relationships that could be construed as a potential conflict of interest.

Publisher's Note: All claims expressed in this article are solely those of the authors and do not necessarily represent those of their affiliated organizations, or those of the publisher, the editors, and the reviewers. Any product that may be evaluated in this article, or claim that may be made by its manufacturer, is not guaranteed or endorsed by the publisher.